



Magnetotelluric and Audiomagnetotelluric Groundwater Survey Along the Humu'ula Portion of Saddle Road Near and Around the Pohakuloa Training Area, Hawaii

By Herbert A. Pierce and Donald M. Thomas



Open-File Report 2009-1135
version 1.1

U.S. Department of the Interior
U.S. Geological Survey

U.S. Department of the Interior
KEN SALAZAR, Secretary

U.S. Geological Survey
Suzette M. Kimball, Acting Director

U.S. Geological Survey, Reston, Virginia: 2009
Revised: September 22, 2009

For product and ordering information:
World Wide Web: <http://www.usgs.gov/pubprod>
Telephone: 1-888-ASK-USGS

For more information on the USGS—the Federal source for science about the Earth,
its natural and living resources, natural hazards, and the environment:
World Wide Web: <http://www.usgs.gov>
Telephone: 1-888-ASK-USGS

On the cover: A north-looking photo of the Saddle Road Area between Mauna Kea and Mauna Loa. Aa lava flows, the saddle, and the south-facing slope of Mauna Kea are visible. Photograph by James B. Murray.

Suggested citation:

Pierce, H.A., and Thomas, D.M., 2009, Magnetotelluric and audiomagnetotelluric groundwater survey along the Humu'ula portion of Saddle Road near and around the Pohakuloa Training Area, Hawaii (ver. 1.1): U.S. Geological Survey Open-File Report 2009-1135, 160 p., available at <http://pubs.usgs.gov/ofr/2009/1135/ofr2009-1135.pdf>.

Any use of trade, product, or firm names is for descriptive purposes only and does not imply endorsement by the U.S. Government.

Although this report is in the public domain, permission must be secured from the individual copyright owners to reproduce any copyrighted material contained within this report.

Contents

Abstract	1
The Big Island Saddle Road MT Study	1
Geologic Environment	2
Hydrology	4
Electromagnetic Natural Source Approach and Methods	9
Field Surveys	10
Resistivity Soundings	11
Discussion	12
Results	13
Cross-Profile Transect PTA4	16
Cross-Profile Transect HSR2	17
Cross Profiles PTA1, PTA2, and PTA3	18
Resistivity Maps at Several Elevations	22
Conclusions	25
Acknowledgments	26
References Cited	28
Appendix A—MT and AMT Stations	30
Appendix B—MT and AMT Sounding Resistivity Plots	32
Appendix C—1D Inversions of the MT and AMT Data	89
Appendix D—Polar Diagrams of Selected Frequencies	104

Figures

1. Map showing stratigraphic formations for volcanoes on the Island of Hawaii.	3
2. A simplified conceptual model of island geology and hydrology	5
3. Shaded relief map of the Digital Elevation Model (DEM) for the county of Hawaii showing well locations (Imata, 2004) plotted in yellow. Most of these wells are located near the coastline. The wells labeled Waikii, PTA, and Kaumana are colored blue and are discussed in the text.	7
4. Map of the magnetotelluric and audiomagnetotelluric station locations	11
5. Electrical transects and station locations mapped along the Humuula Saddle Road	13
6. Profile of the Saddle from Mamalahoa Highway to Kaumana showing resistivities encountered along Saddle Road in the relatively dry volcanic terrain.	14
7. Cross-profile resistivity plot of transect PTA4	17
8. Cross-profile resistivity plot of several stations near the access roads (line HSR2) to the Mauna Kea and Mauna Loa observatories	18
9. Cross-profile resistivity plot of line PTA2	19
10. Cross-profile resistivity plot of resistivities collected along line PTA1	20
11. Cross-profile resistivity plot of transect PTA3	22
12. Map view of resistivity data from MT and AMT stations at a constant elevation of 400 meters above sea level	23
13. Map view of resistivity data taken from MT and AMT stations at a constant elevation of 600 meters above sea level	24

14.	Map view of resistivity data taken from MT and AMT stations at a constant elevation of 800 meters above sea level	25
-----	---	----

Table

A-1.	Magnetotelluric and audiomagnetotelluric station identifiers, locations, and Global Positioning System (GPS) elevations (± 10 meters).....	30
------	---	----

Conversion Factors

Multiply	By	To obtain
Length		
inch (in.)	2.54	centimeter (cm)
foot (ft)	0.3048	meter (m)
mile (mi)	1.609	kilometer (km)
Area		
acre	0.4047	hectare (ha)
square mile (mi ²)	259.0	hectare (ha)
Flow rate		
gallon per minute (gal/min)	0.06309	liter per second (L/s)

Vertical coordinate information is referenced to the insert datum name (and abbreviation) here for instance, "North American Vertical Datum of 1988 (NAVD 88)."

Horizontal coordinate information is referenced to the insert datum name (and abbreviation) here for instance, "North American Datum of 1983 (NAD 83)."

Magnetotelluric and Audiomagnetotelluric Groundwater Survey Along the Humu'ula Portion of Saddle Road Near and Around the Pohakuloa Training Area, Hawaii

By Herbert A. Pierce and Donald M. Thomas

Abstract

The Pohakuloa Training Area (PTA), operated by the U.S. Army on the Big Island of Hawaii, is in need of a reliable potable water supply to sustain ongoing operations by staff and trainees. In an effort to acquire baseline hydrologic data with which to develop a plan for providing that water, a series of magnetotelluric (MT) geophysical surveys was performed that spanned the Mauna Loa/Mauna Kea Saddle region of Hawaii Island. These surveys provided electrical resistivity profiles and resistivity maps at several elevations along the axis of the field measurements that can be interpreted to yield information on the depth to the water table. In 2004, a preliminary sequence of 23 audiomagnetotelluric (AMT) soundings was collected along Saddle Road extending from the Waikii Ranch area, west of the PTA, to Department of Hawaiian Home Lands Humu'ula properties east of the Mauna Kea access road. The results of those soundings showed that highly resistive rocks, consistent with dry basalts, were present to depths of at least one kilometer, the maximum depth to which the AMT technique can reliably reach in Hawaii's rocks. A second survey was conducted in 2008 using MT instruments capable of recovering resistivity data to depths of several kilometers below sea level where saturated formations are known to exist. A total of 30 MT soundings was performed along a roughly east to west transect that extended from the (recently acquired) Keamuku PTA lands on the west to as far as the County of Hawaii's upper Kaumana water supply well to the east. Inversion and processing of the field data yielded an electrical cross-section following the Saddle that roughly parallels the geologic contact between the Mauna Kea and Mauna Loa lavas. Several additional electrical sections were constructed normal to the main transect to investigate the three-dimensional nature of the contact. These resistivity data and models suggest that the elevation of saturated rock in places are 1,000 meters above mean sea level beneath the surveyed region. Highest elevations for water-saturated zones based upon preferred electrical models are located between training area 3 and training area 6 southwest of training area 4.

The Big Island Saddle Road MT Study

The Pohakuloa Training Area (PTA), on the Island of Hawaii, encompasses more than 53,000 hectares of land within the Saddle region that lies between Mauna Kea and Mauna Loa Volcanoes. The lands comprising the PTA include a cantonment area, an airfield, a live-fire range, and extensive lands suitable for maneuvers training, as well as wildlife reserve areas that have been designated critical habitat for a number of species. Some portions of the current PTA lands have been used for troop training purposes for more than 50 years. For the majority of that time, demand for water has been met either through harvesting of surface (spring) water from the upper slopes of Mauna Kea, harvesting catchment water from cantonment buildings, or hauling water from lower elevation wells by tanker

truck. The deficiencies of harvesting spring water in terms of reliability and water quality, the economic costs of hauling water, and the impacts on roads and traffic using Saddle Road, have made consideration of a permanent production water supply well imperative.

Prudent development of a water supply well field involves an initial assessment of the prospects of encountering subsurface groundwater, based on an evaluation of already available geologic and geophysical data, followed by more focused studies intended to provide guidance in selection of a test-hole site that maximizes the likelihood of encountering water at a depth and location where a production well can meet projected demands both reliably and cost effectively. The present work was undertaken as the middle phase of this process—the focused study—in order to yield the information required for the selection of an optimum test-hole site.

In the following section we will discuss the preexisting geologic and geophysical data relevant to identifying a groundwater resource within PTA lands, the field surveys that were conducted for this survey, our analysis and interpretation of the field measurements, and implications of the measurement for prospective groundwater resources within the Saddle region.

Geologic Environment

A recent compilation of geologic data for the major Hawaiian Islands (Sherrod and others, 2007) describes the Island of Hawaii as consisting of five volcanoes that formed in a sequential series from the north toward the south. Figure 1 presents a generalized geologic depiction of the island and shows that Kohala Volcano, the oldest on the island, is believed to have completed its main growth phase of activity about 1.5 million years ago; Kohala was followed by Hualālai Volcano, which, although its surface flows are much younger, completed its growth phase about one million years ago. Hualālai was followed by Mauna Kea, which completed its growth about 300,000 to 500,000 years; Mauna Loa, which is still in its main growth stage; and Kilauea, which is estimated to be about half-way through its development.

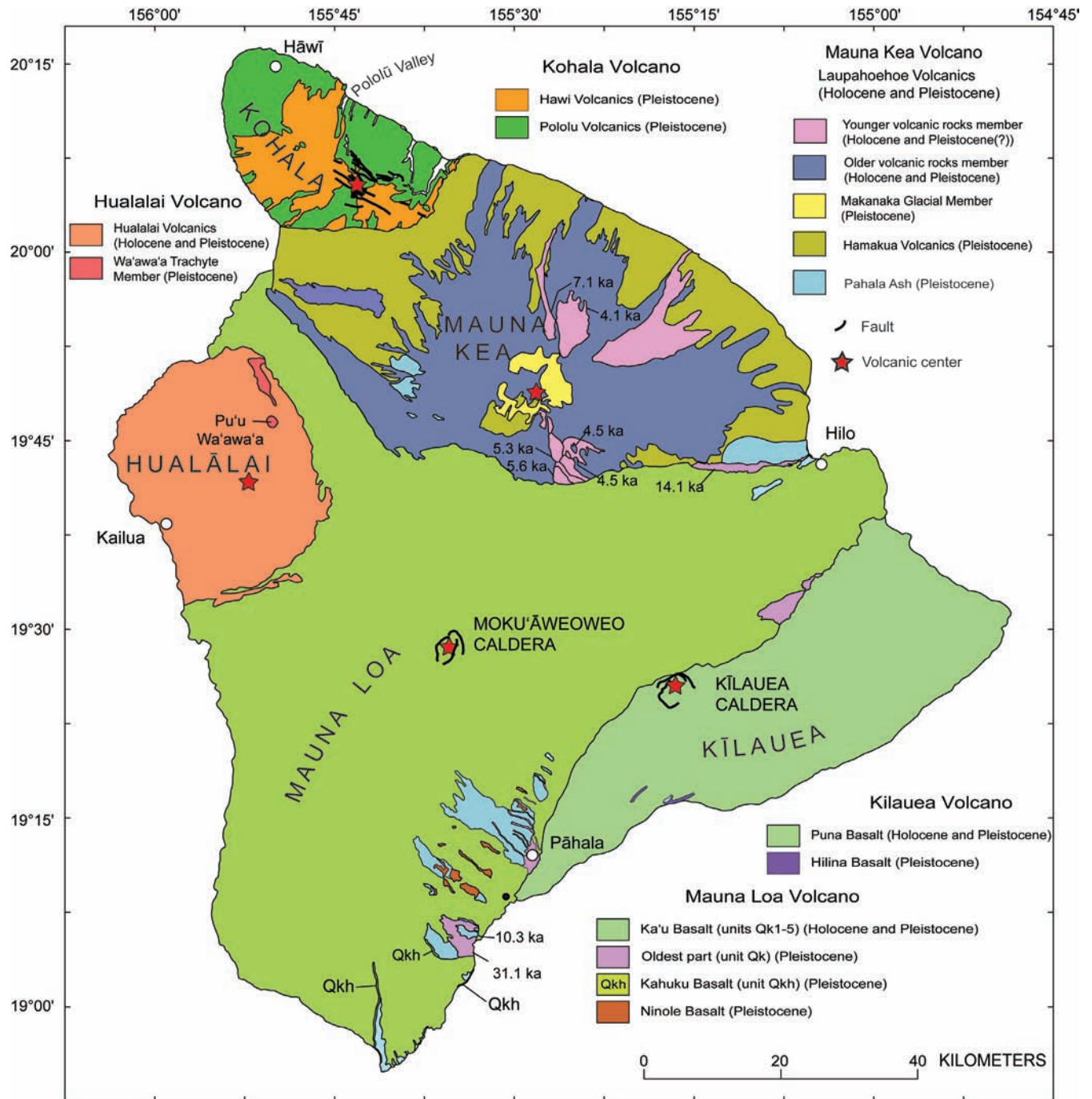


Figure 1. Map showing stratigraphic formations for volcanoes on the Island of Hawaii. Modified from Sherrod and others, 2007. Kiloannum (thousand years), ka.

Because of the sequential progression of volcanic centers on the big island, the younger volcanic systems are typically built on the southern flanks of older volcanoes. Hence, Hualālai and Mauna Kea Volcanoes rest on the southwestern and southern flanks of Kohala Volcano, respectively, whereas Mauna Loa Volcano is built on the southern and southeastern flanks of Mauna Kea and Hualālai

Volcanoes, respectively. Recent research has suggested that Hawaii's volcanoes are active for a span of about 1.5 million years; as a result, there may be interfingering of lava flows of a younger volcano with those of its immediately older predecessor. However, a more typical relation between flows will be that, as activity wanes on the older sister volcano, its flanks will begin to weather and accumulate soil and ash on its ageing surface until the younger sister volcano, during its more voluminous main stage of activity, will send flows up onto the older flank and aggressively extend its surface coverage of the older landscape. Another consideration in the subsurface structure of the volcanoes is that, as the island mass increases during volcano growth, the resultant lithostatic load will cause progressive down-bowing of the Pacific tectonic plate; hence, the growth of the volcano is accompanied by subsidence of the island. A deep research borehole, drilled into the flank of Mauna Kea near Hilo, found subsidence of more than 1 kilometer (km) since the first subaerial flow of Mauna Kea formed the shoreline near the Hilo airport about 400,000 years ago (400 ka). Because subsidence rates are expected to be higher beneath the interior of the island, we can assume that the Mauna Kea flank has subsided by as much as 1.5 km beneath PTA lands. As a result of the succession of volcano growth and subsidence, we can reasonably expect that the northern PTA properties are underlain by subaerial Mauna Kea lavas that are resting atop older subaerial Hualālai lavas that may extend to as deep as 3.5 km beneath the ground surface; below those lavas are likely to lie relatively impermeable submarine rocks made up of mixed volcanic glass fragments (hyaloclastites) and pillow lavas. Toward Hualālai to the southwest, the thickness of the Mauna Kea lavas will decrease while the Hualālai subaerial deposits will thicken. Nearer to Hualālai, the Mauna Kea lavas are covered by a thin carapace of Mauna Loa lavas that are gradually encroaching on both Hualālai and Mauna Kea.

Farther to the east, where Saddle Road crosses recent Mauna Loa lavas, the surface deposits can reasonably be assumed to be a progressively thickening (toward the south) series of Mauna Loa flows overlying the original Mauna Kea flank. Analysis of the slopes within the transition between Mauna Kea and Mauna Loa lavas suggests that there may have been an area of "ponded" lavas where flows generated by Mauna Kea may have interfingered with Mauna Loa lavas in a broad flat plain between the two volcanoes. Unfortunately, we have no exposed analogues of the subsurface stratigraphy of a region bounded by three (probably simultaneously) active volcanic systems; hence a description of the subsurface structure of this region must be considered to be speculative.

Hydrology

A simplified conceptual model of the hydrology for the Island of Hawaii is shown in figure 2 (Anthony, 1997). On the younger volcanic surfaces, the permeability of the basalts is extraordinarily high, and rainfall that strikes the ground will infiltrate rapidly and percolate down to a standing water table or basal lens. With time, the water within the lens gradually migrates toward the shoreline where it is lost to the ocean. On older volcanic surfaces, where soil and ash have accumulated, infiltration rates are lower, and a higher fraction of the rainfall is lost through evapotranspiration (through direct evaporation and plant respiration); when older, less permeable, surfaces are sufficiently steep and rainfall rates exceed the ability of the soils to infiltrate water, surface runoff can further reduce the fraction of rainfall that contributes to recharging of the basal lens.

The accumulation of groundwater within the island is driven by the counterbalancing of hydrostatic head as water accumulates within the lens (or, more accurately, as the elevation of the saturation zone rises above sea level) against the forces that restrain the horizontal flow of water toward the shoreline. With Hawaii's very permeable basalts, the prevailing model anticipates that the elevation of the top of the lens should increase toward the interior of the island at a rate of about 19 centimeters per kilometer (cm/km) [5 feet per mile (ft/mi)] depending on rainfall rates (Stearns and Macdonald,

1946; Hunt, 1996; Anthony, 1997; Bauer, 2003). In instances where buried low-permeability ash zones or nearly vertical cross-cutting volcanic dike systems are present to impede water flow, groundwater will accumulate to substantially higher elevations; water sources formed under these conditions are referred to as “ash bed perched” and “dike-impounded” systems, respectively. These aquifers are typically isolated from the basal lens and have a more restricted aerial extent and lower reserves than basal lens waters.

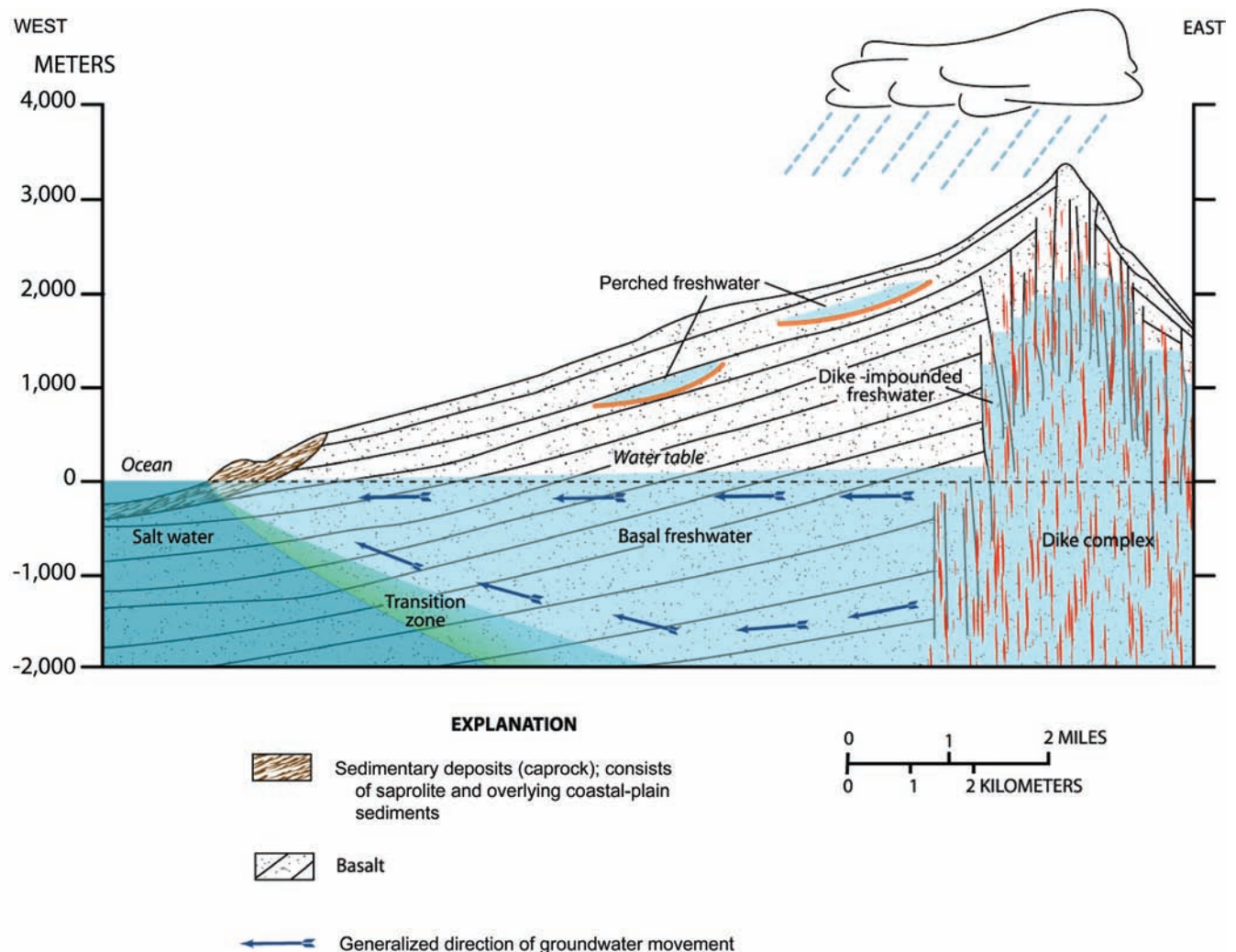


Figure 2. A simplified conceptual model of island geology and hydrology showing major features, such as dike-impounded water, dike complex, perched aquifer, basal freshwater lens, and transition (mixing) zone between freshwater and saltwater.

A secondary effect of the accumulation of water above sea level is the displacement of salt water downward by the increased hydrostatic head and the corresponding hydraulic pressure of the rising lens; because saltwater has a density that is 2.5 percent greater than that of freshwater, the rise of the top of the freshwater lens by 1 meter (m) will displace saltwater downward by 40 m in order to balance the increased hydrostatic head of the freshwater above sea level. Within the context of this static model (Badon-Ghyben, 1888; Herzberg, 1901), the hydrologic conditions below the PTA would usually consist of a relatively thin basal lens. At a 40-km distance from the western shoreline of the island and

50 km from the eastern shoreline, this static model projects the top of the basal lens to be elevated by 7.5 m to 9.5 m above sea level and would be supported by a 300- to 400-m deep freshwater body below. If one considers only the steep rainfall gradients across the Saddle area, ranging from more than 1.52 m to less than .51 m across the crest of the Saddle, the model should also predict that the thickness of the lens would decrease from east to west owing to the substantial changes in recharge to the basal lens.

Owing to the nonstatic conditions within the study area—uneven distribution of rainfall, presence of lava tube conduits, and the highly permeable and highly fractured nature of volcanic rocks—the static Ghyben-Herzberg model does not appear to work everywhere. For example, groundwater wells drilled within a few kilometers of the shoreline have generally substantiated the Ghyben-Herzberg model and have shown elevations at the top of the freshwater lens to be a few meters above sea level. However, as demand for drinking water has increased on the island, wells have been drilled further inland (fig. 3) that have encountered water tables elevated well above those predicted by current models.

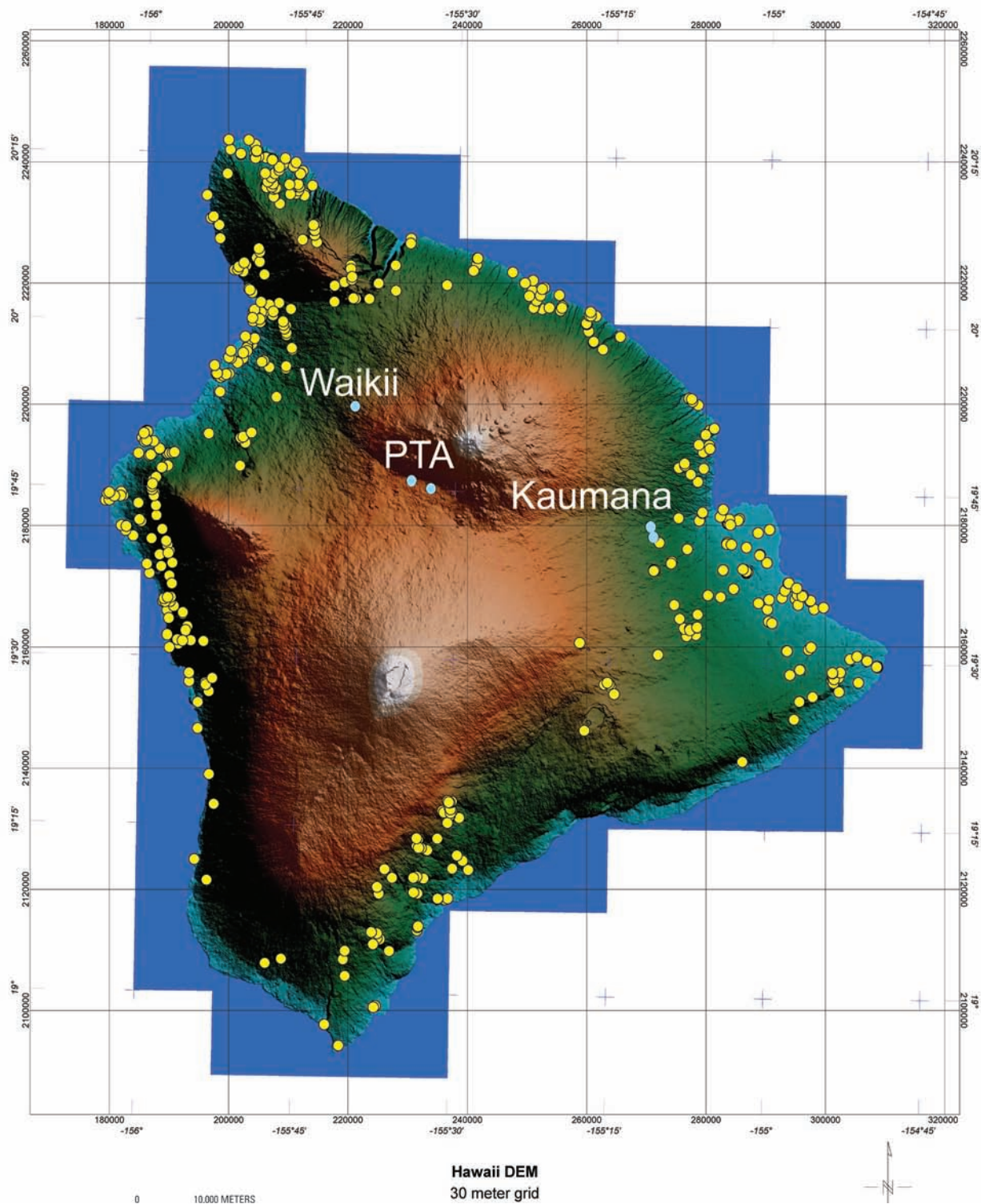


Figure 3. Shaded relief map of the digital elevation model (DEM) for the county of Hawaii showing well locations (Imata, 2004) plotted in yellow. Most of these wells are located near the coastline. The wells labeled Waikii, PTA, and Kaumana are colored blue and are discussed in the text.

Of particular relevance to the present work are two wells drilled approximately 14 km west of the PTA near Waiki'i Ranch, two wells located about 42 km east of the PTA near Kaumana, and a deep research well drilled near the Hilo shoreline. The two Waiki'i Ranch wells are located about 26 km from the western shoreline of the island and are at elevations of 1,298.3 m above mean sea level (amsl) and 1,304.4 m amsl for Waiki'i #1 (drilled in 1983) and Waiki'i #2 (drilled in 1989), respectively. Waiki'i #1 encountered a water table at 459.9 m depth (838 m amsl) and Waiki'i #2 well reached the water table at a depth of 390.1 m (914.3 m amsl). The elevation of the water table found in both wells exceeds that predicted for the basal water table by 800 to 900 m within the island and could be interpreted to suggest much higher water tables will be found further inland. However, these wells are located within an area that is believed to be underlain by Mauna Kea's western rift system; hence, the groundwater in this area could be associated with dike-confined aquifers in the now-buried rift. These wells were rotary drilled and at a time when drilling mud was used. During drilling, the use of drilling mud in wells drilled above the water table usually resulted in the hole being drilled with complete loss of fluid circulation into the formation. Many old wells were drilled without having even cuttings recovered from the hole. As a result, few cuttings were recovered that would allow us to determine whether dike rocks were encountered. The Waiki'i #1 well is a production well [162 gallons per minute (gpm)] and has reliably supplied potable water to a small residential subdivision on the former Waiki'i Ranch lands since its installation in 1983.

The two Kaumana wells include the U.S. Geological Survey (USGS) Kaumana Observation Well, drilled in 1995, and the nearby Saddle Road A production well (2,100 gpm), drilled in 1998; both wells are located about 12 km from the eastern shoreline of the island. The USGS well was drilled from an elevation of 547.4 m amsl and encountered the water table at an elevation of 243.8 m amsl; the Saddle Road A well was drilled from an elevation of 582.1 m amsl and encountered the water table at 292.6 m amsl. Again, these wells show groundwater present at elevations that are more than 200 m higher than would be predicted for the basal lens. Our current geologic interpretation of Mauna Kea's structure in the immediate vicinity of these wells predicts neither a significant rift system nor the likelihood of a fault system that could reasonably be expected to impound groundwater to these elevations. Water level monitoring in the Kaumana Observation Well shows a significant but not overwhelming sensitivity to changes in seasonal recharge with variations of about 10 m between periods of high rainfall and lower rainfall recharge.

Finally, the Hawaii Scientific Drilling Project well that was drilled near the eastern shoreline of the island (Stolper and others, 2009) also provides data relevant to the elevation of the groundwater table within the interior of Mauna Kea. This borehole was continuously cored to a depth of about 3,500 m below sea level. The well's location near the shoreline anticipated that it would encounter a thin basal lens at sea level and that deeper aquifers would be uniformly saturated with sea water. Instead, the bore encountered multiple layers of both freshwater and saline water that were associated with specific horizons in the stratigraphic section: the basal lens was evident in the first few meters of drilling and was underlain by sea water; a second, artesian freshwater system was encountered at approximately 300 m below sea level and was associated with soil and ash horizons that marked the transition from Mauna Loa to Mauna Kea lavas; additional strongly artesian freshwater systems were subsequently encountered below depths of 2,000 m, to as deep as 3,100 m, within permeable pillow lavas that were confined by compacted and indurated hyaloclastite intervals. The significance of these findings to the present effort is that they demonstrate that hydrostatic pressures and the elevation of the freshwater lens within Mauna Kea's freshwater system are substantially higher than would have been expected from our current model of Hawaii's hydrology. Further, they provide independent data that the elevated water tables present in the Kaumana wells are the result of much higher elevations of the basal lens within Mauna Kea.

For the sake of completeness, we should also note the results of two shallower bores drilled within PTA-controlled properties in the 1960s. These holes were drilled to investigate water resources within the boundaries of PTA lands; the first, Pohakuloa Test Hole (TH) #1, was drilled in 1965 from an elevation of 1,943 m to an elevation of 1,939.5 m amsl [1,001 feet (ft) deep]. The second, Pohakuloa TH #2, was drilled from an elevation of 1,828.7 m to an elevation of 1,722 m amsl (350 ft deep). Neither test hole was deep enough to encounter the saturated zone.

In summary, the traditional models of the groundwater hydrology for Hawaii would anticipate that relatively small quantities of groundwater are stored within the island's volcanoes and that the elevation of the water table beneath PTA properties and the Saddle region would be no more than about 10 m above sea level. In recent years, research and groundwater wells have demonstrated that the island hydrology is much more complex and that much larger quantities of water are stored within Mauna Kea and possibly other volcanoes on the Island of Hawaii. Groundwater monitoring and production wells that have been drilled closest to the PTA properties suggest that freshwaters may be elevated by as much as 800 m above sea level within Mauna Kea but are at least 300 m below ground surface.

Electromagnetic Natural Source Approach and Methods

Electromagnetic (EM) soundings are conducted to determine variations in the electrical resistivity of the Earth with depth (Cagniard, 1950, 1953; Tikhonov, 1950; Wait, 1962; Keller and Frischknecht, 1966; Dmitriev and Berdichevsky, 1979; Vozoff, 1986; 1991; Spies and Frischknecht, 1991; Simpson and Bahr, 2005). This study employed two EM techniques that use natural-source, broadband, multifrequency EM signals from geomagnetic variations (MT) and atmospheric electrical discharges (AMT) as an energy source. Variations in the frequency and amplitude of the natural signals induce currents in the Earth's subsurface; the electrical and magnetic response, when measured on the surface, is dependent on the formation conductivity and magnetic permeability. The EM signals are measured, recorded, filtered, and processed in a way that enables us to determine the ground resistivity and phases over a range of depths (Swift, 1962; Simpson and Bahr, 2005). The techniques applied in our cross-island surveys were the audiomagnetotelluric (AMT) method (data recorded in 2004), which records and processes frequencies that range from about 10 to about 100,000 hertz (Hz), and the magnetotelluric (MT) method (data recorded in 2008), which records and processes signals in the frequency range of 0.0007 to 357 Hz. The AMT method offers a more detailed image of the subsurface resistivity beneath a receiver station and can collect an adequate dataset for an individual station in a few hours, but its depth of penetration is limited to about 1 km. The MT method provides a much greater depth of penetration, up to several tens of kilometers, but its use of a lower frequency range requires a much longer data collection period at individual stations.

In application, both techniques make a series of orthogonal electrical and magnetic measurements in either a linear array or a surface grid; the amplitude and frequency data are recorded and processed and ultimately inverted to construct a one-dimensional (1D) sounding of resistivity against depth, and then the individual soundings are stitched together to form profiles (for a linear array) or map image if processed as a grid. The resulting images reflect the resistivity structure of the geologic formations within the sensing range of the network of stations used in the field program.

The relevance of the subsurface resistivity structure to the present work is based on the influence of water on the electrical conductivity of geologic materials. Rocks, in the present case basalts that are entirely dry, will be highly resistive to the conduction of electricity. They will have inferred resistivities in excess of 10,000 ohm-meters (Ωm). The introduction of (fresh) water will progressively reduce these resistivities, and when saturated, Hawaii basalts will have resistivities ranging from as low as several tens of ohm-meters to about 600 Ωm . The presence of dissolved ions (salt) in the water will further

reduce resistivity, and saltwater-saturated basalts generally have resistivities in the range of about 3 Ωm to a few tens of ohm-meters. Hence, the resistivity image produced by the AMT and MT techniques can enable us to infer the depth to saturation in the ground (the water table). Thus, in an island environment, we may infer the depth to the saltwater transition below the freshwater lens and, in some cases, the thickness of the freshwater-bearing aquifers.

However, there are important caveats to the above idealized application of these techniques because the resistivities of the subsurface formations are dependent on a range of other factors that make an unequivocal interpretation of subsurface conditions a challenge:

1. The morphology of the subsurface formations strongly affects their resistivity; ash beds are much less resistive than stratigraphic units made up of pahoehoe and a'a lavas. Similarly, the higher porosity of pahoehoe lavas has lower resistivities than a'a lavas of similar thickness.
2. The degree of weathering or alteration of the rocks also affects resistivity since water-saturated clays and zeolites will have substantially lower resistivities than saturated pristine basalts.
3. Formation temperatures have a strong influence on the conductivity of saturated rocks; heated geothermal fluids (that typically also have elevated ion or salt contents) passing through subsurface formations will show significantly lower resistivities than rocks saturated with ambient temperature waters.
4. The impedance estimates from MT and AMT soundings are often affected by near-surface galvanic and induction conductivity structures. These structures give rise to dimensionality problems and can be a source of distortion (Berdichevsky and Dmitriev, 1976.; Groom, 1988; Groom and Bailey, 1989a, 1989b, 1991; Chakridi, and others, 1992; Groom and others, 1993; McNeice and Jones, 2001; Jones and Garcia, 2003; Martí and others, 2005).
5. It is important that users of EM sounding data understand that the 1D and two-dimensional (2D) models are not unique. In a "layered-Earth" model that is generated by inversion of the data sets, the thickness and conductivity of the individual units are interrelated derived parameters where it is difficult to assign unique values to both parameters. For instance, a unit of 100-m thickness and 300- Ωm resistivity is not easily distinguishable from a 150-m thick unit of 200- Ωm resistivity. Carefully locating MT and AMT stations to reduce noise, performing static shifts to remove galvanic effects, editing to remove poorly resolved impedances and phases, and D+ smoothing of the curves prior to inversion are completed to ensure that the values represent the subsurface resistivity variations as accurately as possible. Likewise, the processing procedures during inversion are designed to test a multitude of layers and resistivities in a way that provides a "best fit" to the field data.

Hence, interpretation of the resistivity profiles must rely on what is geologically and hydrologically reasonable within a surveyed terrain.

Field Surveys

Field survey stations along Saddle Road west and east of the PTA were restricted to a narrow band coincident with the surface contact between the Mauna Kea and Mauna Loa lavas. The 2008 MT survey employed four Phoenix MTU-5A MT receivers, with one dedicated as a remote reference in the Aalii Makai pasture of Parker Ranch. The 2004 AMT survey used a single Geometrics EH-4 AMT receiver. Sites were chosen so that stations were as far away as possible from power lines, roads, and other anthropogenic noise sources. Background electric and magnetic field strengths were monitored prior to recording, and stations were relocated if interfering signals were too high. The MT soundings at

each station consist of measurement of orthogonal electric and magnetic fields collected over a range of frequencies from 0.0008 to 357 Hz with multiple receivers. Data collection was automatically conducted overnight, between the hours of 22:00 and 06:00 local time, in order to acquire a full complement of the lowest frequencies during the (electrically) quietest time of the day. A fixed remote reference station collected magnetic field data over the entire survey campaign, which were later used during robust processing to remove anthropogenic and other extraneous noise collected at the individual sounding sites.

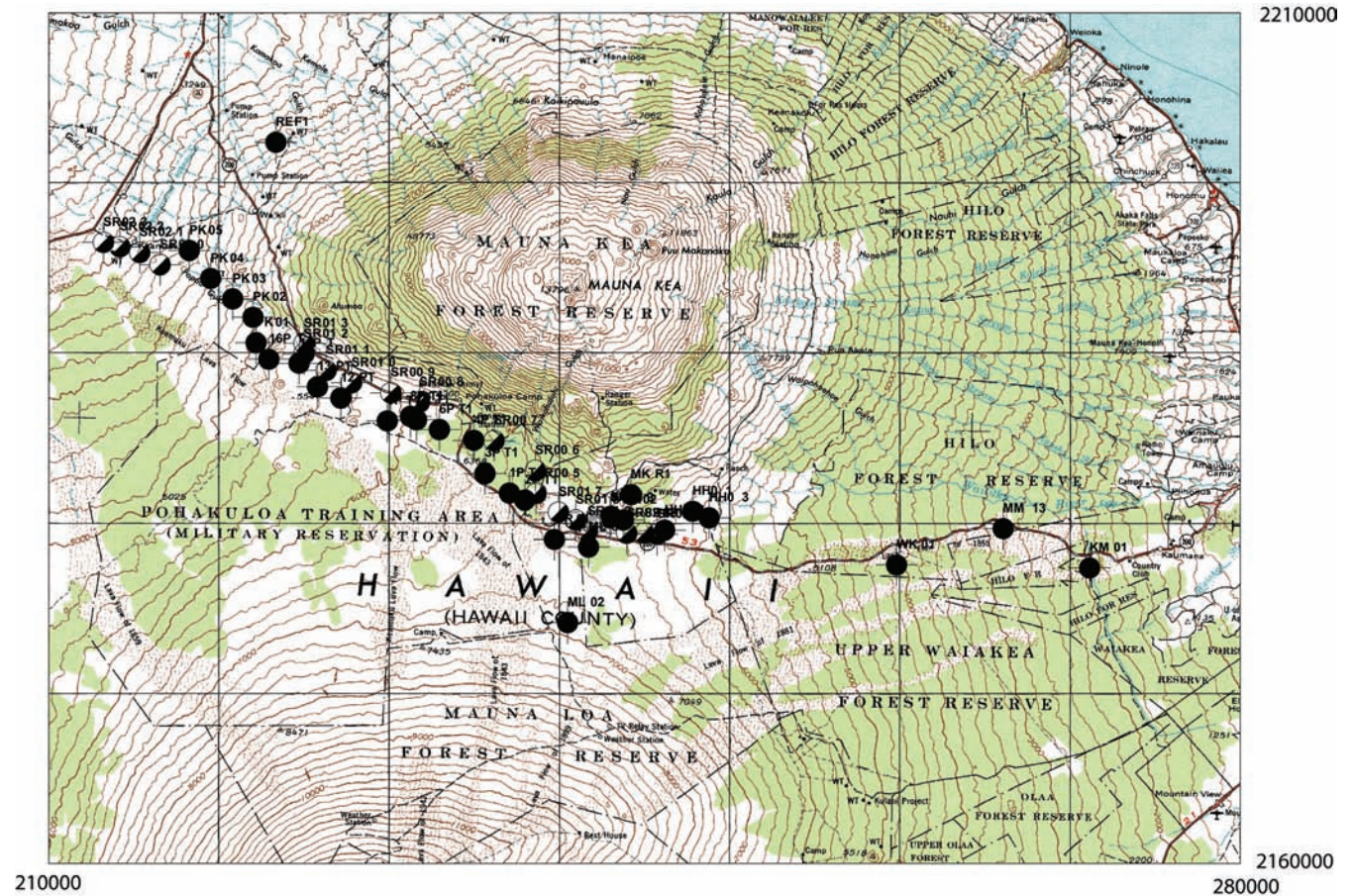


Figure 4. Map of the magnetotelluric (MT) and audiomagnetotelluric (AMT) station locations. Solid circles are the MT locations where data were collected in 2008. Half-white/half-black circles are the AMT station locations where data were collected in 2004. Universal Transverse Mercator (UTM) grid is 10 kilometers on a side, taken from the Hawaii 1:100,000-scale topographic map of Hawaii Transverse Mercator projection [base latitude (BL) = 0° , central meridian (CM) = -153°].

During the MT survey campaign, we made several short, “cross-profile” transects in addition to the long east-west series across the Saddle. These shorter surveys were designed to provide us with a sense of the three dimensionality of the along-Saddle profile.

Resistivity Soundings

Within the collected field data, the impedance (Z) is obtained from measurements of the electric and magnetic fields. The MT and AMT methods used in this survey measure orthogonal magnetic (H_x ,

H_y , and H_z) and electric fields (E_x and E_y) so that the impedance can be described as a complex tensor to account for anisotropy.

The AMT soundings do not have a vertical magnetic coil (H_z) or the associated tipper that is calculated from the vertical field.

The MT impedance tensor (Z) contains four complex components that relate the measured electric (E) and magnetic (H) fields:

$$\begin{bmatrix} E_x \\ E_y \end{bmatrix} = \begin{bmatrix} Z_{xx} & Z_{xy} \\ Z_{yx} & Z_{yy} \end{bmatrix} \times \begin{bmatrix} H_x \\ H_y \end{bmatrix} \quad (1)$$

The impedances are computed from the records using a remote reference, robust processing scheme that applies coherency processing with a cutoff of 0.85 and a secondary Rho variance scheme with a 0.75 cutoff. All the MT soundings collected use remote H_x and H_y fields from the station REF1 (fig. 4) as reference. All the AMT soundings use a local magnetic reference (Gamble and others, 1979a, b).

Once the phase and resistivities are estimated from the impedances, the electrical dimensionality is investigated, and an inversion approach chosen. Skews (Swift, 1962) and direct current (DC) resistivity soundings (Zohdy and Jackson, 1969) from the PTA Saddle Road area were used to ascertain dimensionality.

The electrical section models are generated from the edited and smoothed curves using Occam's inversion (deGroot-Hedlin and Constable, 1990) with a uniform half-space of 100 Ωm as a starting model for the inversions. Once a series of models is generated, resistivity cross-sections and associated maps are made. The electrical sections and maps at slices of various elevations are compared with the known geology, borehole data, and hydrologic information, if available.

If the geologic structures can be assumed to be 2D, then the tensor Z can be rotated to the angle corresponding to the strike of the geology to get a rotated tensor Z' . For Z' , Z'_{xy} and Z'_{yx} are maximized and Z'_{xx} and Z'_{yy} are minimized. The angle θ_0 that maximizes $Z'_{xy}^2 + Z'_{yx}^2$ is the principal direction of Z . The principal direction of Z and the Z -strike is evaluated for each frequency. They are often the same, though they need not be. The way the Z -strike is calculated results in two possible geologic strike directions. It is important that the geologic setting be understood prior to using these values.

Discussion

MT and AMT profiles and maps of inverted resistivity data show anomalous areas of high and low resistivities along the geologic contact between Mauna Loa, Hualālai, and Mauna Kea volcanic rocks (fig. 6). East of the PTA, rocks associated with a series of cinder cones near the Mauna Kea access road indicate the geology is electrically resistive. Another small area of high resistivity associated with Puu KeeKee on the west side of the PTA indicates the surficial geology is resistive and may be associated with a southwestern rift from Mauna Kea. From these electrical sections, estimates of depth to water can be made on the basis of the resistivities and gradients (figs. 6–9). This estimated piezometric surface roughly follows the topography and ranges from 500 to 1,200 m below the surface of the Humu'ula Saddle Road. From the electrical section models, we estimate that the shallowest water on PTA property is between training areas 6 and 3, southwest of training area 4. Real induction arrows (MT station 4PT1, Appendix D) suggest that the resistivity low is to the southwest of the MT site in training area 4.

Results

[illegible]

13

Plots of the 1D inversions can be found in Appendix C, and polar diagrams for selected frequencies are in Appendix D. Figure 5 maps the locations of electrical sections (red dashed line) and are used to investigate the electrical structure parallel and normal to the Humu'ula Saddle Road. The locations of the electrical sections are tied to the digital elevation model (DEM) plotted in fig. 3 so that elevations can be extracted along the profiles to correct the MT and AMT data for topography. Figure 6 is a plot of our longest electrical section made from a combination of MT and AMT soundings along Saddle Road and presents a 2D image of 1D inversions spanning the Saddle from Mamalahoa Highway on the west (left) to the upper Kaumana water supply well to the east (right) with the depth of the model extending down to sea level. The color distribution presents higher resistivities in the warmer spectrum, and low resistivities are presented as colder colors (note resistivity scale to right of plot).

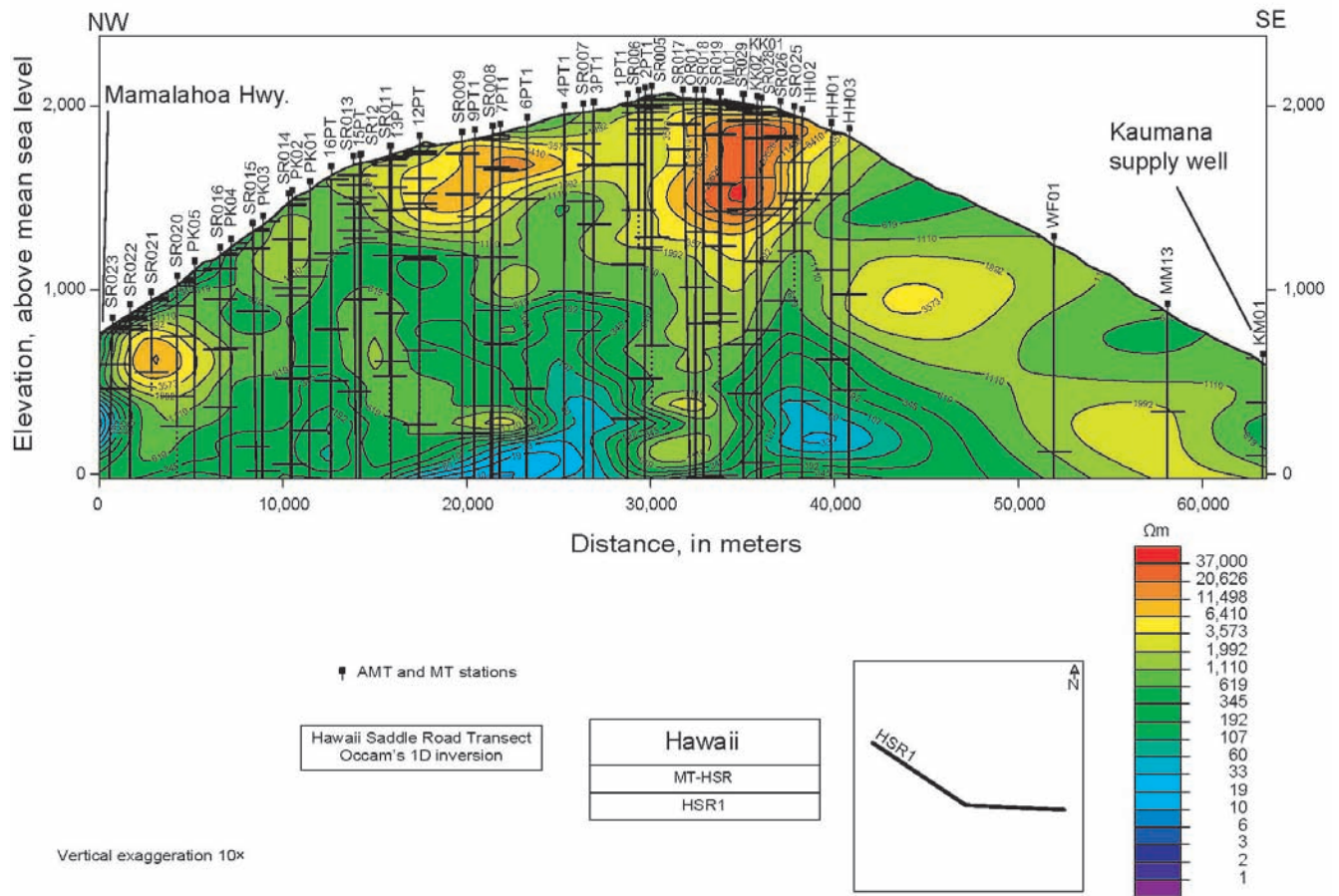


Figure 6. Profile of the Saddle from Mamalahoa Highway to Kaumana showing resistivities encountered along Saddle Road in the relatively dry volcanic terrain. Plot is looking north with west to the left and east to the right. Warm colors are resistive, and cool colors are conductive. Distances and elevations are in meters. Note the blue conductive zones near the center of the plot below at elevation of approximately 500 meters; these cool-colored conductive zones are potential drilling targets. Ohm-meter, Ωm .

The resistivity structure of the Saddle region spans a broad range of resistivities and reveals complex geologic and hydrologic features. To the extreme right, the sounding near the Kaumana well (fig. 6) gives us an important baseline in that the known depth to the water table at that location is

approximately 300 m amsl. There is no known evidence of a buried rift zone in that area; hence, we can establish that Mauna Kea basalts saturated with freshwater have a resistivity of $\sim 600 \Omega\text{m}$. Although this is at the upper range for freshwater saturated basalts, it is not unreasonable given both the low salt content of the rainfall recharge typical of inland regions on the island and the relative youth and absence of weathering of Mauna Kea's lavas.

Moving westward along the profile, a band of increased resistivity is encountered near sea level that increases in elevation roughly in parallel with the surface slope and is capped by a highly resistive formation near the crest of the saddle. Gravity surveys conducted on Mauna Kea (Kauahikaua and others, 2000) have suggested that a buried rift zone may extend toward the south-southeast from Mauna Kea's summit; the presence of buried intrusive lavas, which have higher resistivities than eruptive basalts, may be responsible for the increased band of resistivity as our transect crossed a dike system. The extremely high, shallow resistivities beneath the crest of the Saddle are not unexpected: rainfall rates decline rapidly as the summit is approached, and at the time of the surveys, an extended drought had deprived the Saddle region of significant rainfall for more than a year. The geology within that area may play a significant role as well, since this area is marked by a number of cinder cones that are probably accompanied by buried intrusives.

Below and slightly east of the shallow resistive formations in figure 6, at approximately the 40,000-m marker on the horizontal axis, is an area of intermediate to low resistivities. If we accept the $619 \Omega\text{m}$ contour as our saturation zone, then the local water table may extend to an elevation of about 1,000 m amsl. Certainly, this is a much higher elevation for the basal groundwater than conventional models would predict; however, the presence of (an inferred) rift system that would impede groundwater movement toward the east may account for a substantially higher water table than expected.

The much lower resistivities observed near sea level in this area are difficult to interpret unequivocally; the resistivities are well below the values found higher in the section but are at the far upper range for expected resistivities of sea-water-saturated basalt. The presence of saltwater near sea level beneath an extraordinarily thick freshwater aquifer is unlikely based on hydrological principals; barring the presence of a perching formation, a freshwater aquifer at a substantial elevation above sea level would normally be underlain by an even thicker layer of freshwater below sea level. Two other alternatives seem more likely to account for the lower resistivities found in this area:

1. If the nearly vertical, more resistive formations located west of the low resistivity zone are because of feeder dikes for the multiple cinder cones located on and near the crest of the Saddle, then the low resistivities near sea level can reasonably be attributed to hydrothermal alteration of the older eruptive basalts into which the system of dikes was intruded. Hydrothermal alteration normally produces more clays within the rock and consequently lowers the resistivity of the altered formations.
2. Alternatively, elevated water temperatures are known to reduce the resistivity of freshwater as well as saltwater, and it is possible that the low resistivities flanking the (inferred) dike system are associated with hydrothermally heated groundwater. Whether the source of the heat is the dike system or whether the dike system is simply channeling thermal water from the interior of Mauna Kea cannot be determined with the data we currently have available. With respect to the availability of groundwater at accessible depths, the moderate to low resistivity feature located below stations SR025 and SR026 suggests that water could be accessed at a depth of about 1,000 m amsl below this portion of the Saddle (table A-1).

Progressing further to the west, the resistive shallow zone continues beyond station 12PT1, but following the $619 \Omega\text{m}$ contour, there appears to be a broad feature that is consistent with a large zone of

saturation, again, at an elevation of about 1,000 m amsl. This area is also underlain by a lower-than-expected resistivity near sea level and can be attributed to the same conditions as cited for areas below stations SR025 and SR026. In terms of assessing the likelihood of encountering usable quantities of water, a target somewhat east of station 6 PT1 would appear to be the most favorable location for further exploratory work.

Continuing westward, the 619- Ω m contour begins to drop rapidly west of station 16 PT1. The area in which this occurs is near Hualālai Volcano, and it is likely that the geology in this region will be a complex interface between Mauna Kea lavas and underlying Hualālai subaerial flows as well as buried features that may include cinder cones similar to those on the Mauna Kea surface. Nonetheless, the rapidly dropping elevation of the apparent water table is not unexpected since this area receives sporadic low rainfall, and wells drilled west of the end of our transect, at lower elevations on the Hualālai flank, have not encountered groundwater levels that are substantially above sea level (for example, Well no. 8–4953 has a water table elevation of about 1 m amsl). (We note here that the profile presented does not include the Waikii wells as the profile passes more than 9 km to the south of the Waikii wells.)

To provide a better understanding of the three-dimensional nature of the survey area, a series of short (1.5–8 km long) resistivity surveys was conducted perpendicular to Saddle Road; the results are presented in figures 7 through 11. The longest of these, HSB2, was constructed from MT and AMT stations collected near the Mauna Kea and Mauna Loa observatory access roads. They show some of the electrical structures oriented north-south across the Saddle Road both near PTA lands as well as toward the east near the observatory roads. They show a low resistivity zone associated with Mauna Kea that may be water or with perhaps clay (ash) plus water.

Cross-Profile Transect PTA4

Transect PTA4 (fig. 7) extends in a northeast-to-southwest direction and crosses the main Saddle profile about 10 km east of the Saddle crest. The surface geology across the transect makes a transition from Mauna Kea lava and ash or soils on to the young Mauna Loa pahoehoe and a’ā lava flows at station SR025. Overall, the profile shows a resistivity gradient that is decreasing in elevation to the southwest: this would not be inconsistent with a progressively deepening Mauna Kea surface below the encroaching Mauna Loa lava flows. The low resistivity formations near sea level may again be the result of prior thermal alteration of now-buried formations or currently active thermal water issuing from the core of Mauna Kea along the inferred rift system that extends through this area.

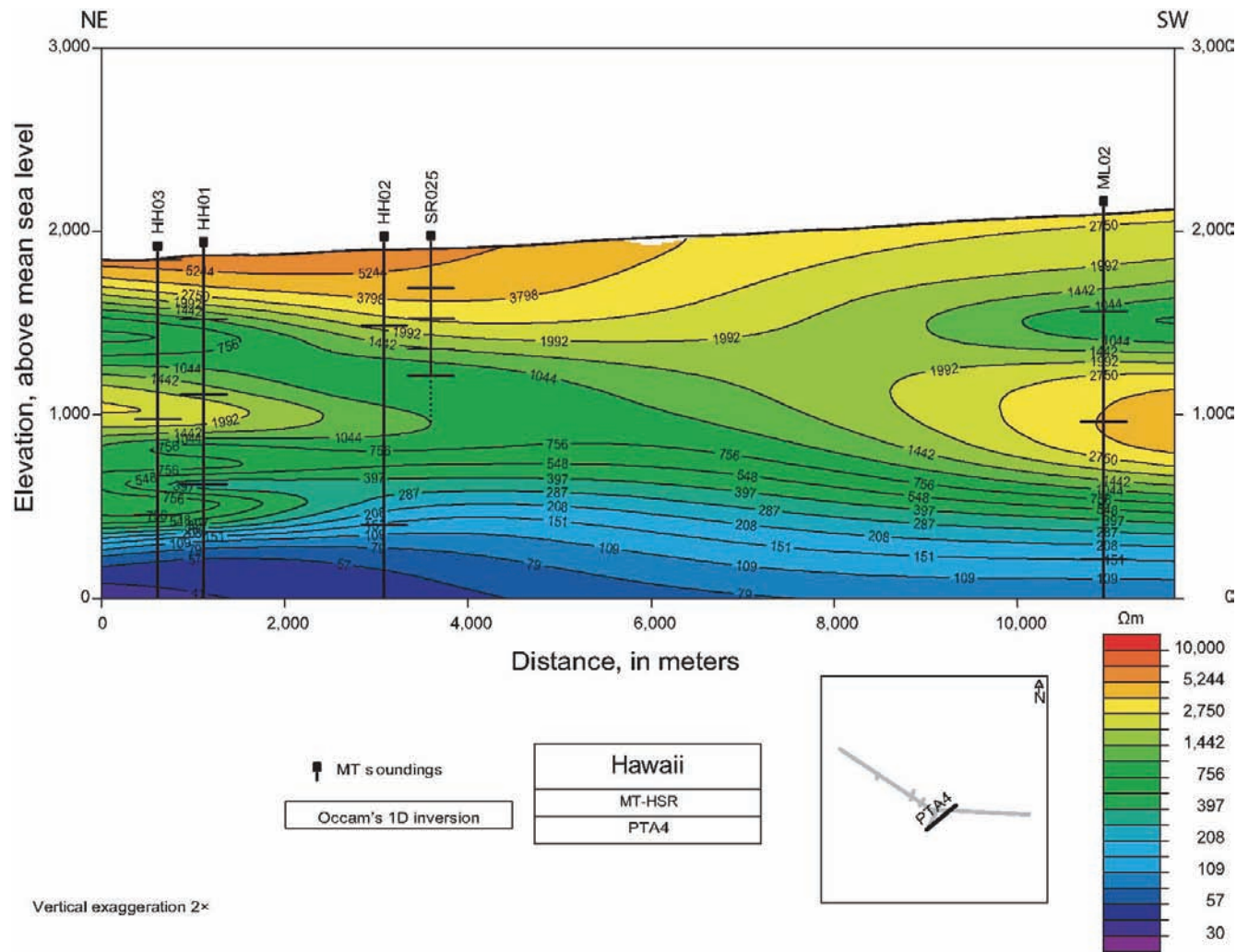


Figure 7. Cross-profile resistivity plot of transect PTA4, which trends northeast to southwest, left to right, looking to the southeast. Note the flat-lying low resistivity zone near the bottom of the plot. This horizontal low resistivity zone likely represents the water table.

Cross-Profile Transect HSR2

Transect HSR2 (fig. 8) would seem to substantiate the latter interpretation. Although the two surveys are located in close proximity to each other, the PTA4 survey is oriented along a transect that would be roughly parallel to the topographic elevation of Mauna Kea's slope, whereas HSR2 is more nearly perpendicular to the slope. Hence, the low resistivity feature near sea level is seen to thin rapidly from the northeast as the transition is made from Mauna Kea along the observatory access road and toward Mauna Loa where the latter's younger lava flows are encroaching onto the older Mauna Kea surface. We also note the moderately resistive feature between ML01 and ML02 at an elevation of approximately 1,500 m. This may well correspond to a perched aquifer that has accumulated atop one or more ash beds that mark the top of the older Mauna Kea surface and that is now buried by Mauna Loa lavas.

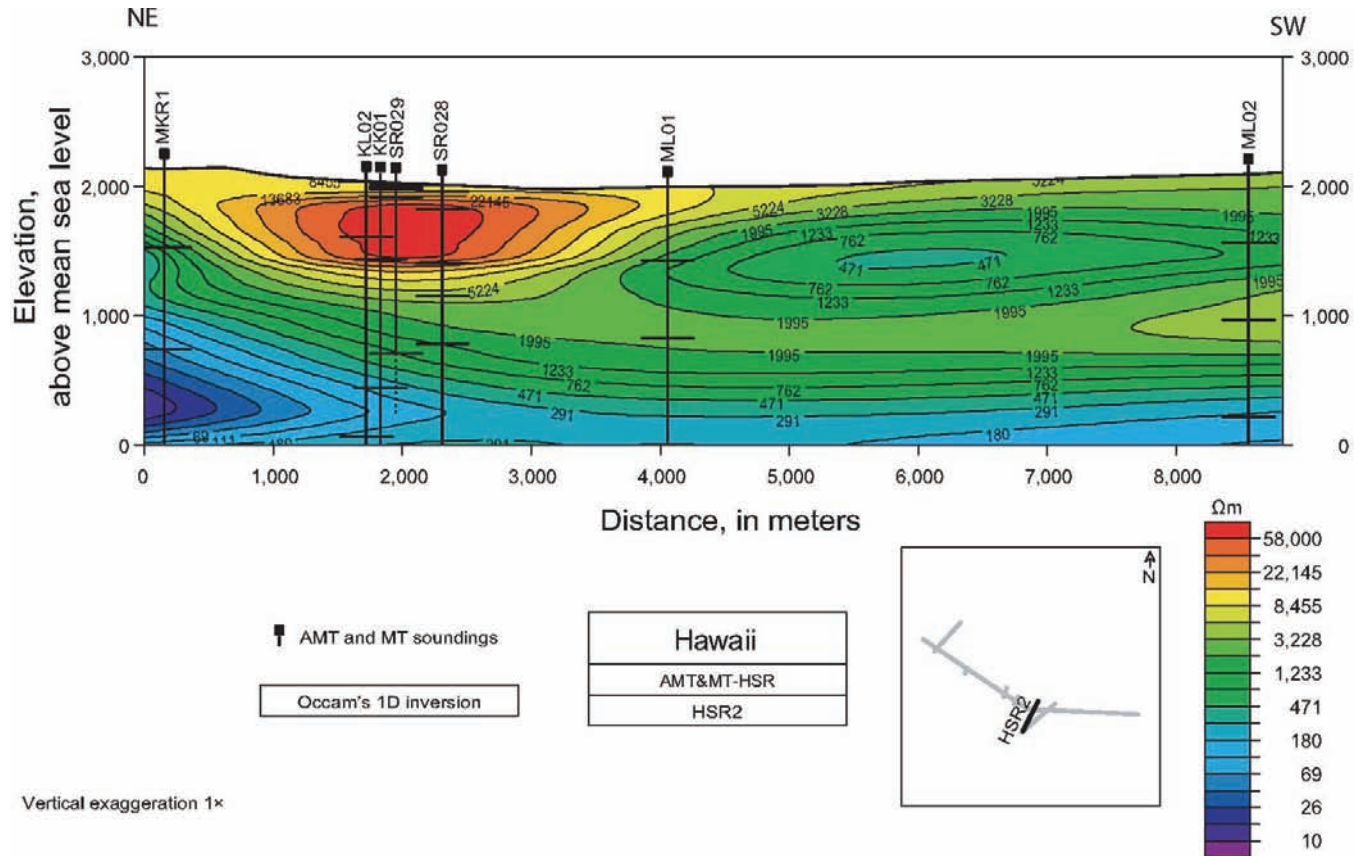


Figure 8. Cross-profile resistivity plot of several stations near the access roads (line HSR2) to the Mauna Kea and Mauna Loa observatories. Note the low resistivity wedge-shaped zone beneath MT station MKR1. This resistivity low may be a drilling target, but it is more than 15 kilometers east of the PTA property.

Cross Profiles PTA1, PTA2, and PTA3

Cross profiles PTA2 and PTA1 were conducted at distances of approximately 1 and 2 km west of the HSR2 profile respectively. Both profiles show an intermediate to high resistivity on their northeastern stations but significantly lower resistivity to the southwest. PTA2 shows the low-resistivity formations to quite high elevations (more 1,800 m amsl), whereas PTA1 shows a broader resistivity low to elevations slightly higher than 1,000 m amsl. Interpretation of these profiles is problematic. Such low resistivities at a single station on a transect, as seen in PTA2 (fig. 9), introduce some doubt that the modeled values reflect a significant feature. The conversion of the field data into the 2D profiles can cause “edge effects” that are difficult to control during the processing; hence, the southwestern end of the PTA2 modeled profile needs to be considered with some skepticism. The PTA1 modeled profile (fig. 10) shows a substantially broader low-resistivity interval at a somewhat greater depth that is sensed by two of the three stations and provides some degree of validation to the PTA2 low-resistivity zone.

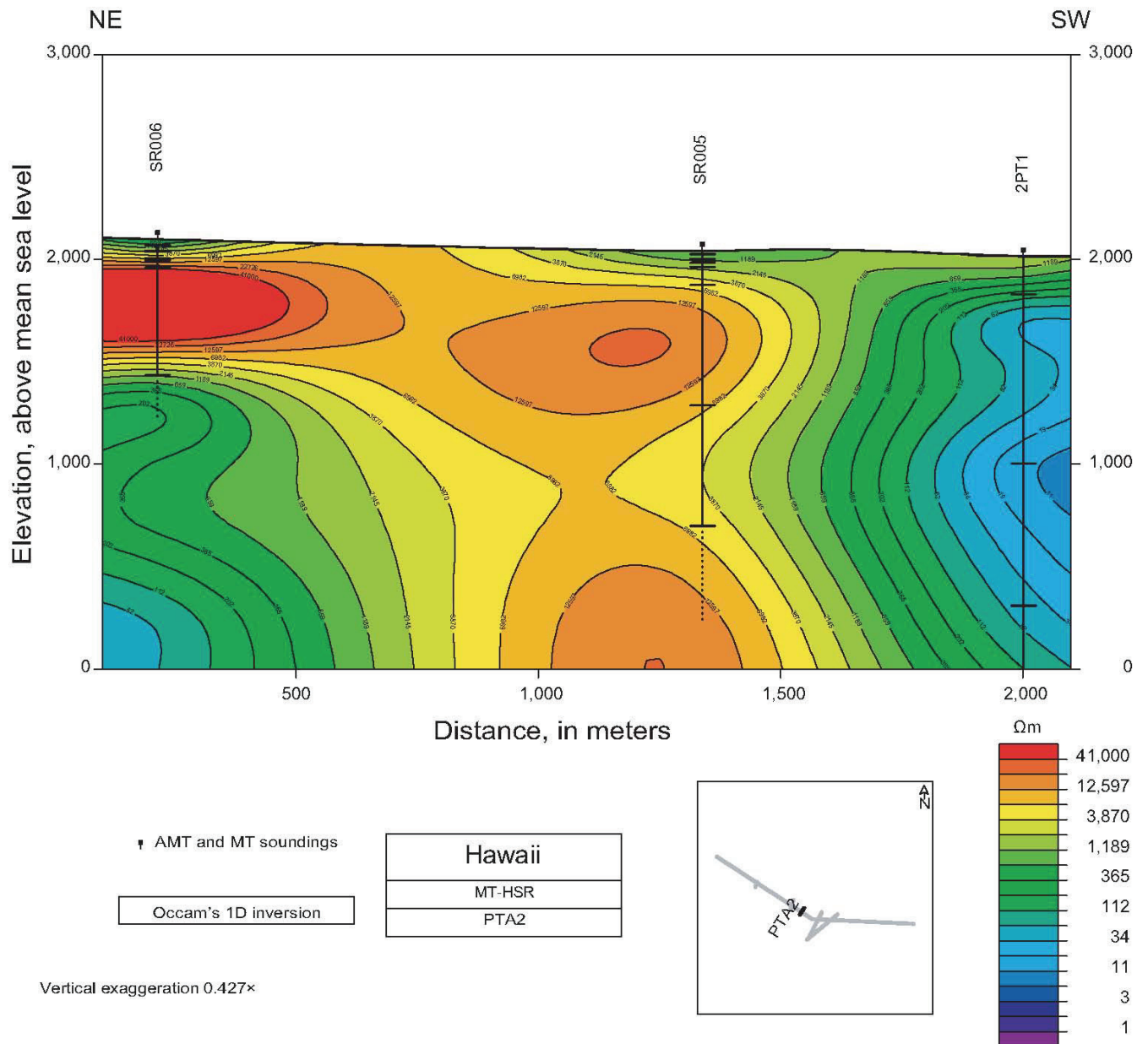


Figure 9. Cross-profile resistivity plot of line PTA2, which trends northeast to southwest. The resistivity low on the southwestern end of the line is defined by only one sounding station.

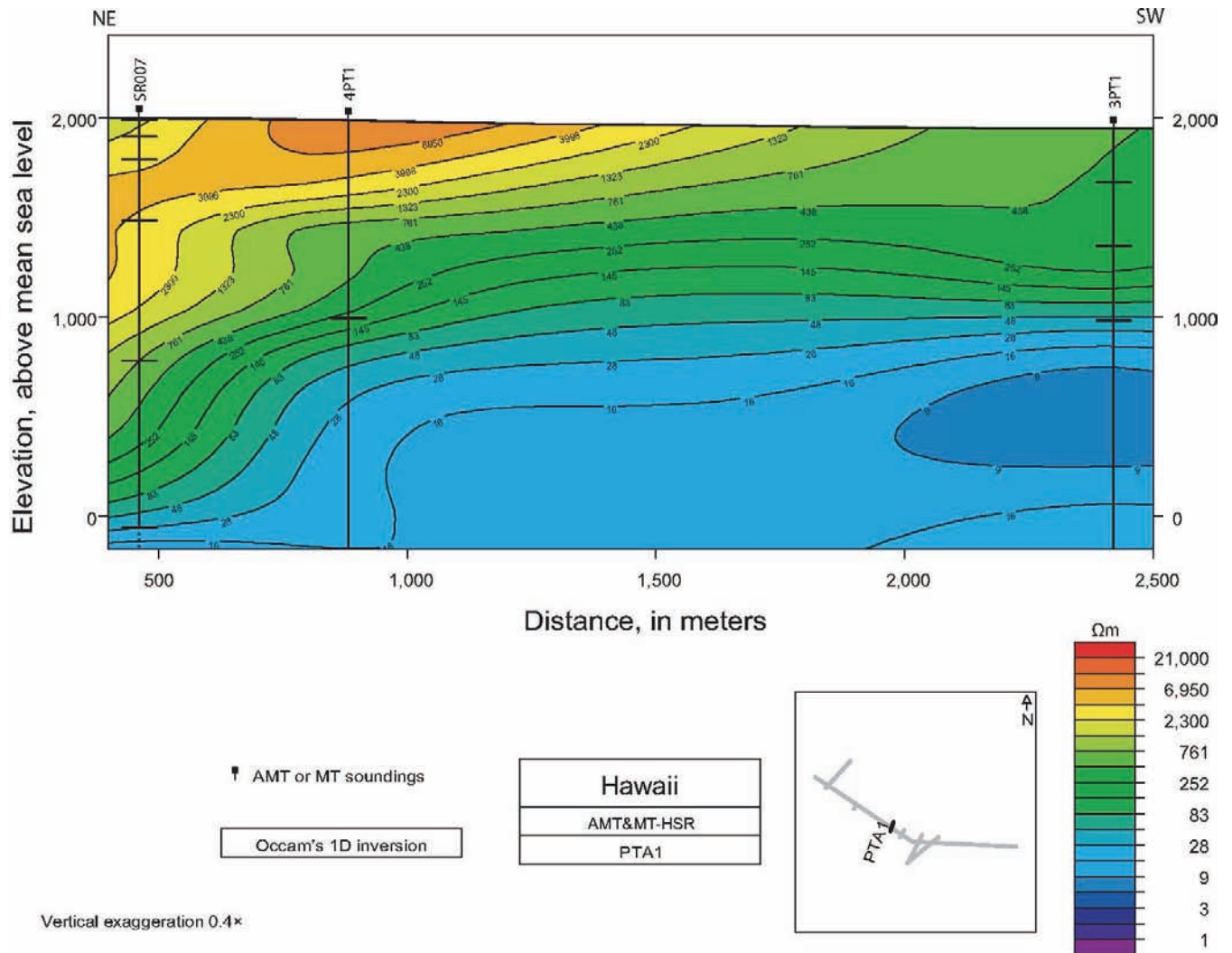


Figure 10. Cross-profile resistivity plot of resistivities collected along line PTA1 from northeast to southwest. Data are from three stations near the western conductor seen on electrical section HSR1 in figure 6. The low, representing water, is towards the southwestern end of the electrical section.

As we move west along the Saddle, the geologic history of the subsurface has become progressively more complex. Whereas the eastern end of the cross-Saddle transect can reasonably be assumed to be sounding into strata made up entirely of Mauna Kea lava flows, albeit with a possible rift system having been intruded into them, the central and western portion of the transect more likely images lavas derived from both Mauna Kea and Hualālai as well as possibly Mauna Loa. Included within this region may also be remnants, now buried, of a rift system from Hualālai. Further, a topographic analysis of the southern flank of Mauna Kea above the PTA indicates a grade of nearly 40 percent; the slopes on the eastern and western flanks of the mountain at similar elevations are about one-half that gradient. Grades of this steepness are often associated with gravitational slumping of an island volcano's unbuttressed flank. These slumps produce steep scarps on the footwall or island side called pali. This is similar to the current situation with Kilauea's southern flank at the Hilina Pali and the sequence of slip faces east and west of the pali.

Finally, we also need to consider the weathering history of Mauna Kea. We are currently in the Holocene interglacial epoch, but there is extensive documentation (Stearns and Macdonald, 1946; Wolfe and Morris, 1996; Sherrod and others, 2007) of recent glaciation at Mauna Kea's summit prior to about 10,000 years ago. This evidence includes glacial moraines flanking Mauna Kea's summit. In addition, unique morphologies of some summit eruption products have been postulated to be the result of their extrusion beneath glacial cover, and glacial polishing of surface rocks has been widely identified within the summit area. Given Mauna Kea's age, it is not unreasonable that its summit has been glaciated multiple times during the last approximately 300 ka (nor is it unlikely that Hualālai, during its mature stages of growth, could have also been glaciated even further back in time).

The relevance of this history to the hydrology of the Saddle region arises from the potential impacts of the geology on the subsurface permeability. Fault systems are known to produce a type of rock termed "fault gouge," which is fine-grained material that weathers rapidly to clay and reduces formation permeability; hence, fault systems are recognized as confining formations that can impede transport of water. In an analogous process, glaciation produces rock "fines" during the transport of the rocks down slope. Whether carried by wind or by water, deposition of these fines and their subsequent weathering within the Saddle region will also substantially reduce the permeability of the now-buried soil horizons. These low permeability horizons could enable substantial quantities of water to accumulate within the formations accessed by these two profiles. Further, the fact that the modeled resistivities are so much lower than those found toward the east further supports this interpretation. If the formations showing resistivities of less than 20 Ωm were in unweathered basalts, then we would have to conclude that they were saturated with either ambient temperature sea water or geothermal fluids. The former option is unsupportable scientifically from the hydrology, and the latter, although possible, seems unlikely given the absence of a recognized, recently active rift zone within the area. Hence, it is reasonable to conclude that saturated formations are present south and southwest of the cross-saddle profile where PTA1 and PTA2 were performed.

The final cross profile, PTA3 (fig. 11), is similar to the prior two in that an unusually shallow low-resistivity formation is found. Similar to PTA1, the low-resistivity zone is observed beneath two of the three stations in this transect; hence we can have some confidence that it corresponds to a buried feature. The subsurface geologic conditions for this transect are as follows: SR013 (northernmost station) and SR012 (central station) are both located on, or very close to, the sloping flank of Mauna Kea and are likely responding to conditions within a sequence dominated by lava flows; station 15PT is located on a less steeply sloped surface and may be responding to both ponded lavas and alluvium in the shallow stratigraphic section but, below 1,000 m, is likely into the buried Mauna Kea flank. We also note that, in this area, we have approached an inferred western rift zone of Mauna Kea (Fiske and Jackson, 1972; Sherrod and others, 2007) and that there are several late-stage eruptive vents scattered around these stations. Hence, an interpretation most consistent with the resistivity patterns observed is that the high-resistivity northeast of station SR013 is because of the dike complex of this rift system; the central low-resistivity feature may be associated with water leakage of dike-impounded water from the rift system that is flowing downward toward the southwest. In consideration of the steep resistivity gradients seen beneath the central station, it seems likely that any inferred water source identified here could be limited in extent.

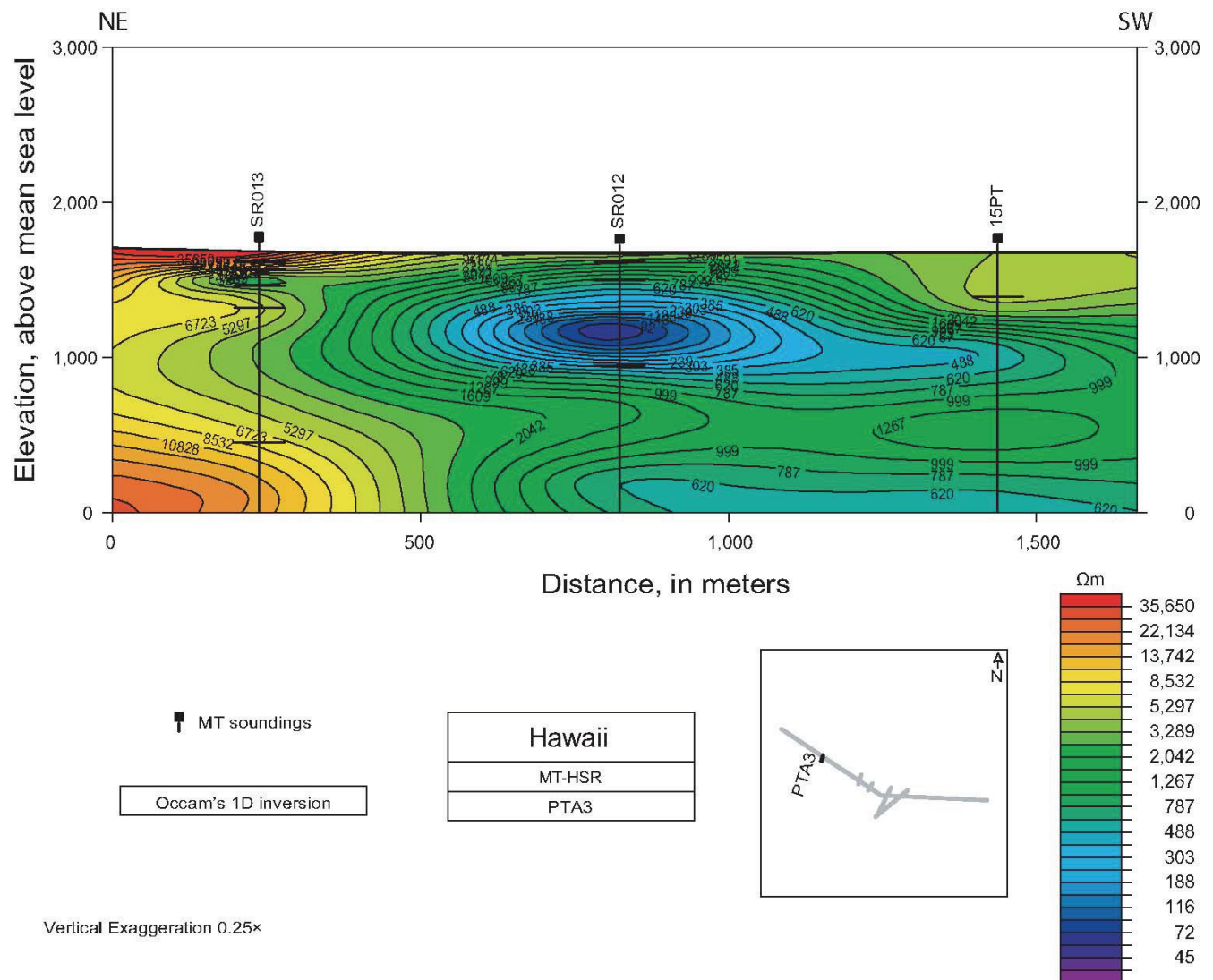


Figure 11. Cross-profile resistivity plot of transect PTA3 trending northwest to southeast. Note that the resistivity low centered near AMT station SR012 extends to the south towards MT station 15PT.

Resistivity Maps at Several Elevations

Using all the MT and AMT data, we mapped the modeled resistivities through the Saddle at constant elevations of 400 m amsl (fig. 12), 600 m amsl (fig. 13), and 800 m amsl (fig. 14) to provide a map view of the resistivity lows. The 400 m (amsl) slice through the region shows a broad resistivity low that corresponds to an inferred southwestern rift system of Mauna Kea and may reflect dike-impounded water, thermal water, or hydrothermally altered formations that are saturated with freshwater. The presence of fresh groundwater east of the rift at an elevation of nearly 300 m provides supporting evidence that saturation extends to at least the elevation of this section. Further to the west, a broad low-resistivity feature is observed that extends toward the southwest of Saddle Road; this feature is centered between our stations 4PT1 and 6PT1. As noted above, this low resistivity is likely to be associated with clay-rich stratigraphy that is probably saturated with freshwater and possibly associated

with faulting of the southern flank of Mauna Kea during its major growth phase (prior to the presence of Mauna Loa forming on its south flank). Although the low resistivities are also consistent with saturation with thermal waters, the absence of evidence for a nearby rift system or other intrusive activity makes this interpretation unlikely. Farther west still, a third conductive feature is mapped southwest of the point at which Saddle Road strikes toward the northwest and begins to climb over Mauna Kea's western flank. The features responsible for the low resistivity may be associated with the dike complex of Mauna Kea's western rift system.

Figure 12. Map view of resistivity data from MT and AMT stations at a constant elevation of 400 meters above sea level. Note the low-resistivity zones near stations 6PT1 and MKR1

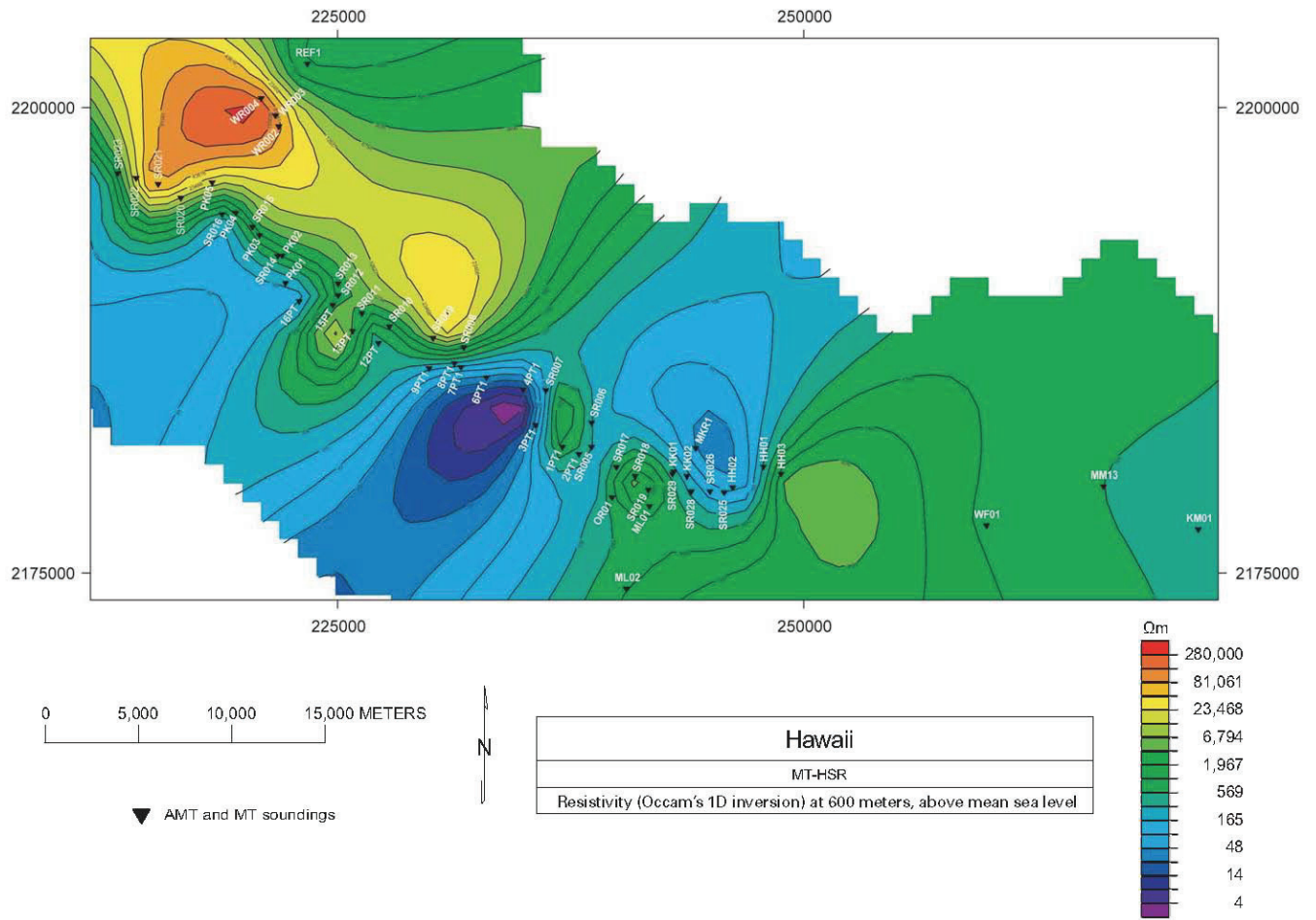


Figure 13. Map view of resistivity data taken from MT and AMT stations at a constant elevation of 600 meters above sea level. Note the low resistivity zones near stations 6PT1 and MKR1.

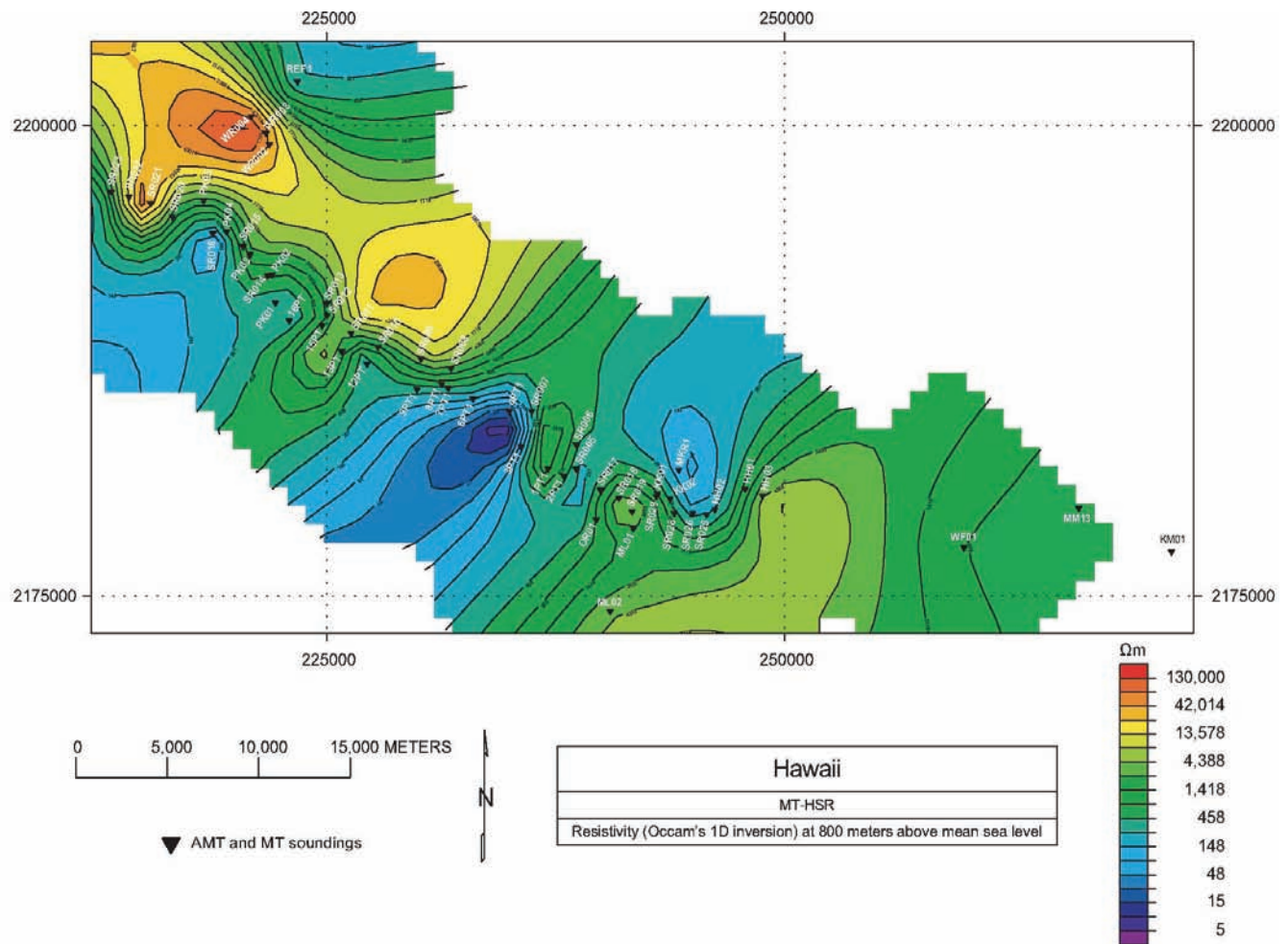


Figure 14. Map view of resistivity data taken from MT and AMT stations at a constant elevation of 800 meters above sea level. Note the low resistivity zones near stations 6PT1 and MKR1

Conclusions

The nature of shield volcanoes assures that near-horizontal fractures and thin-skinned basalt layering are present throughout most of the shield deposited above sea level. These subaerial formations are known to have extraordinarily high permeability. In such an environment, we would expect that only limited quantities of fresh groundwater would accumulate within the islands before discharging through coastal springs. However, recent drilling has shown that groundwater accumulates at substantially higher elevations than has previously been expected. The present study was undertaken in an effort to better define the elevation of the saturation zone across the center of the island through the Saddle area between Mauna Kea and Mauna Loa, to develop insights into the island's groundwater storage capacity, and to provide guidance on developing a reliable groundwater supply for a variety of potential uses—potable drinking water, water for fire control, and water for drought mitigation.

Whereas the AMT soundings provided us with a detailed image of the shallow resistivity across the Saddle, the longer and more deeply penetrating MT surveys enabled us to map subsurface resistivities down to and well beyond sea level beneath the Saddle. The resistivity structure developed from these soundings reveals a much more complex structure than was expected and suggests that

structural and lithologic features, although making up a small fraction of the volume of the shield volcanoes, play a much larger role in groundwater flow than has been previously assumed. Modeled resistivities suggest that groundwater saturation may extend to as high as 1,000 m above sea level within the Saddle and enable us to identify three general locations (fig. 15) where prospects for recovering significant quantities of groundwater may be indicated to be the most favorable.

These locations include an area immediately east of the Mauna Kea Observatory access road, near the center of the Saddle, within training area 4, and toward the southwest of the intersection of the current Saddle Road alignment with the western boundary of PTA-controlled lands. Although the modeled resistivities are suggestive of significant groundwater resources south of the current Saddle Road alignment, our surveys did not extend far enough south to fully detail the extent of those inferred structures; hence, our conclusions are less certain there.

As a final cautionary note, we emphasize that the results of these surveys cannot confirm the existence of recoverable water resources at the modeled depths. The techniques applied are the most reliable method we have available to us for the assessment of subsurface saturation conditions short of drilling a test well. Our intent in this work is to provide a basis on which to exclude some areas where resistivities are high enough to assure that formations are unsaturated and to identify sites where formation resistivities are consistent with saturated conditions and thus more likely to encounter recoverable water resources.

Acknowledgments

USGS investigations of the Pohakuloa Training Area property are conducted in cooperation with the U.S. Department of the Army, Hawaiian Homelands, and Parker Ranch. Many thanks to all who helped and especially to Ed Uchida, U.S. Army; Mr. and Mrs. Ken Kanihoe and Guy Kanihoe of Hawaii; Ryan North and Jose Llopis, U.S. Army Corps of Engineers; and Sean O'Neal, University of Hawaii. Thanks to Allen Crider, Ben DeJong, Jim Murray, Mike Ryan, and Jeff Wynn (USGS) for field support.

References Cited

- Anthony, S.S., 1997, Evaluation of the U.S. Geological Survey Ground-Water Data-Collection Program in Hawaii, 1992: U.S. Geological Survey Water-Resources Investigations Report No. 97-4232, 76 p.
- Badon-Gyben, W., 1888, Nota in verband met de voorgenomen putboring nabij Amsterdam [Notes on the probable results of well drilling near Amsterdam]: Tijdschrift van het Koninklijk Instituut van Ingenieurs, v. 9, p. 8–22.
- Bauer, G.R., 2003, A study of the ground-water conditions in North and South Kohala districts, Island of Hawaii, 1991–2002: Hawaii Commission on Water Resources Management Report PR-2003-01, 74 p.
- Berdichevsky, M.N., and Dmitriev, V.I., 1976, Basic principles of interpretation of magnetotelluric sounding curves, *in* Adam, A., ed., *Geoelectric and geothermal studies*: Budapest, Hungary, Commission of the Academies of Socialist Countries Geophysical Monograph, Akademi Kiado, p. 165–221.
- Cagniard, Louis, 1950, Procédé de prospection géophysique [Procedure of geophysical prospecting]: French Patent 1025683, 6 p.
- Cagniard, Louis, 1953, Basic theory of the magneto-telluric method of geophysical prospecting: *Geophysics*, v. 18, no. 3, p. 605–635.
- Chakridi, R., Chouteau, M., and Mareschal, M., 1992, A simple technique for analyzing and partly removing distortion from the magnetic impedance tensor; Application to Abitibi and Kapuskasing data (Canada): *Geophysics Journal International*, v. 108, p. 917–929.
- deGroot-Hedlin, C.D., and Constable, S.C., 1990, Occam's inversion to generate smooth, two-dimensional models from magnetotelluric data: *Geophysics*, v. 55, p. 1613–1624.
- Dmitriev, V.I., and Berdichevsky, M.N., 1979, The fundamental model of magnetotelluric sounding: Piscataway, N. J., Institute of Electrical and Electronics Engineers Proceedings of the IEEE, v. 67, no. 7, p. 1034–1044.
- Fiske, R.S., and Jackson, E.D., 1972, Orientation and growth of Hawaiian volcanic rifts—The effect of regional structure and gravitational stresses: London, Proceedings of the Royal Society Series A, v. 329, August 22, p. 299–326.
- Gamble, T.D., Goubau, W.M., and Clarke, J., 1979a, Magnetotellurics with a remote reference: *Geophysics*, v. 44, p. 53–68.
- Gamble, T.D., Goubau, W.M., and Clarke, J., 1979b, Error analysis for remote reference magnetotellurics: *Geophysics*, v. 44, p. 959–968.
- Groom, R.W., 1988, The effects of inhomogeneities on magnetotellurics: University of Toronto Ph.D. dissertation, 213 p.
- Groom, R.W., and Bailey, R.C., 1989a, Some effects of multiple lateral inhomogeneities in magnetotellurics: *Geophysical Prospecting*, v. 37, p. 697–712.
- Groom, R.W., and Bailey, R.C., 1989b, Decomposition of magnetotelluric impedance tensors in the presence of local three-dimensional galvanic distortion: *Journal of Geophysical Research*, v. 94, n. B2, p. 1913–1925.
- Groom, R.W., and Bailey, R.C., 1991, Analytic investigations of the effects of near-surface three-dimensional galvanic scatterers on MT tensor decompositions: *Geophysics*, v. 56, n. 4, p. 496–518.
- Groom, R.W., Kurtz, R.D., Jones, A.G., and Boerner, D.E., 1993, A quantitative methodology to extract regional magnetotelluric impedances and determine the dimension of the conductivity structure: *Geophysical Journal International*, v. 115, p. 1095–1118.

- Herzberg, A., 1901, Die wasserversorgung einiger Nordsee bader [The water supply of parts of the North Sea coast in Germany]: *Journal Gasbeluchtung und Wasserversorgung*, v. 44, p. 815–819, p. 842–844.
- Hunt, C.D., 1996, *Geohydrology of the island of Oahu, Hawaii*: U.S. Geological Survey Professional Paper 1412 B, 54 p.
- Imata, Ryan, 2004, *Hawaii, Hawaii well database*: Honolulu, Commission on Water Resources Management, Department of Land and Natural Resources.
- Jones, A.G., and Garcia, X., 2003, Okak Bay AMT data-set case study; Lessons in dimensionality and scale: *Geophysics*, v. 68, n. 1, p. 70–91.
- Kauahikaua, J., Hildenbrand, T., and Webring, M., 2000, Deep magmatic structures of Hawaiian volcanoes, imaged by three-dimensional gravity models: *Geology*, v. 28, n.10, pp. 883–886.
- Keller, G.V., and Frischknecht, F.C., 1966, *Electrical methods in geophysical prospecting*: London, Pergamon Press, 519 p.
- Martí, A., Queralt, P., Jones, A.G., and Ledo, J., 2005, Improving Bahr's invariant parameters using the WAL approach: *Geophysical Journal International*, v. 163, p. 38–41.
- McNeice, G.W., and Jones, A.G., 2001, Multisite, multifrequency tensor decomposition of magnetotelluric data: *Geophysics*, v. 66, n. 1 p. 158–173.
- Sherrod, D.R., Sinton, J.M., Watkins, S.E., and Brunt, K.M., 2007, *Geologic map of the state of Hawai'i*: U.S. Geological Survey, Open-File Report 2007–1089, available only at <http://pubs.usgs.gov/of/2007/1089/>.
- Simpson, F., and Bahr, K., 2005, *Practical magnetotellurics*: Cambridge University Press, 254 p.
- Spies, B.R., and Frischknecht, F.C., 1991, Electromagnetic sounding, *in* Nabighian, M.N., ed., *Electromagnetic methods in applied geophysics*: Tulsa, Oklahoma, Society of Exploration Geophysicists, *Investigations in Geophysics* no. 3, p. 285–422.
- Stearns, H.T., and Macdonald, G.A., 1946, *Geology and ground-water resources of the island of Hawaii*: Hawaii Division of Hydrography Bulletin 9, 363 p., 2 folded maps in pocket (scale 1:125,000) [includes plates].
- Stolper, E.M., DePaolo, D.J., and Thomas, D.M., 2009, Deep drilling into a mantle plume volcano—The Hawaii scientific drilling project: *Scientific Drilling*, no. 7, p. 4–14.
- Swift, C. M., 1962, A magnetotelluric investigation of an electrical conductivity anomaly in the southwestern United States: Massachusetts Institute of Technology Ph.D. dissertation, 211 p.
- Tikhonov, A.N., 1950, The determination of the electrical properties of deep layers of the earth's crust: *Doklady Akademii Nauk SSR* [Russian Academy of Sciences], v. 73, p. 295–297.
- Vozoff, Keeva, 1986, *Magnetotelluric methods*: Tulsa, Oklahoma, Society of Exploration Geophysicists, *Geophysics Reprint Series* no. 5, 763 p.
- Vozoff, Keeva, 1991, The magnetotelluric method; chap. 8 *of* Nabighian, M.N., ed., *Electromagnetic methods in applied geophysics*: Tulsa, Oklahoma, Society of Exploration Geophysicists *Investigations in Geophysics*, v. 2, no. 3, parts A and B, p. 641–712.
- Wait, J.R., 1962, Theory of magnetotelluric fields: U.S. Department of Commerce, National Bureau of Standards, *Journal of Research, Radio Propagation*, v. 66D, p. 509–541.
- Wolfe, E.W., Morris, J., 1996, *Geologic map of the island of Hawaii*: U.S. Geological Survey, *Miscellaneous Investigations Map I-2524-A*, scale 1 : 100,000.
- Zhody, A.A.R., and Jackson, D.B., 1969, Application of deep electrical soundings for groundwater exploration in Hawaii: *Geophysics*, v. 34, n. 4, p. 584–600.

Appendix A—MT and AMT Stations

Table 1. Magnetotelluric and audiomagnetotelluric station identifiers, locations, and Global Positioning System (GPS) elevations (± 10 meters).

[GPS elevations are in meters. Universal Transverse Mercator (UTM) coordinates are in meters, North American Datum (NAD) 83 with a central meridian of -173° and base latitude of 0° (zone 5)]

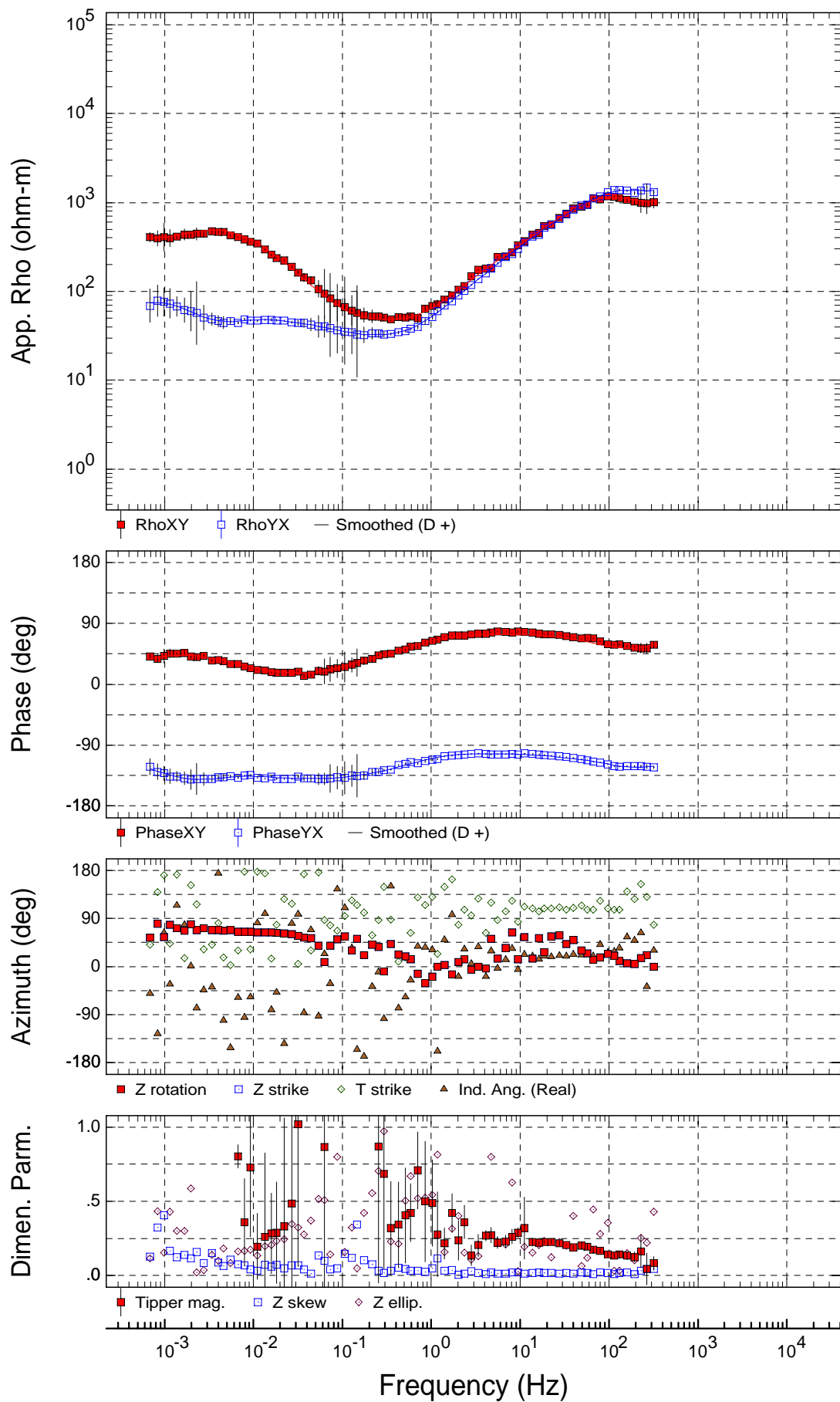
Station	Easting	Northing	Elevation
12PT	227188.2	2187337	1753
13PT	225808.7	2187989	1716
15PT	224720.5	2189378	1698
16PT	222941.5	2189612	1600
1PT1	237076.8	2181773	2028
2PT1	237965.4	2181372	2028
3PT1	235622.7	2182939	1974
4PT1	234960.4	2184832	1990
6PT1	232977.6	2185486	1909
7PT1	231622.7	2186051	1871
8PT1	231261.7	2186256	1863
9PT1	229909	2185997	1823
HH01	247847.7	2180700	1902
HH02	246206.3	2179603	1956
HH03	248798.1	2180320	1845
KK01	243050.6	2180418	2073
KK02	243755.3	2180183	2033
KM01	271149.9	2177371	631
MKR1	244211.4	2181706	2155
ML01	241721.8	2178597	2024
ML02	240485.9	2174173	2122
MM13	266081.1	2179673	891
OR01	239729.5	2179066	2034
PK01	222190.5	2190572	1558
PK02	222004.2	2192067	1494
PK03	220812.7	2193154	1372
PK04	219527.3	2194371	1254
REF1	223371.4	2202369	1239
PK05	218272	2196000	1105
WF01	259820.8	2177566	1288
SR005	238620	2181756	2071
SR006	238620	2183063	2067
SR007	236181	2184821	2035
SR008	231786	2187107	1883
SR009	230122	2187623	1834
SR010	227792	2188235	1779
SR011	226313	2188954	1725
SR012	225016	2189920	1704
SR013	225016	2190555	1622
SR014	221776	2192028	1489
SR015	220431	2193580	1332

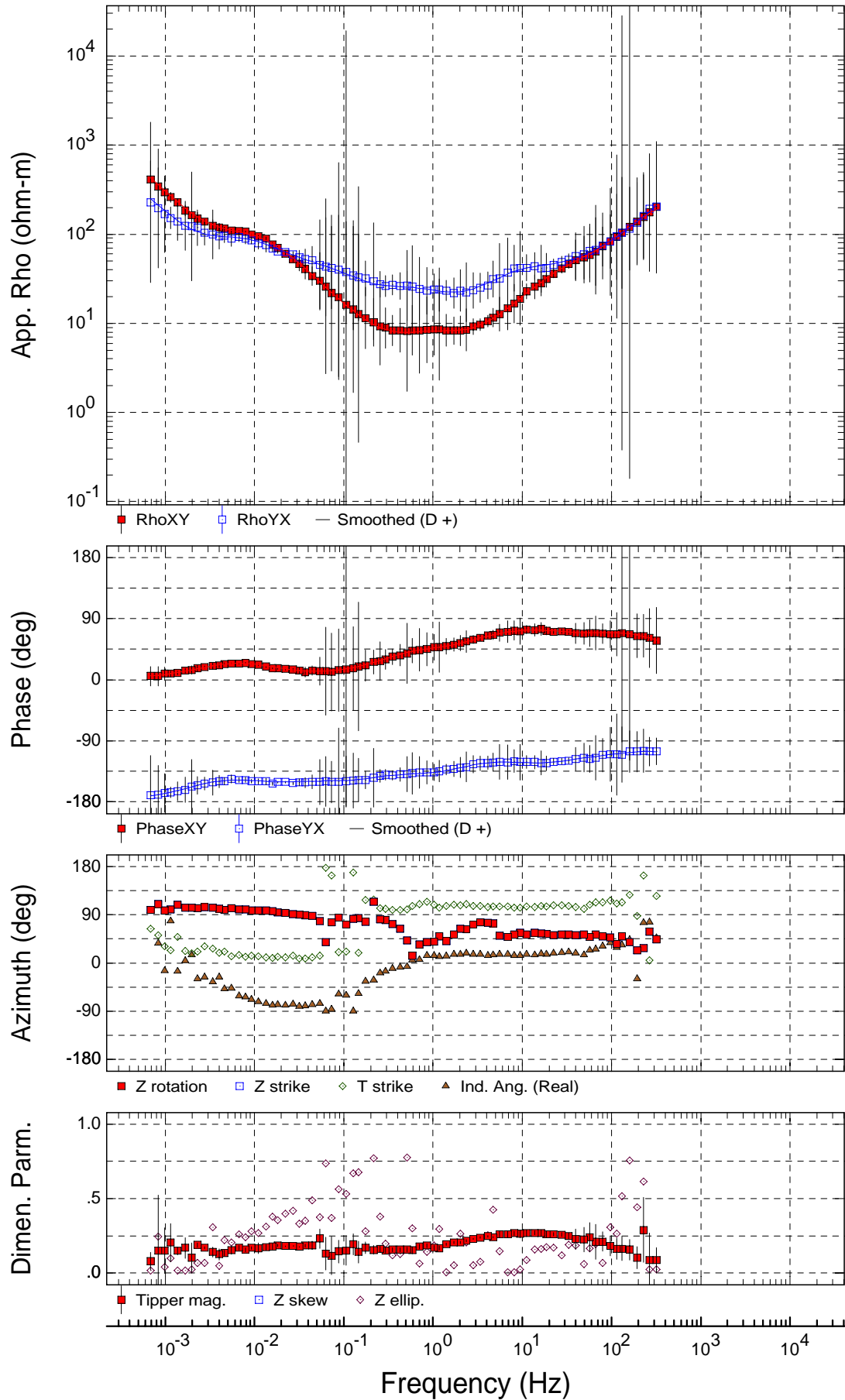
Station	Easting	Northing	Elevation
SR016	218778	2194263	1215
SR017	239948	2180658	2074
SR018	240965	2180195	2075
SR019	241671	2179495	2053
SR020	216564	2195170	1064
SR021	215355	2195885	979
SR022	214194	2196229	905
SR023	213213	2196480	839
SR025	245751	2179350	1967
SR026	244995	2179410	1992
SR028	243972	2179409	2008
SR029	242988	2180312	2078

Appendix B—MT and AMT Sounding Resistivity Plots

USGS
Rotation: PA

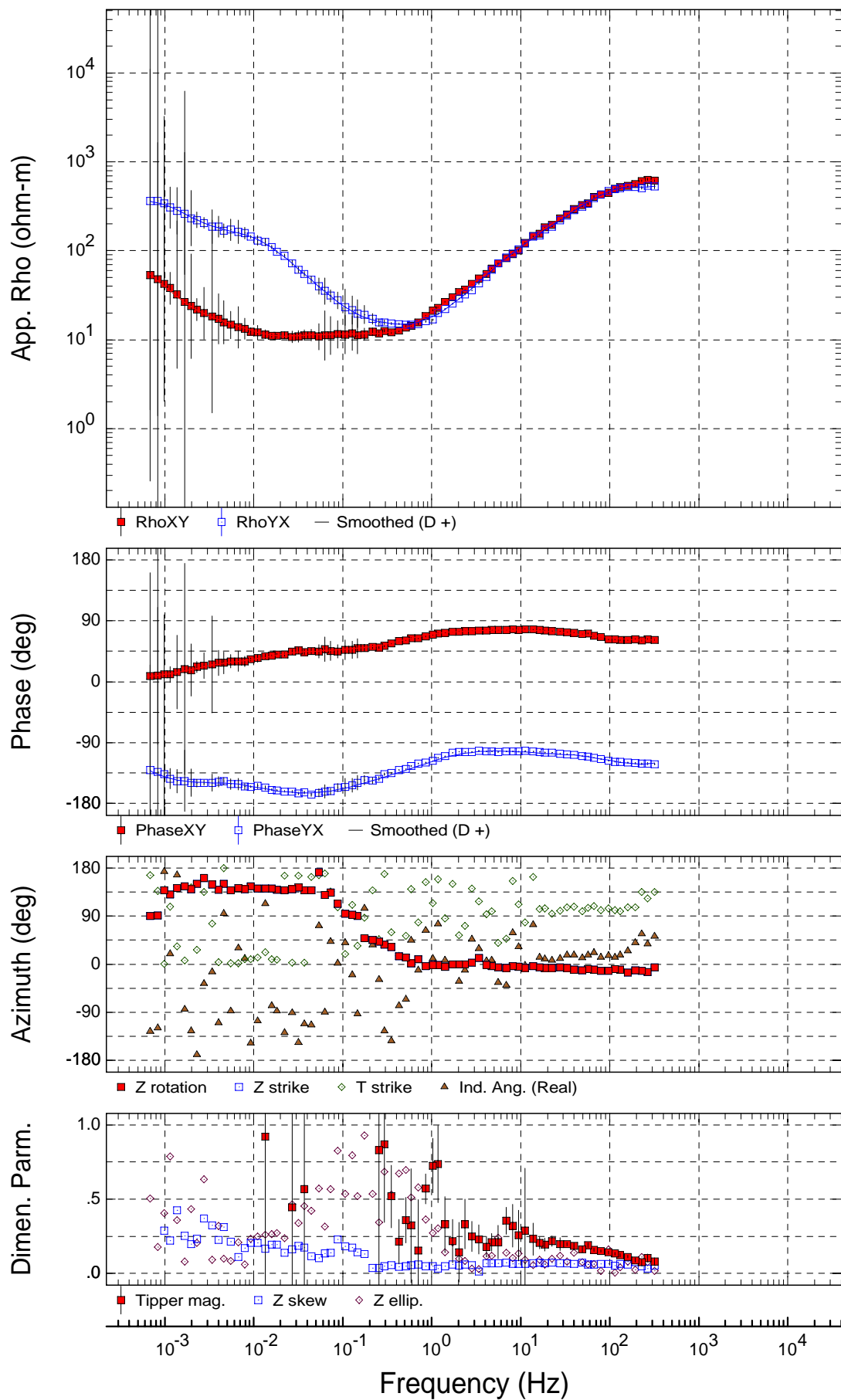
Sounding 1PT1

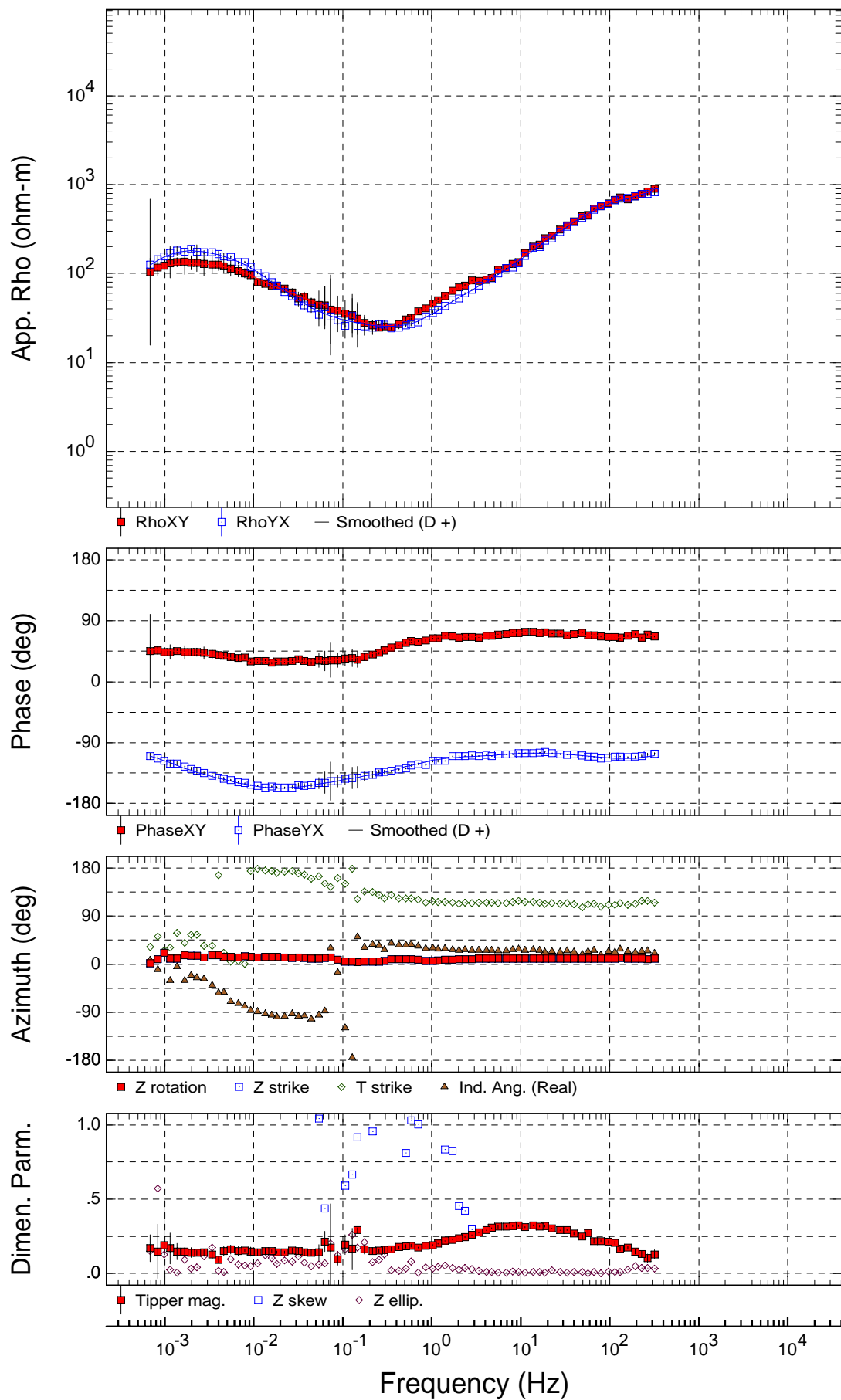


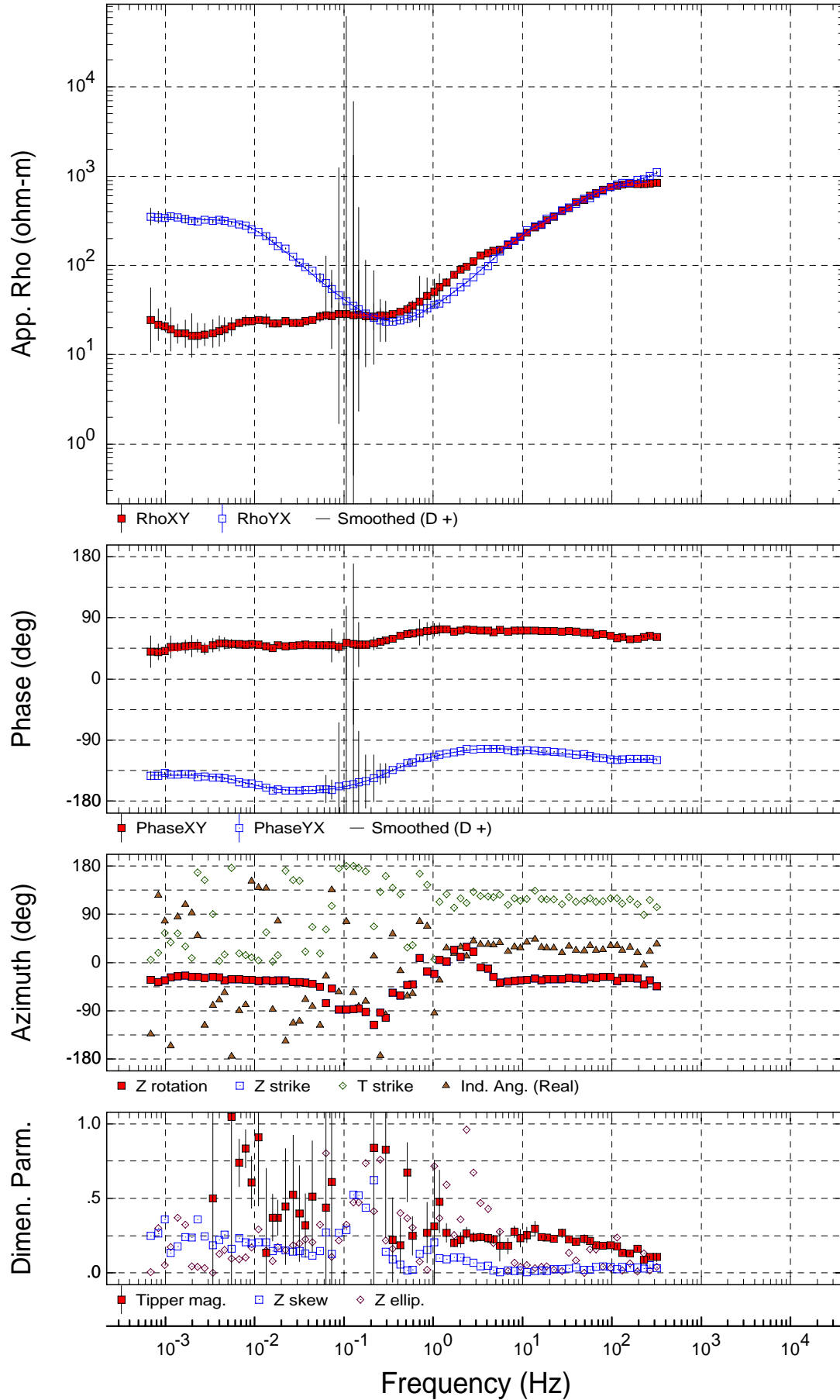


USGS
Rotation: PA

Sounding 3PT1

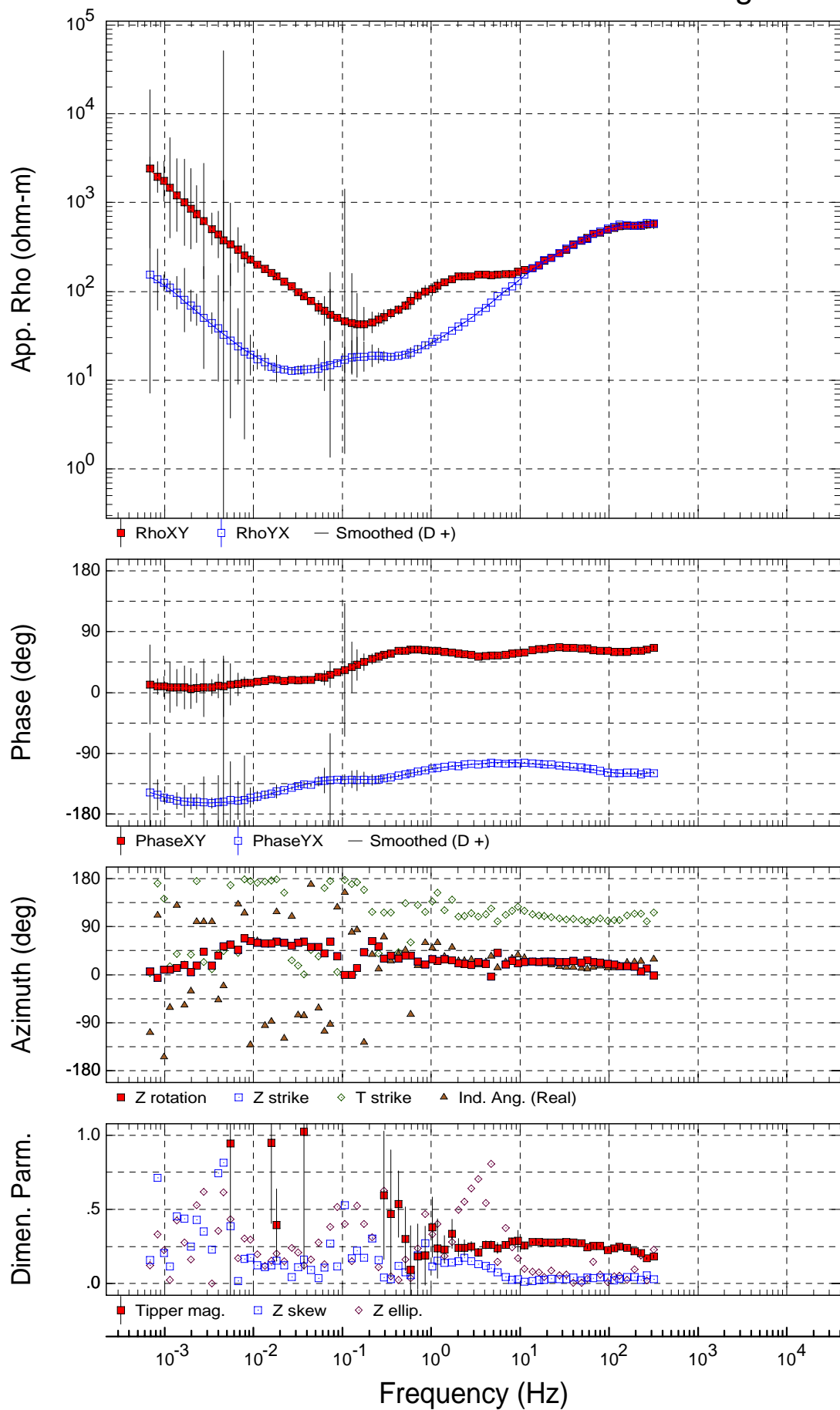


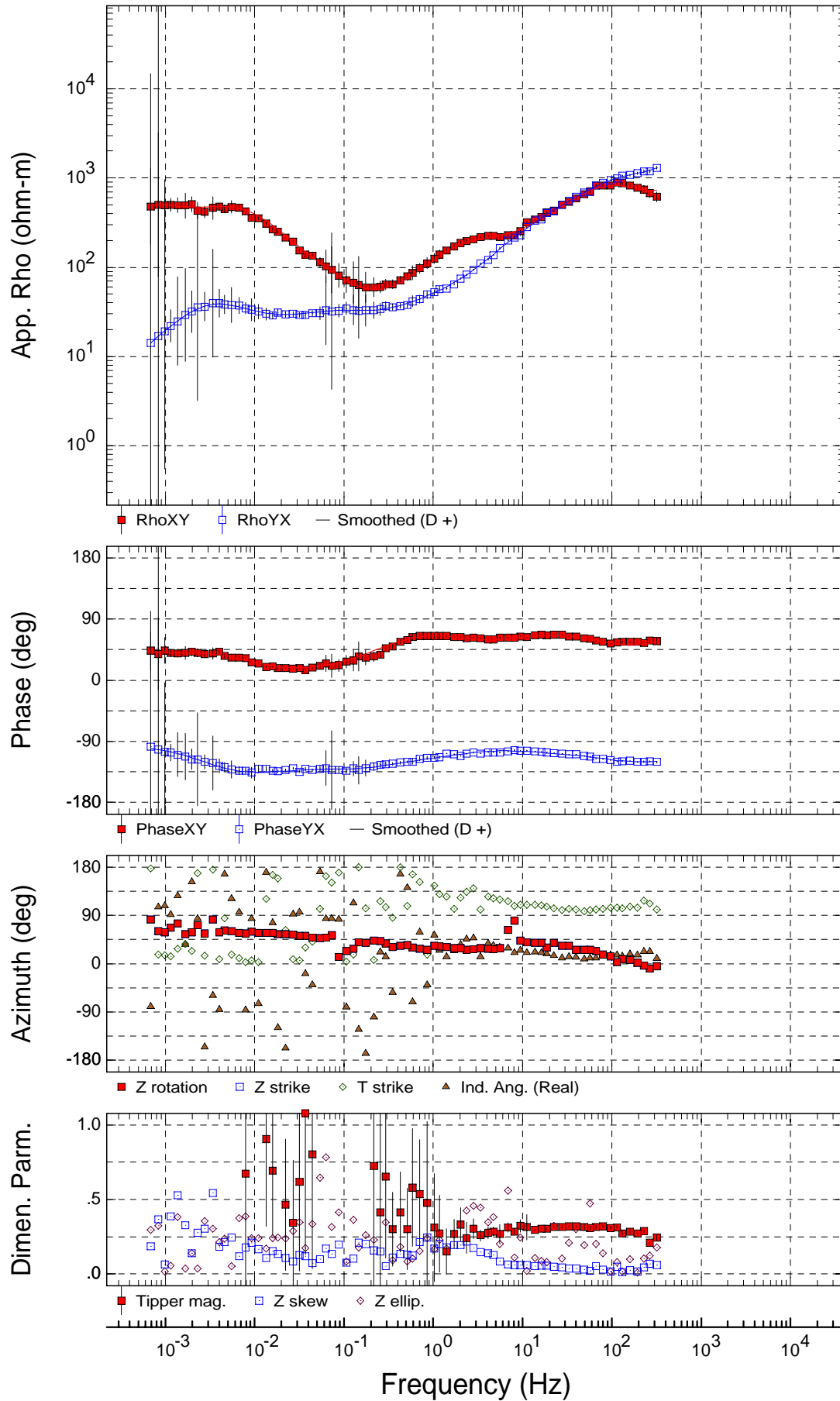




USGS
Rotation: PA

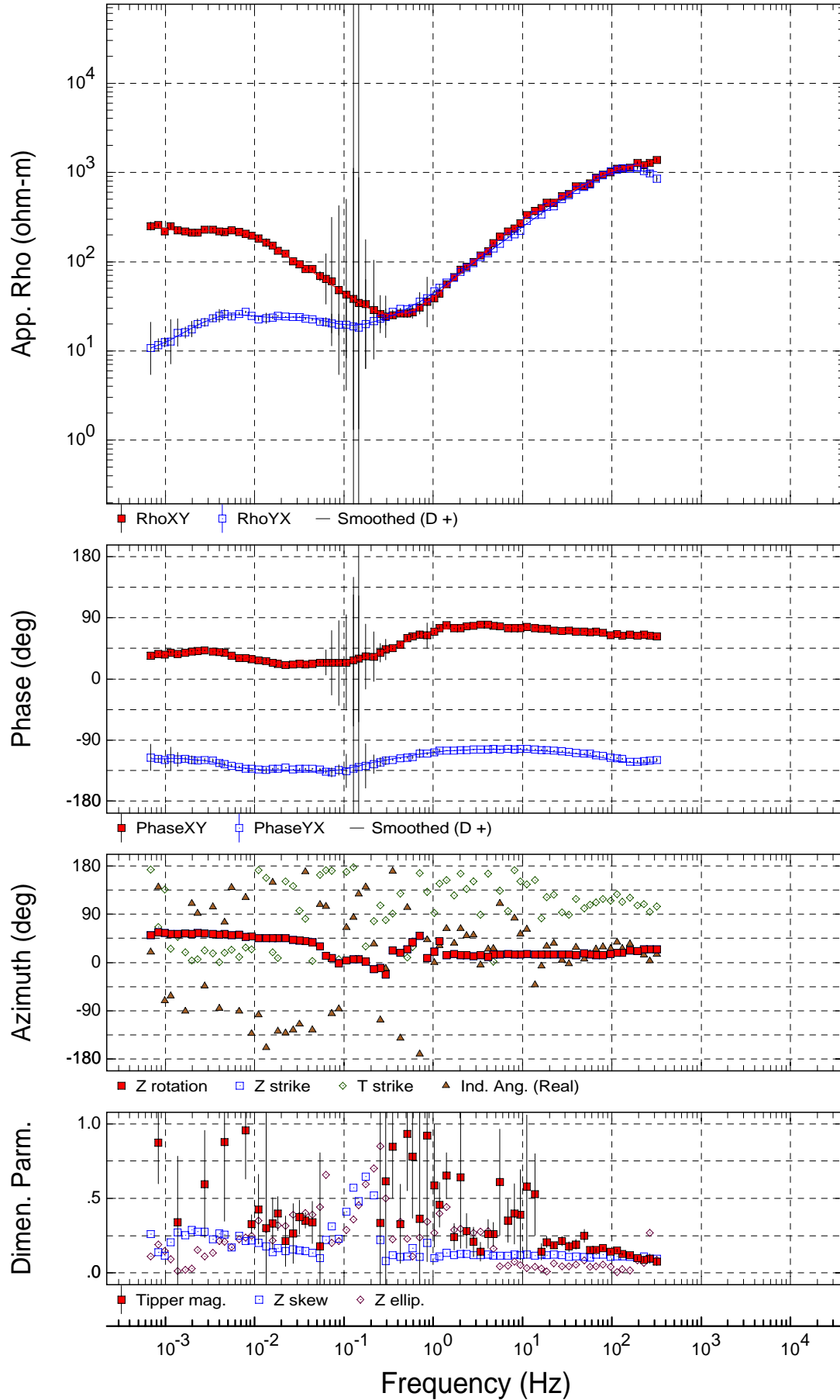
Sounding 7PT1

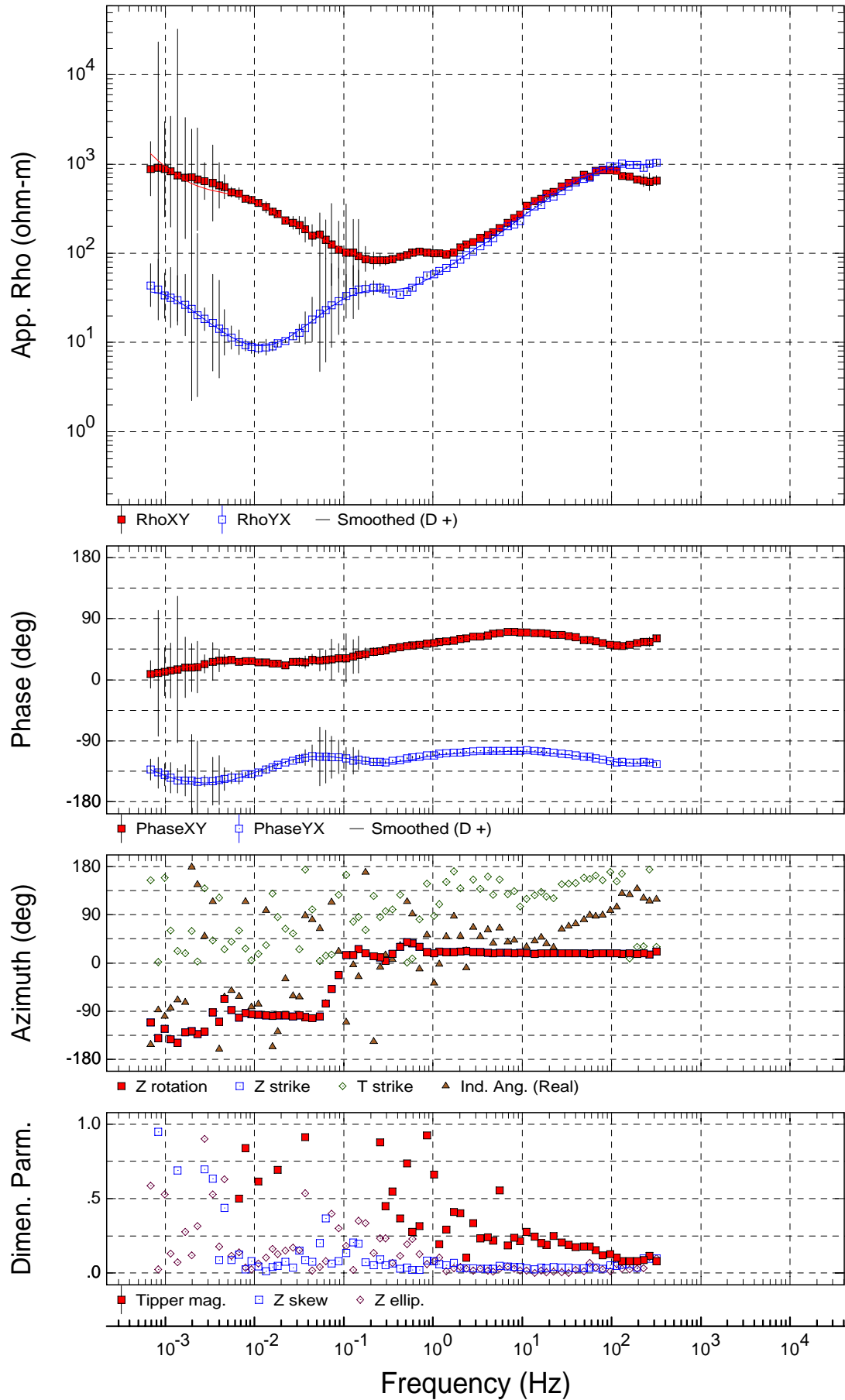




USGS
Rotation: PA

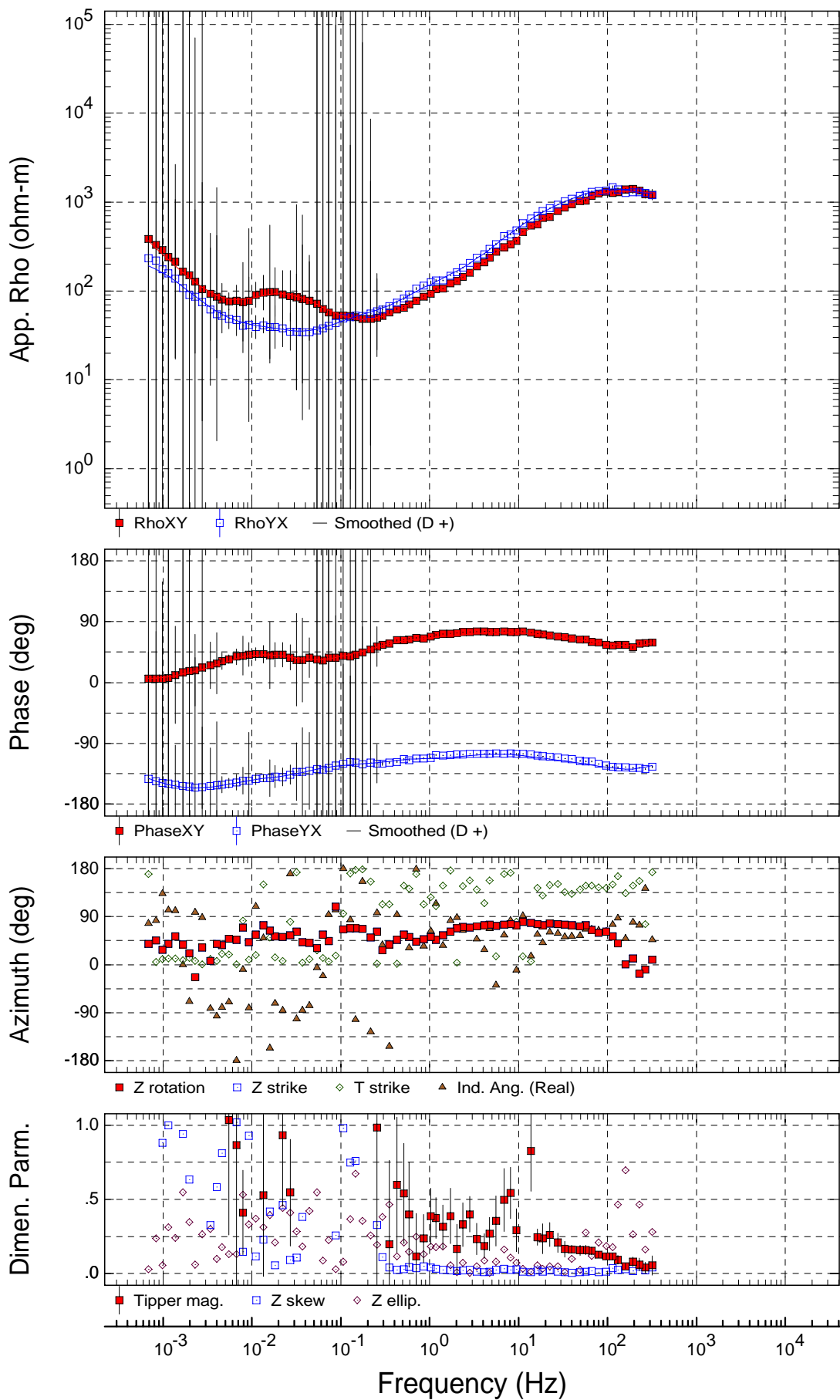
Sounding 9PT1





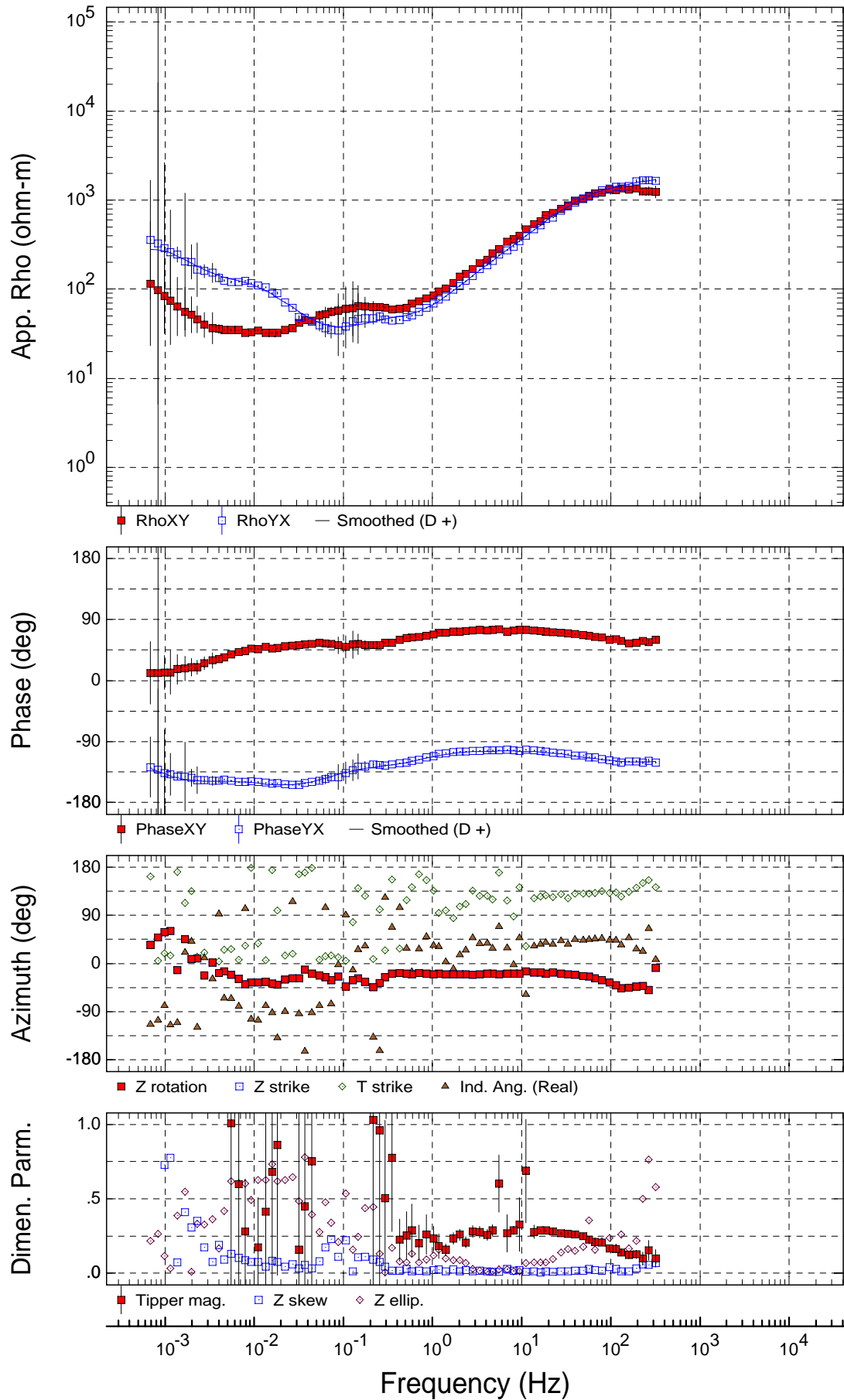
USGS
Rotation: PA

Sounding 13PT



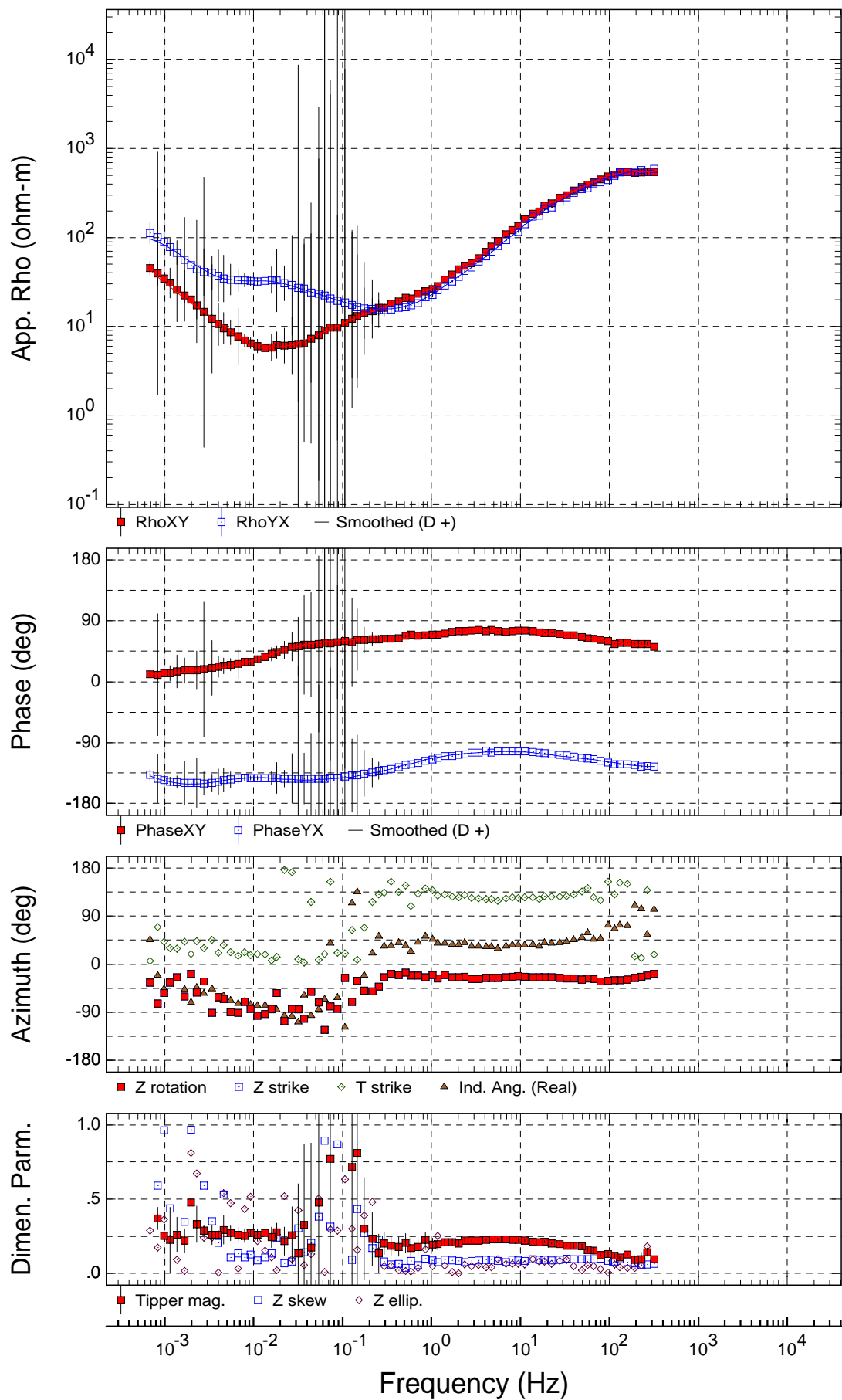
USGS
Rotation: PA

Sounding 15PT



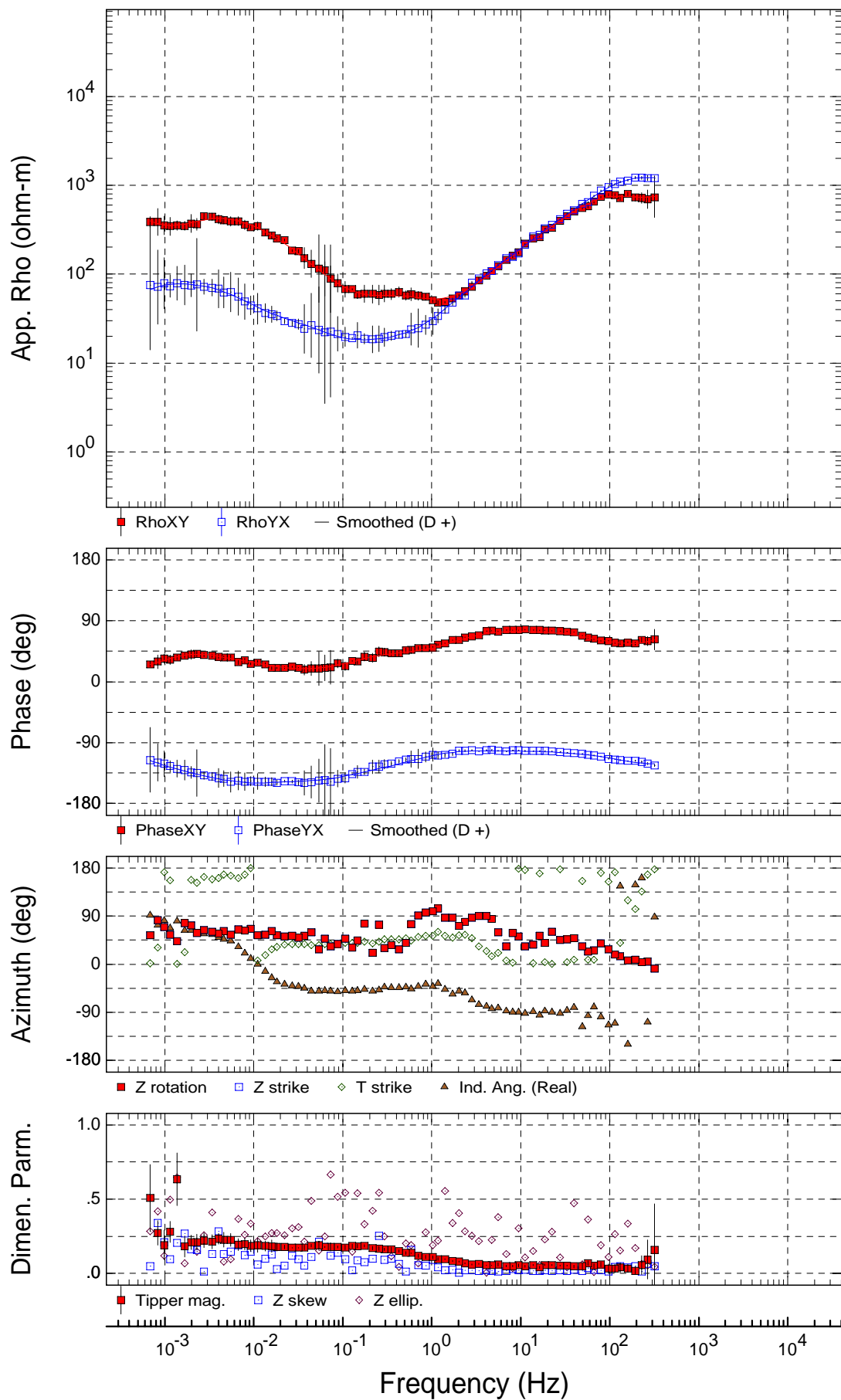
USGS
Rotation: PA

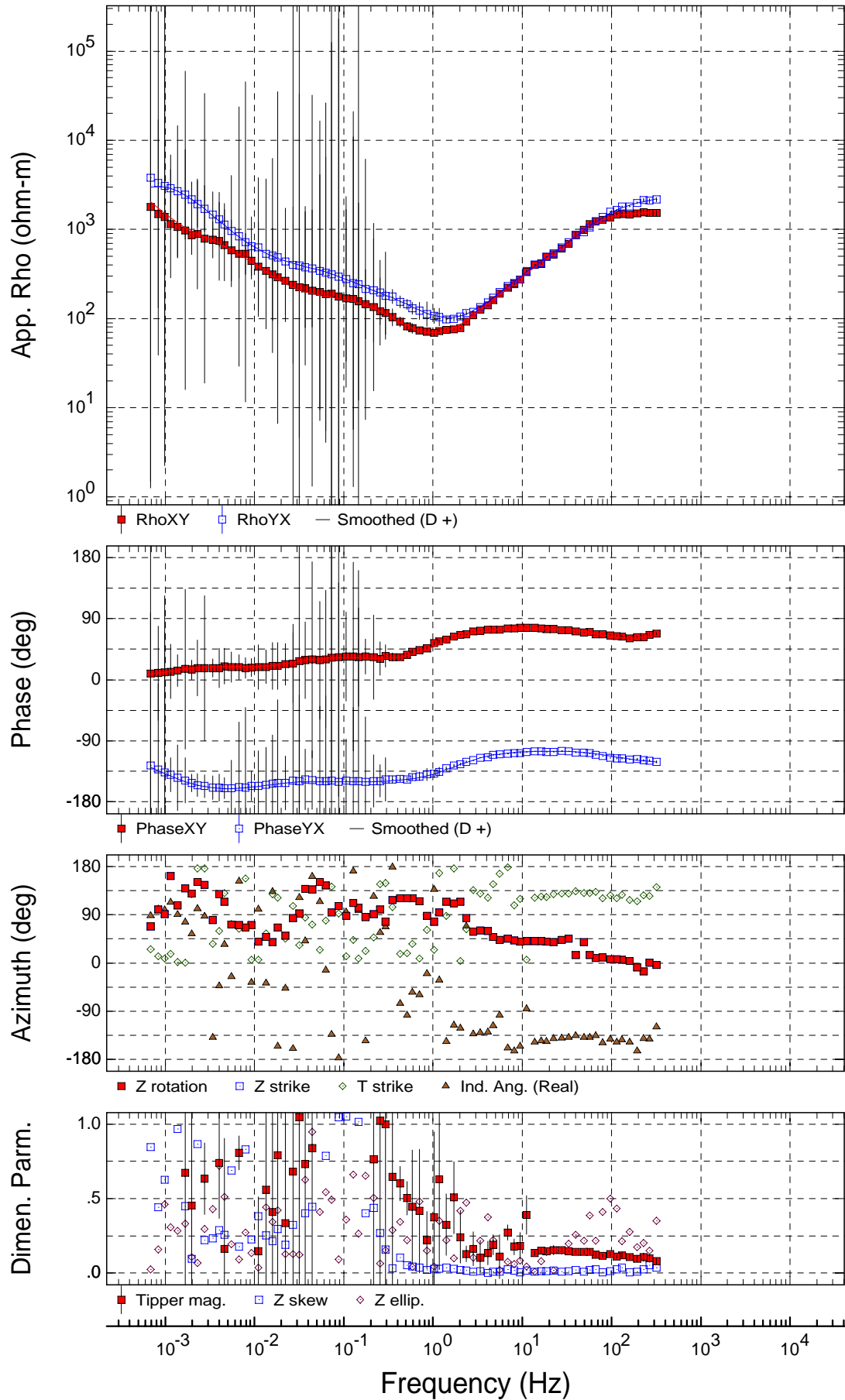
Sounding 16PT



USGS
Rotation: PA

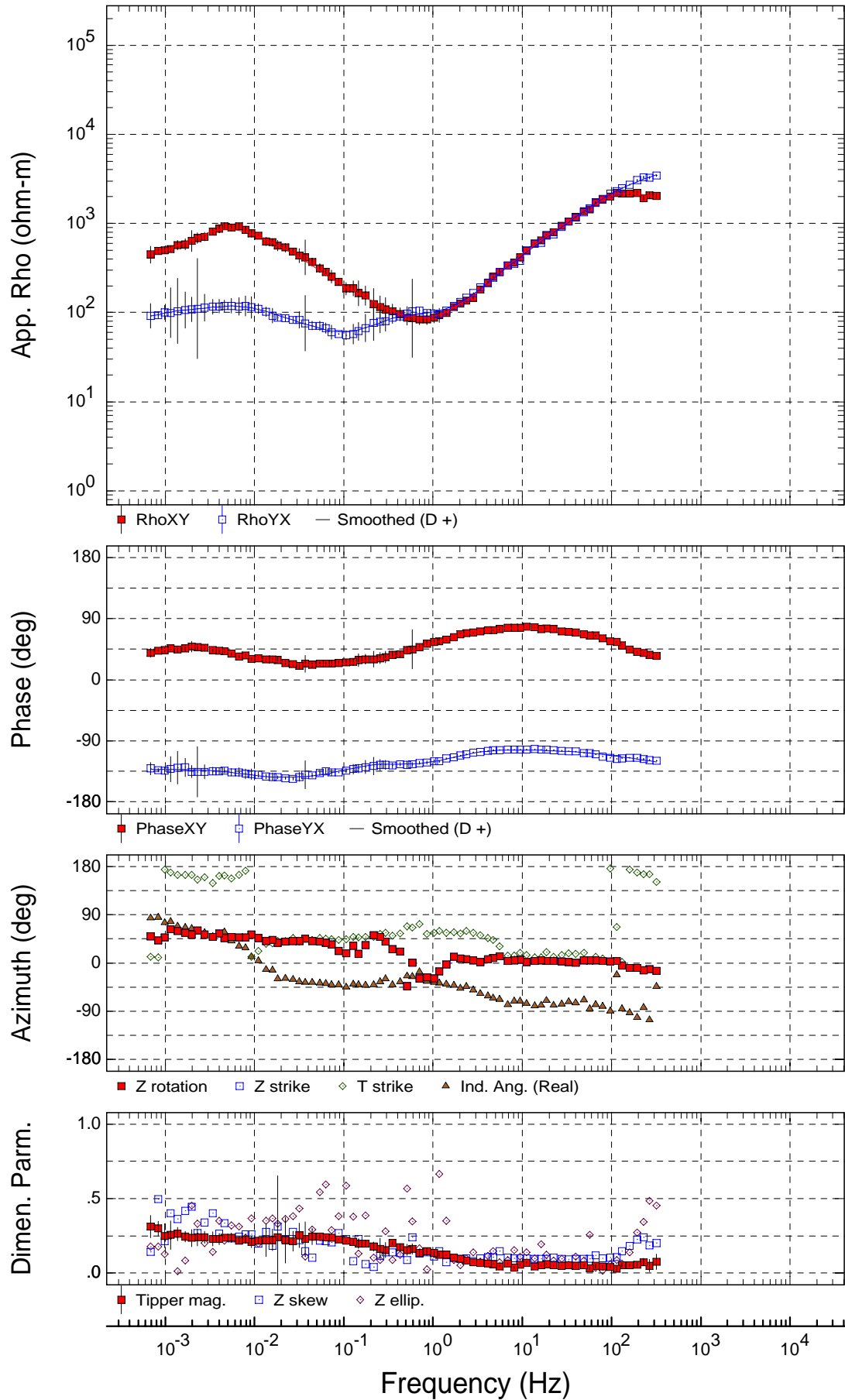
Sounding HH01

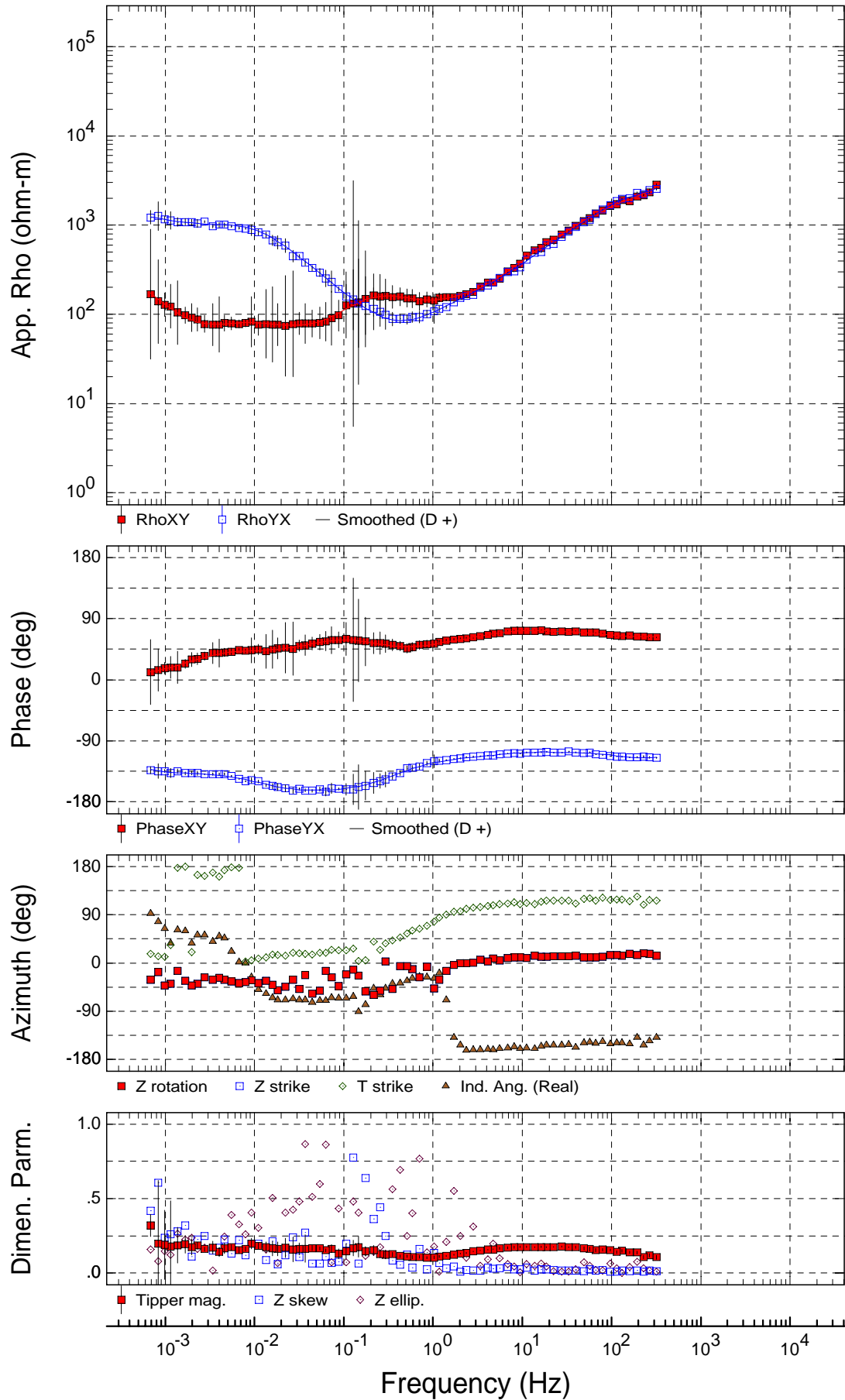




USGS
Rotation: PA

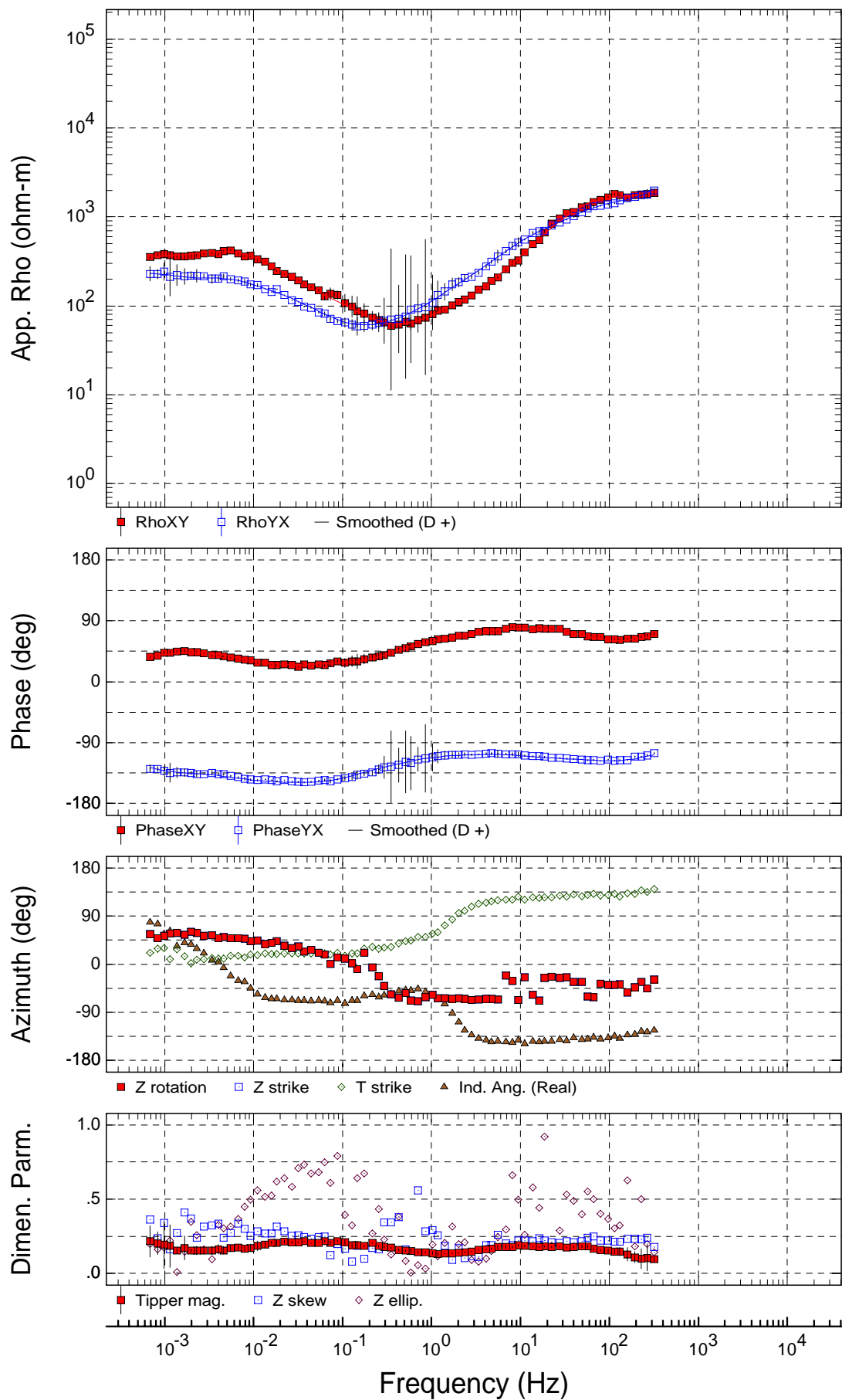
Sounding HH03





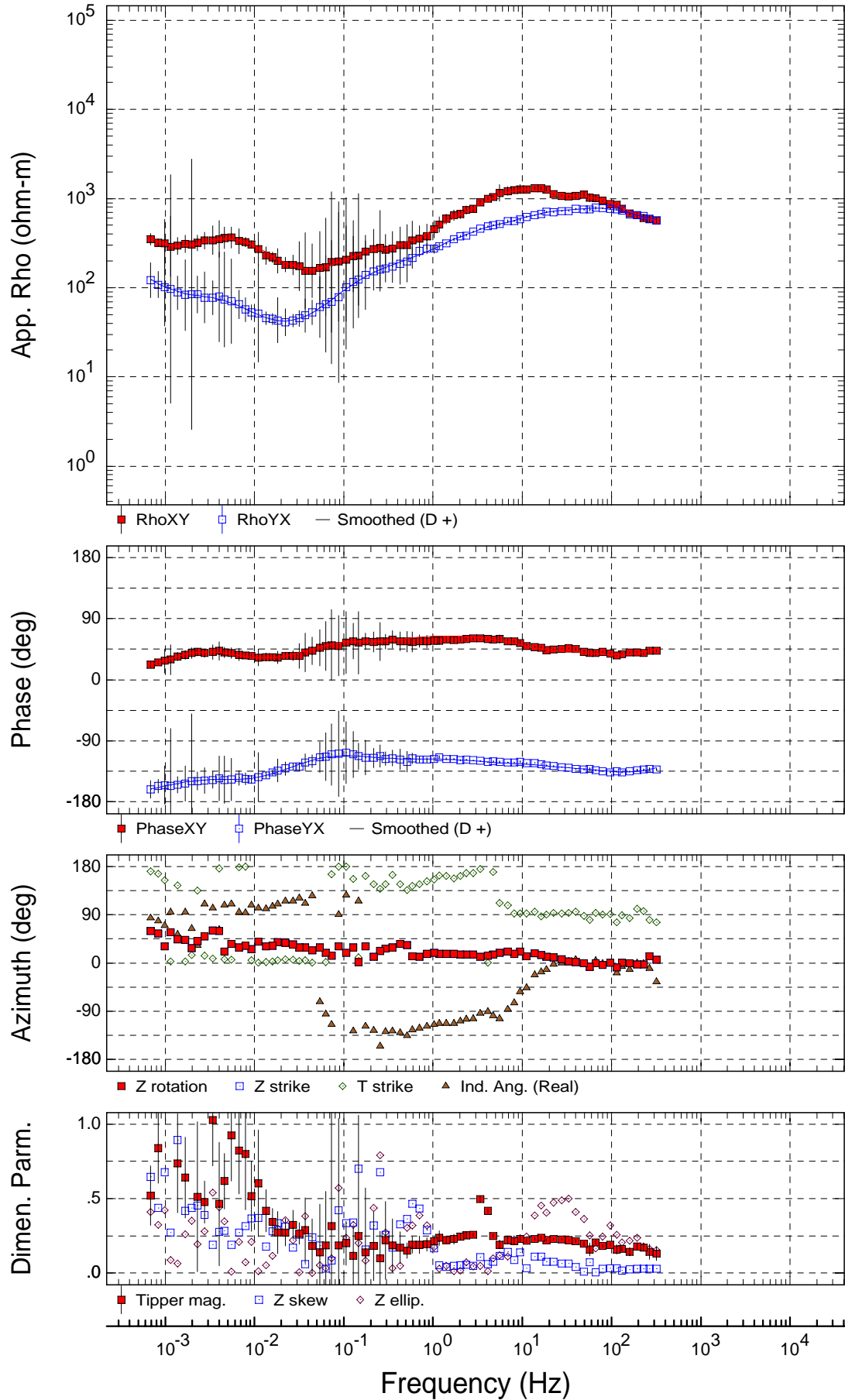
USGS
Rotation: PA

Sounding KK02



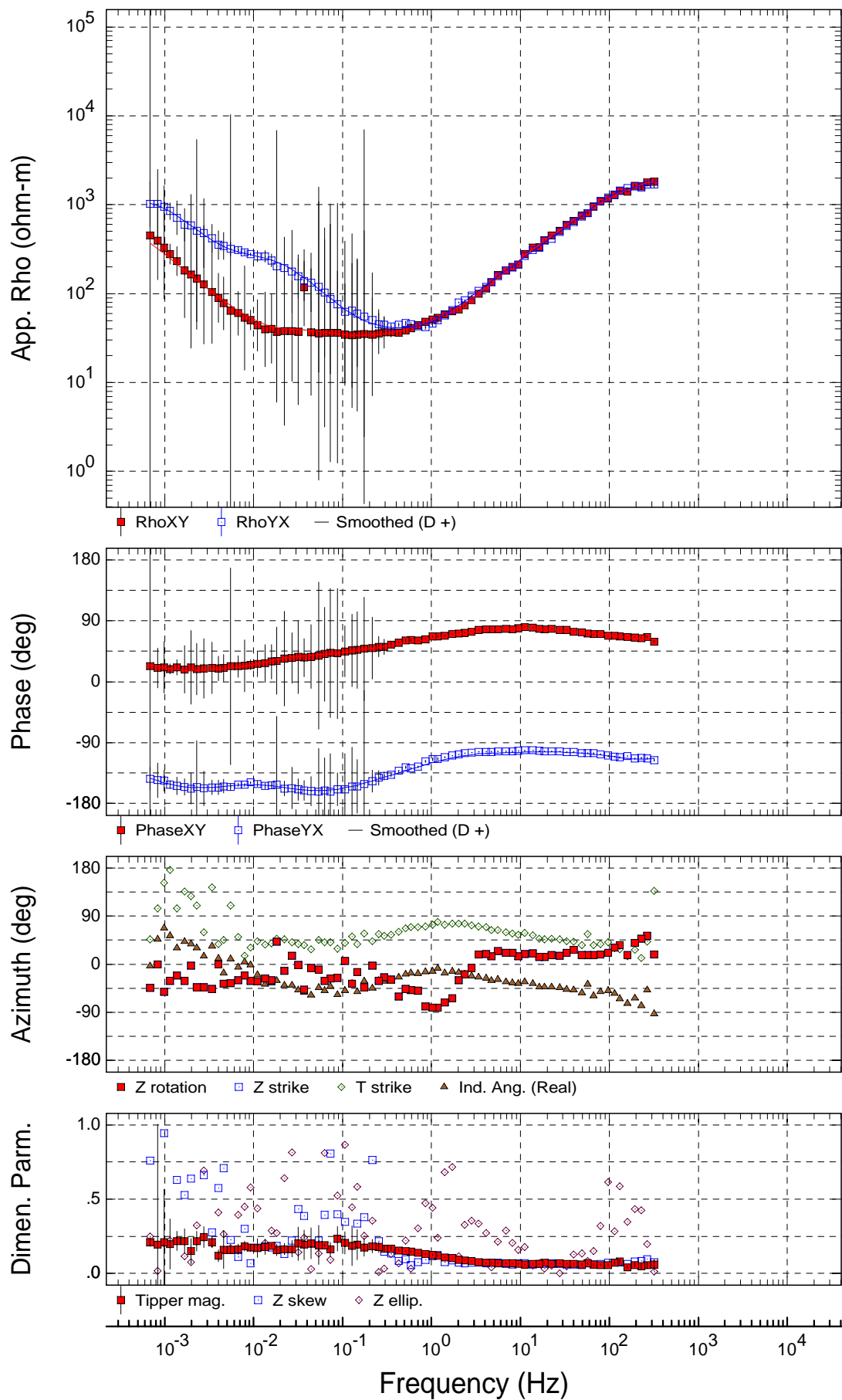
USGS
Rotation: PA

Sounding KM01



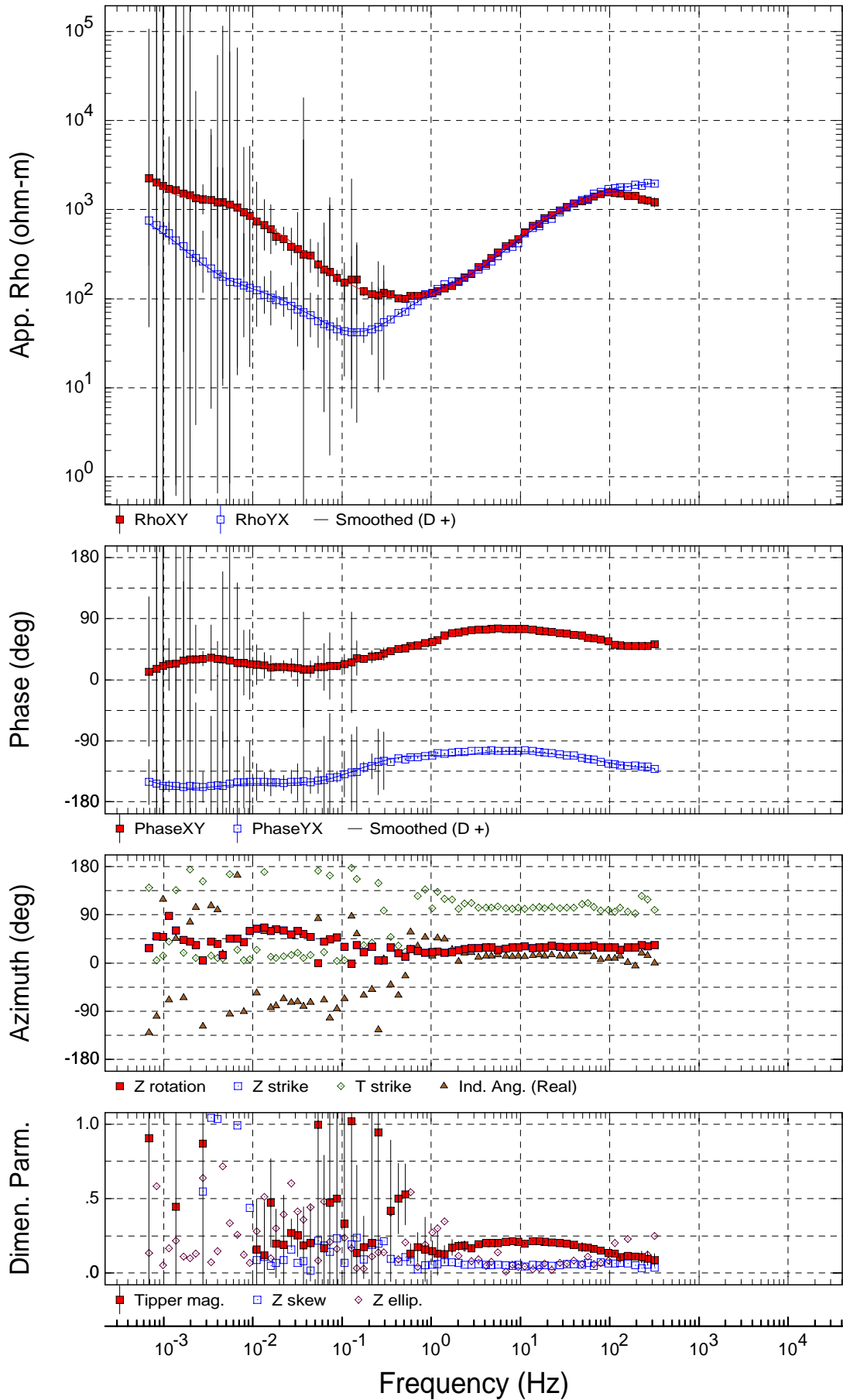
USGS
Rotation: PA

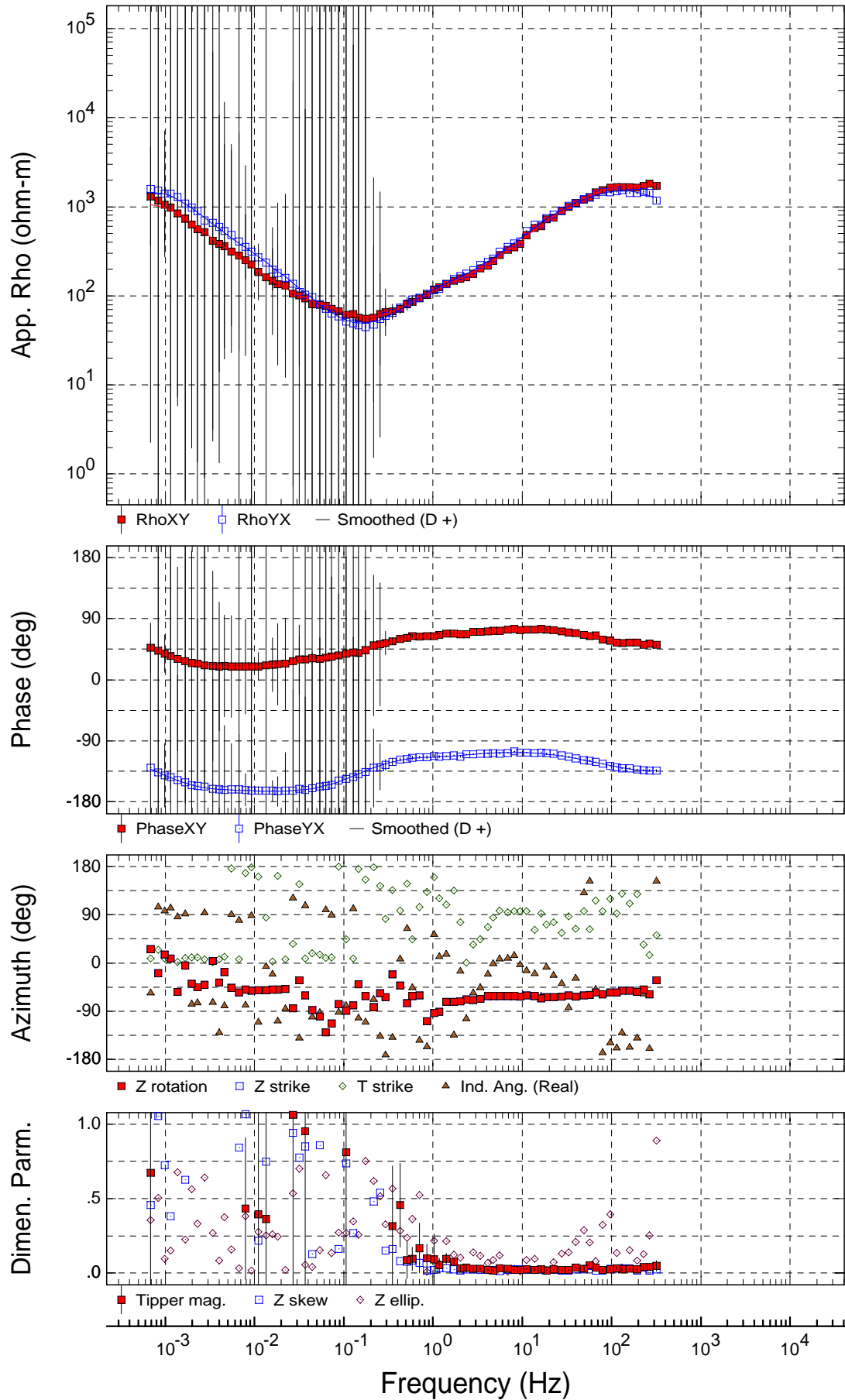
Sounding MKR1

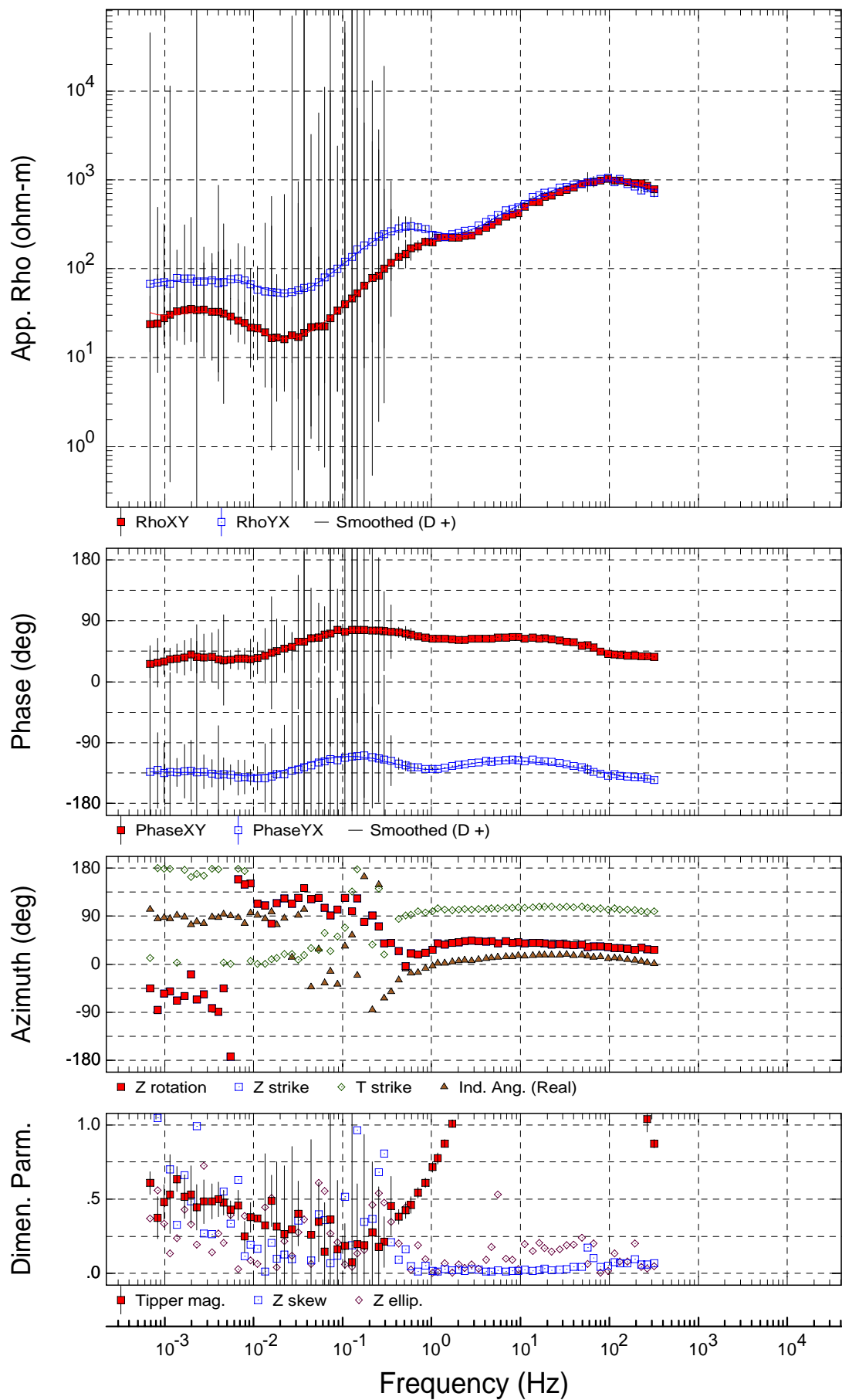


USGS
Rotation: PA

Sounding ML01

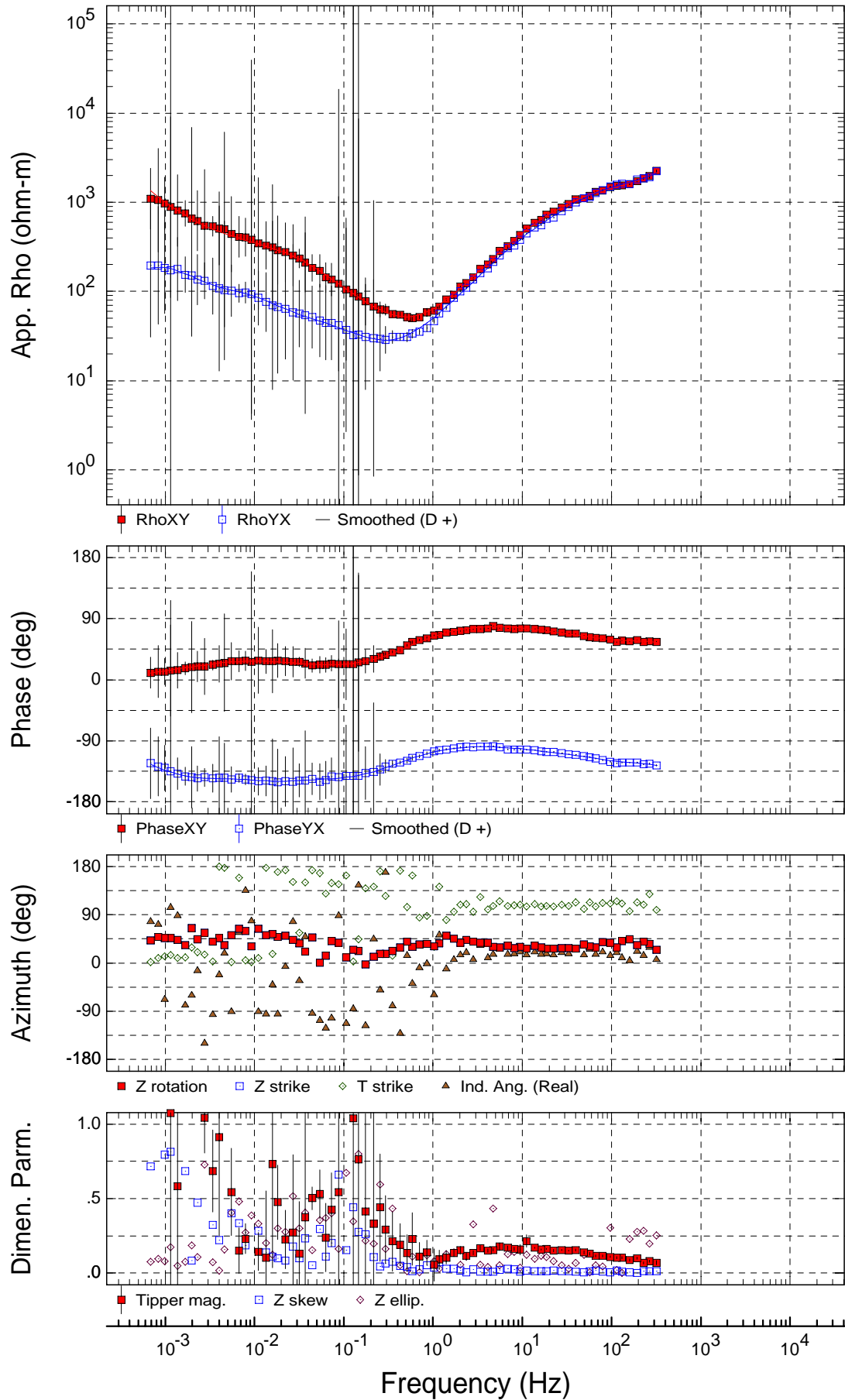


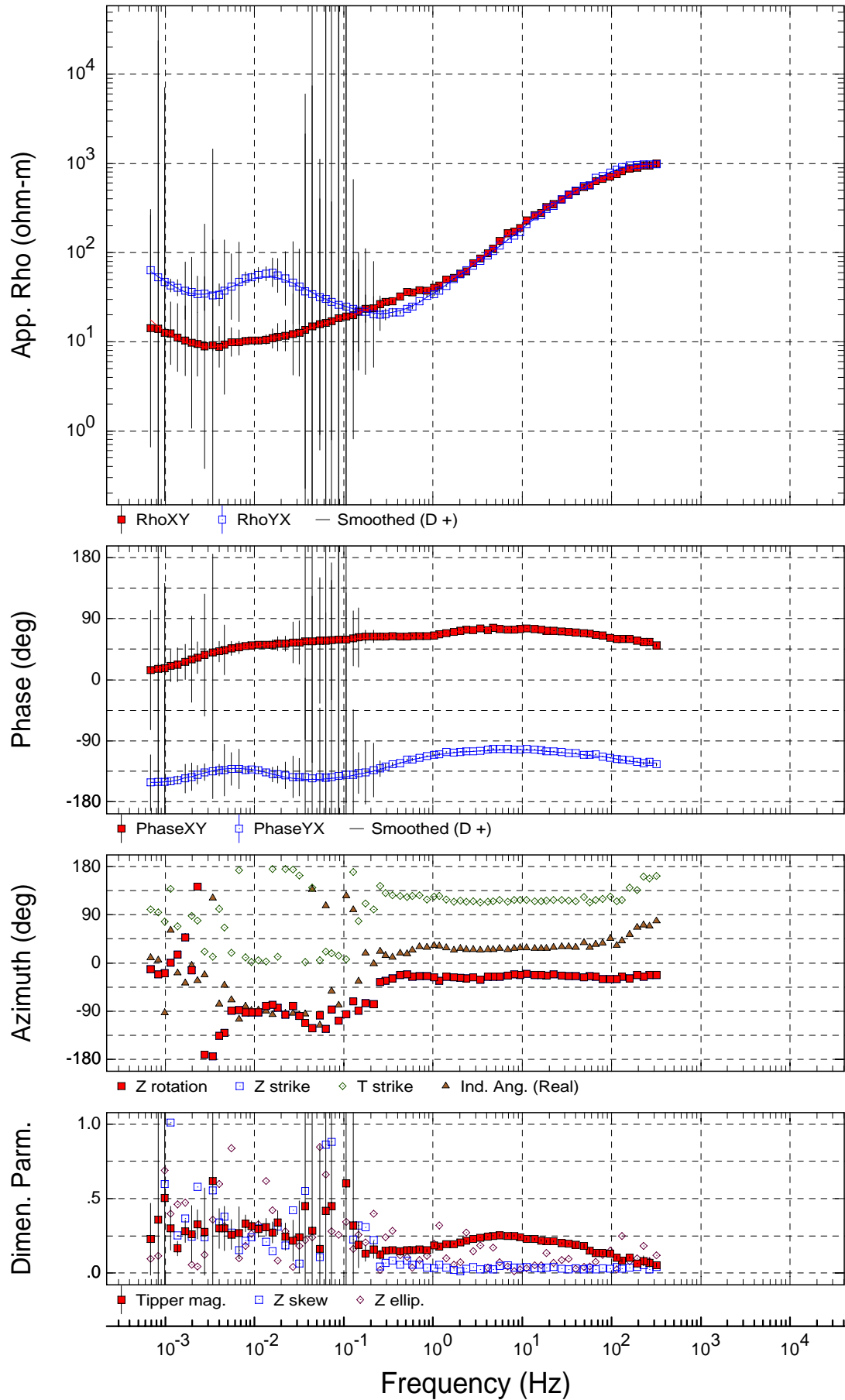




USGS
Rotation: PA

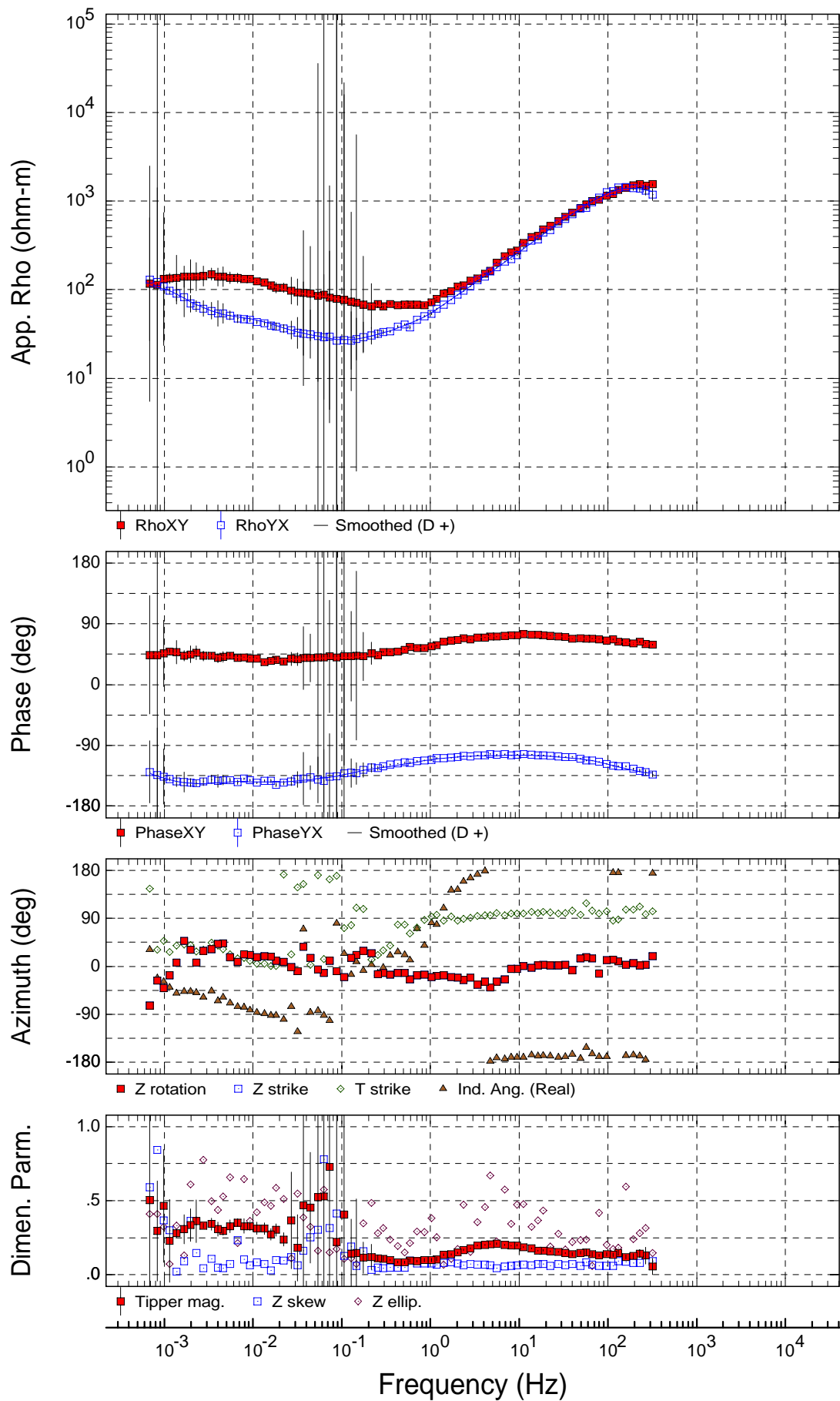
Sounding OR01





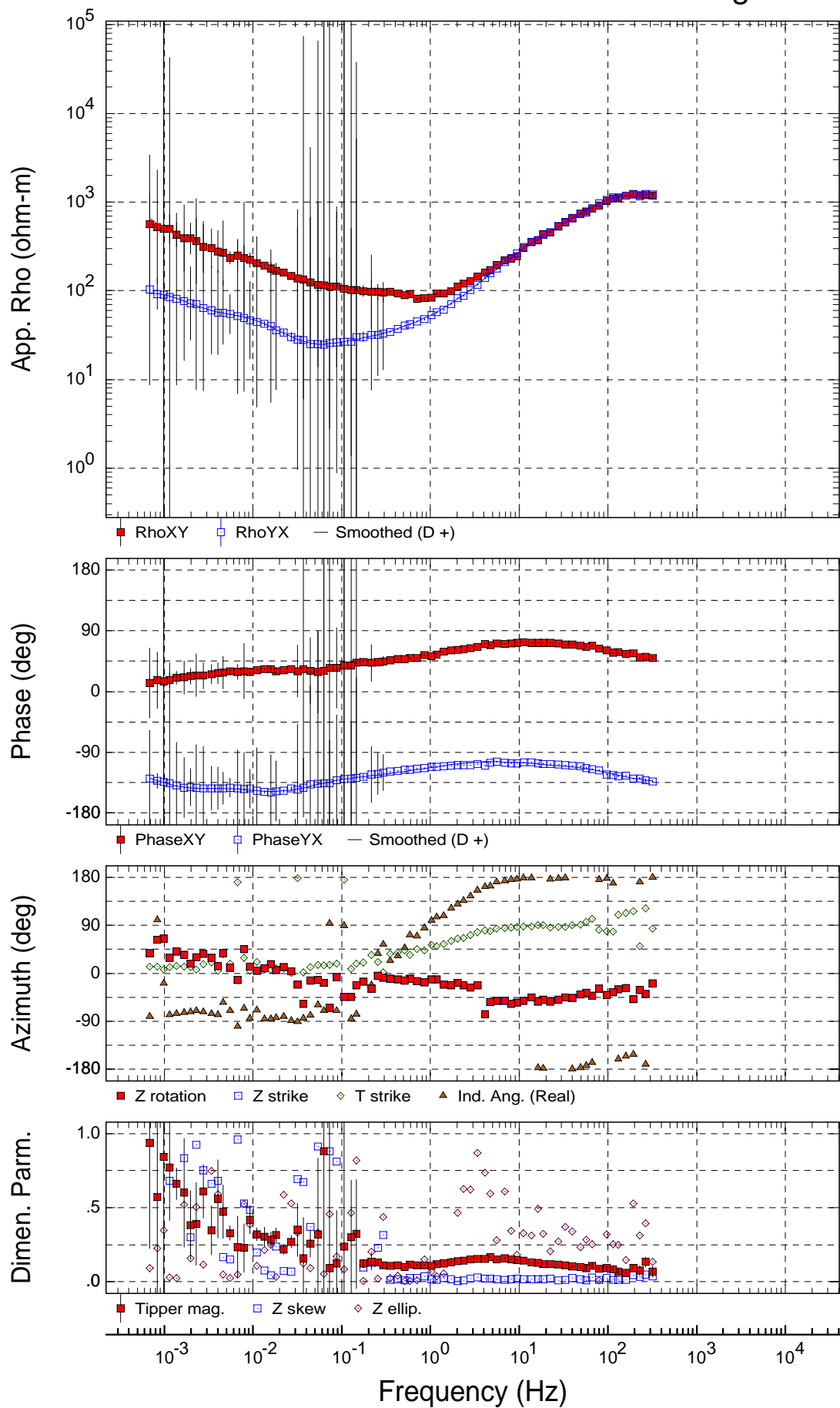
USGS
Rotation: PA

Sounding PK02



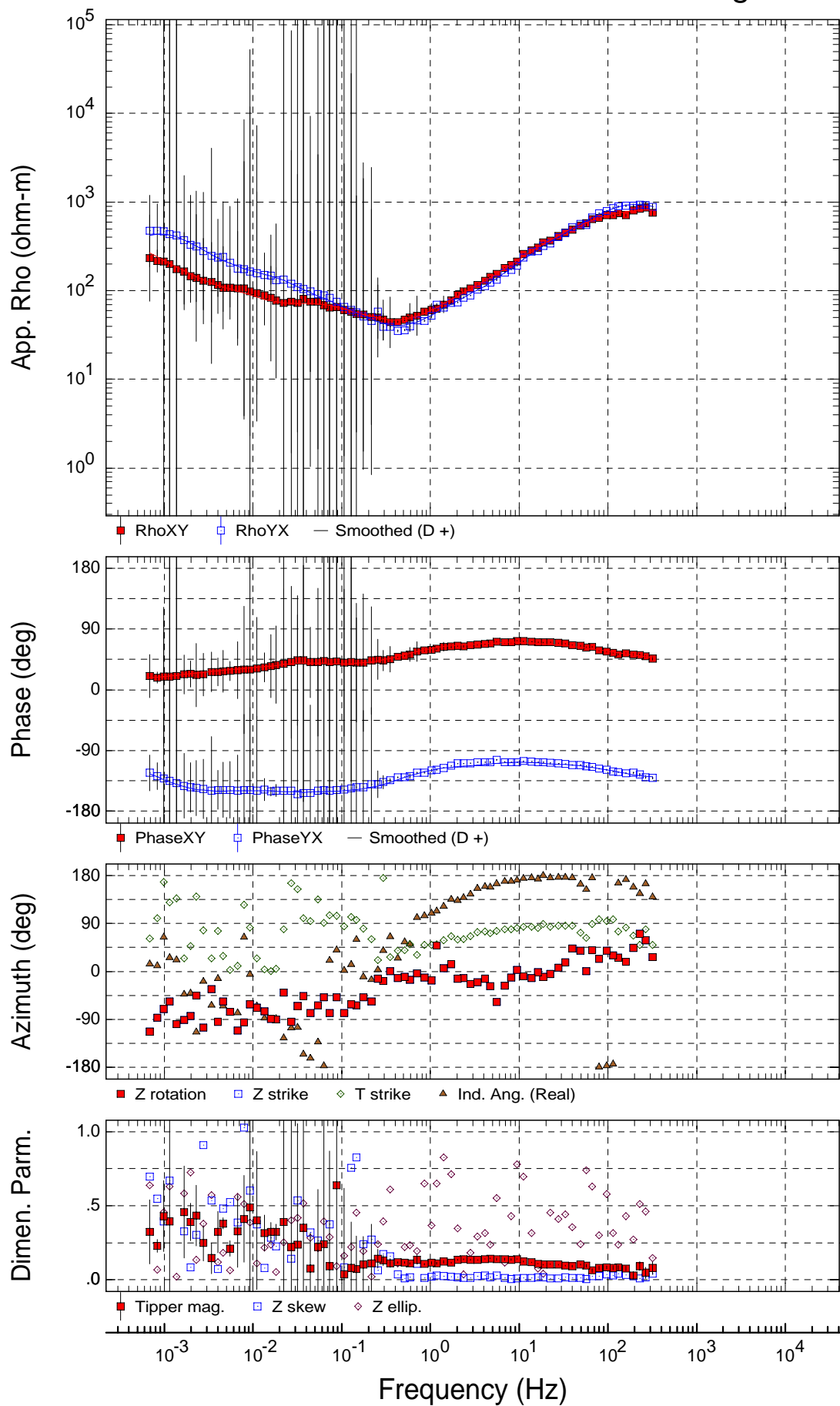
USGS
Rotation: PA

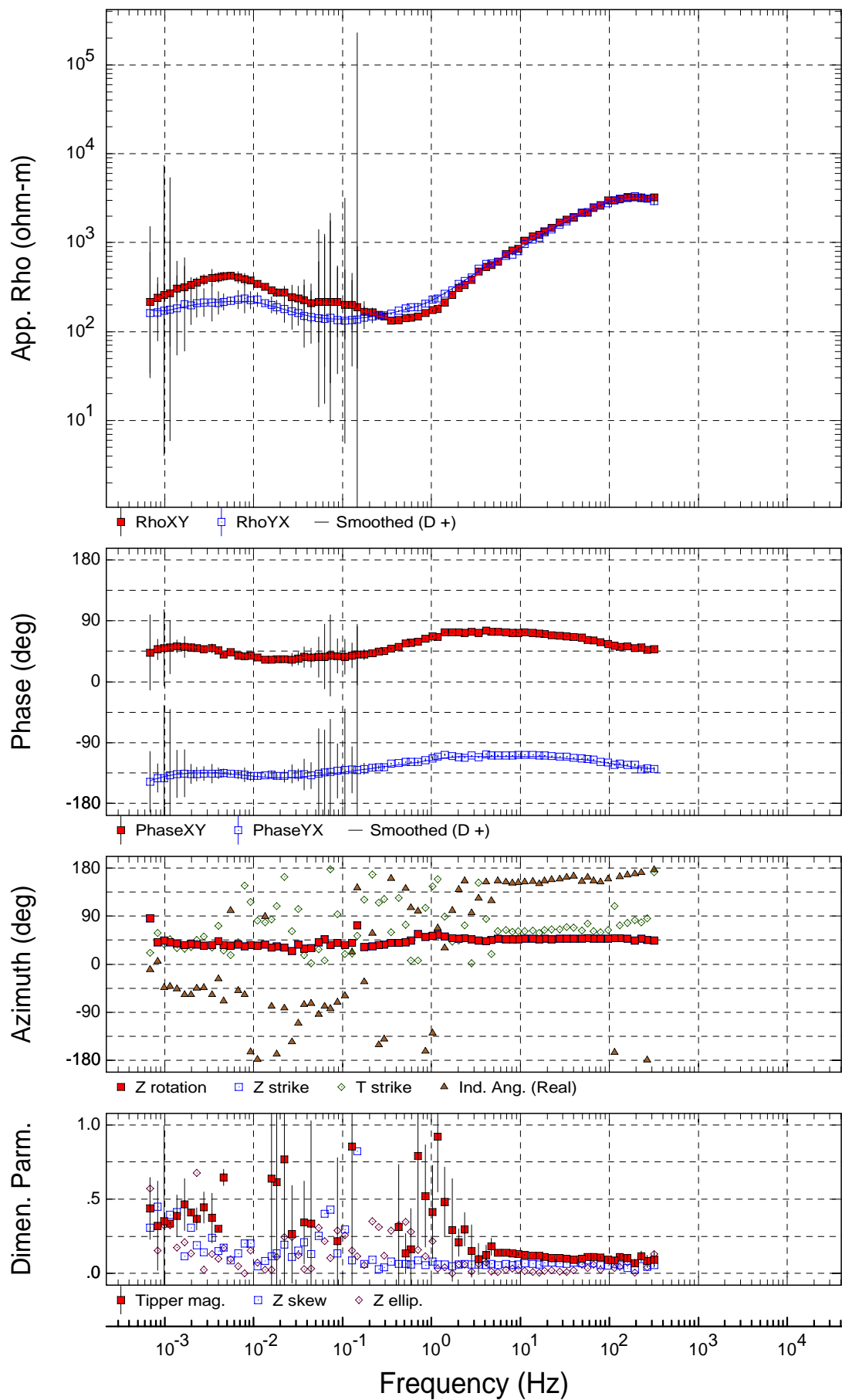
Sounding PK03



USGS
Rotation: PA

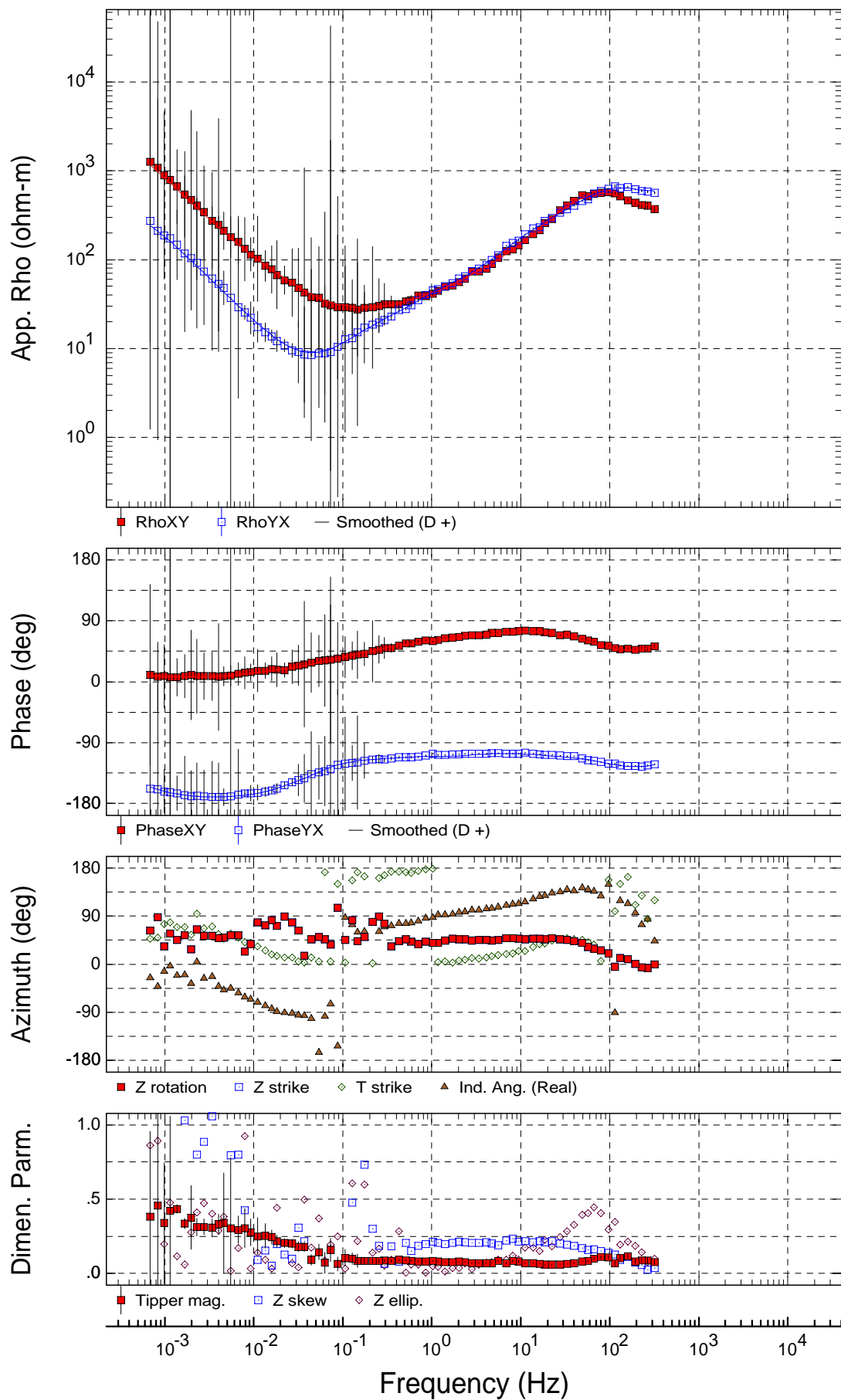
Sounding PK04





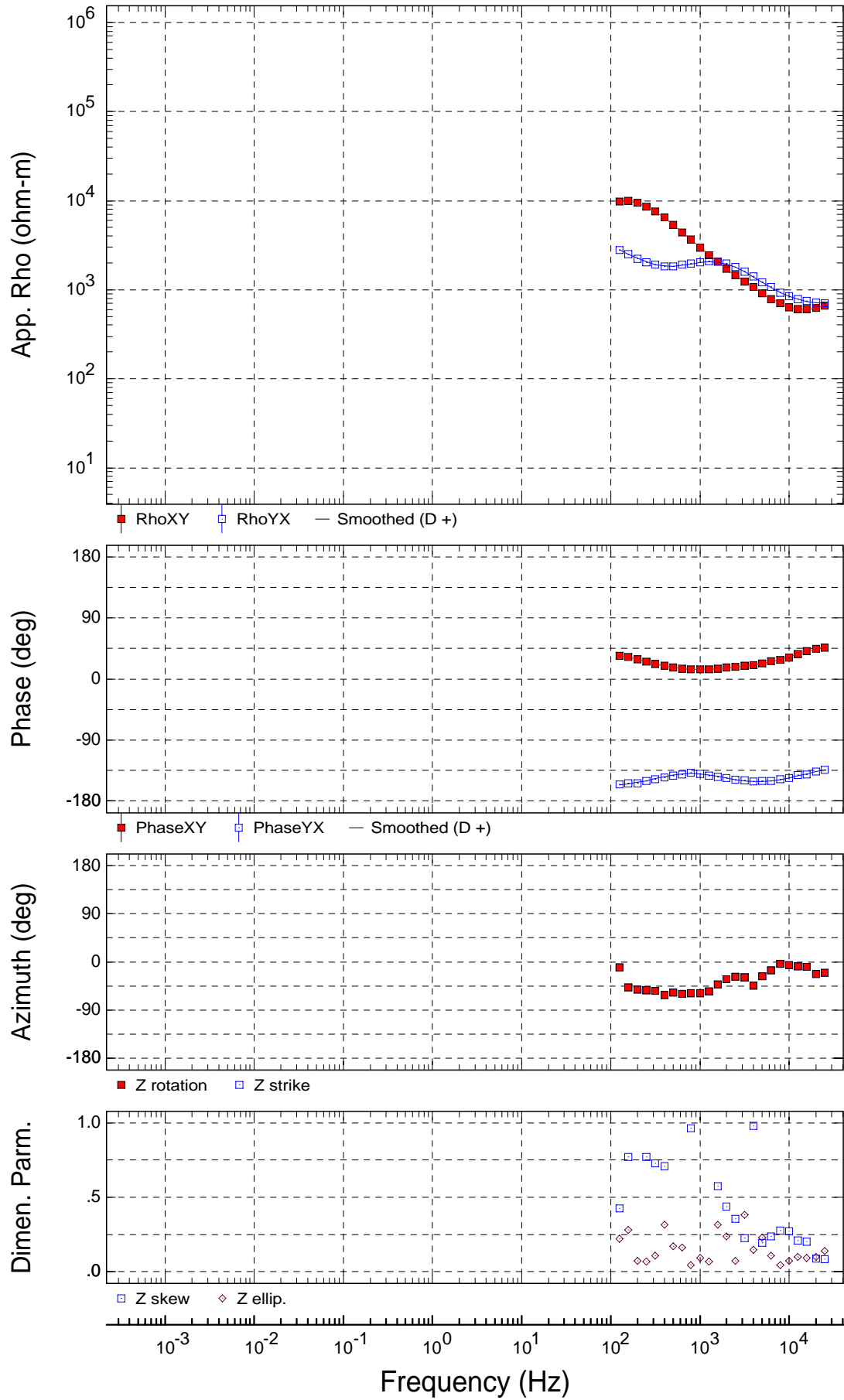
USGS
Rotation: PA

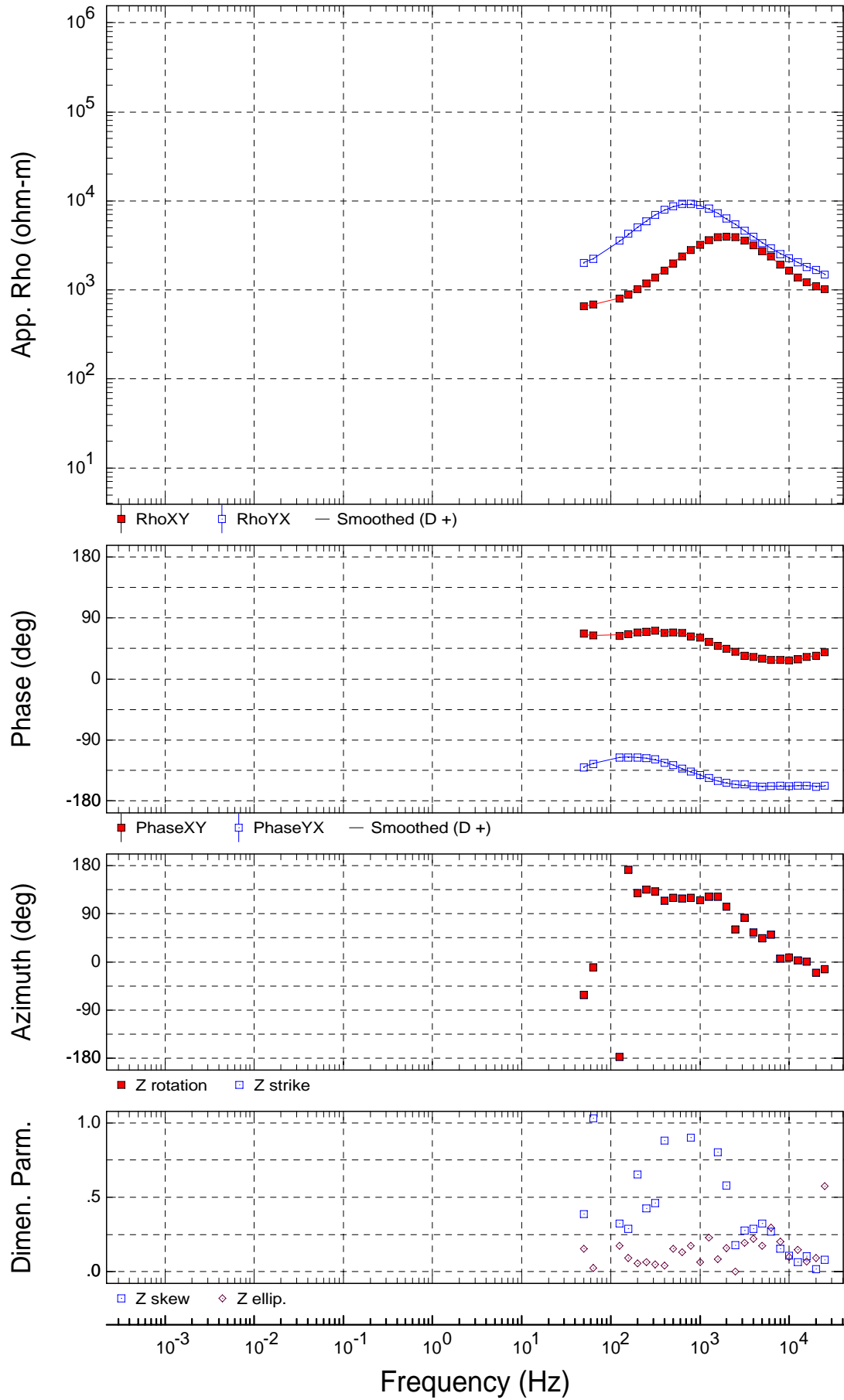
Sounding REF1



USGS
Rotation: PA

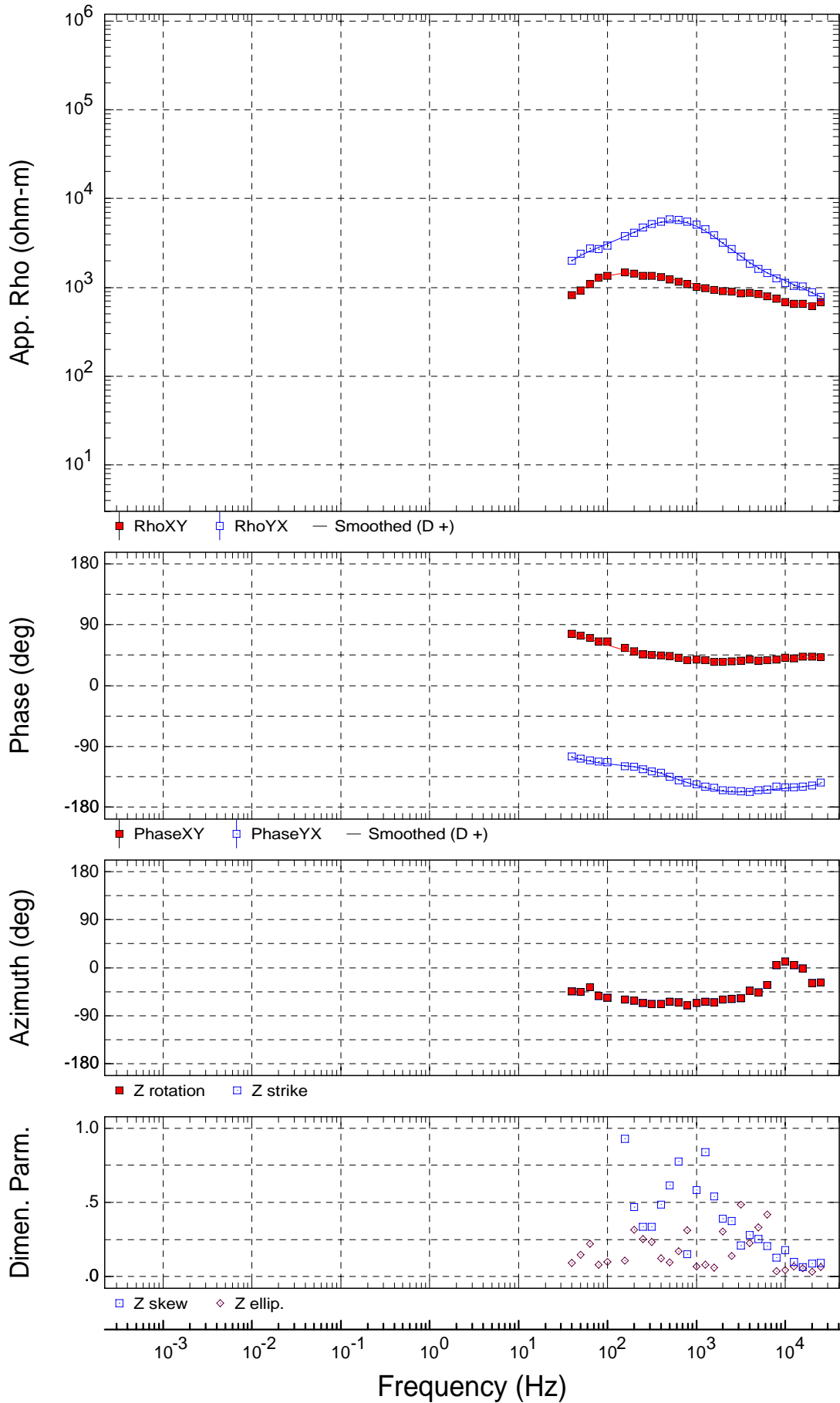
Sounding SR005

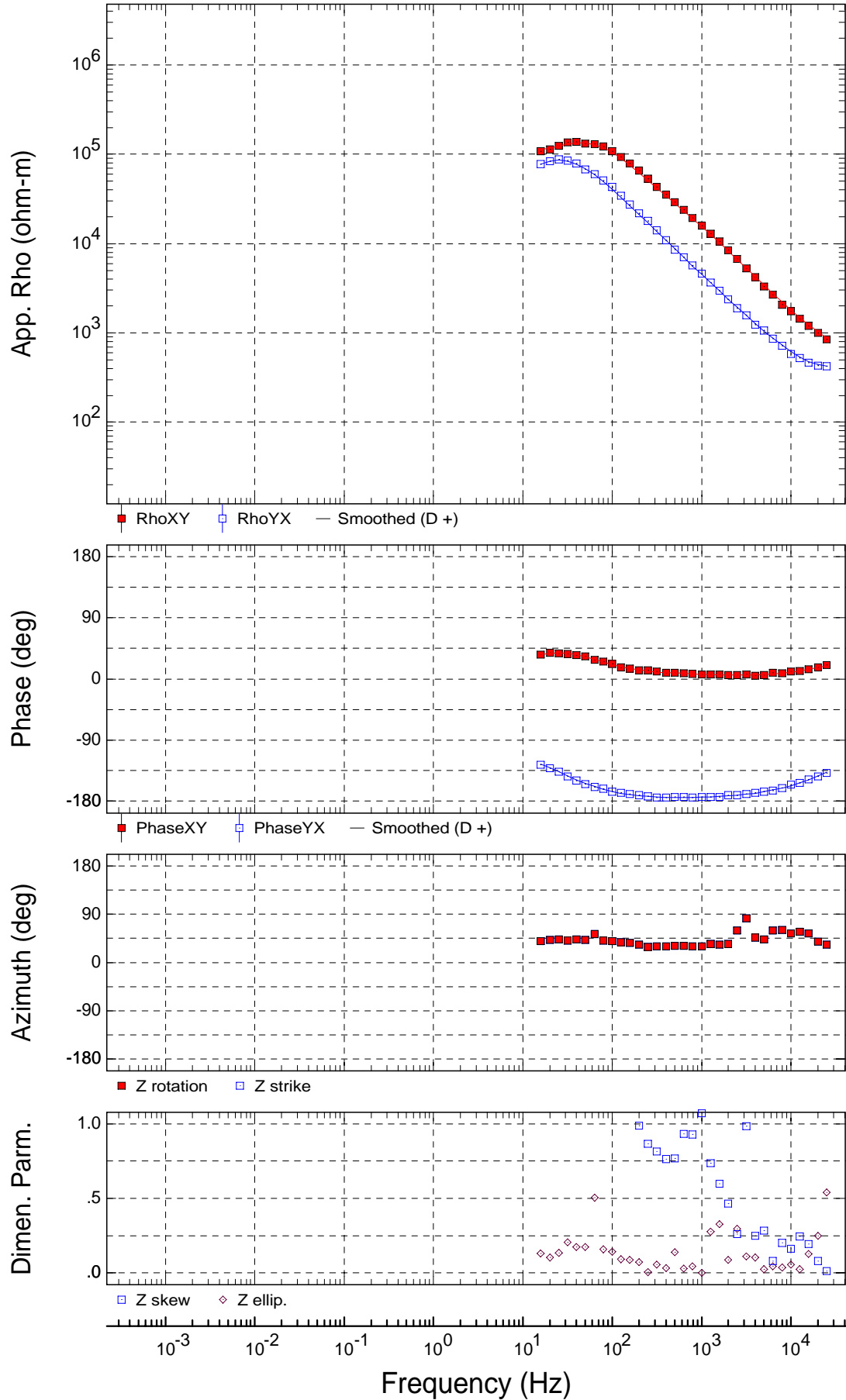


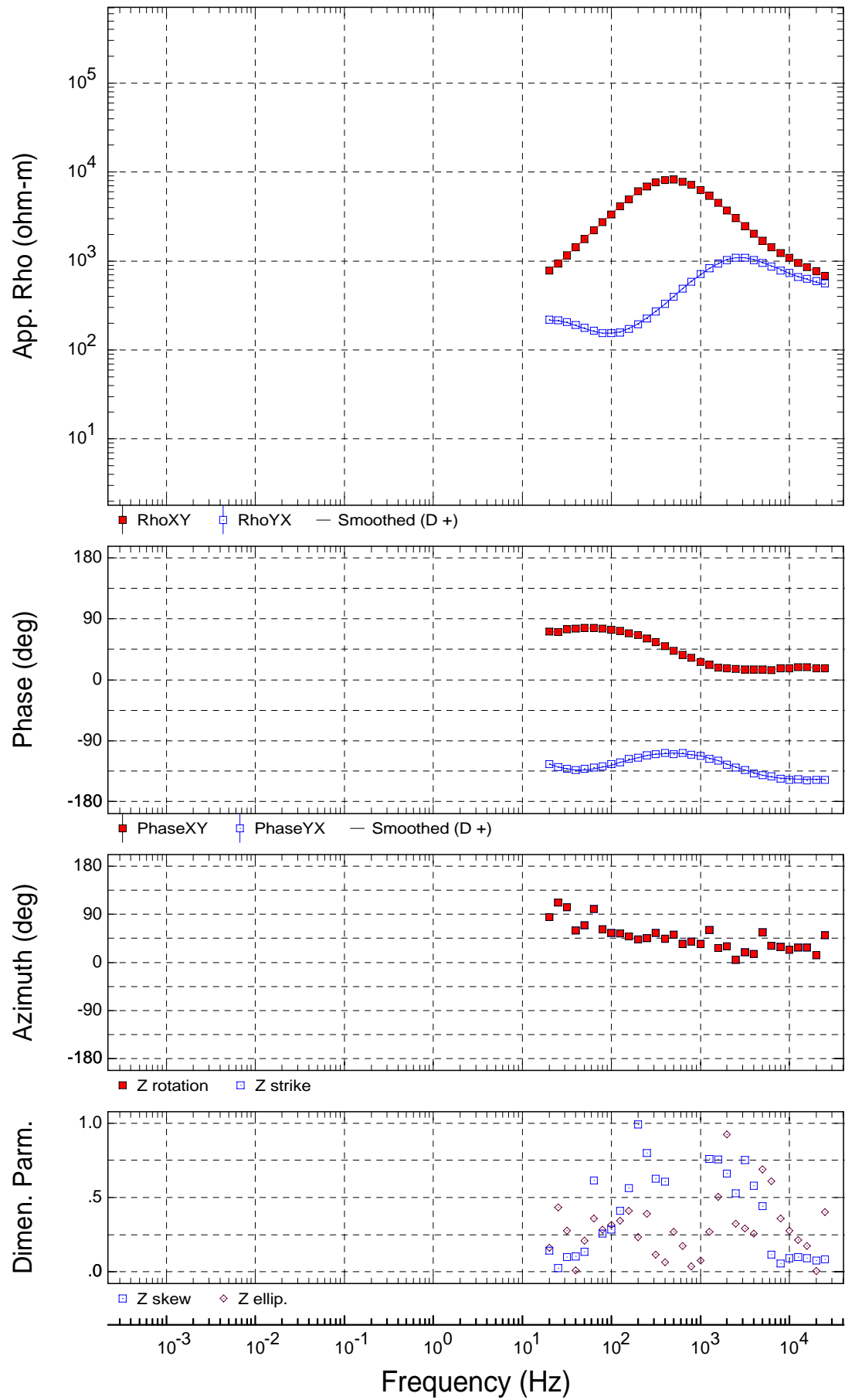


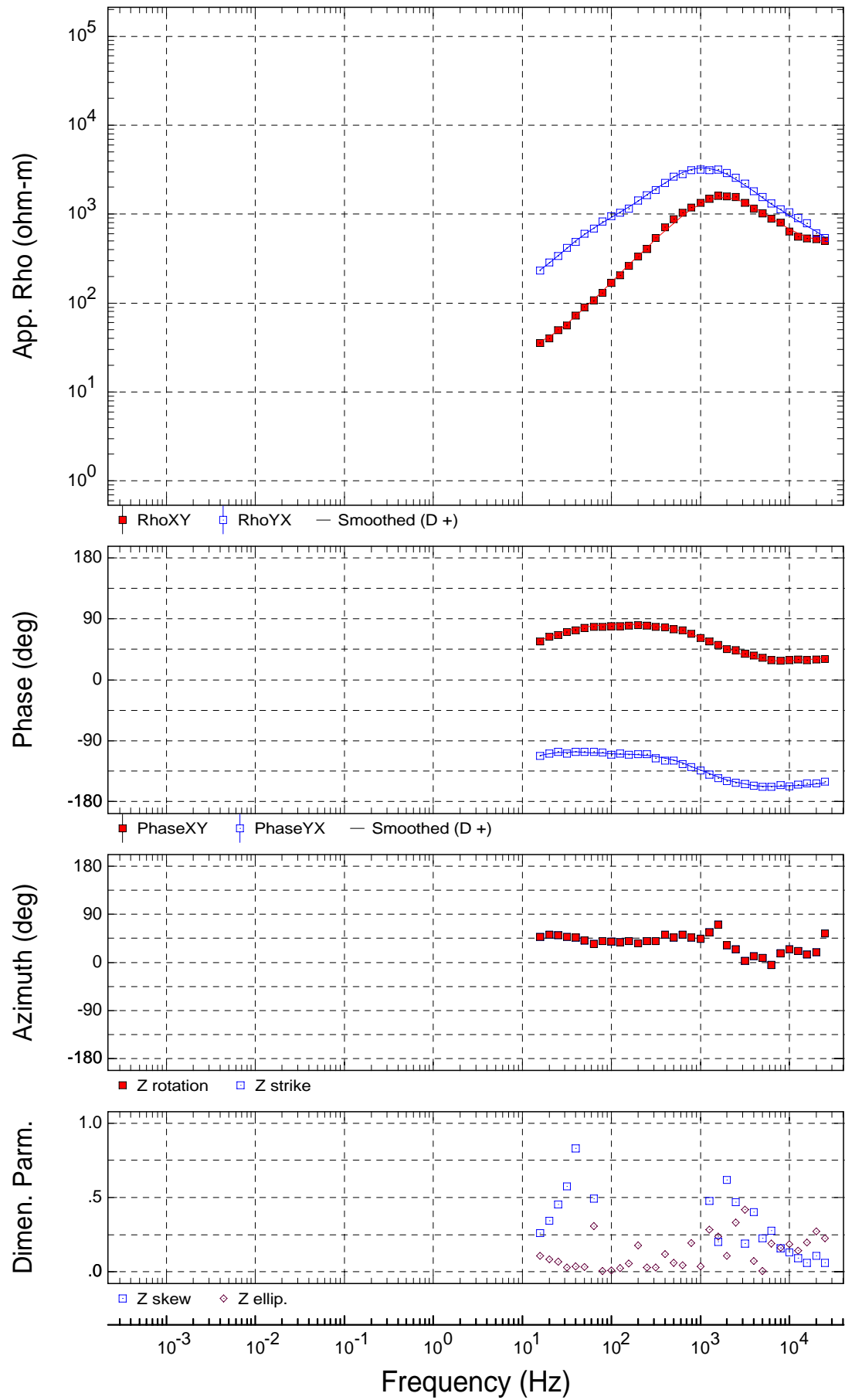
USGS
Rotation: PA

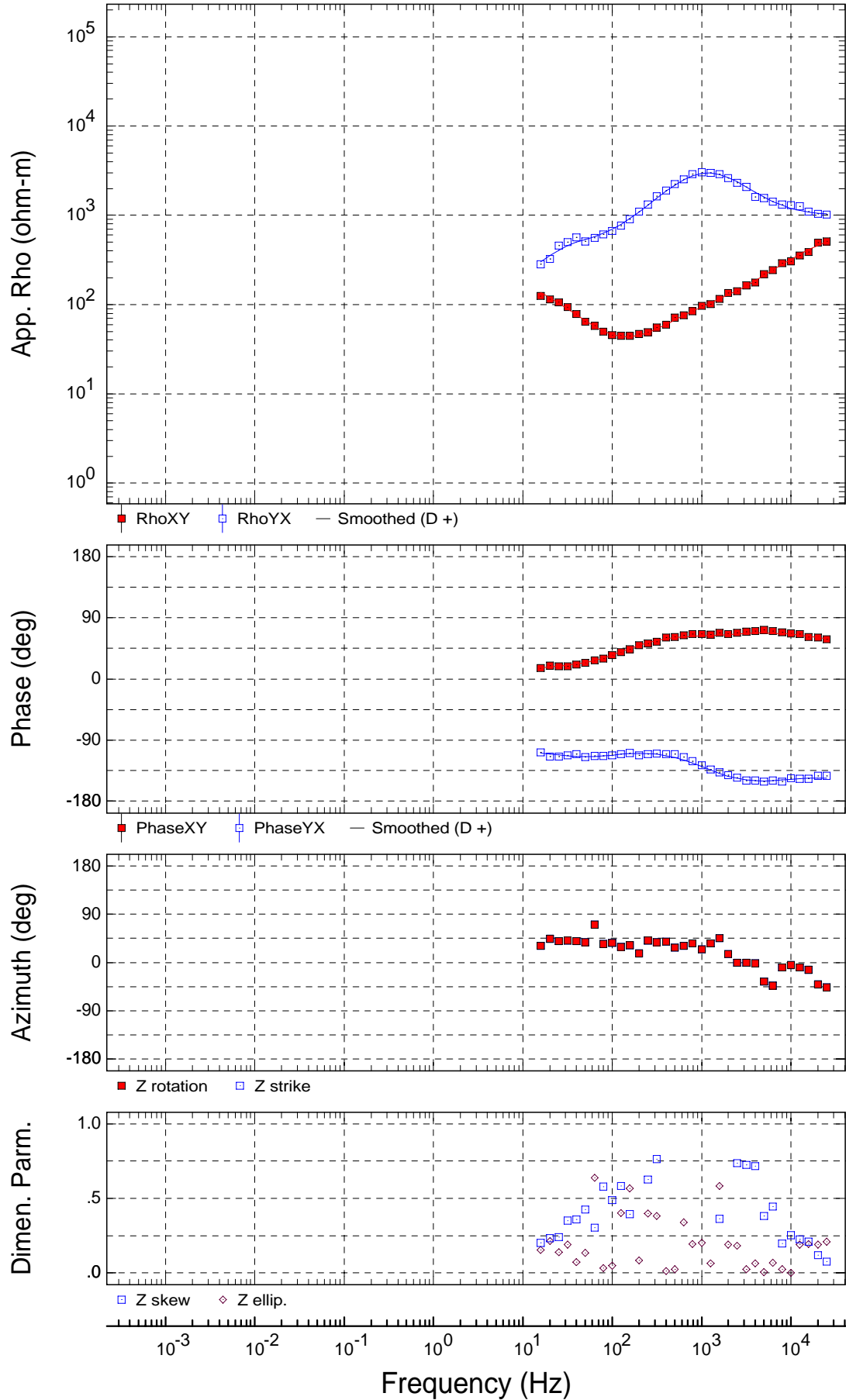
Sounding SR007

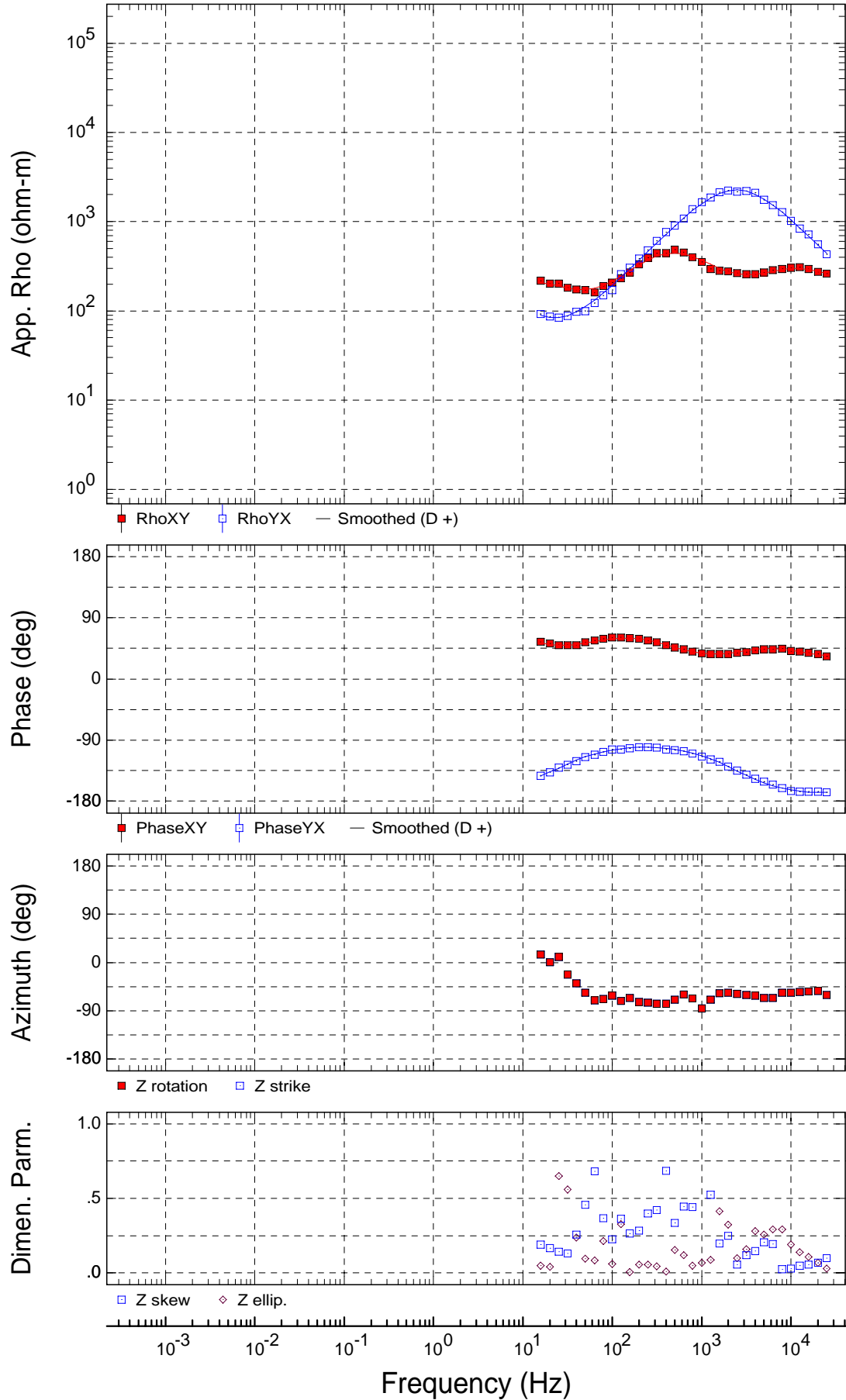


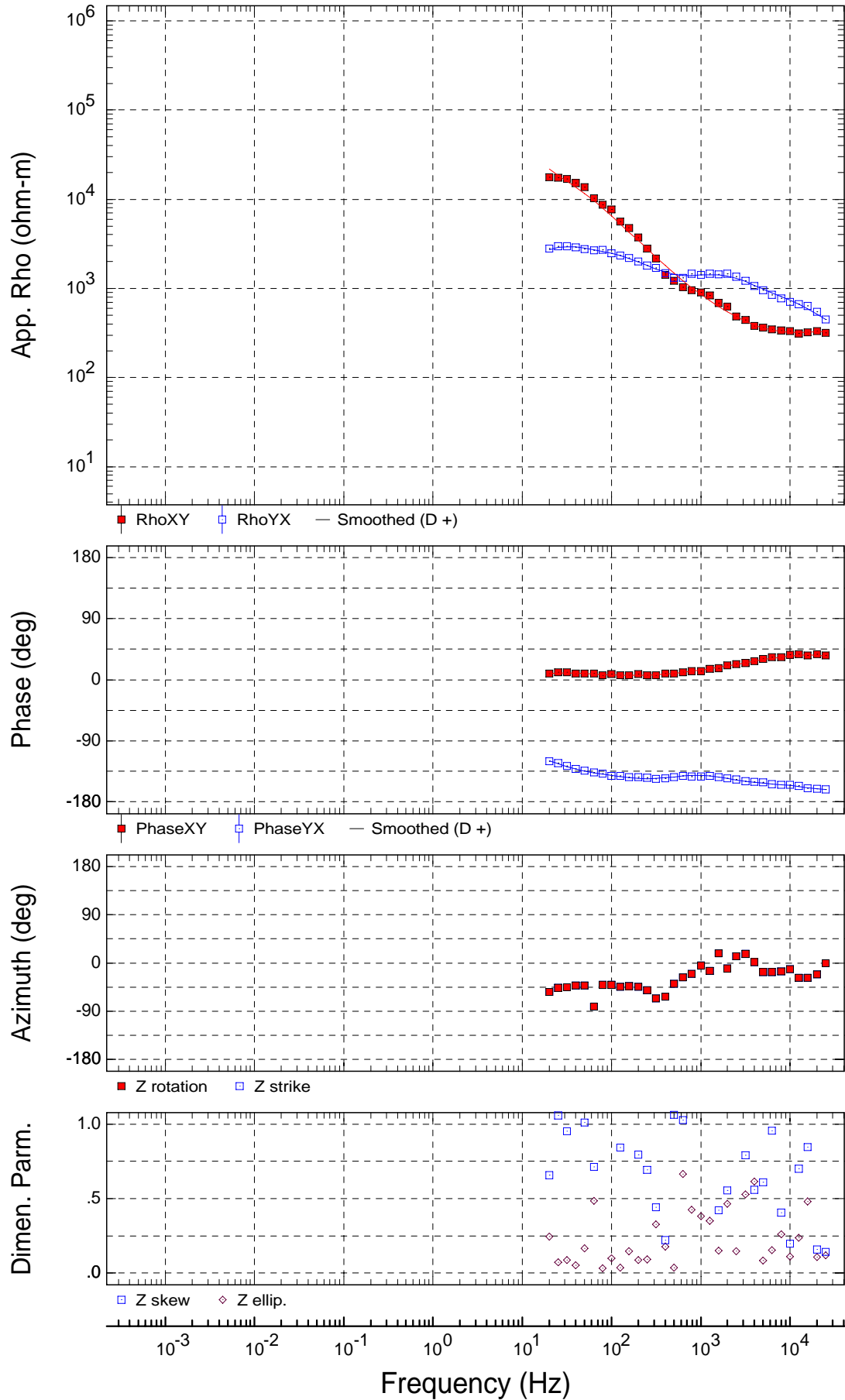


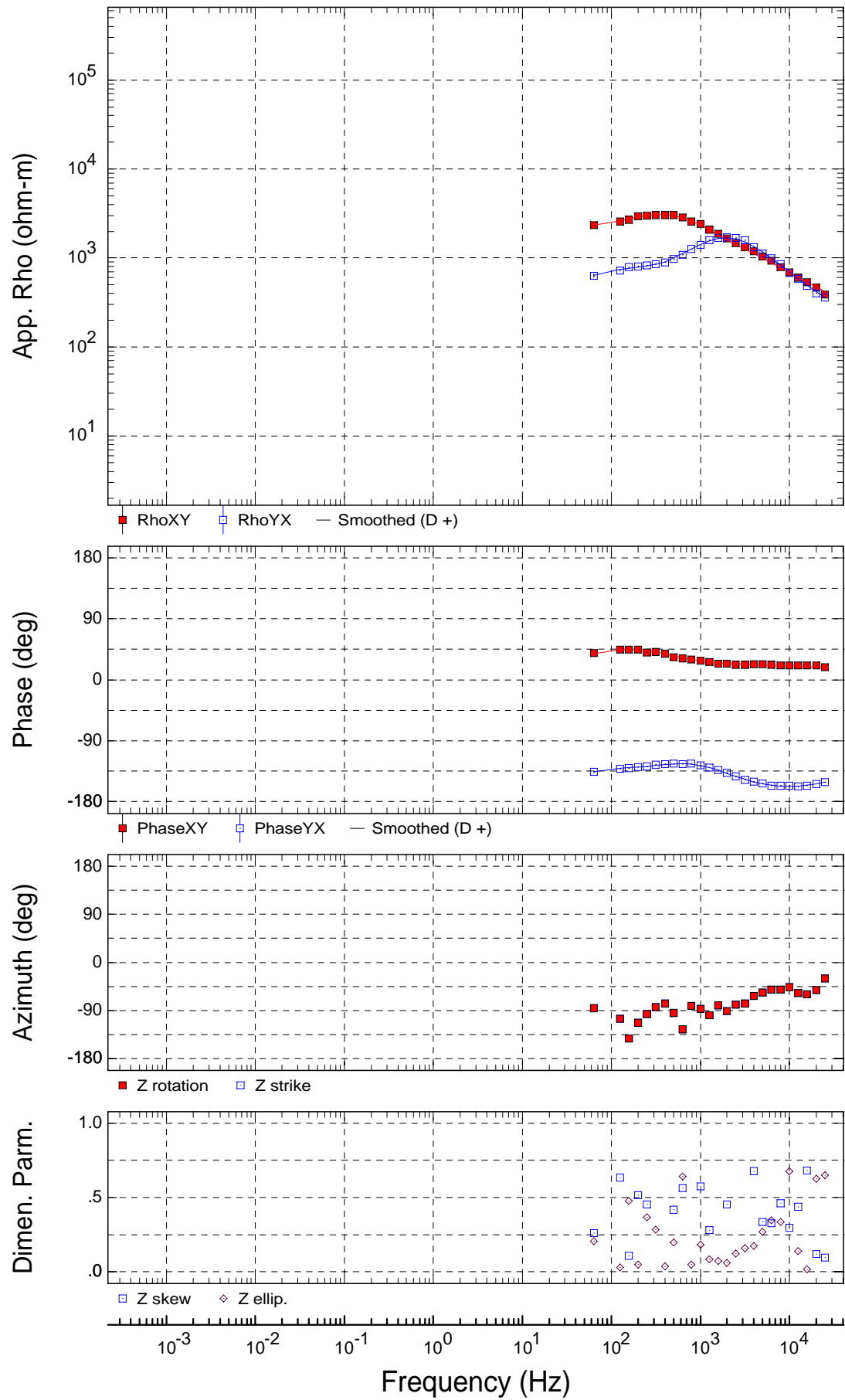


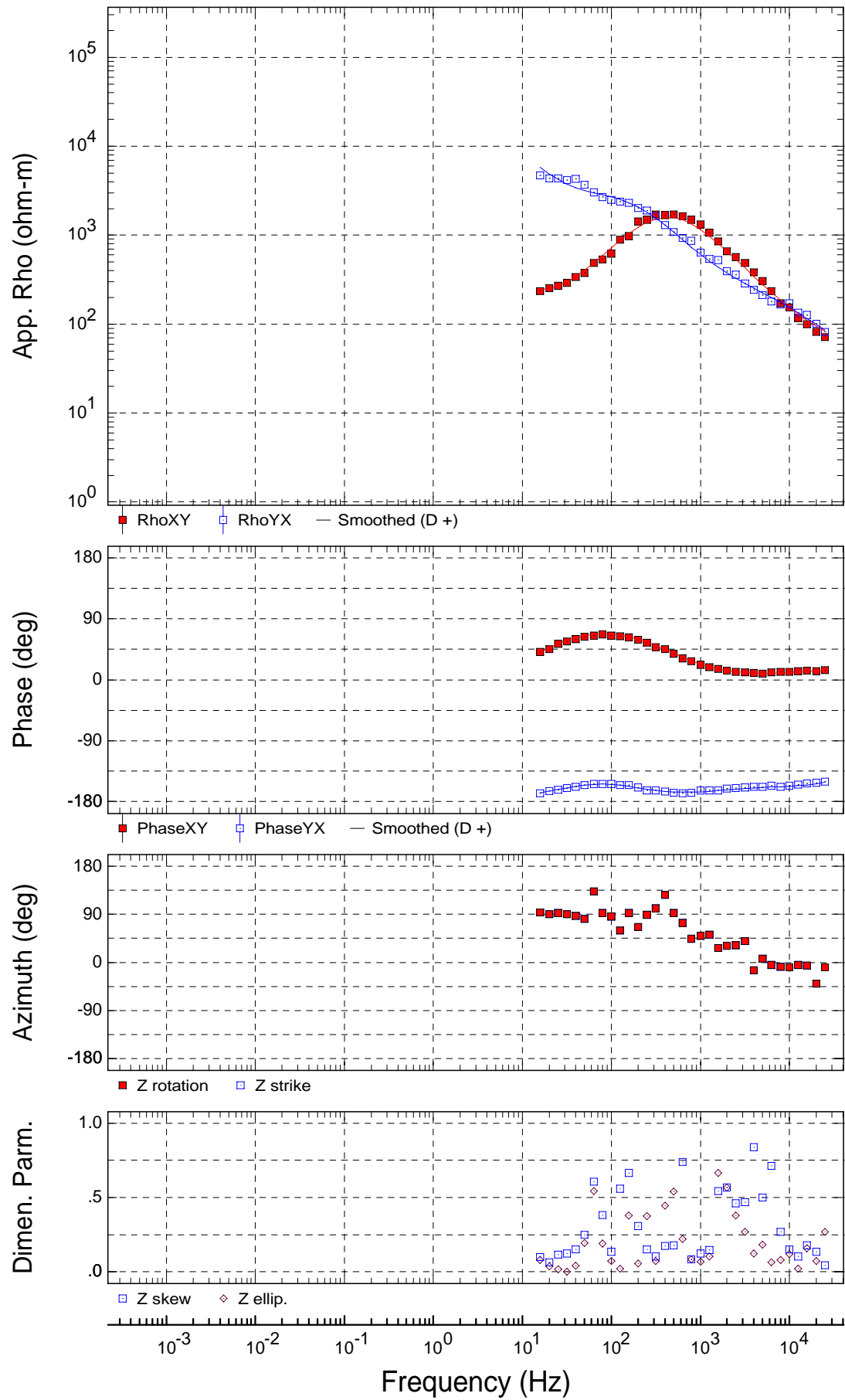


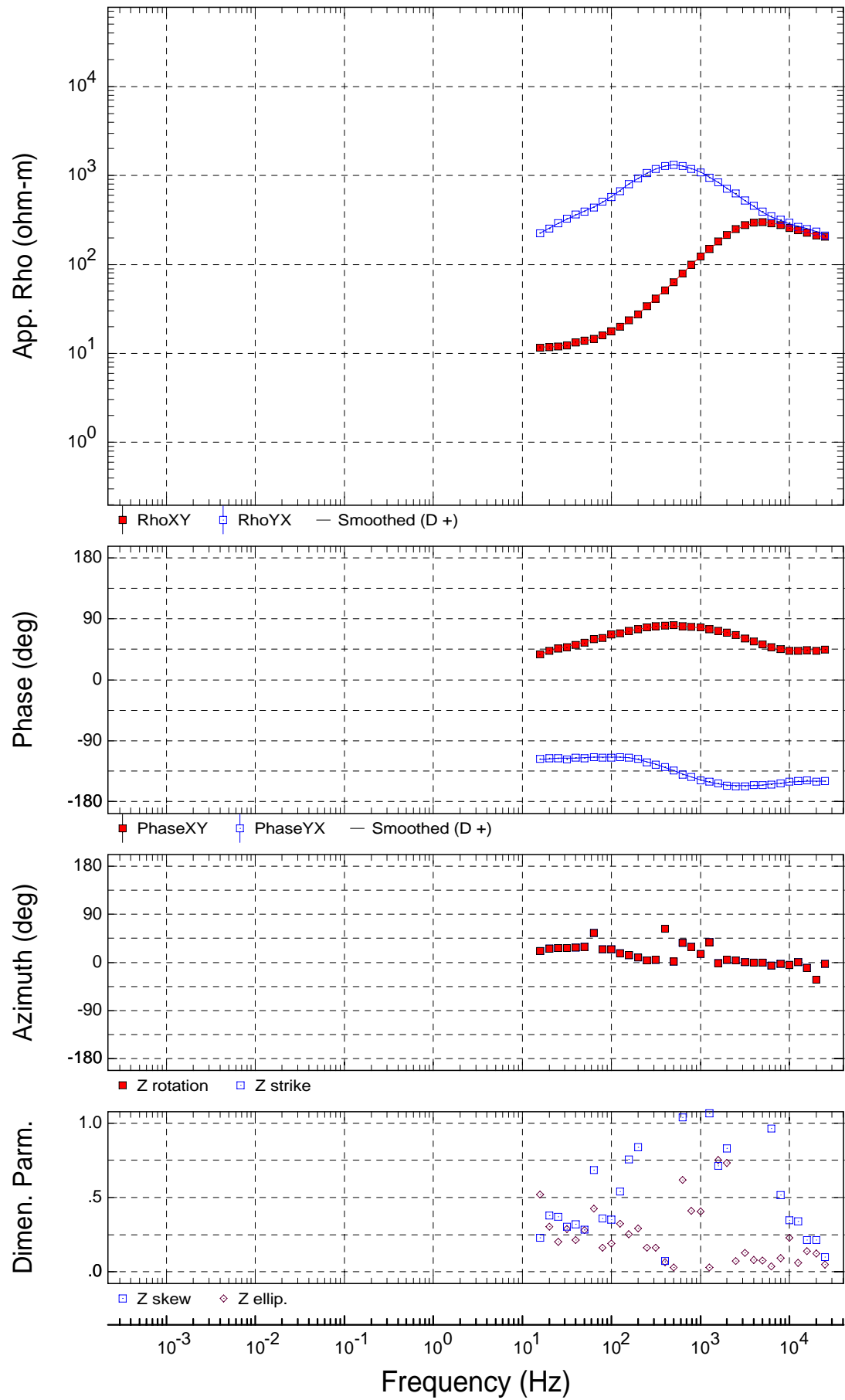


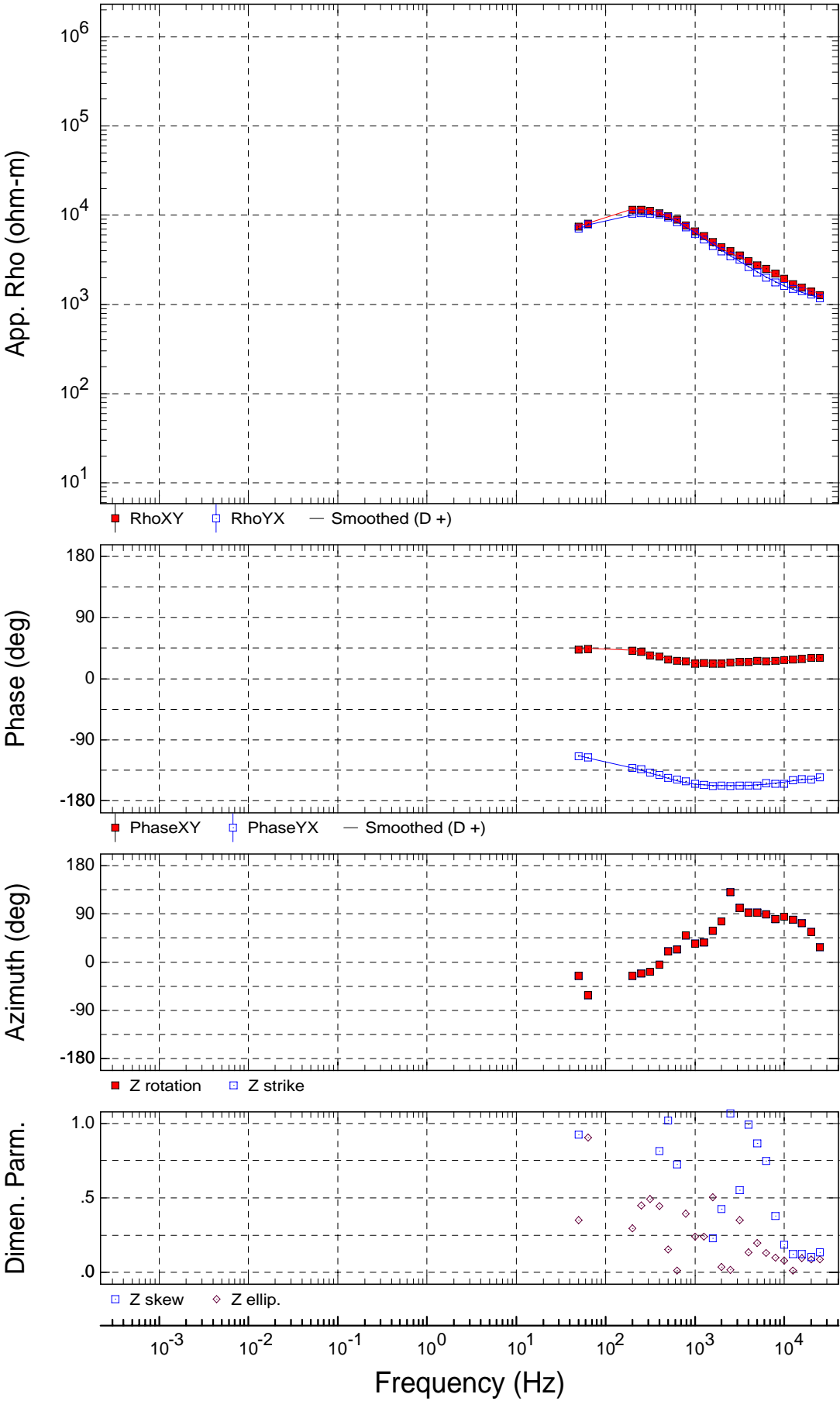


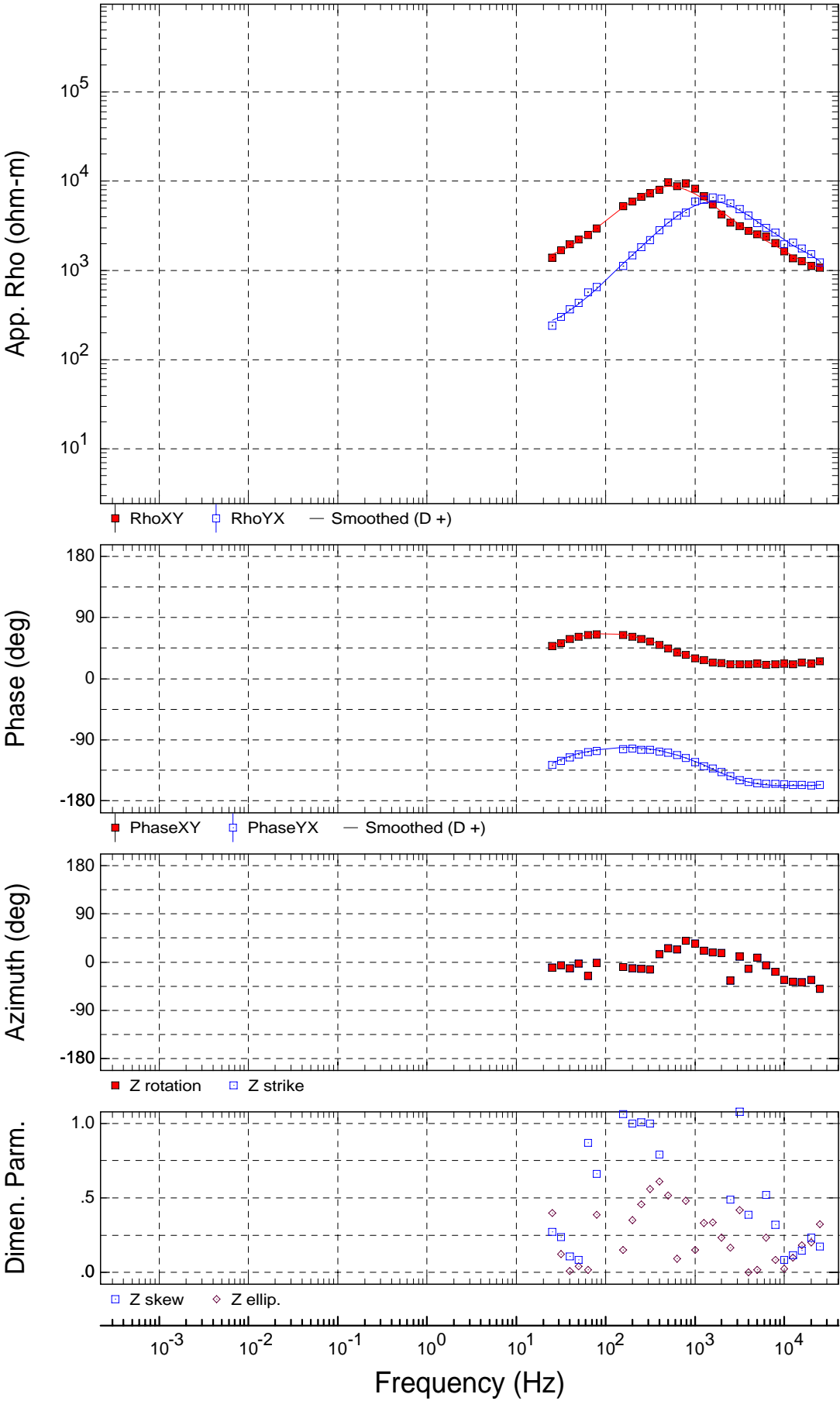


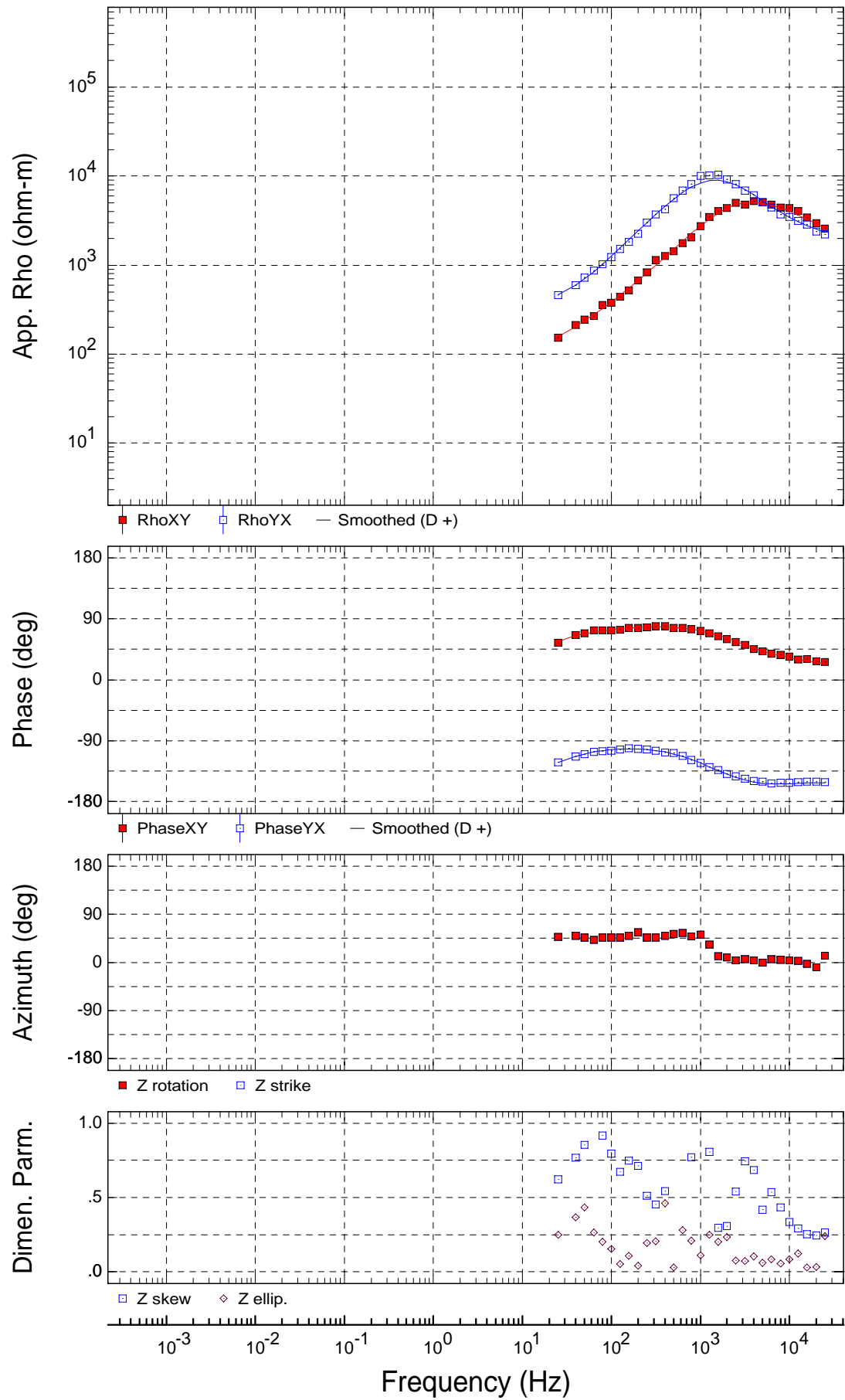


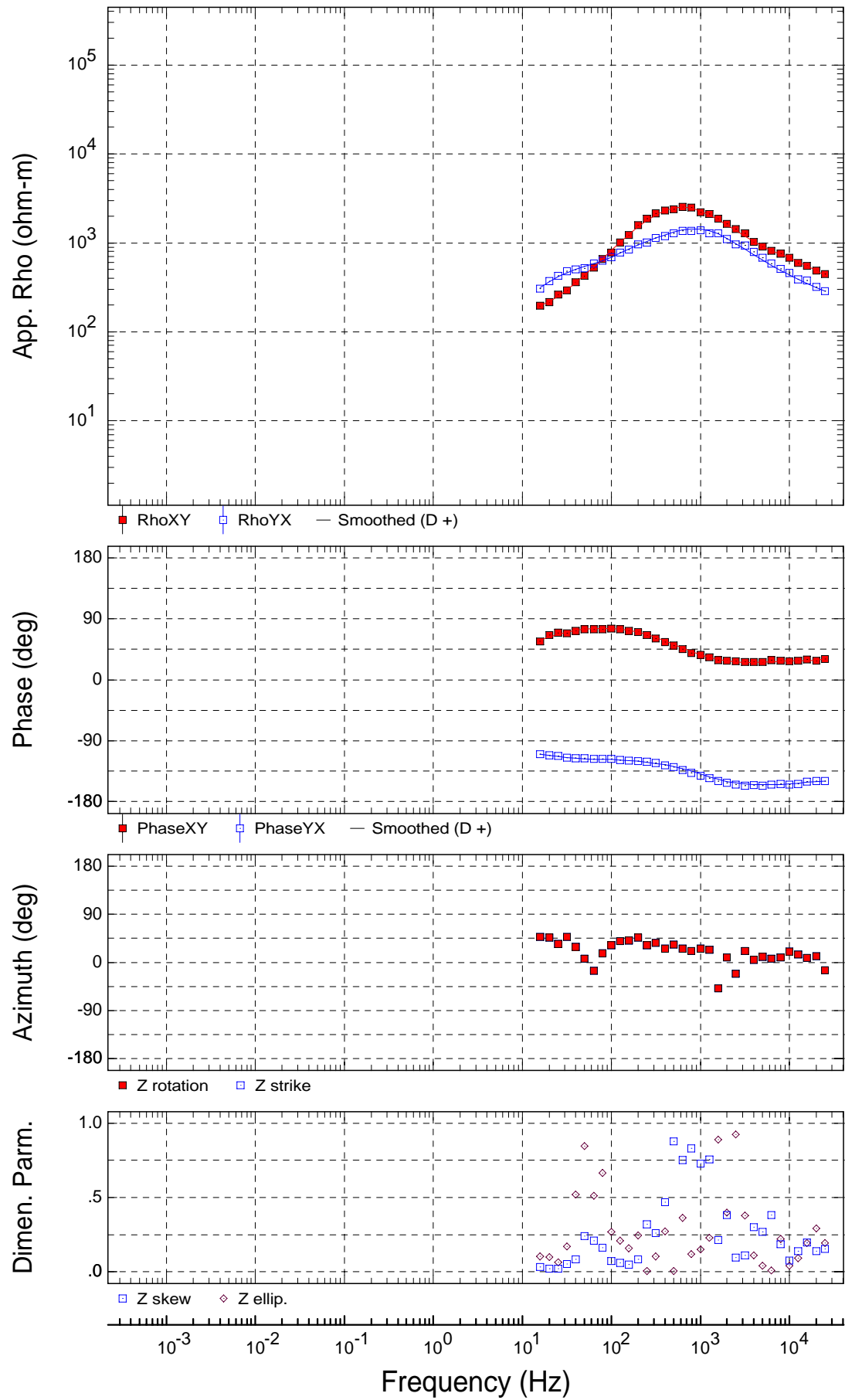


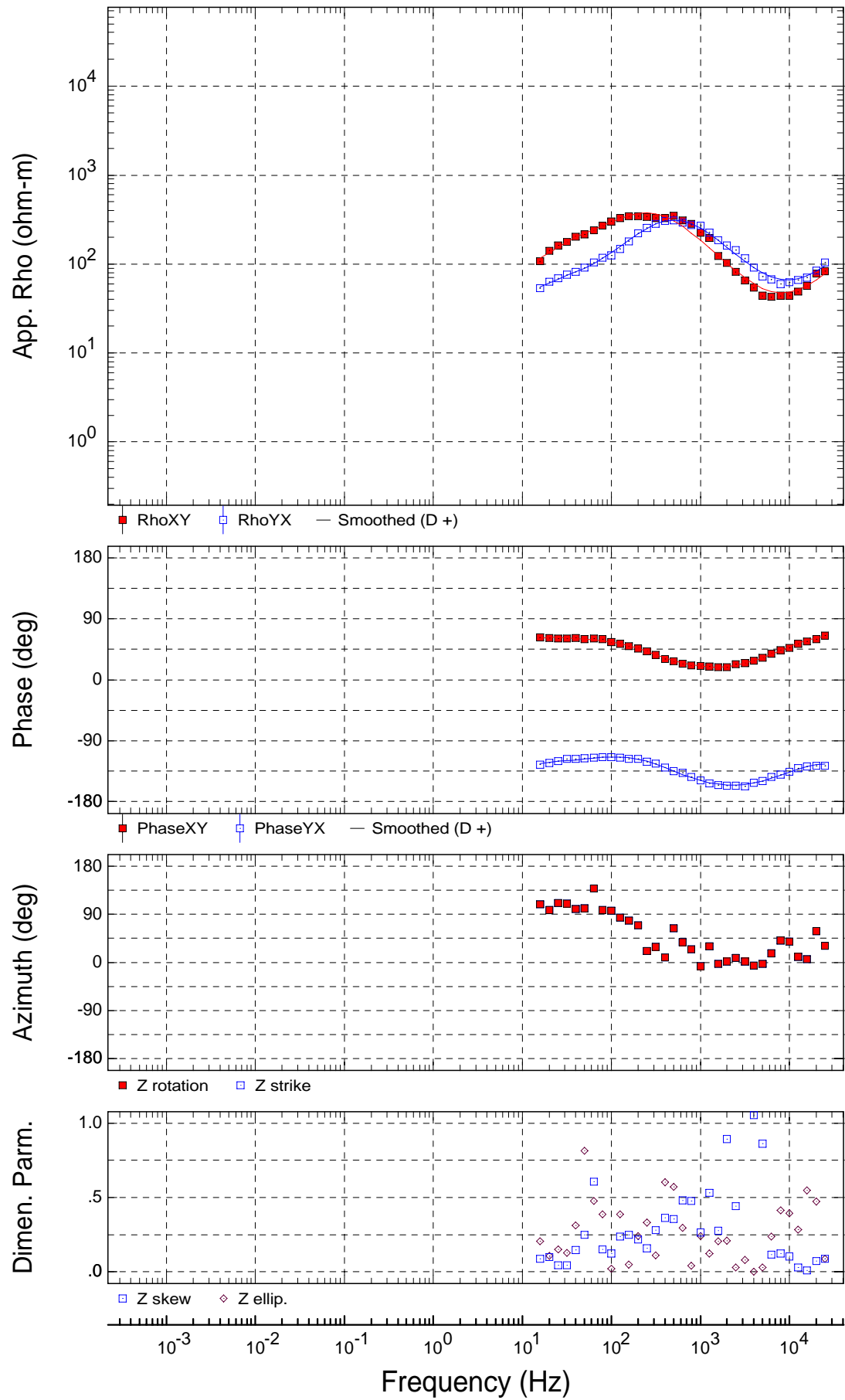


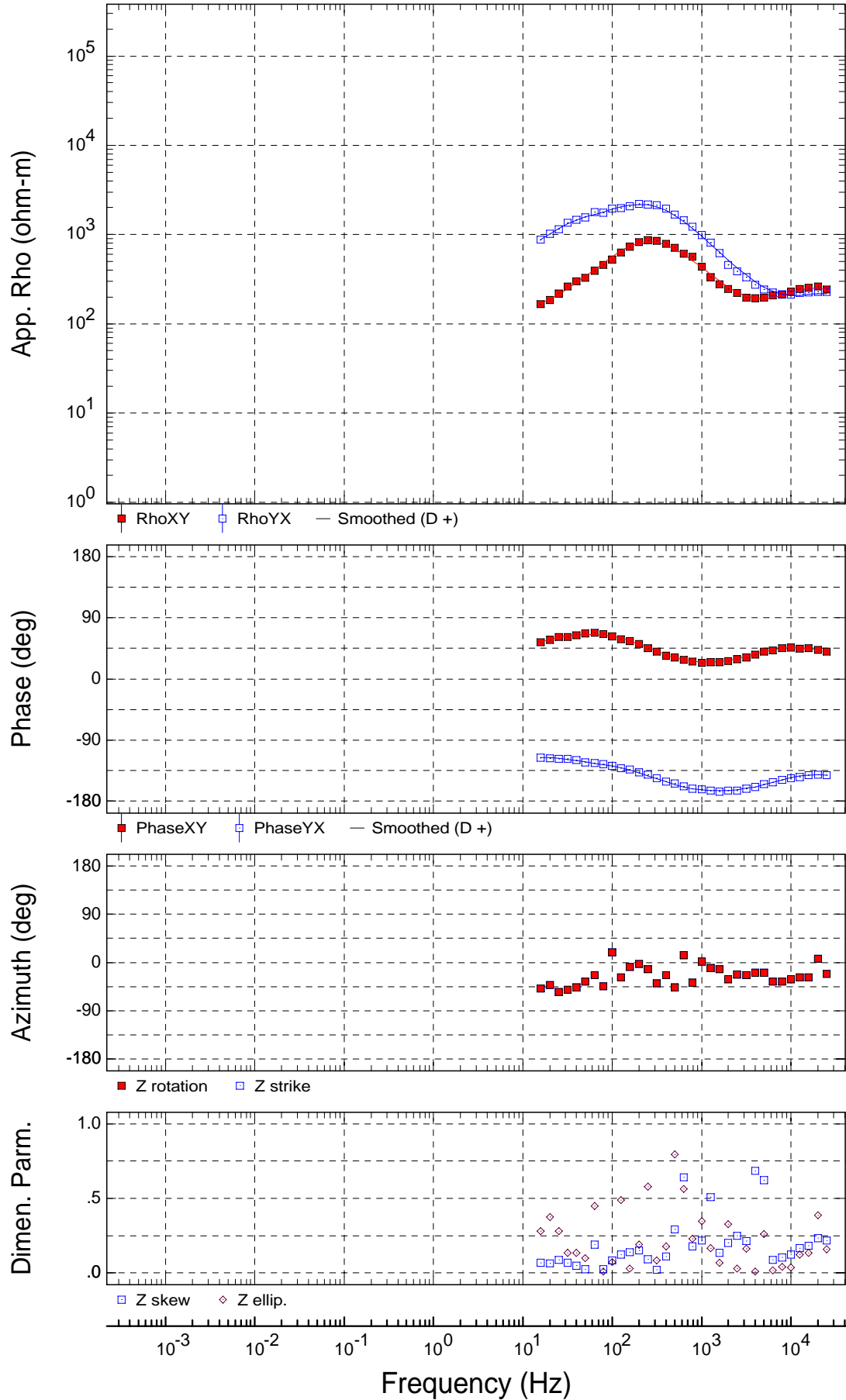






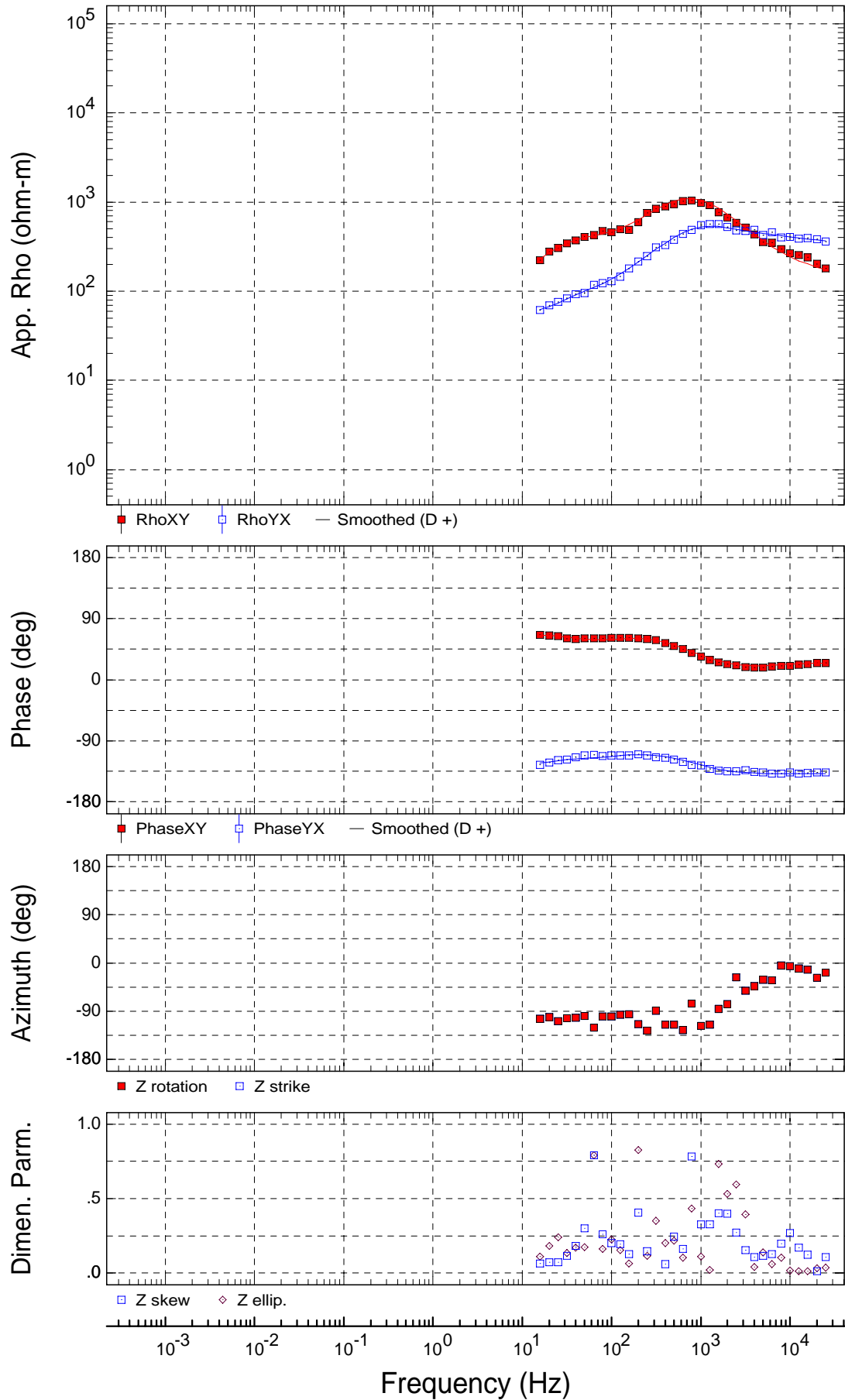


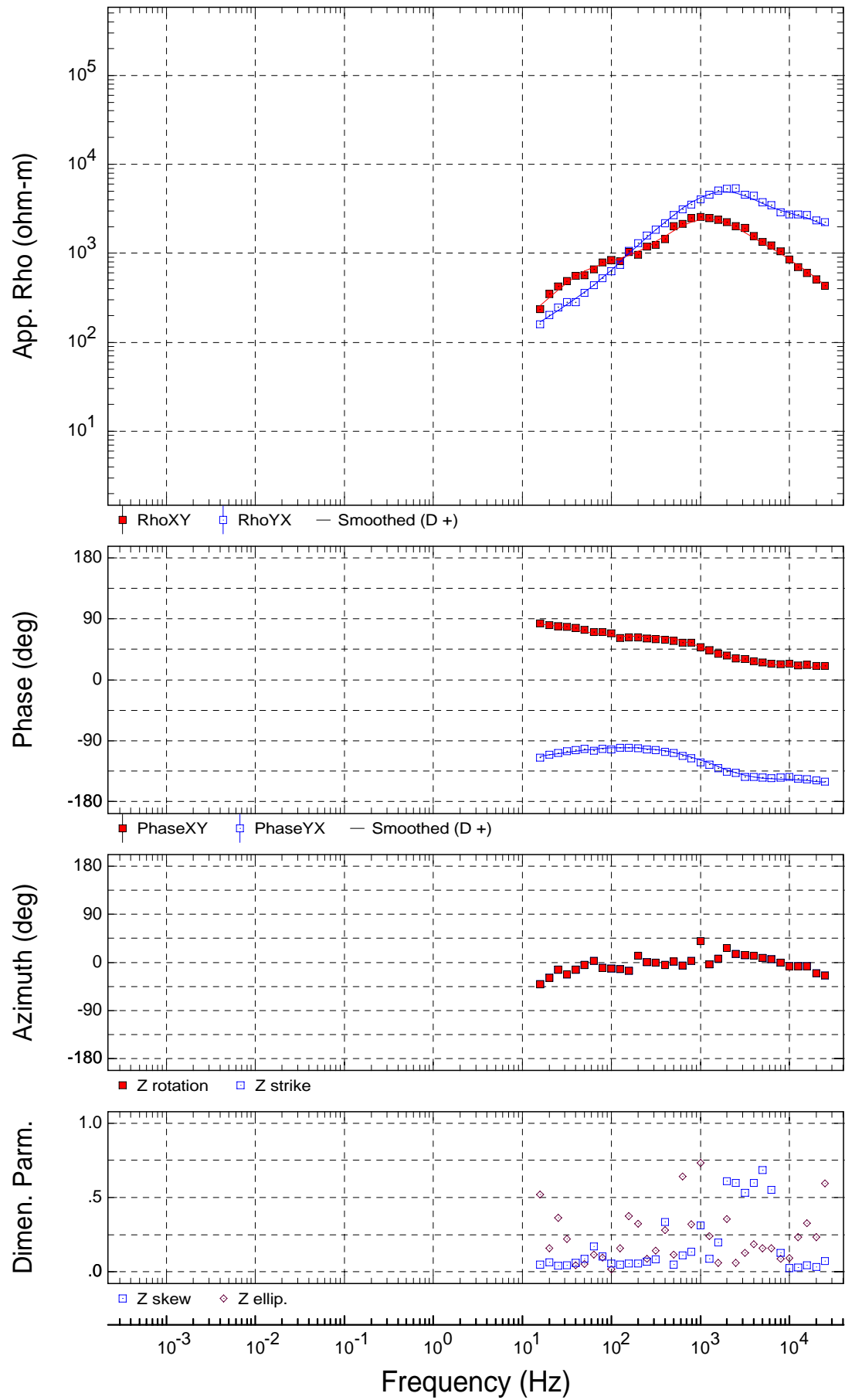


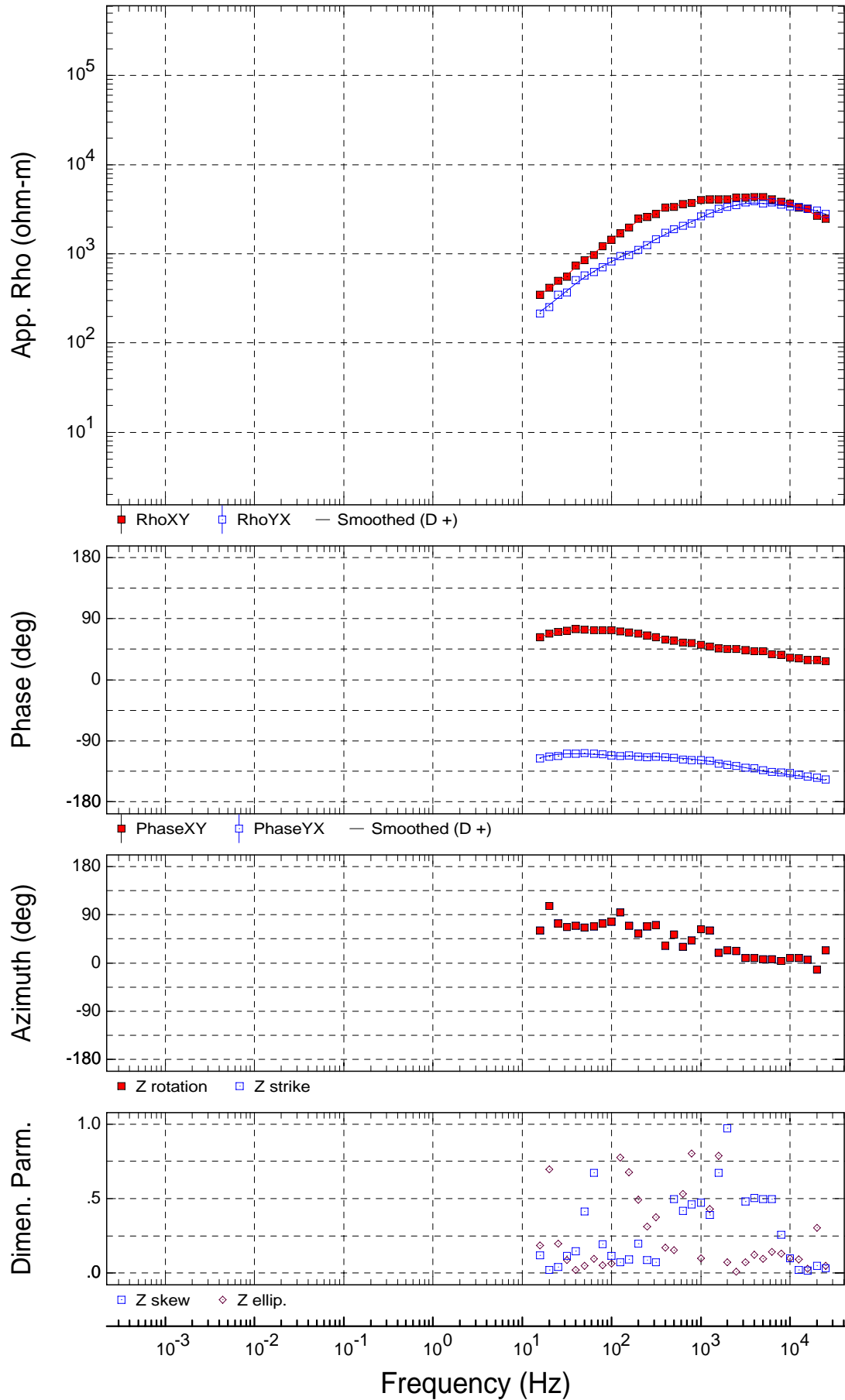


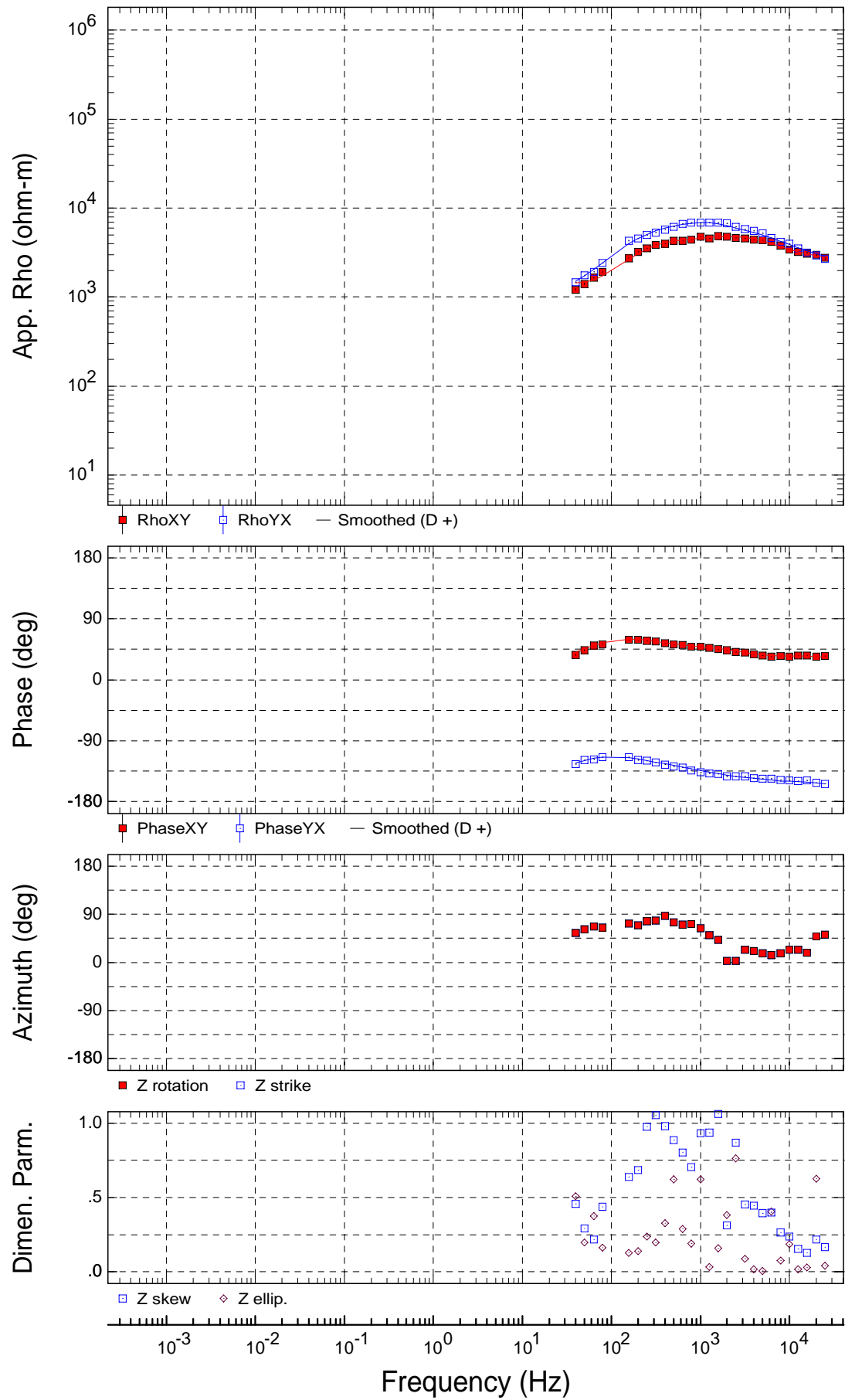
USGS
Rotation: PA

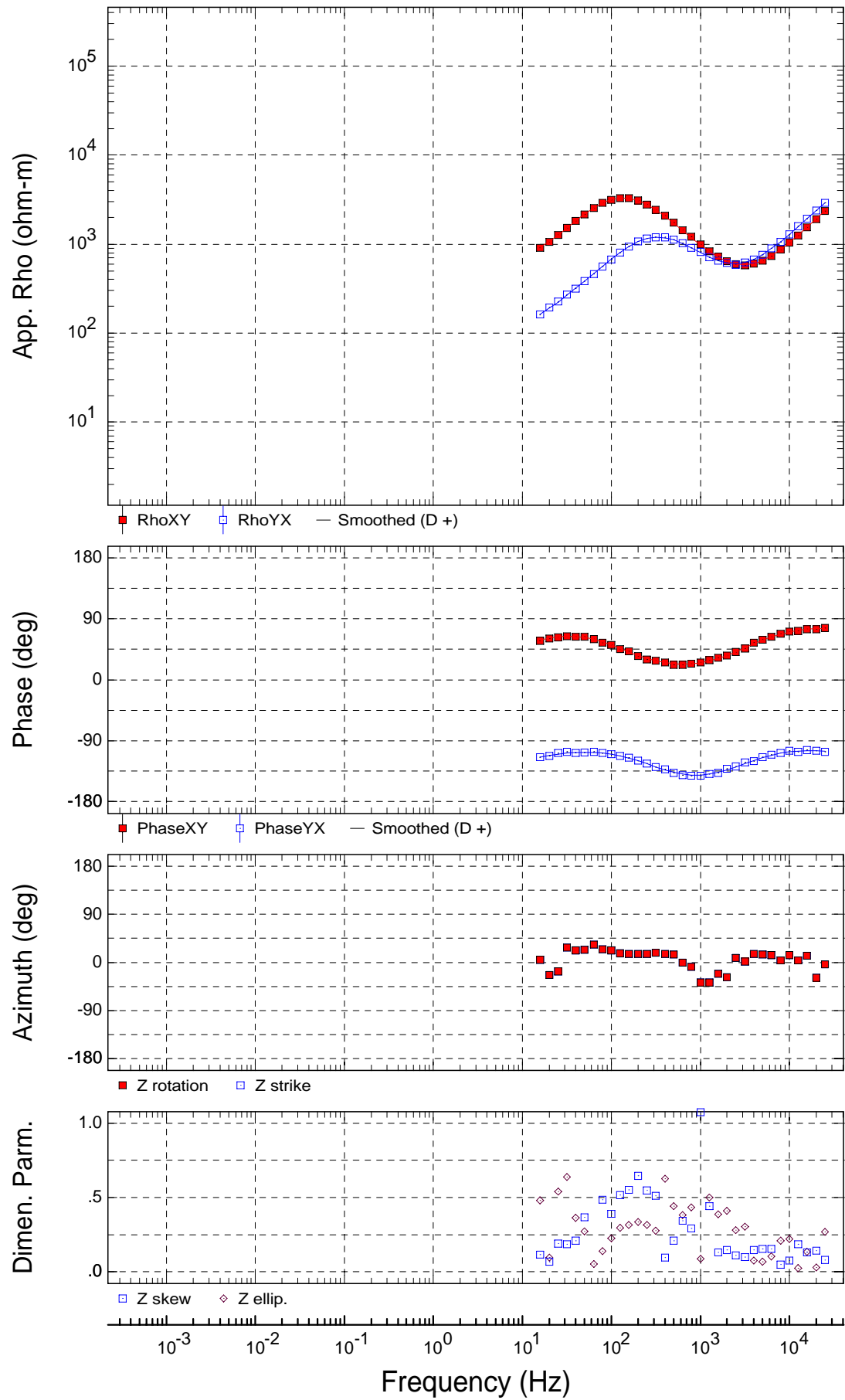
Sounding SR023





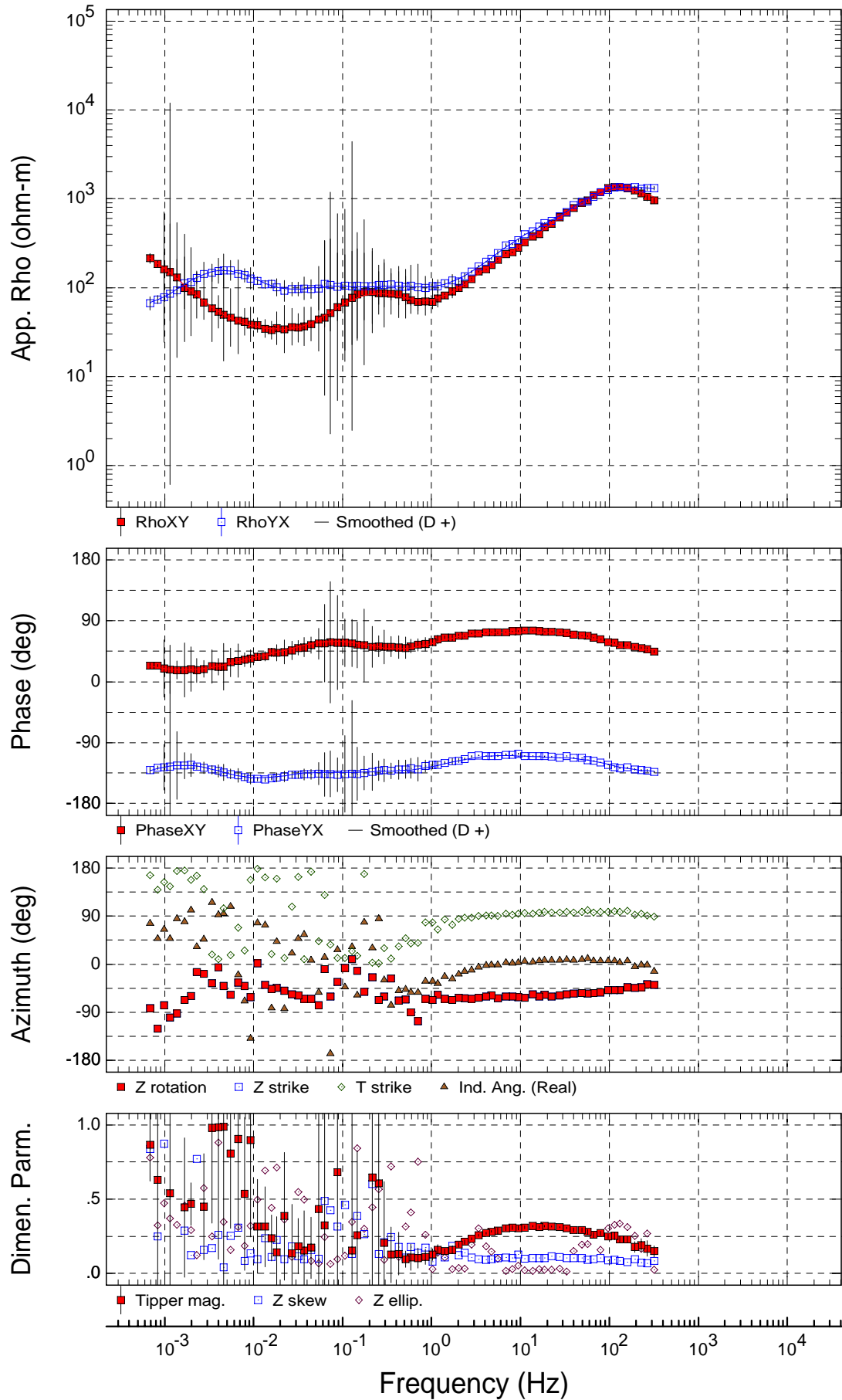


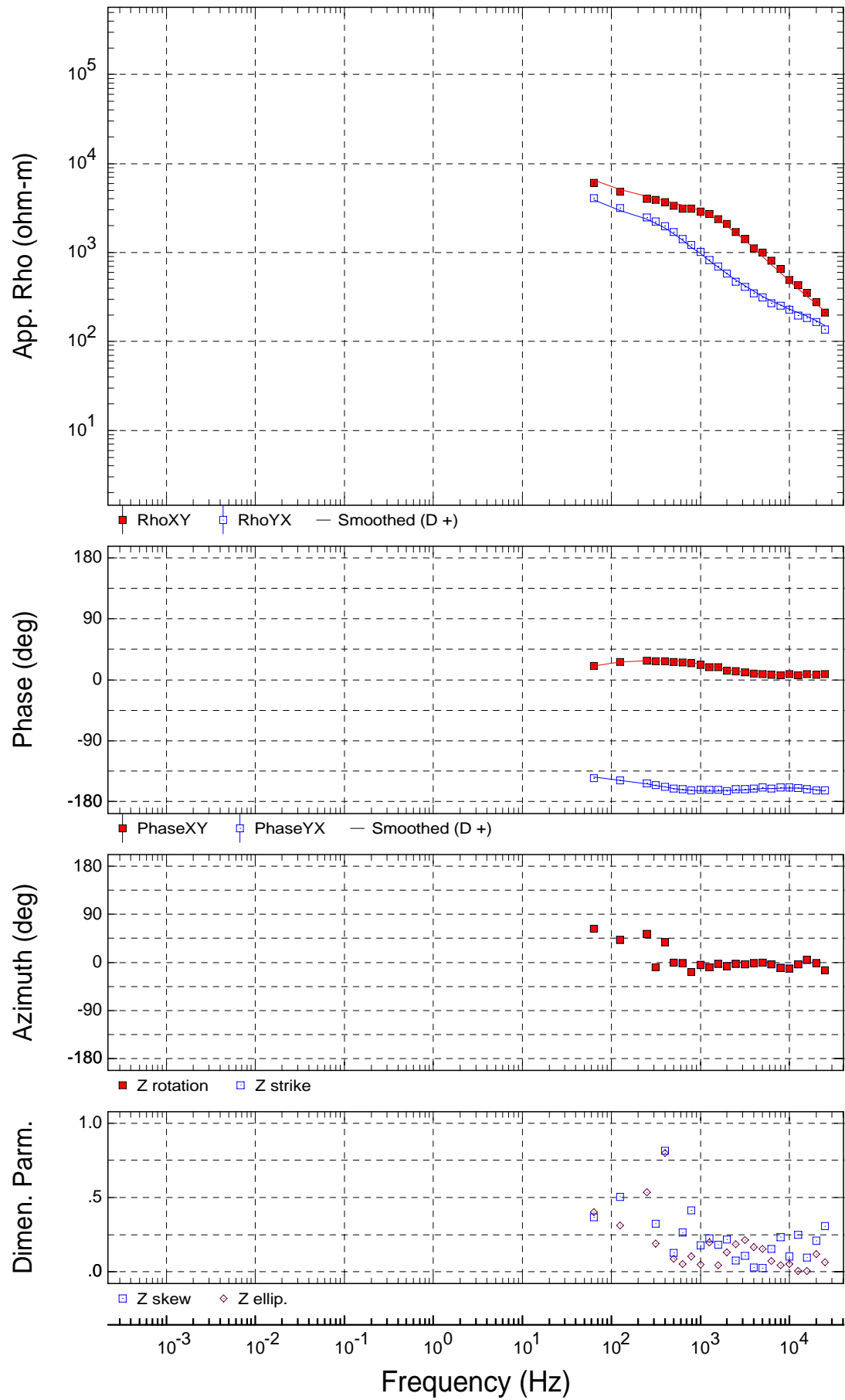




USGS
Rotation: PA

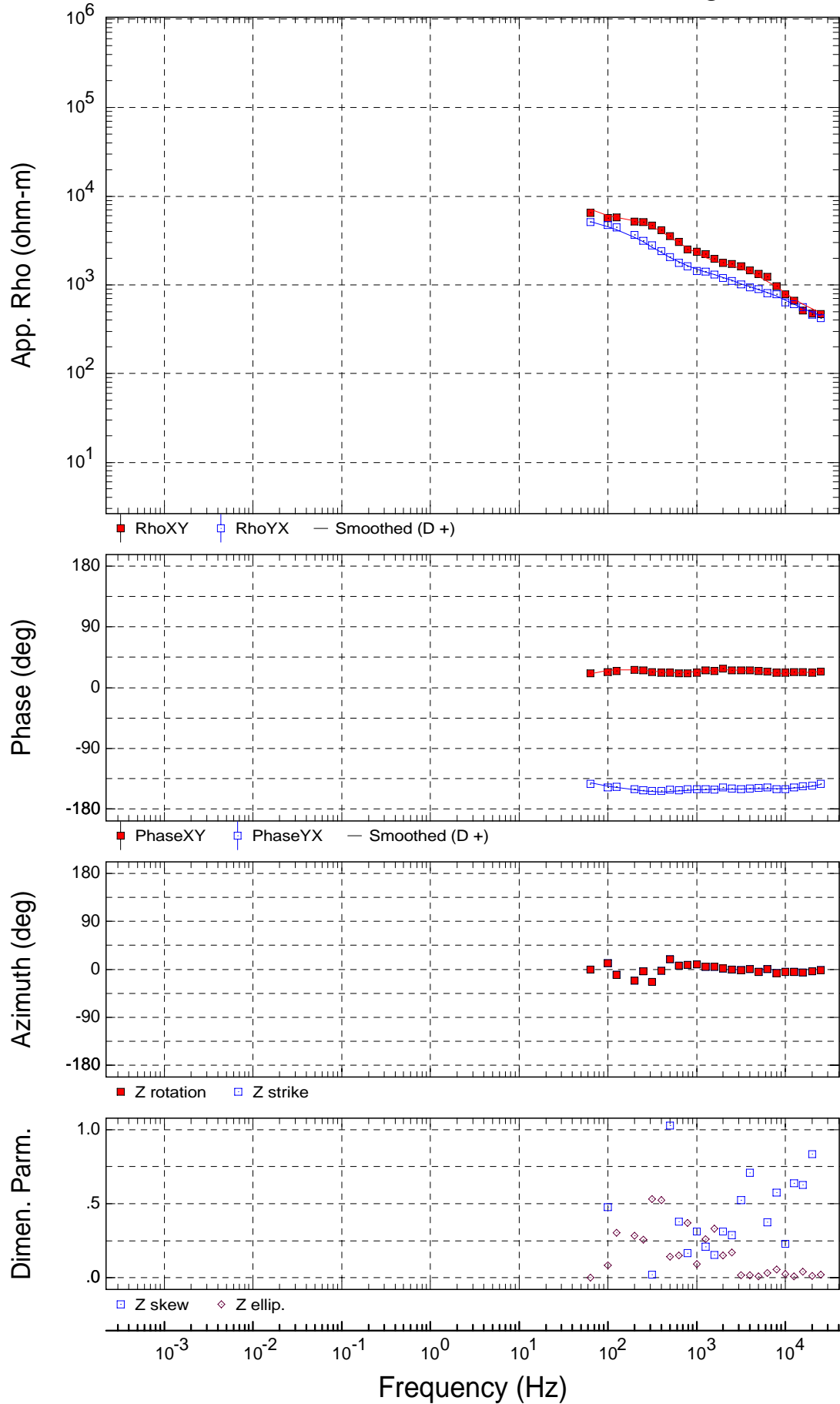
Sounding WF01





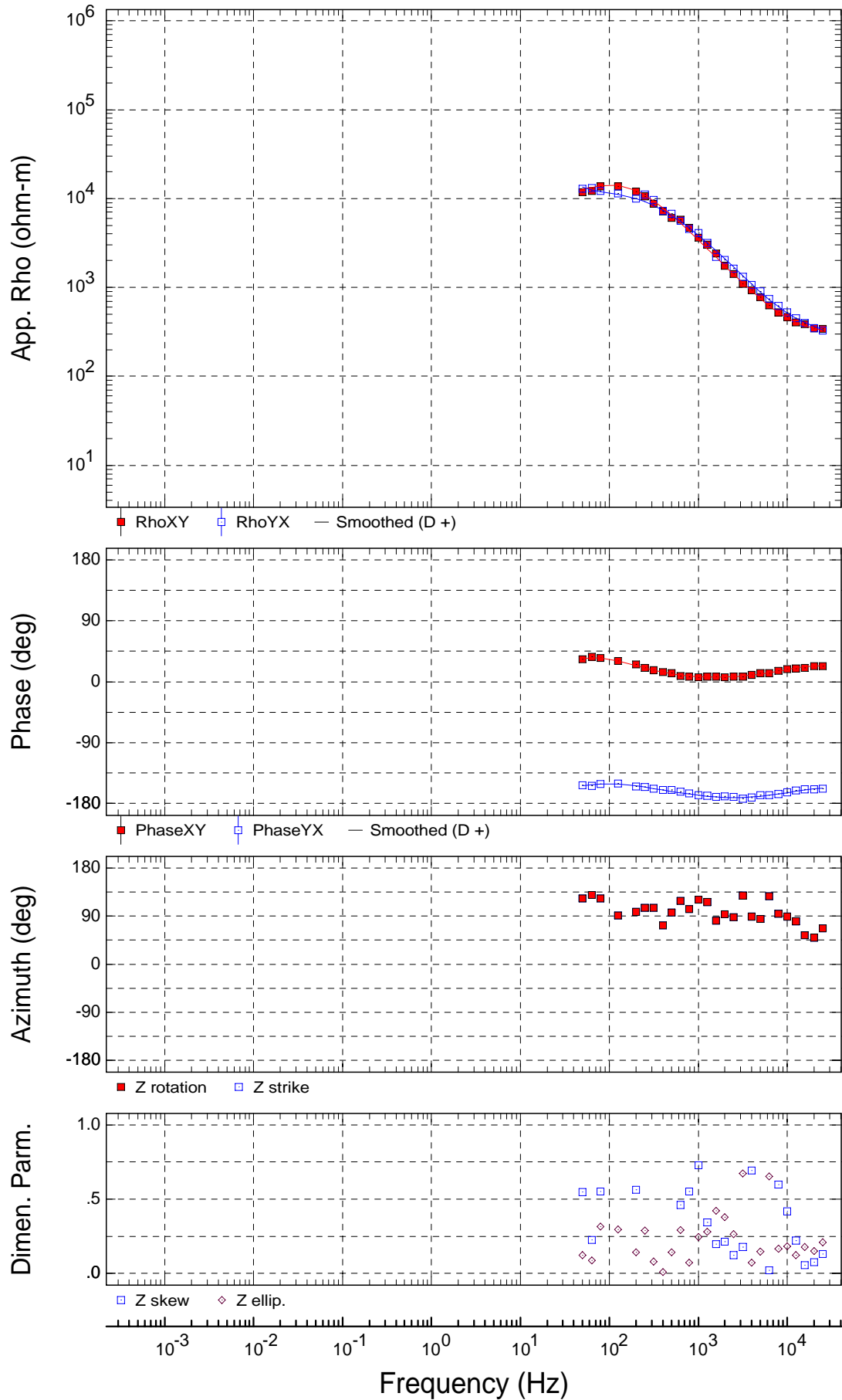
USGS
Rotation: PA

Sounding WR003

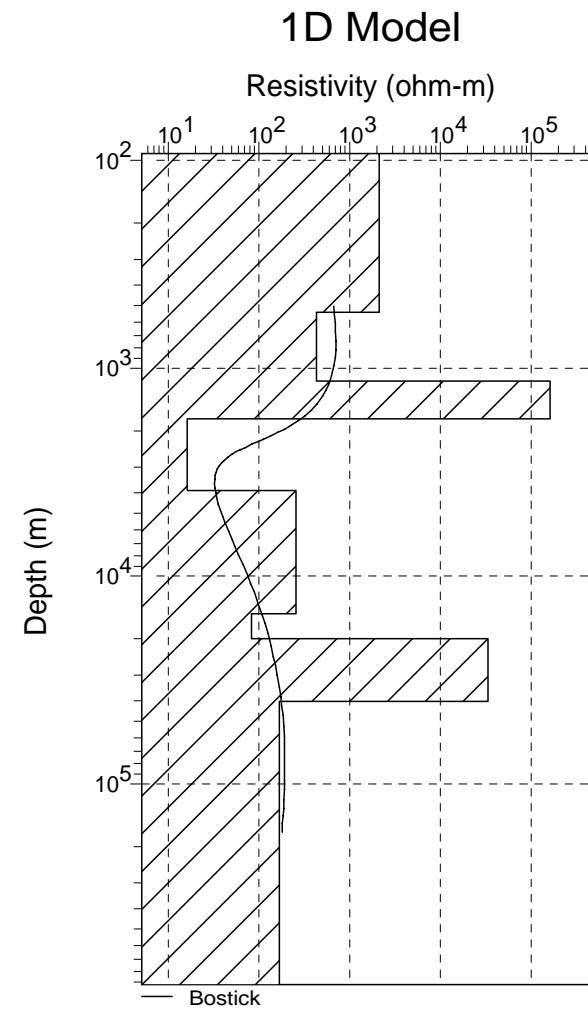
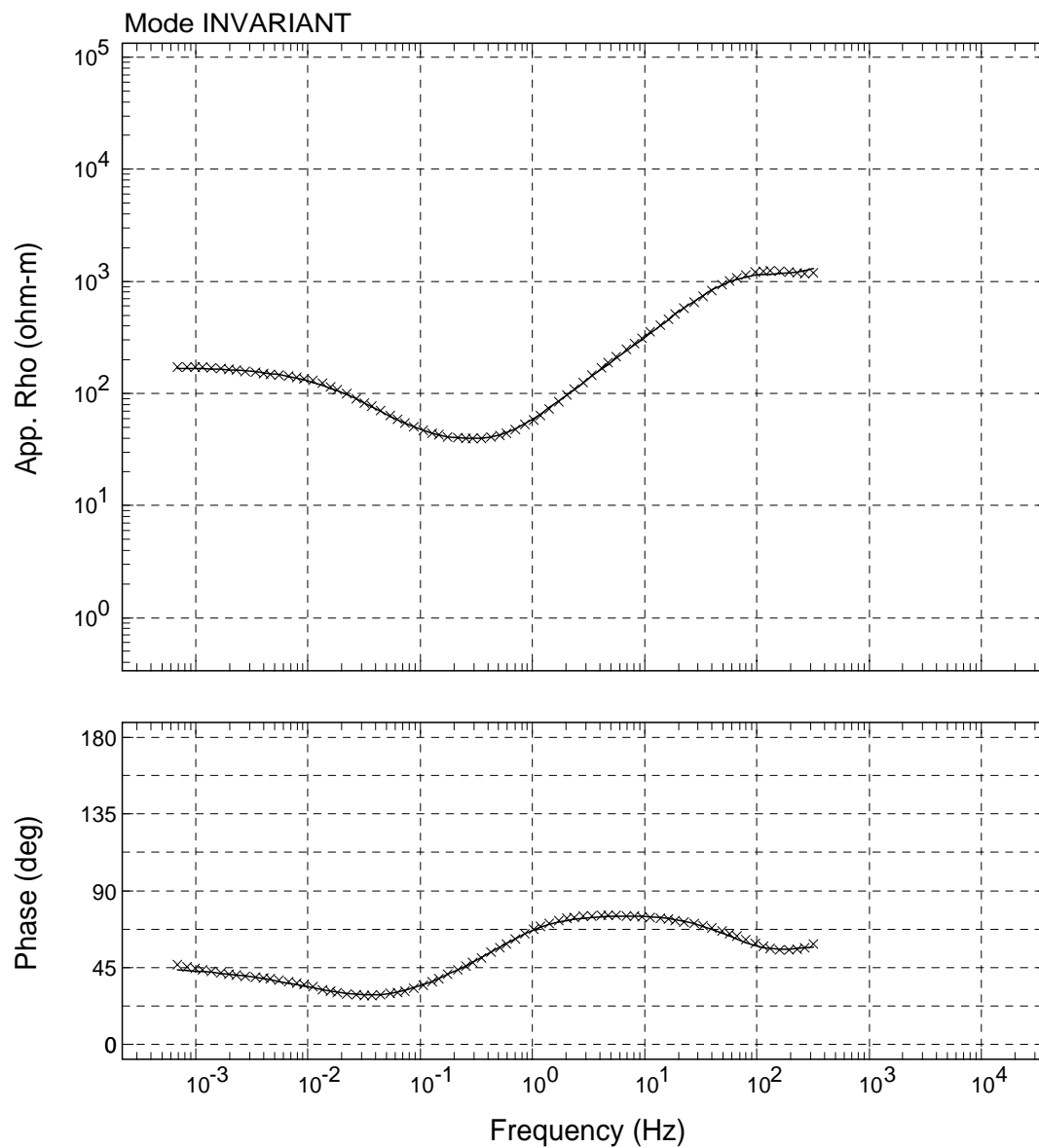


USGS
Rotation: PA

Sounding WR004



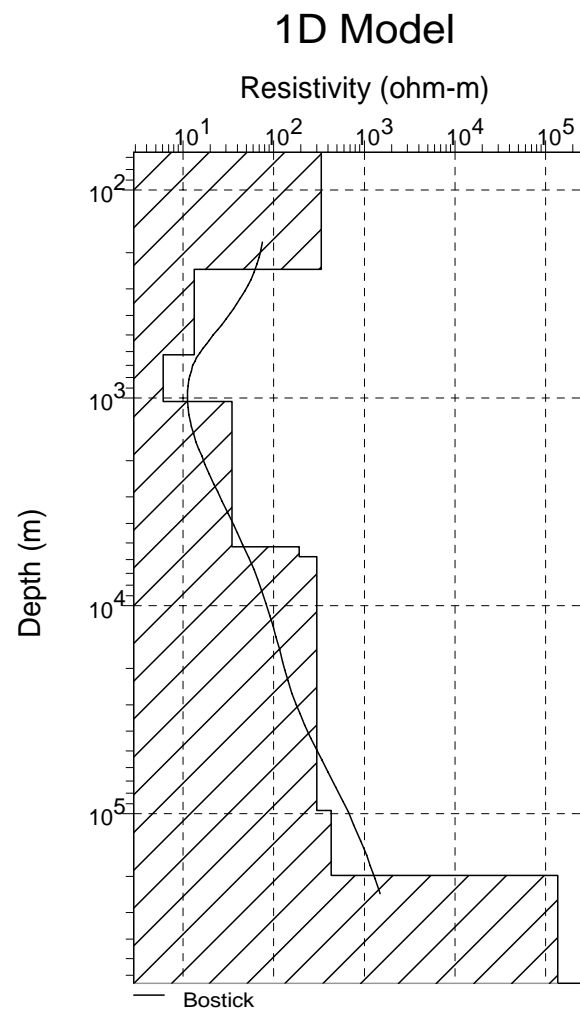
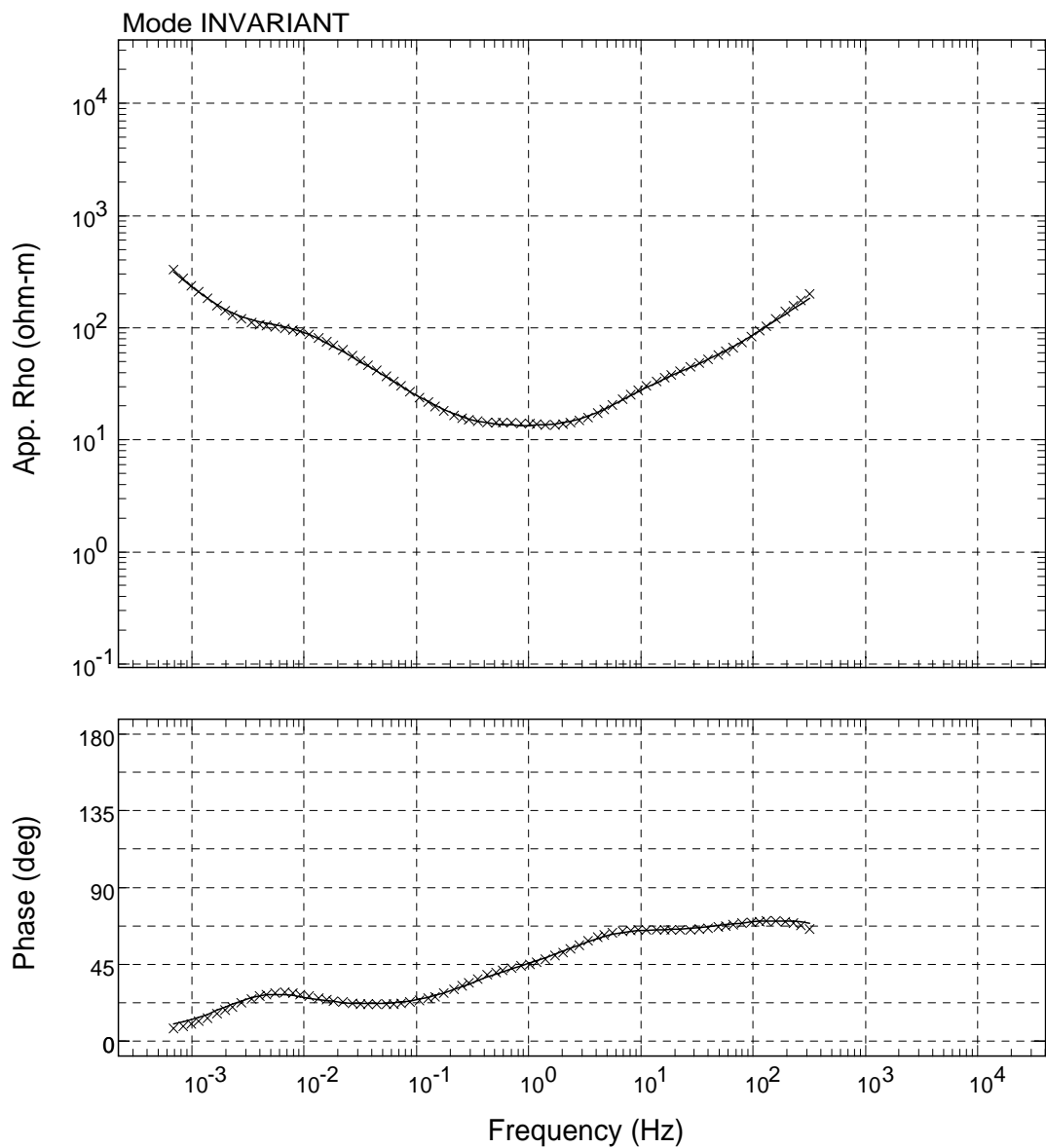
Appendix C—1D Inversions of the MT and AMT Data



Sounding: 1PT1

Area: Hawaii

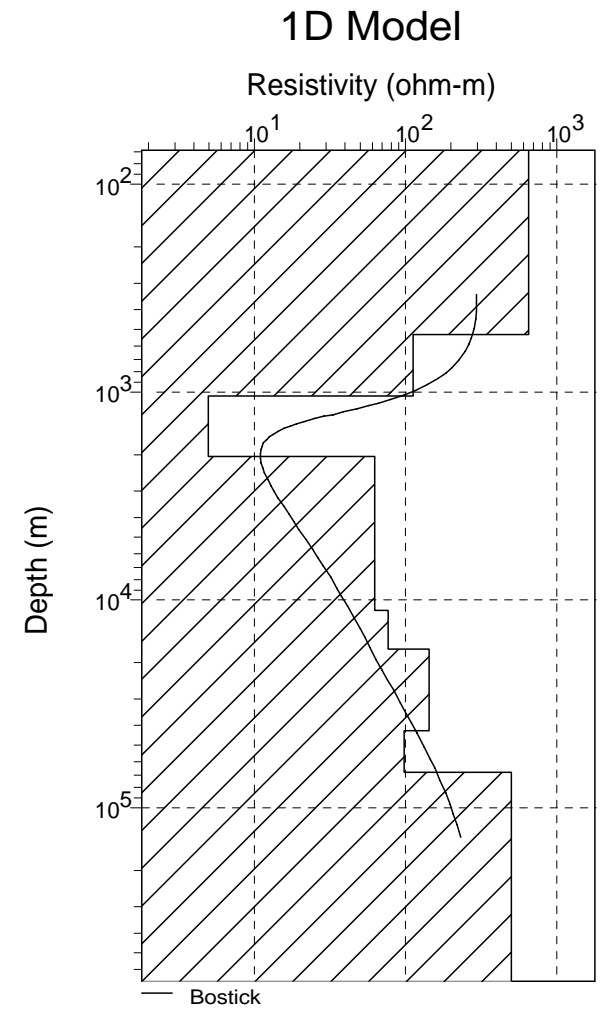
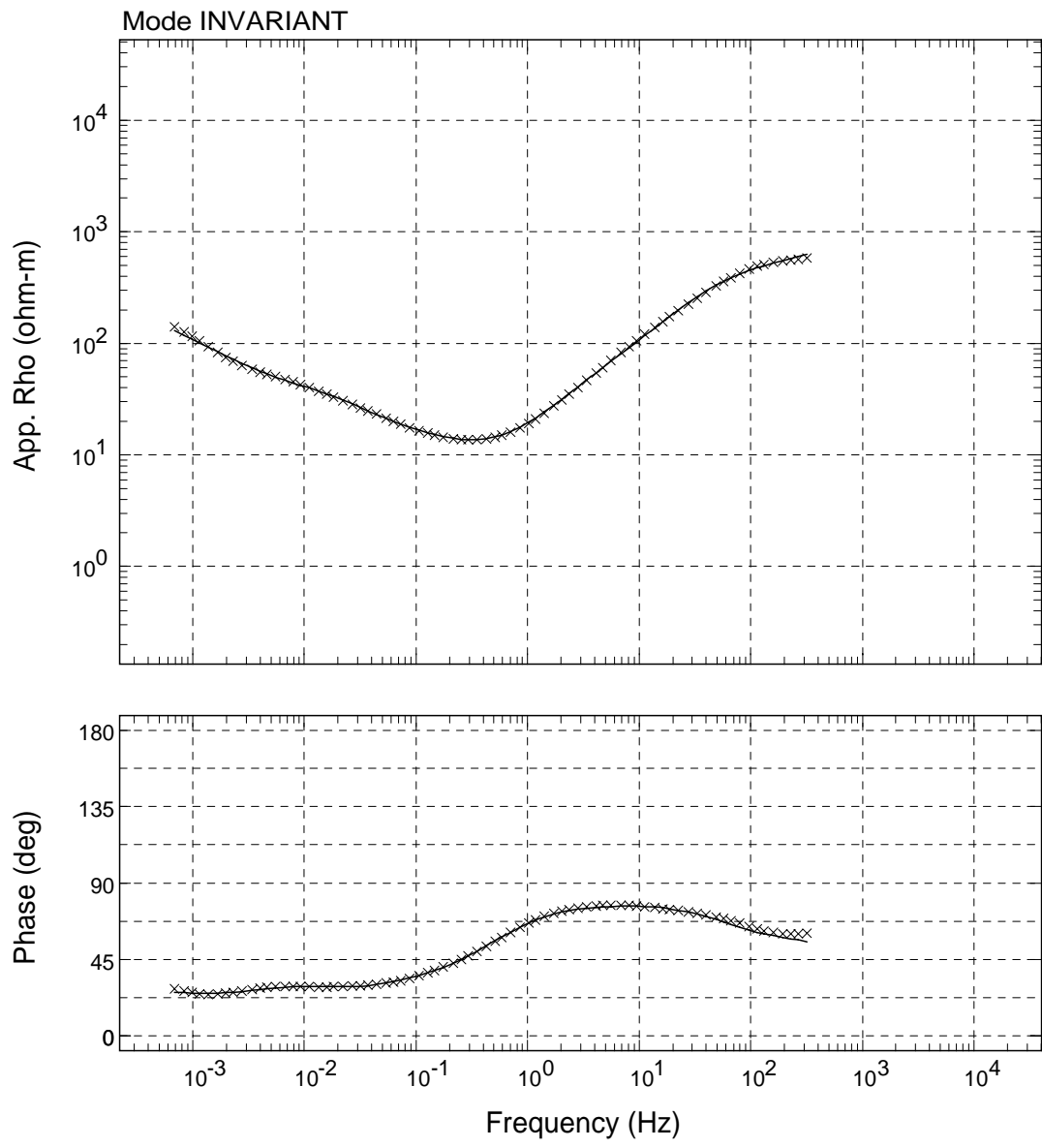
USGS - 01/Jun/2009



Sounding: 2PT1

Area: Hawaii

USGS - 01/Jun/2009

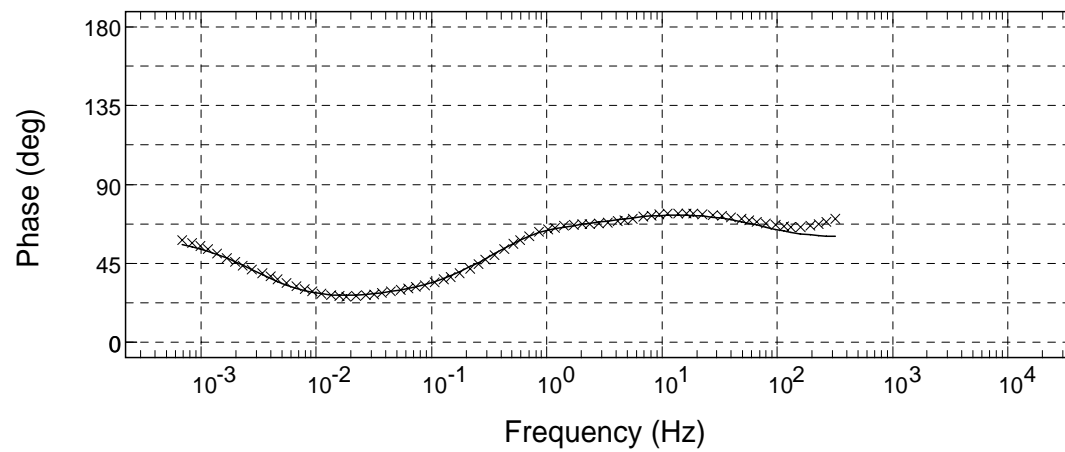
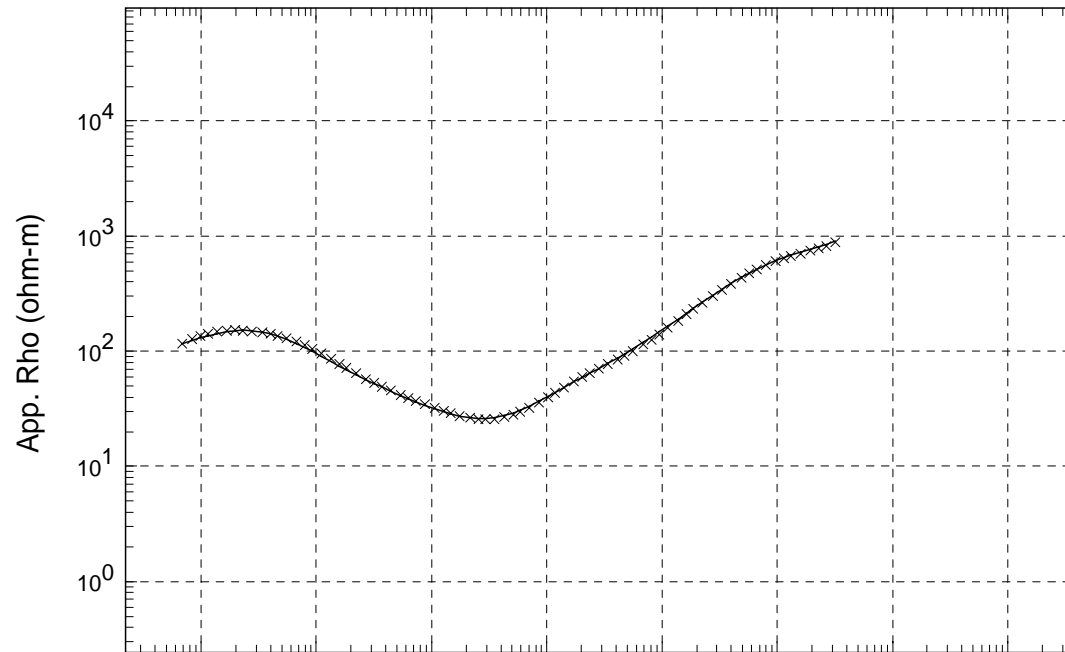


Sounding: 3PT1

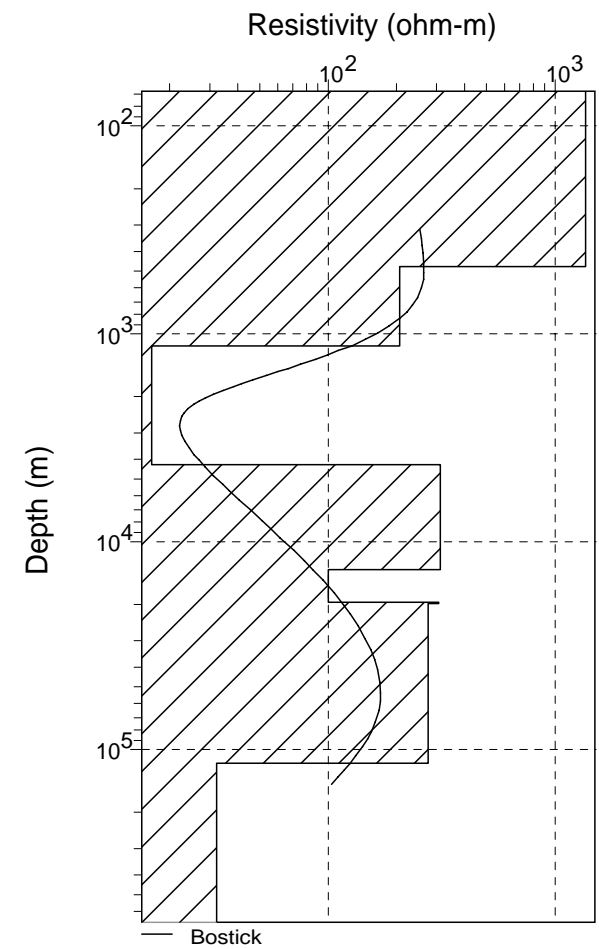
Area: Hawaii

USGS - 01/Jun/2009

Mode INVARIANT



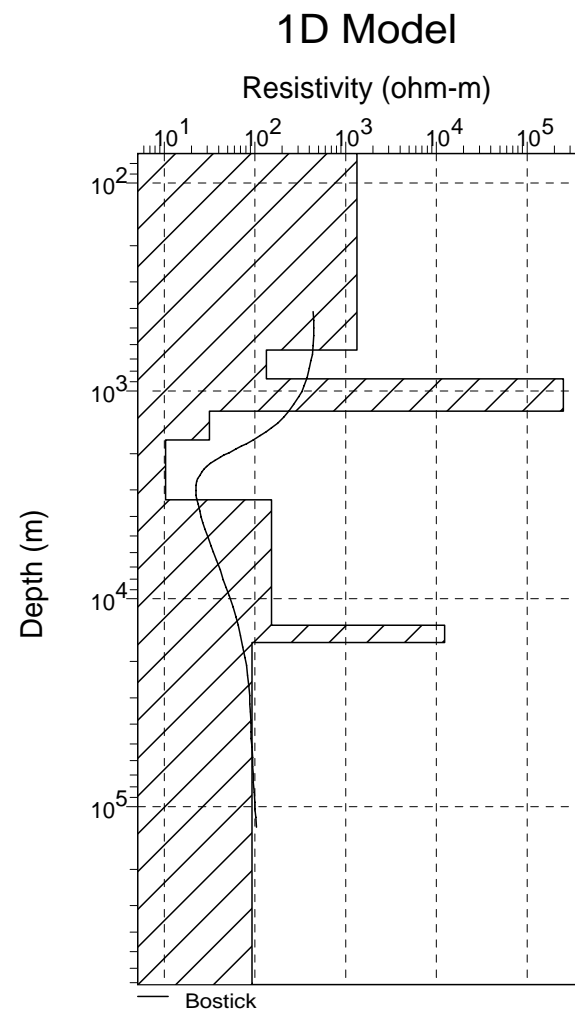
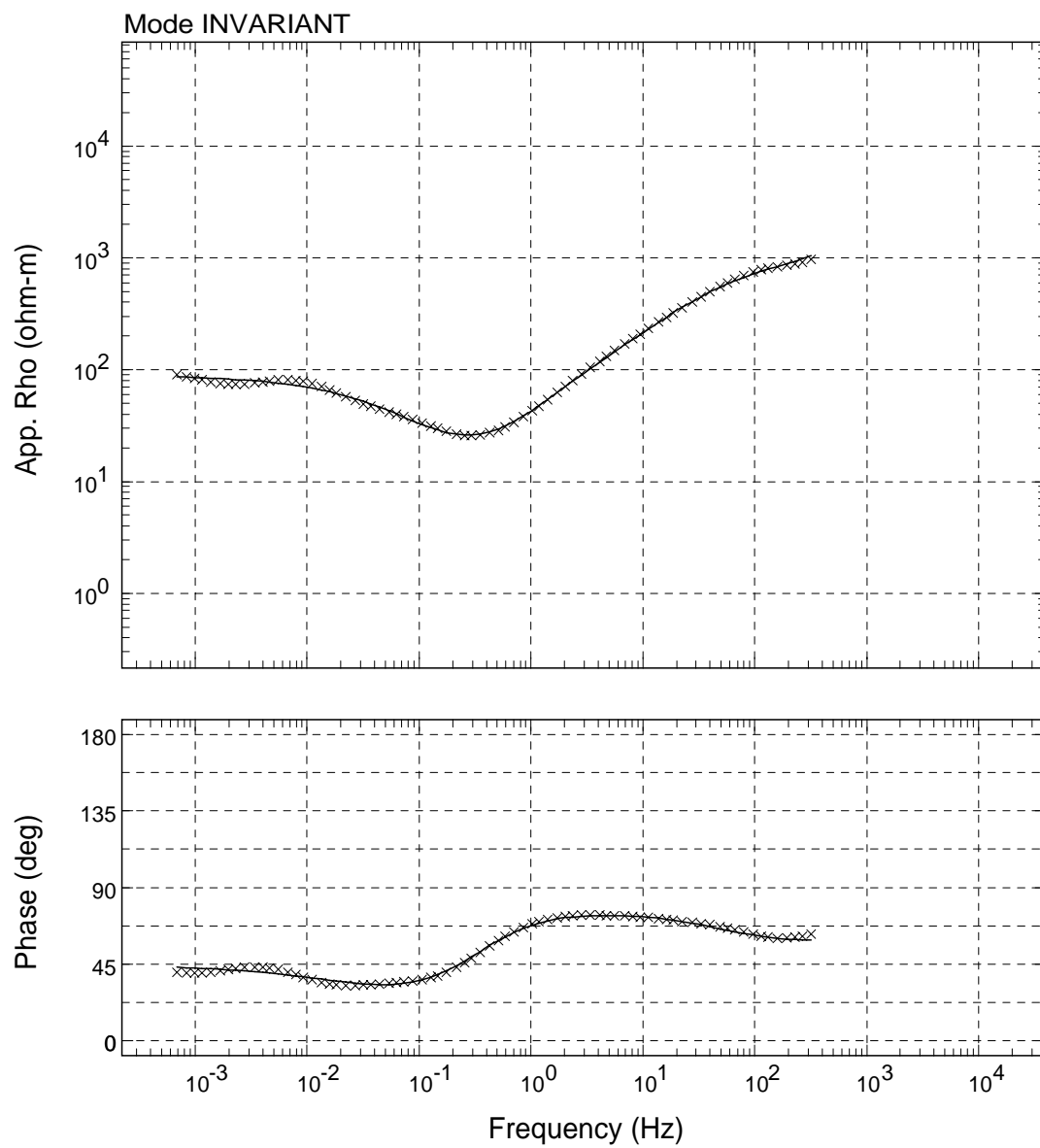
1D Model



Sounding: 4PT1

Area: Hawaii

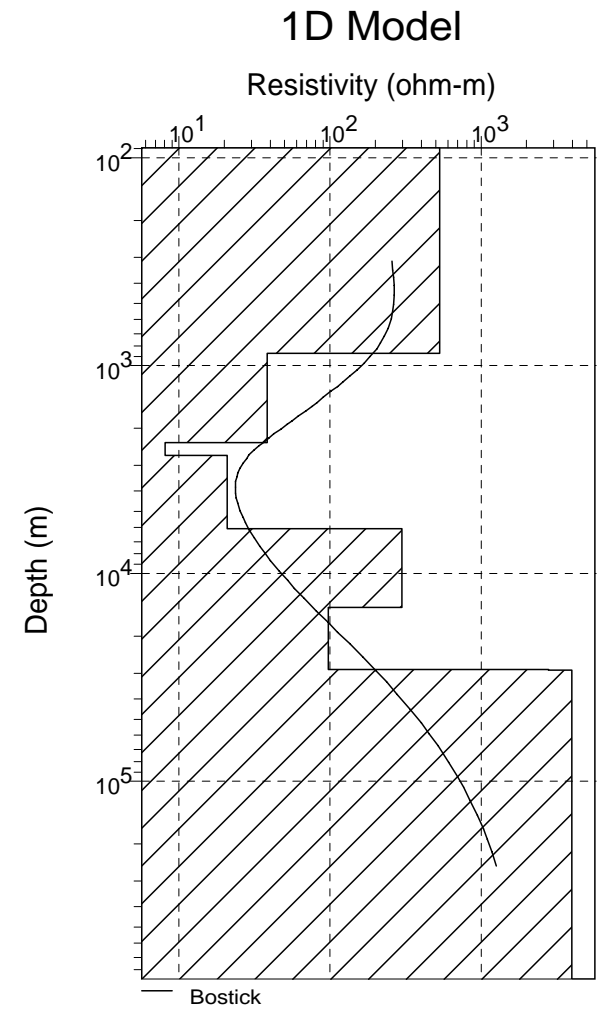
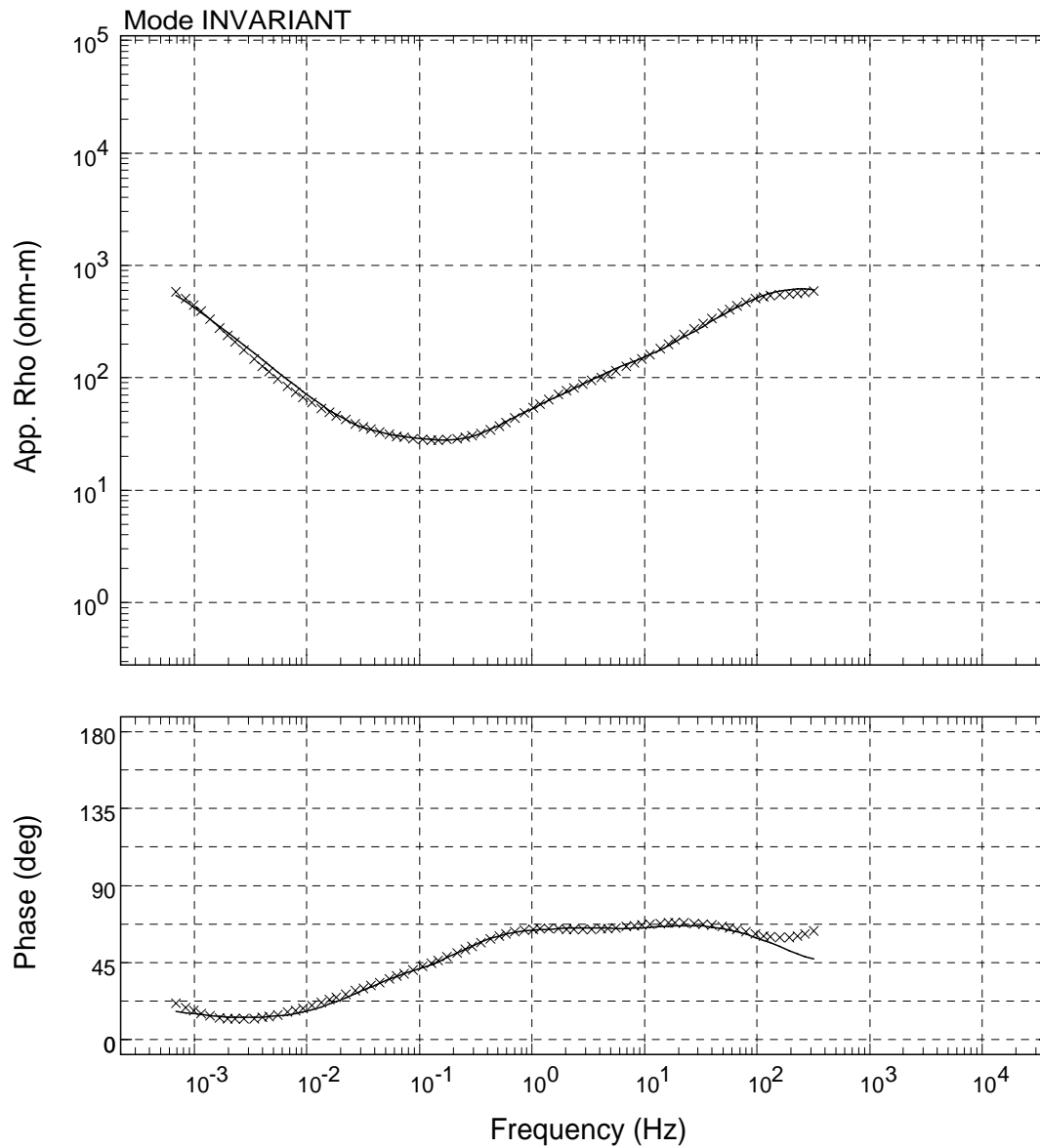
USGS - 01/Jun/2009



Sounding: 6PT1

Area: Hawaii

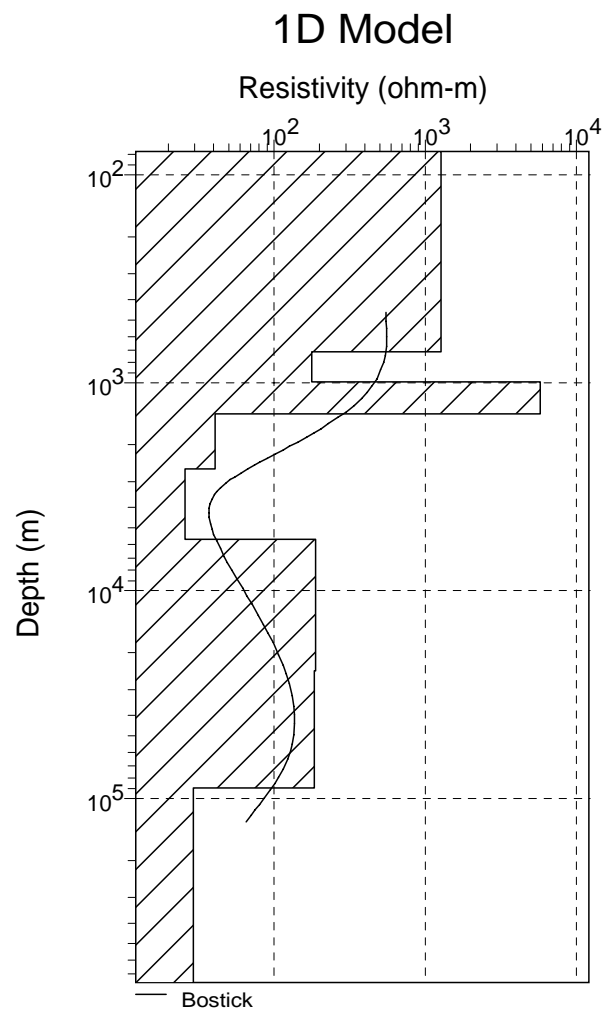
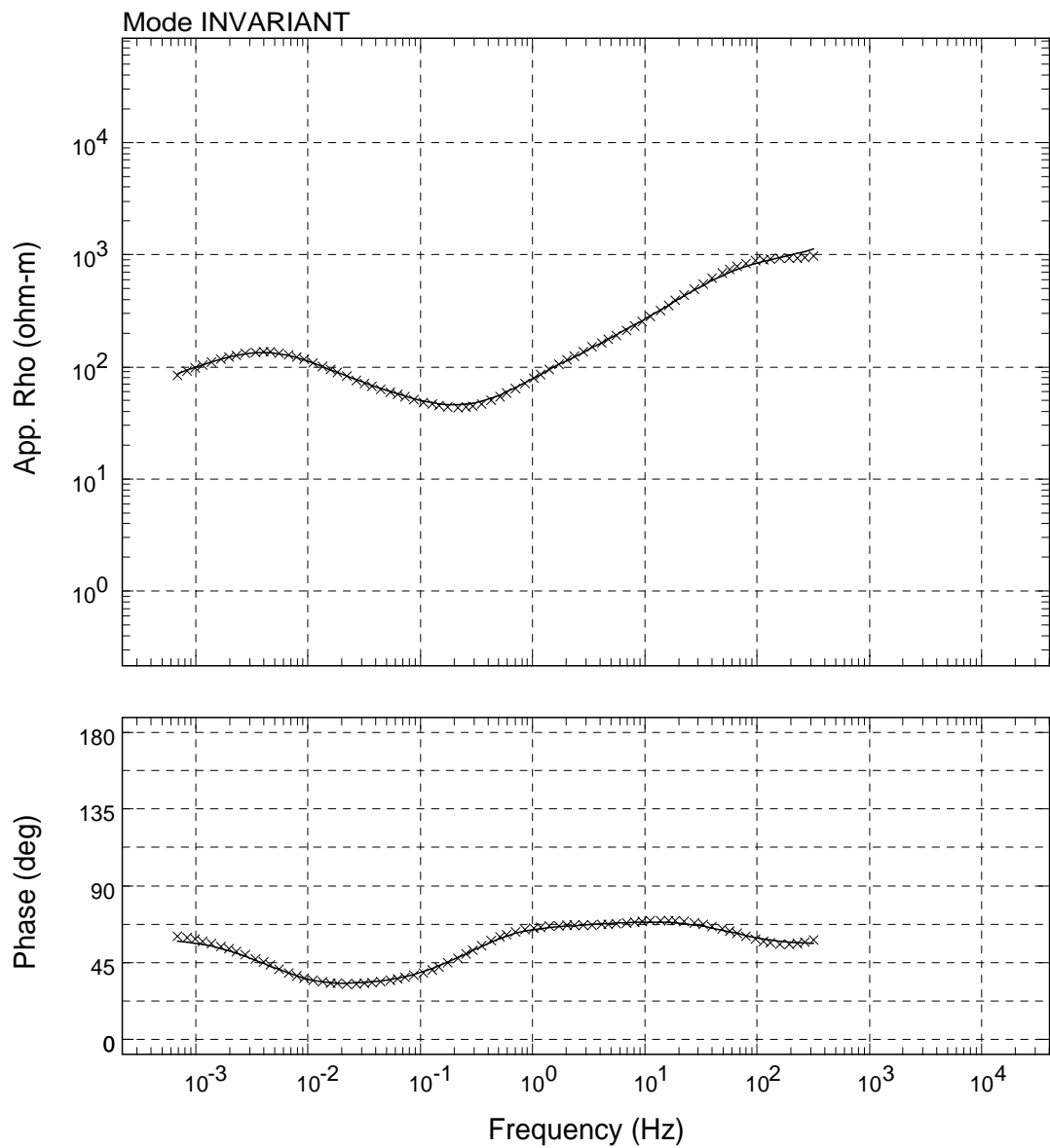
USGS - 01/Jun/2009



Sounding: 7PT1

Area: Hawaii

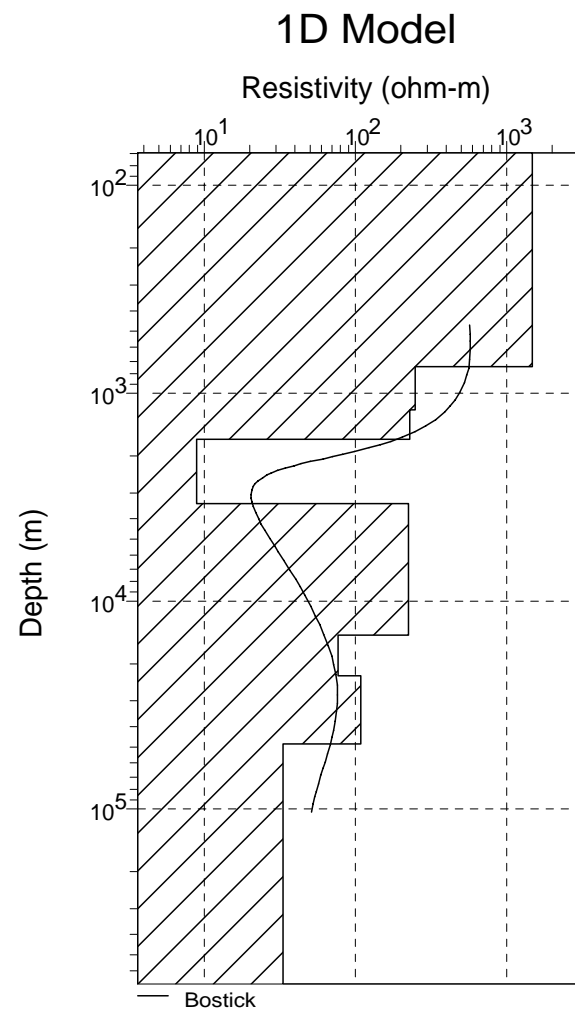
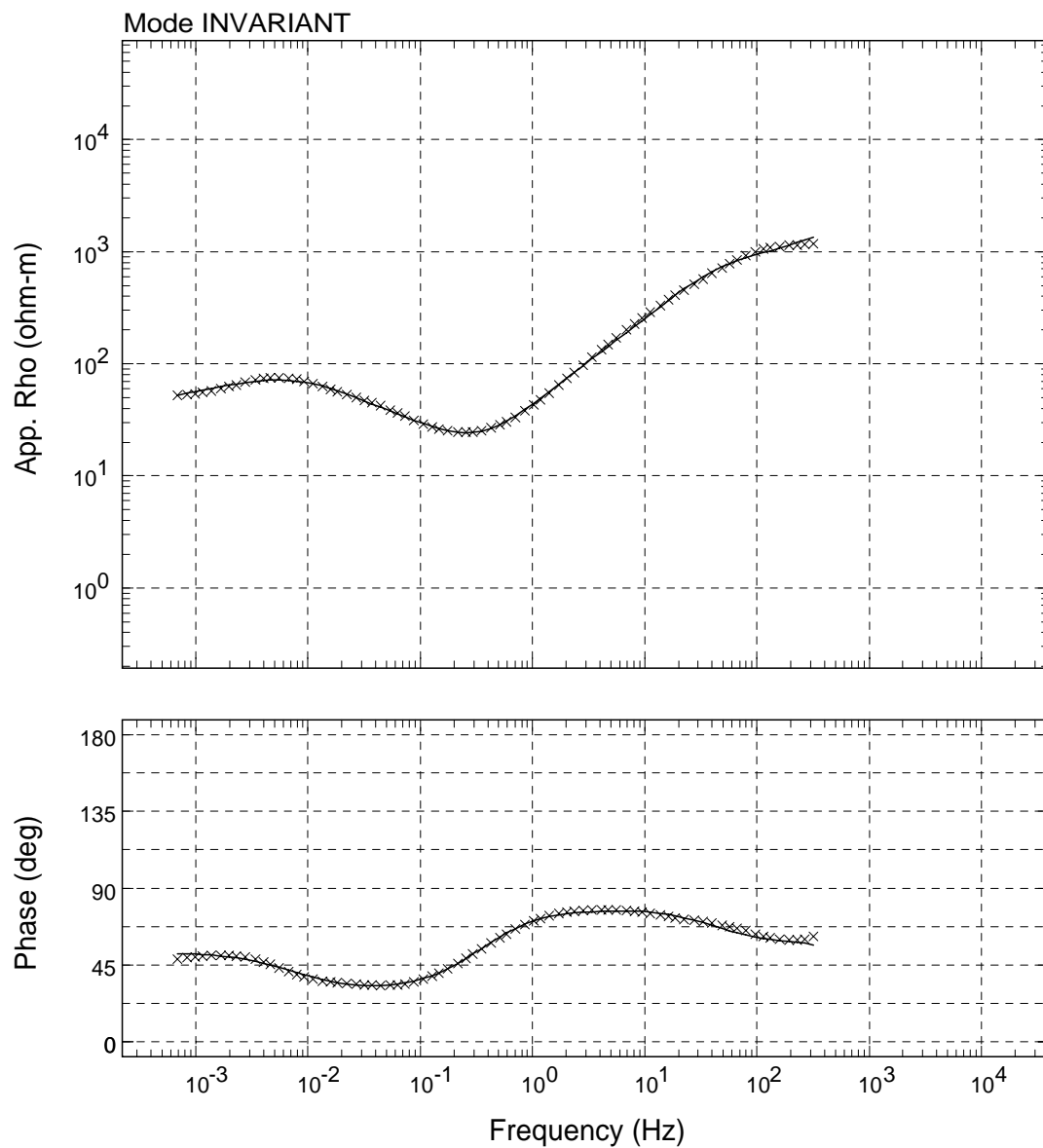
USGS - 01/Jun/2009



Sounding: 8PT1

Area: Hawaii

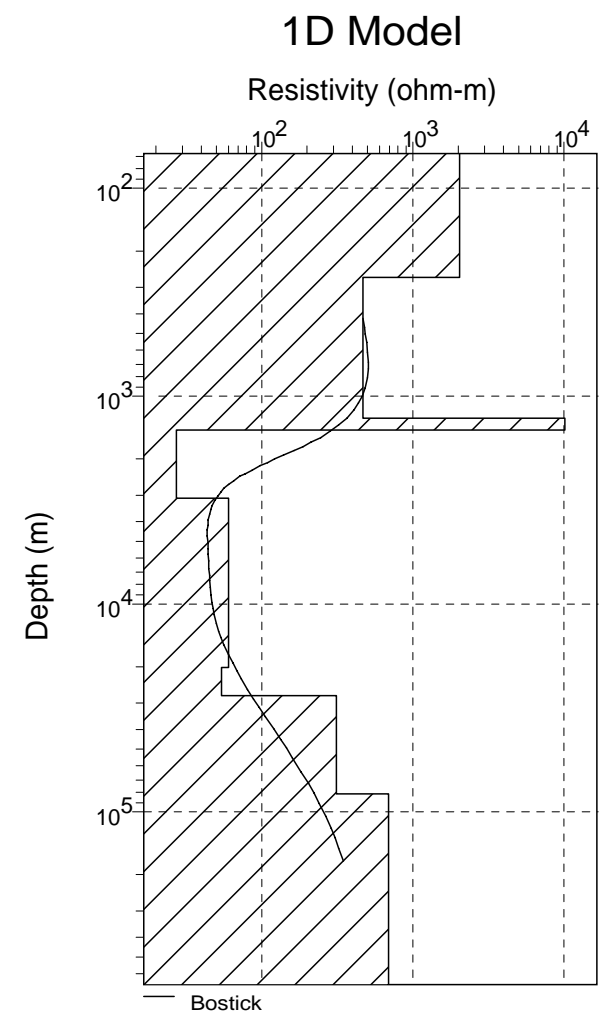
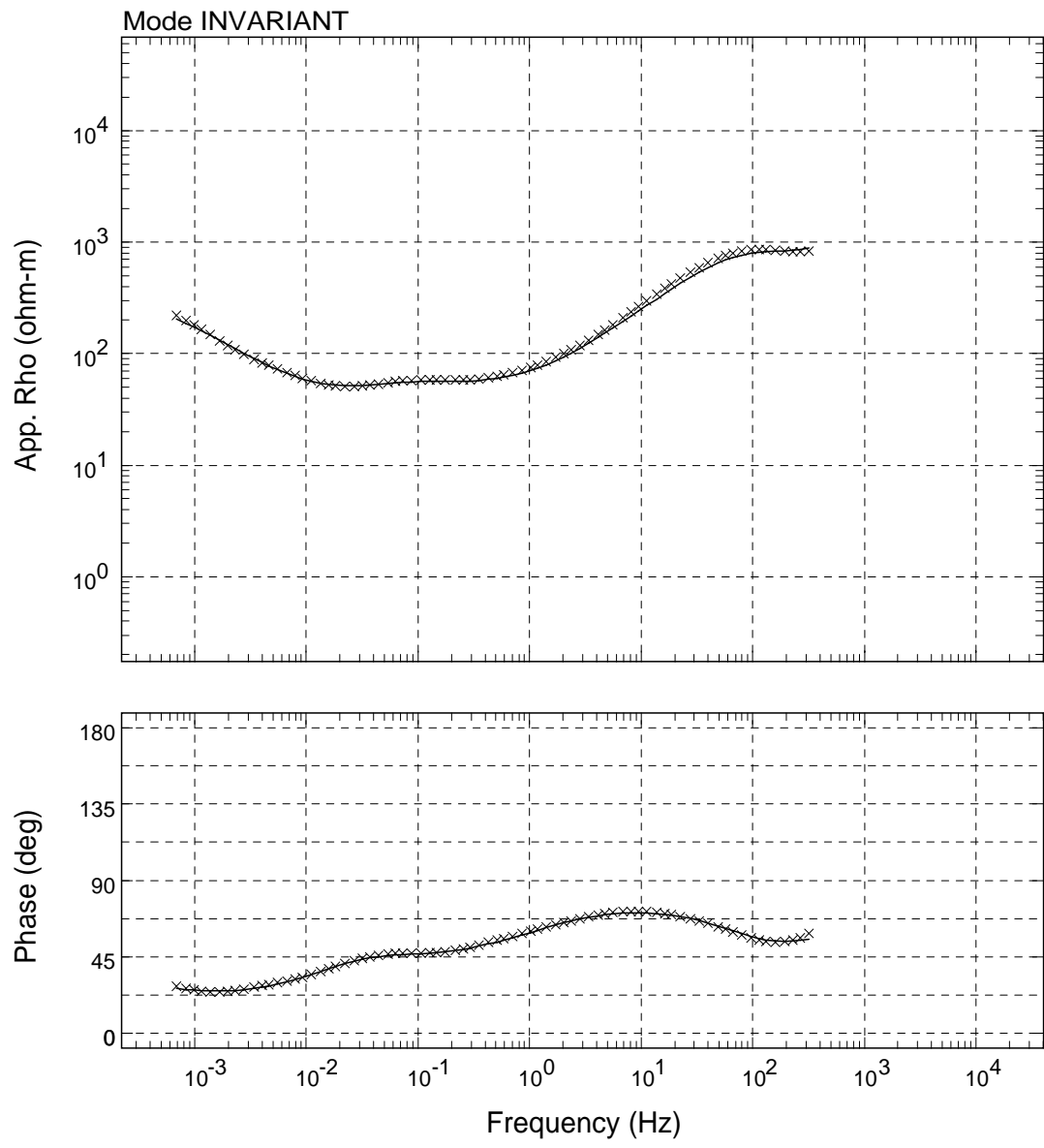
USGS - 01/Jun/2009



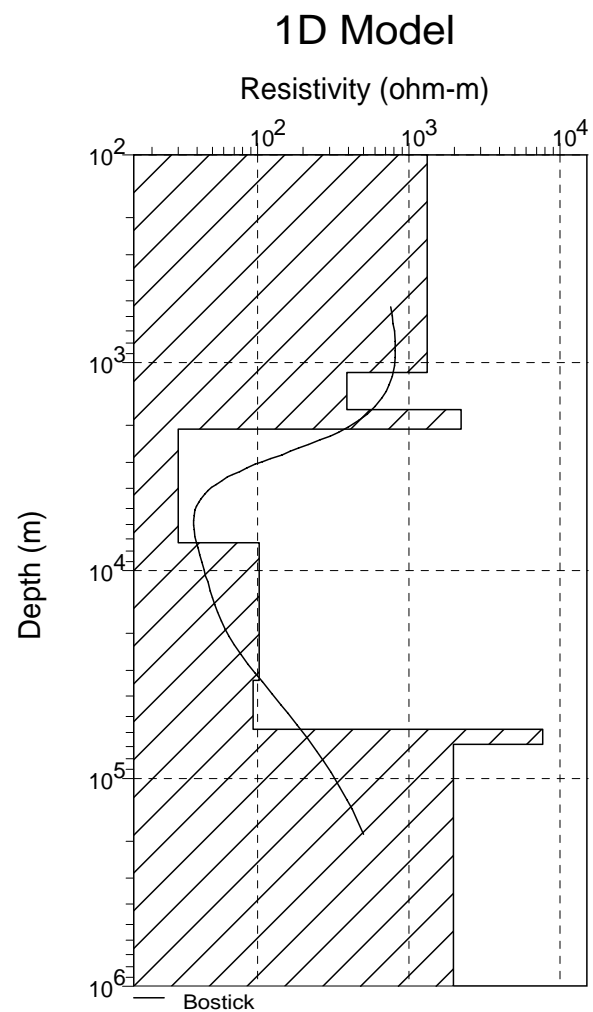
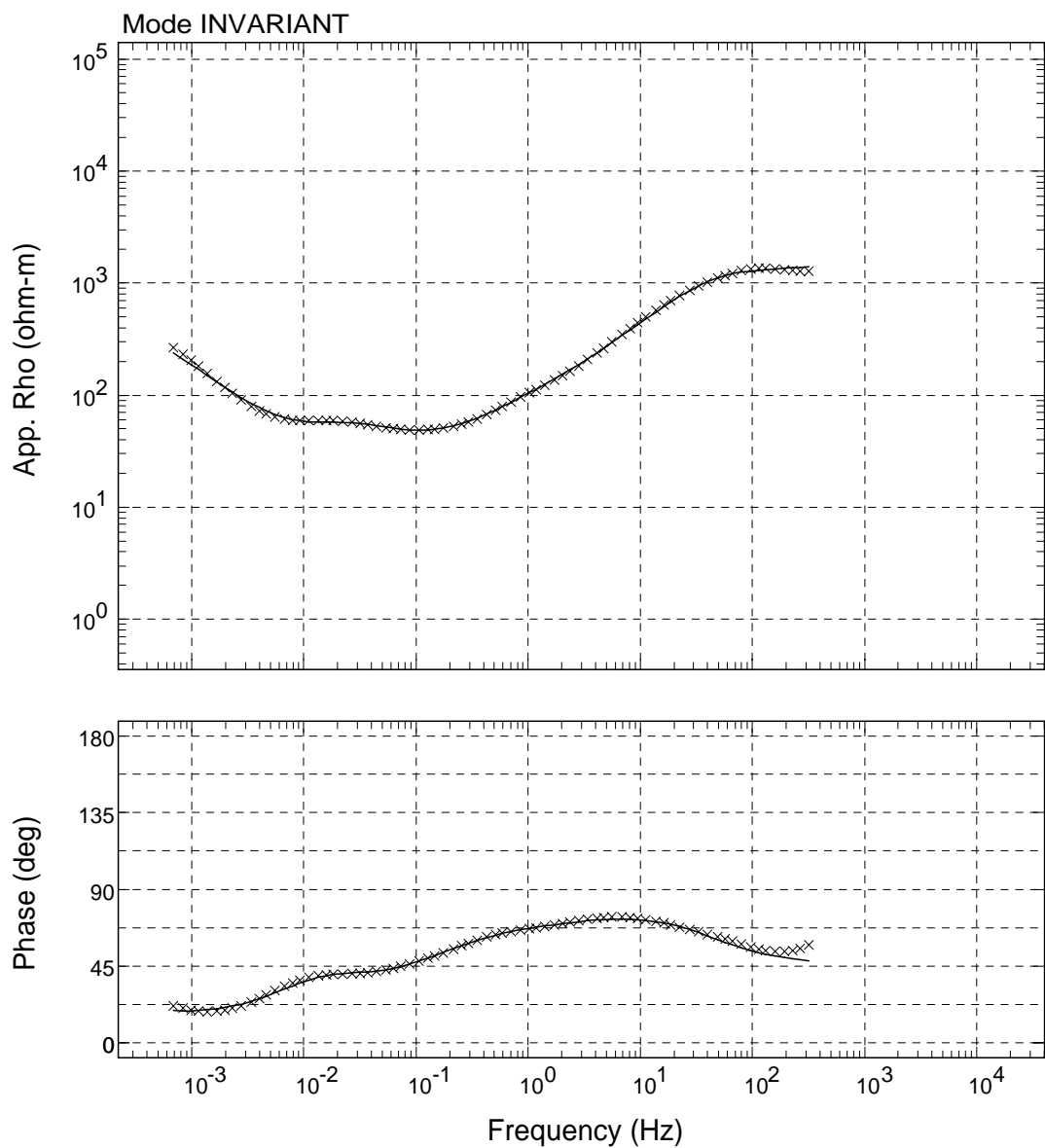
Sounding: 9PT1

Area: Hawaii

USGS - 01/Jun/2009



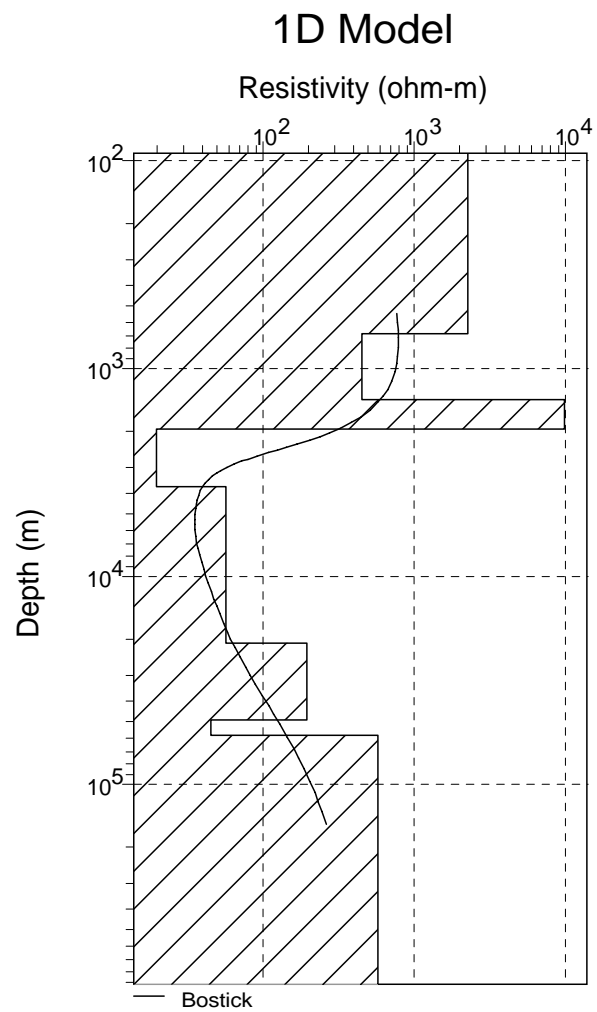
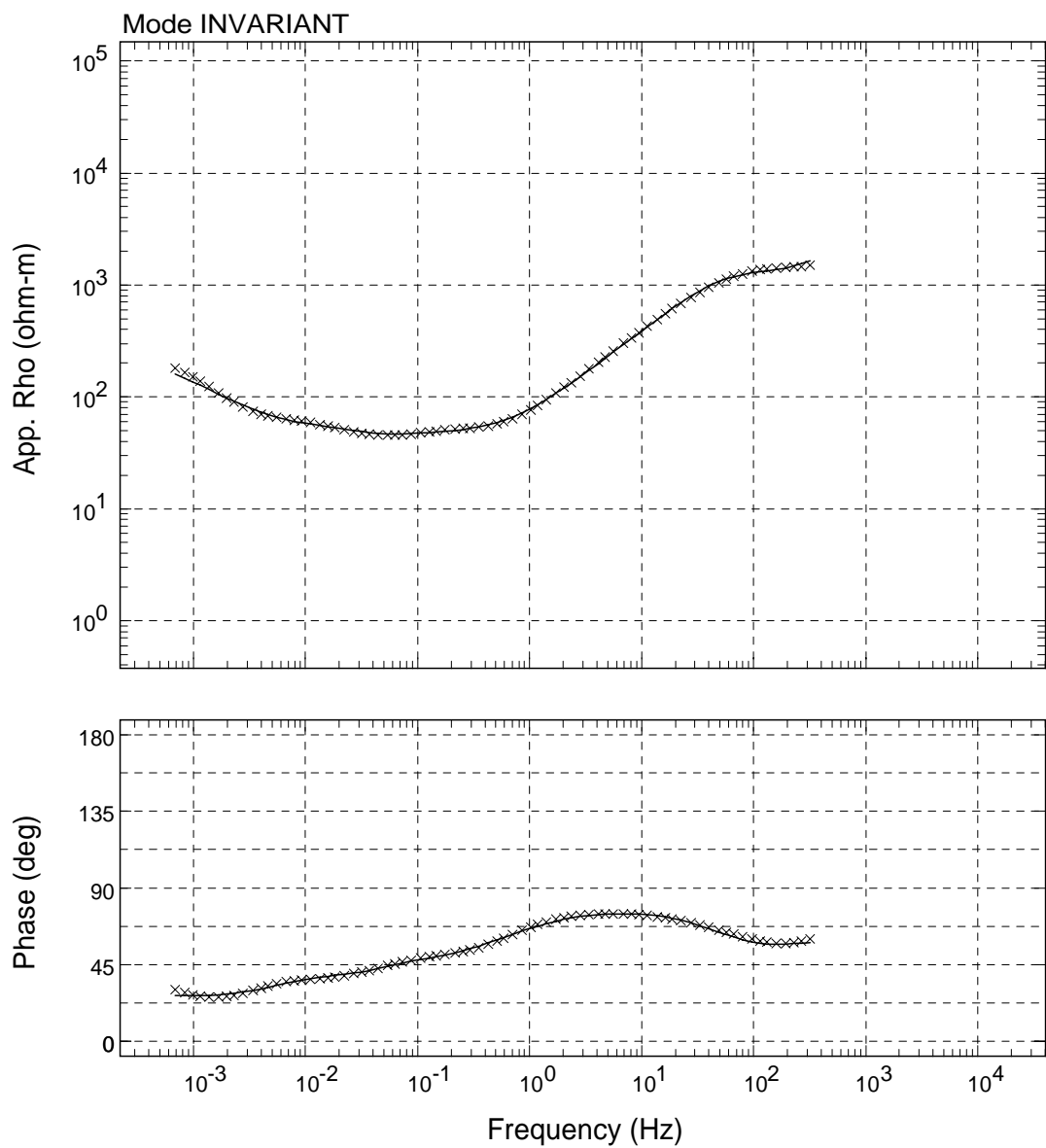
Sounding: 12PT
Area: Hawaii
USGS - 01/Jun/2009



Sounding: 13PT

Area: Hawaii

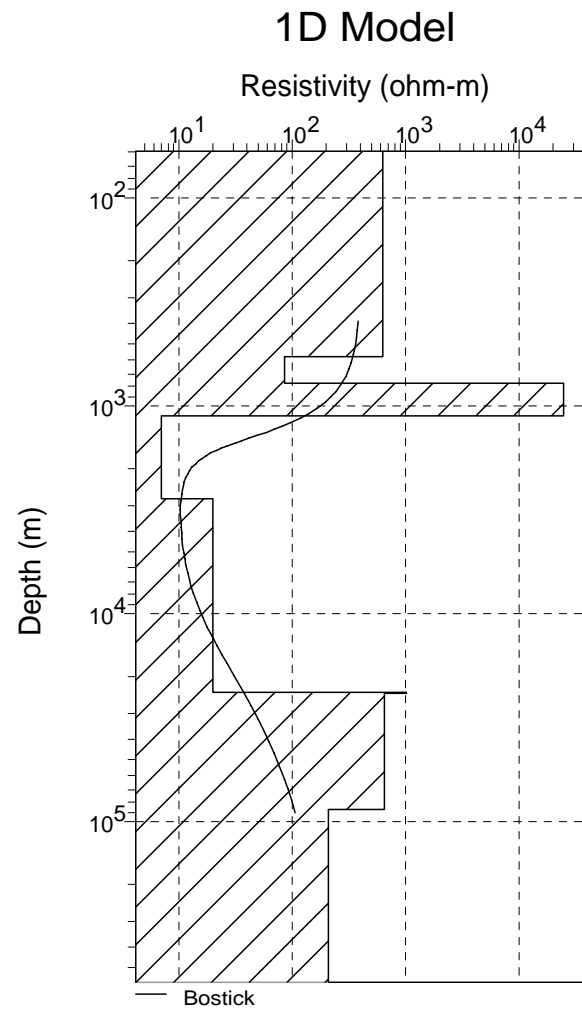
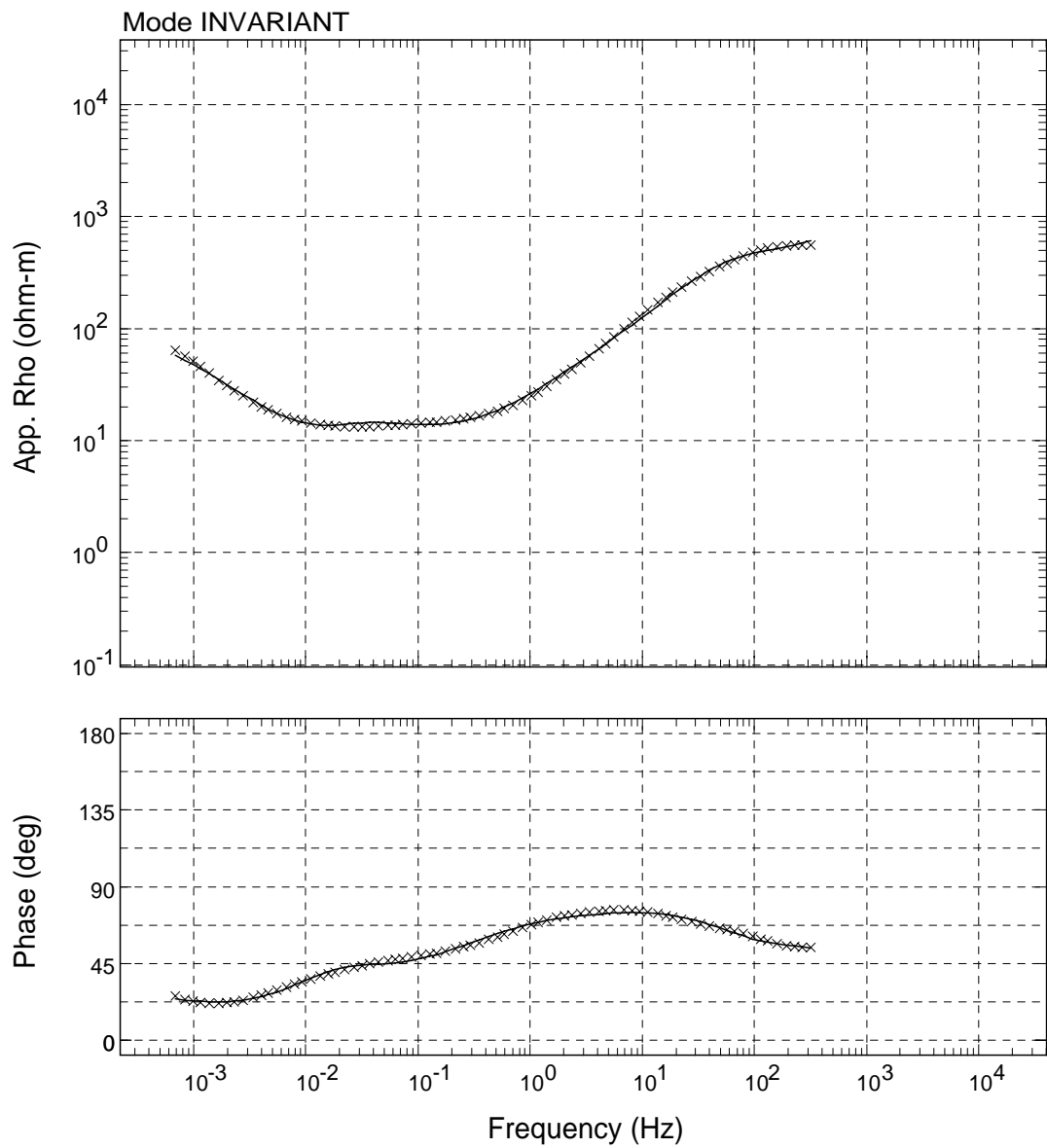
USGS - 01/Jun/2009



Sounding: 15PT

Area: Hawaii

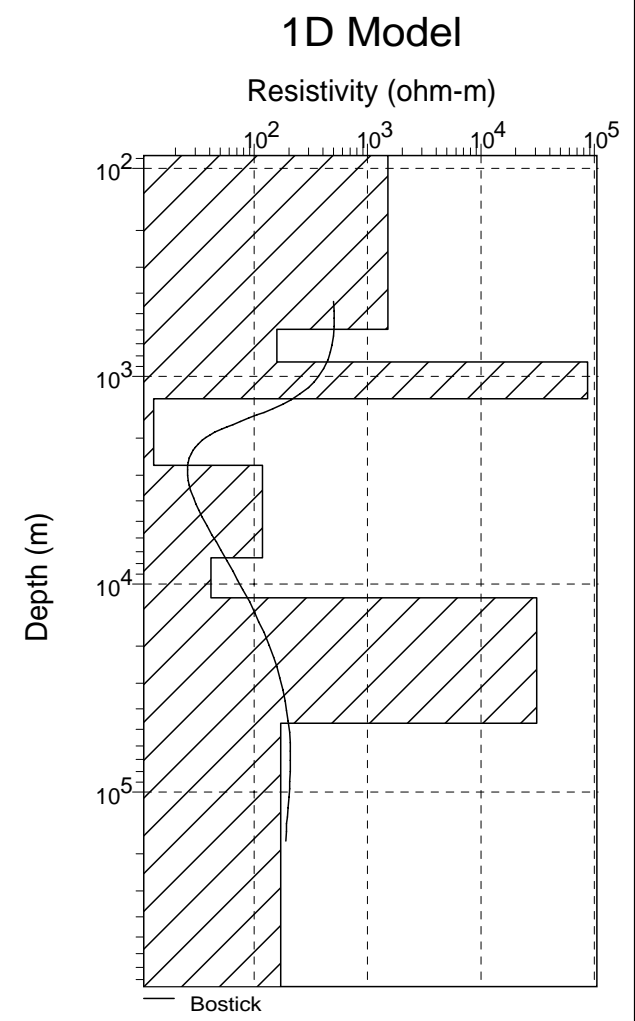
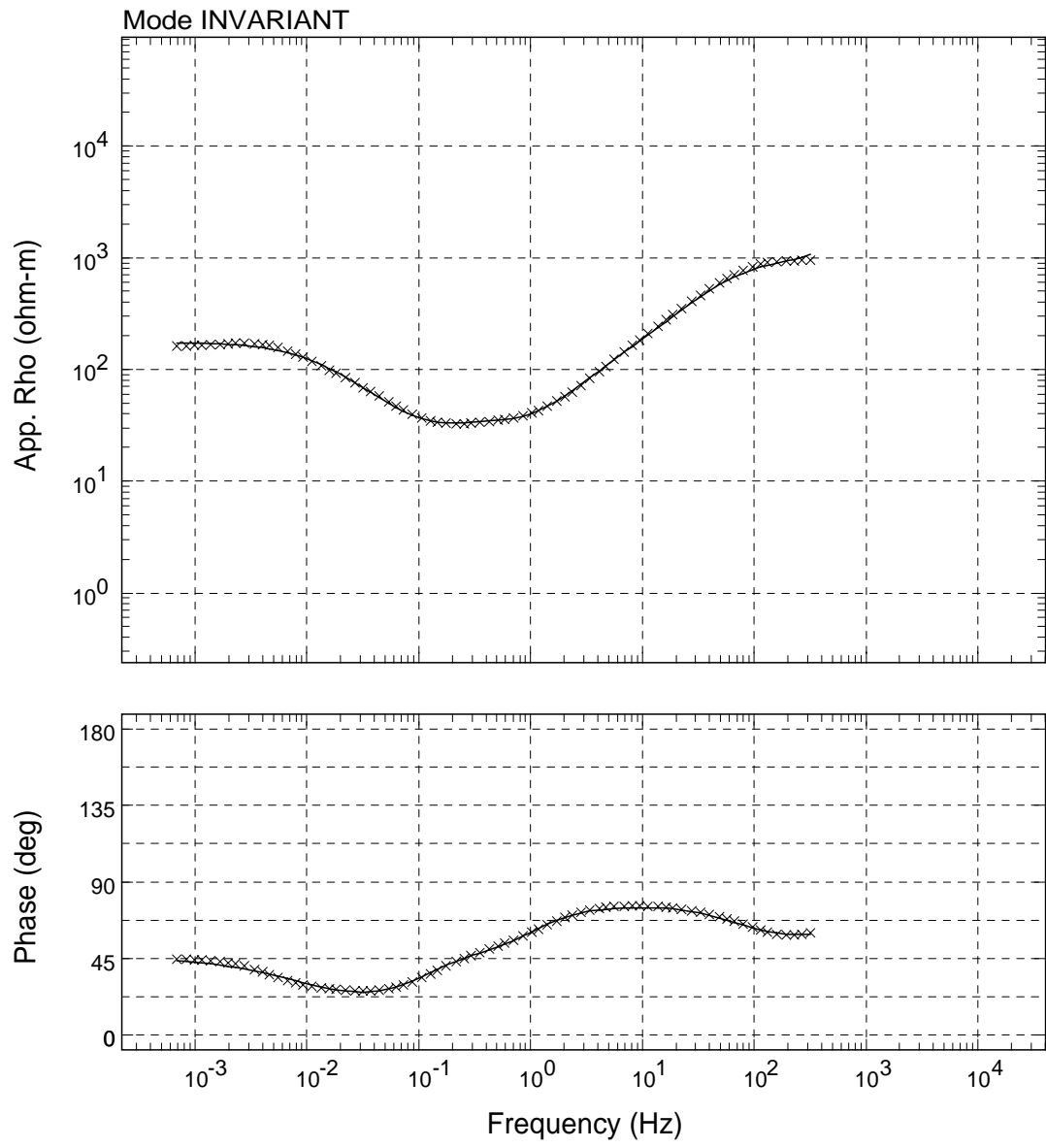
USGS - 01/Jun/2009



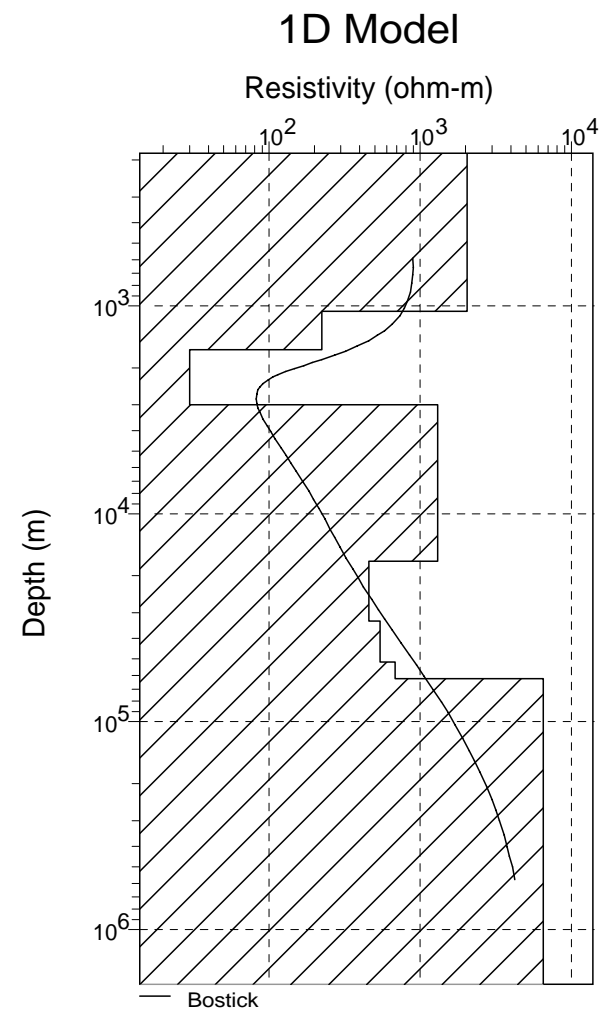
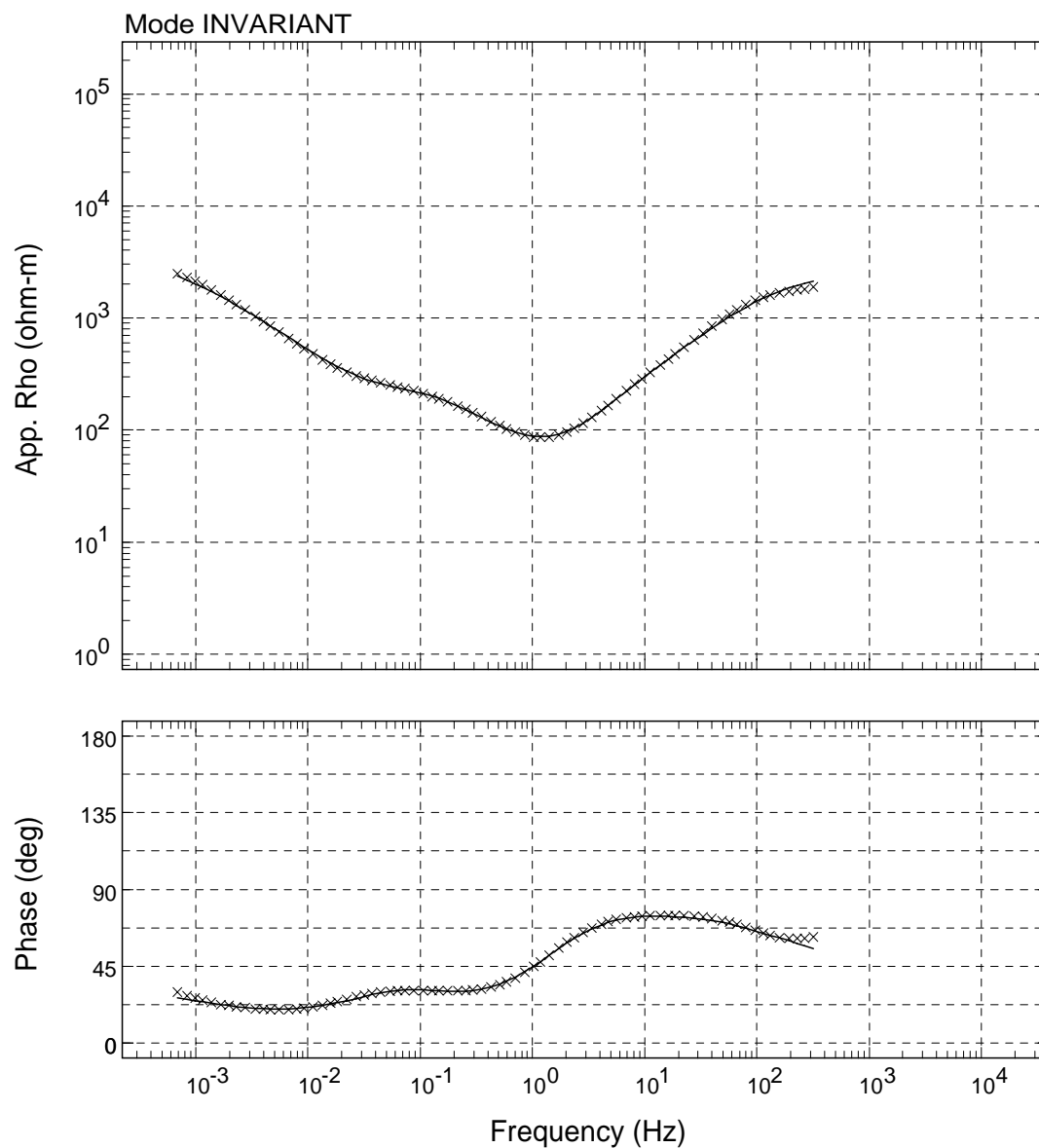
Sounding: 16PT

Area: Hawaii

USGS - 01/Jun/2009



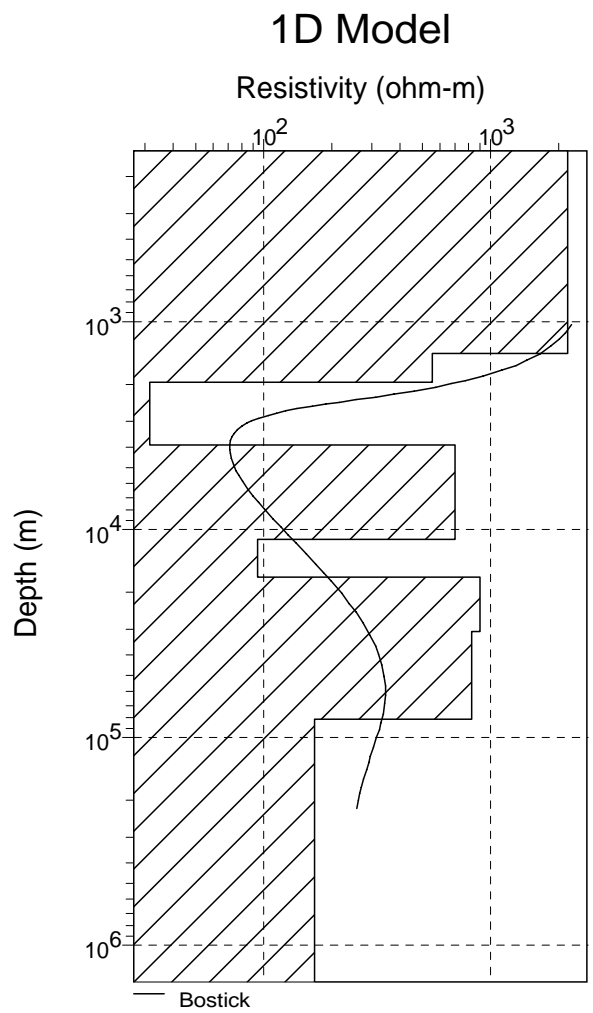
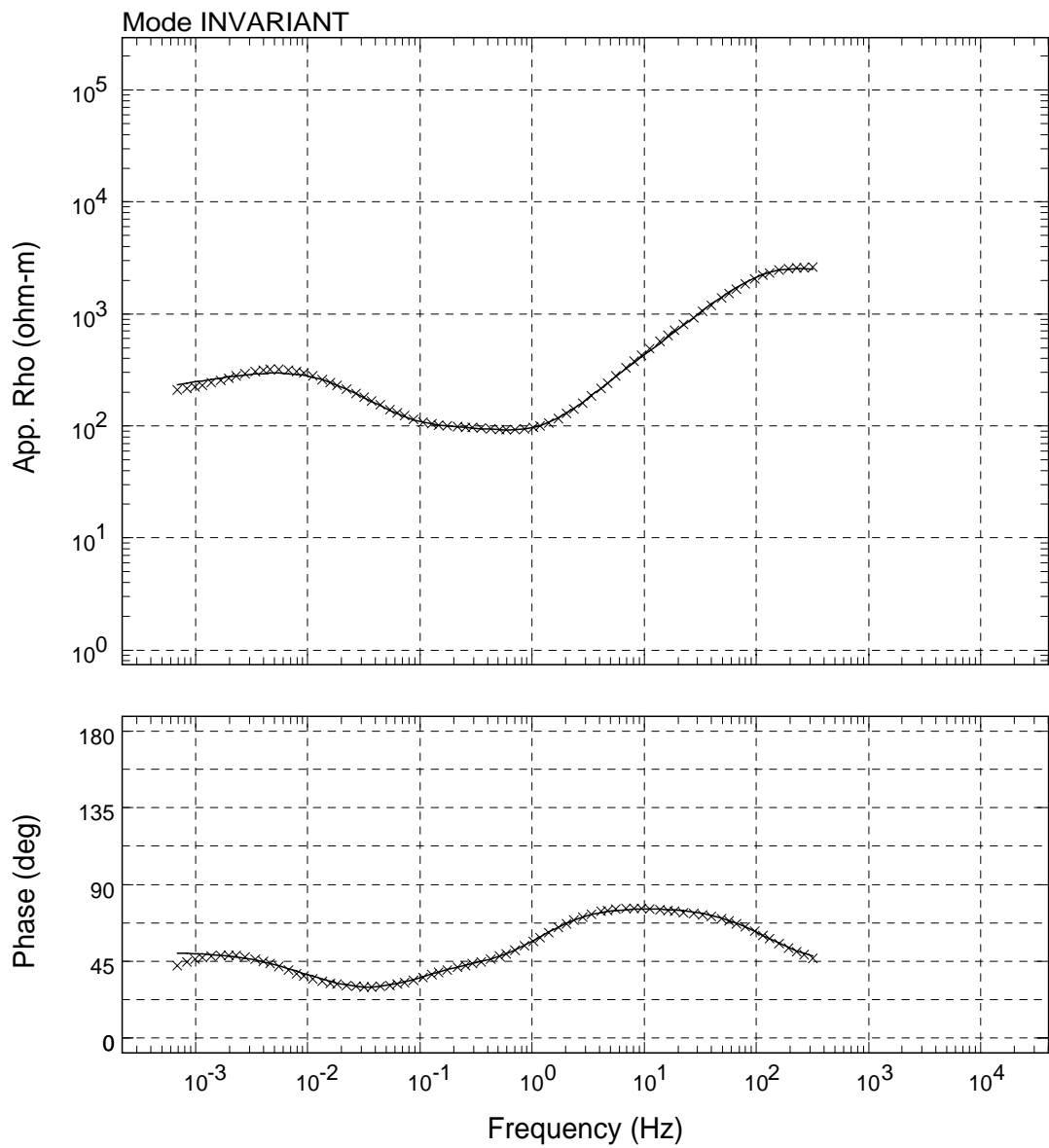
Sounding: HH01
Area: Hawaii
USGS - 01/Jun/2009



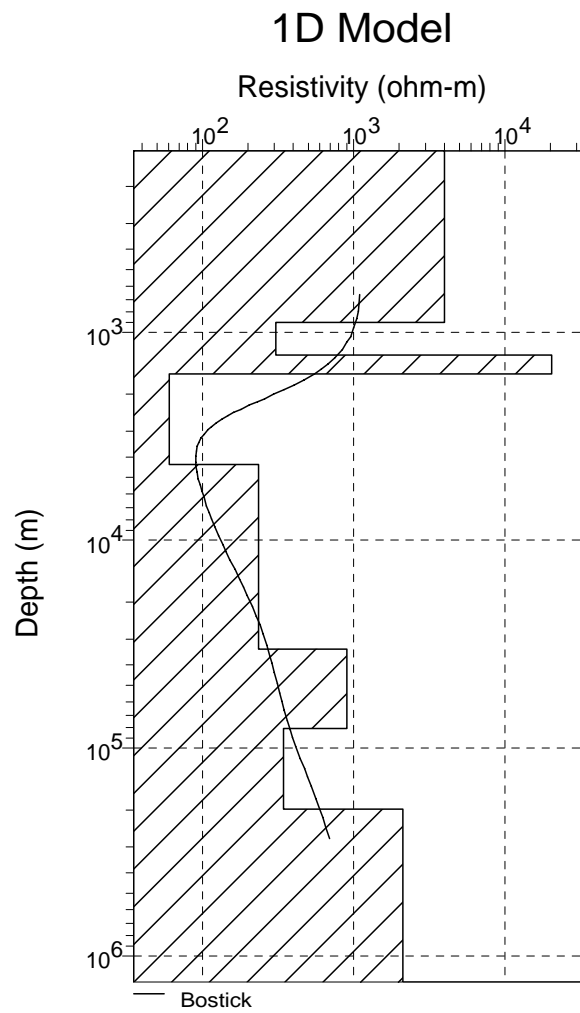
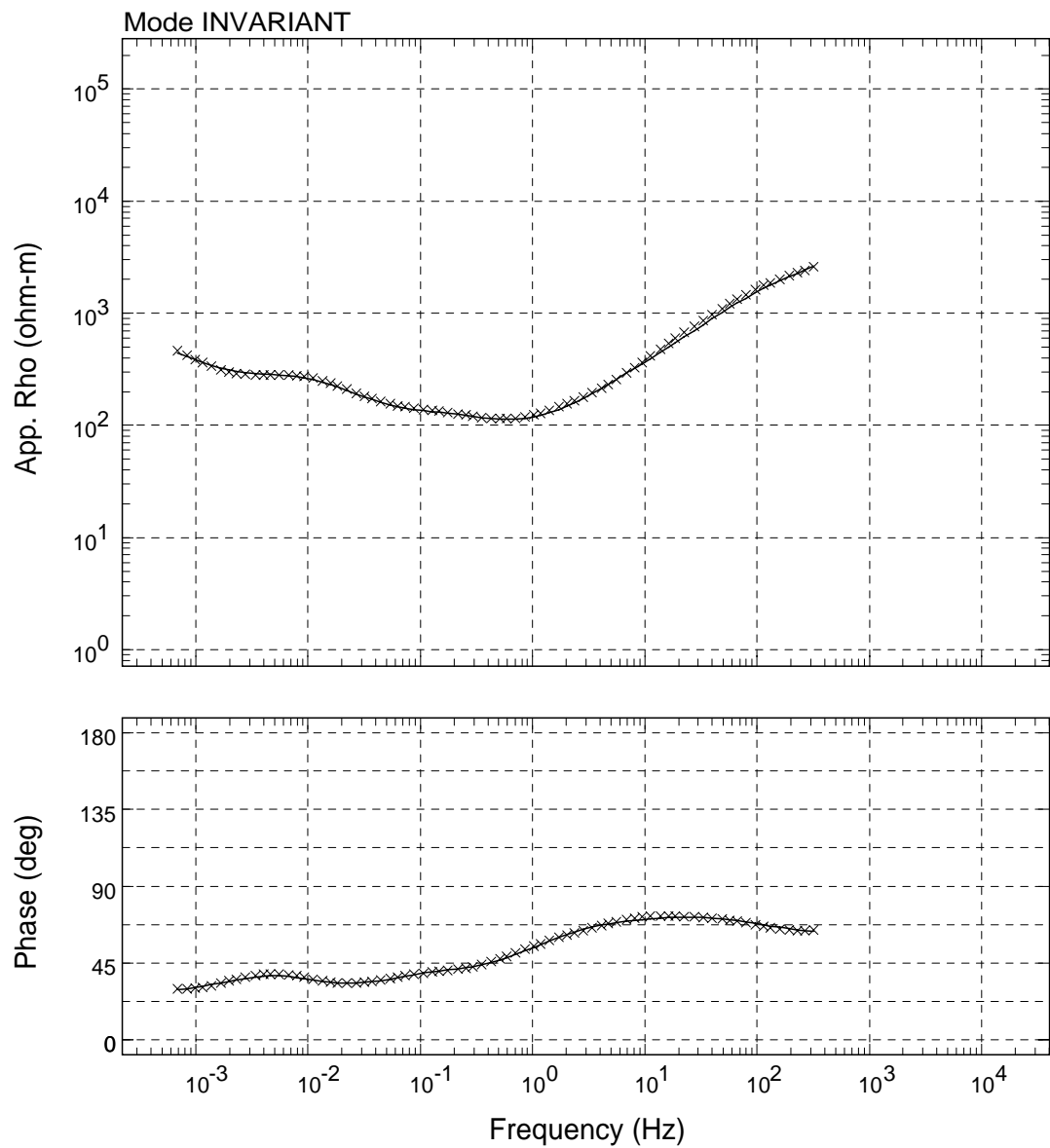
Sounding: HH02

Area: Hawaii

USGS - 01/Jun/2009



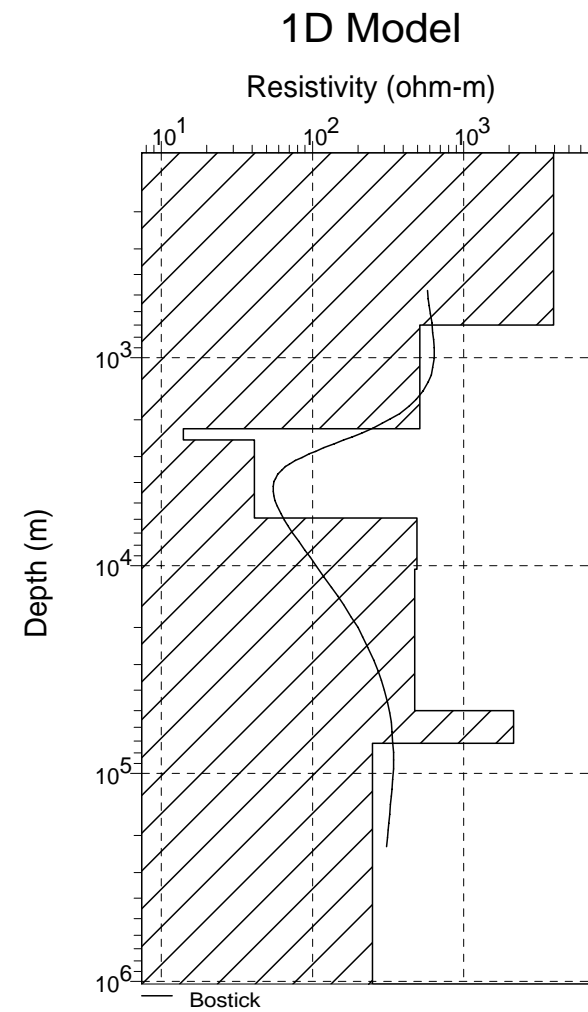
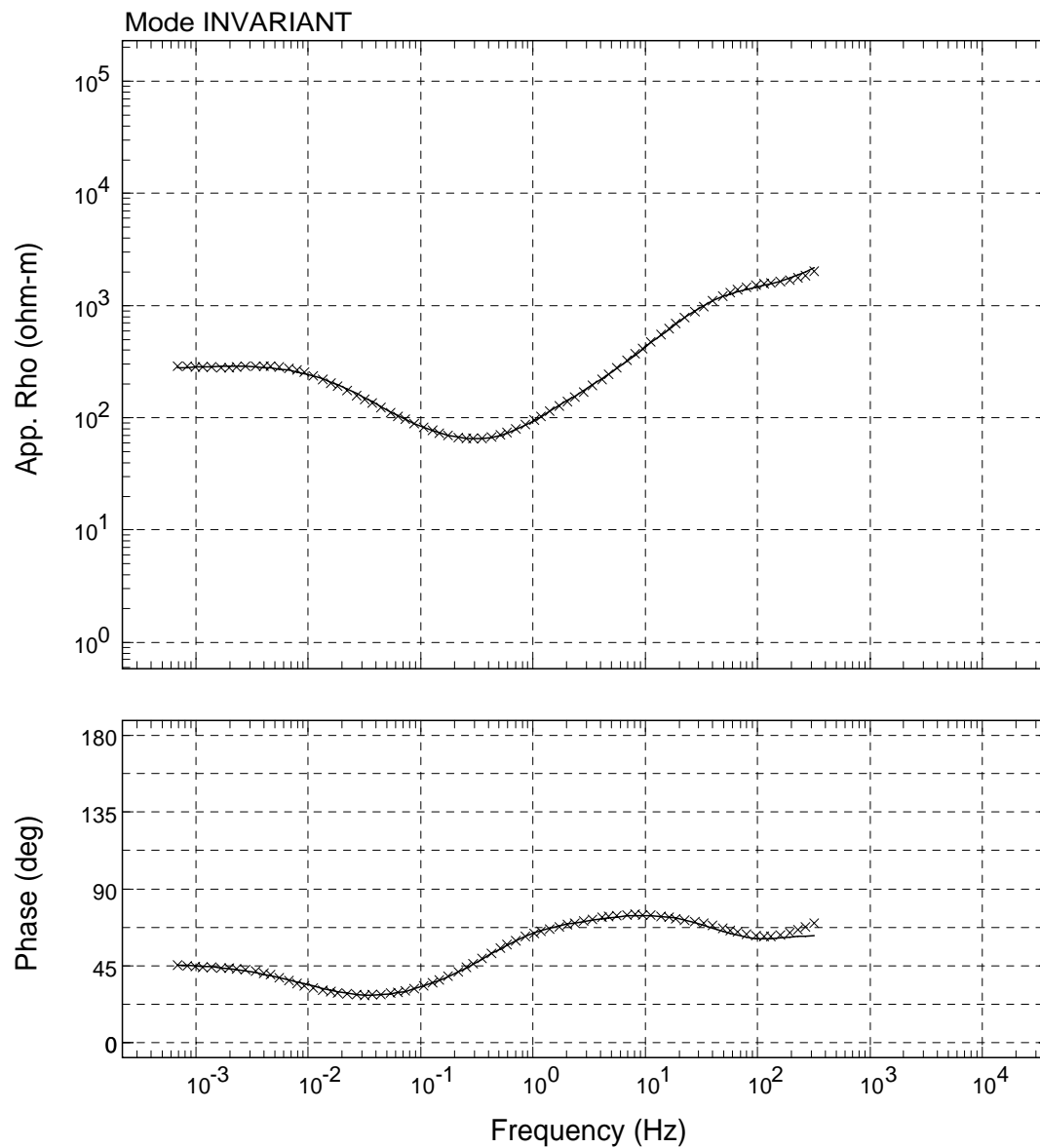
Sounding: HH03
Area: Hawaii
USGS - 01/Jun/2009



Sounding: KK01

Area: Hawaii

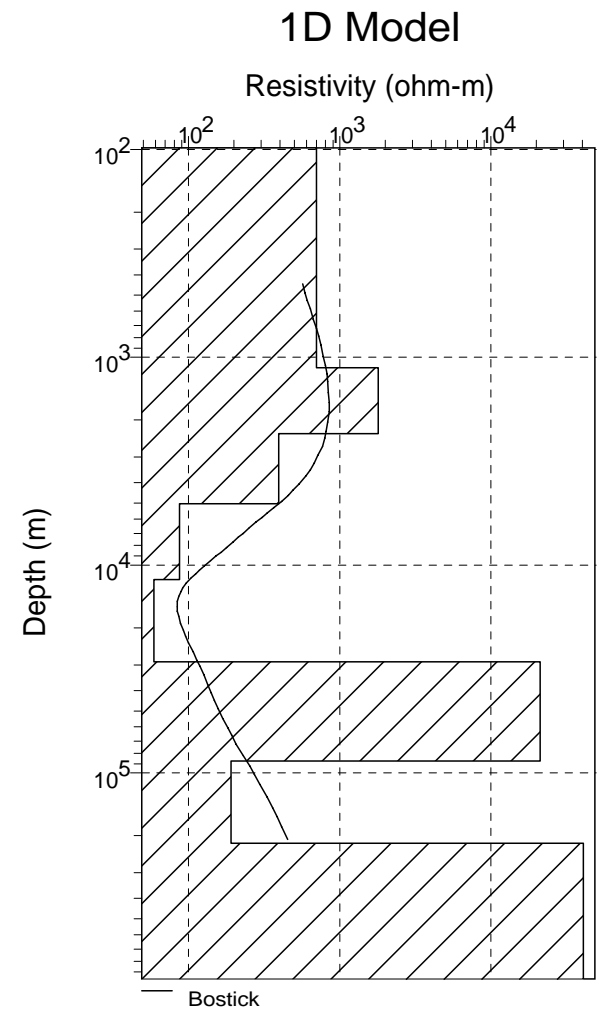
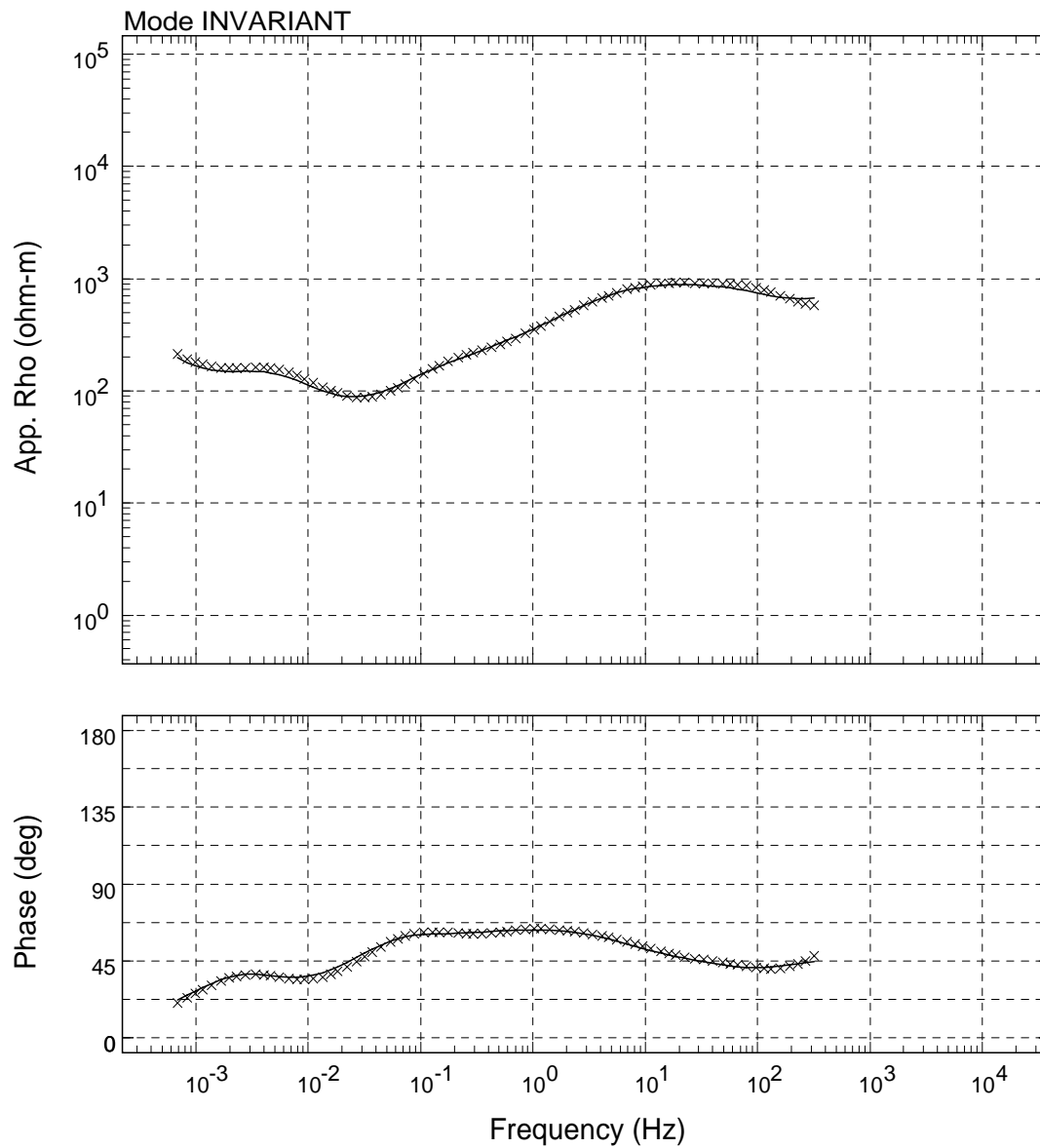
USGS - 01/Jun/2009



Sounding: KK02

Area: Hawaii

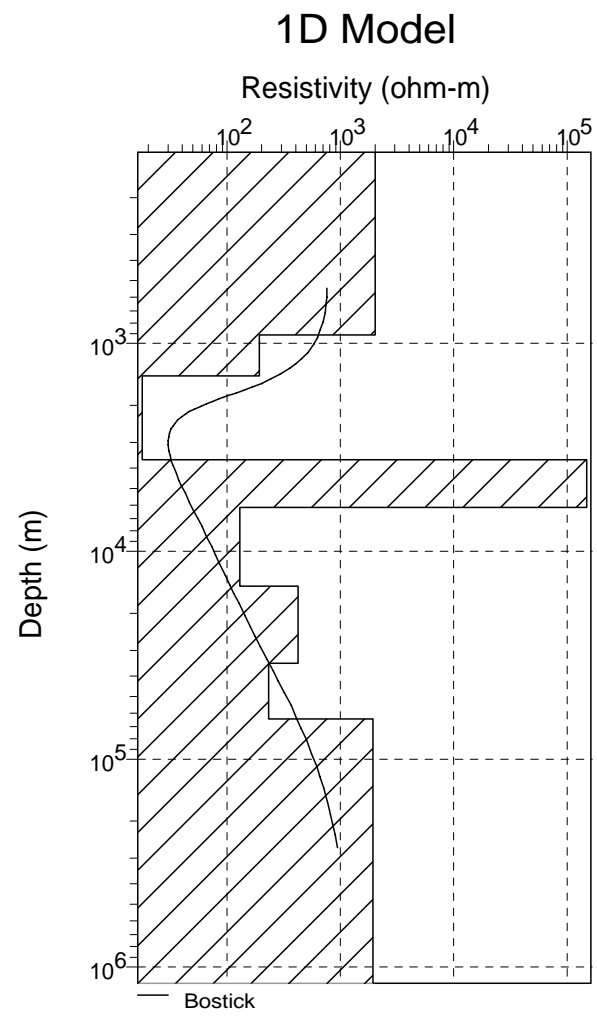
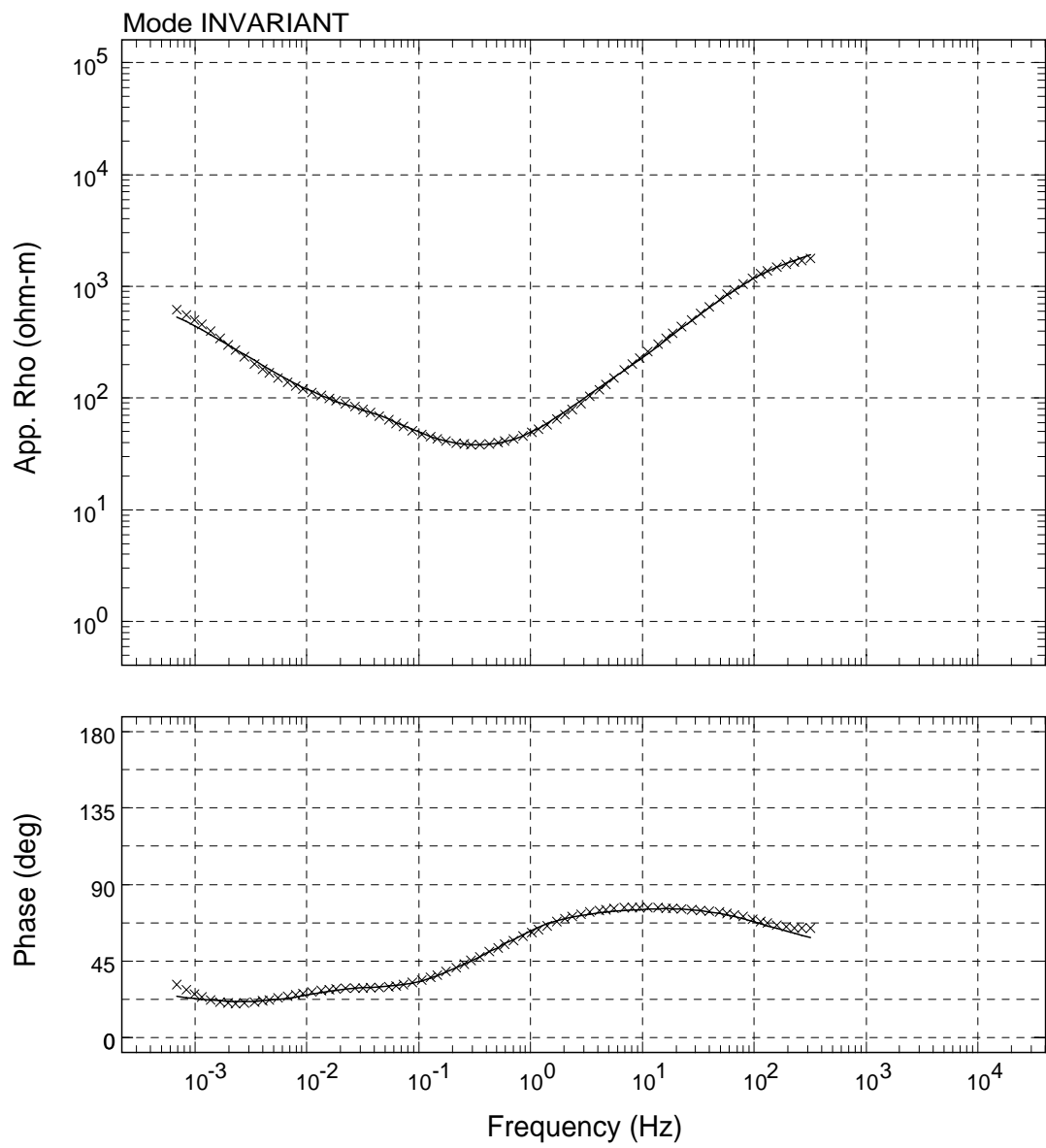
USGS - 01/Jun/2009



Sounding: KM01

Area: Hawaii

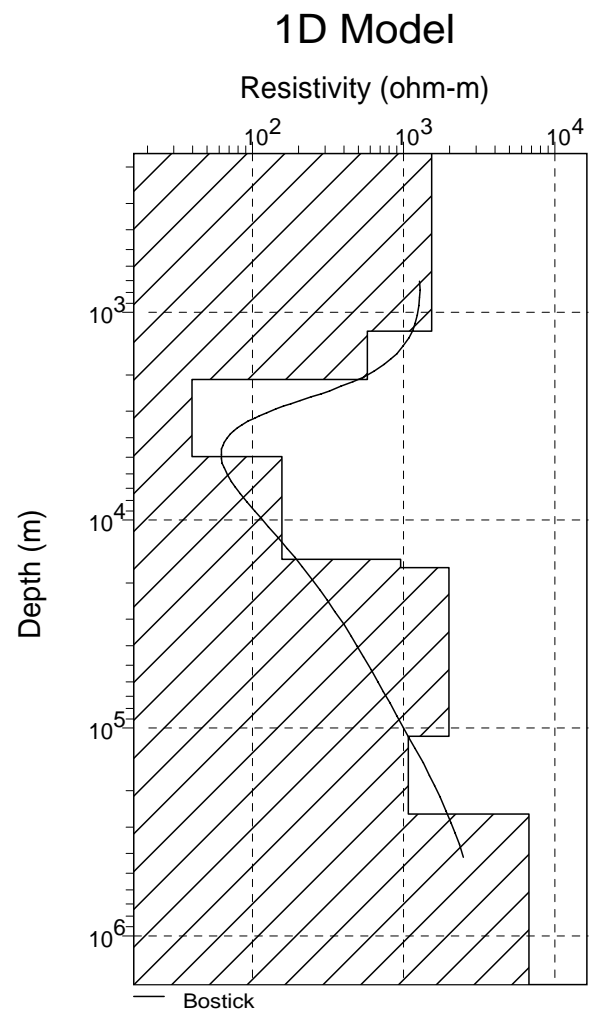
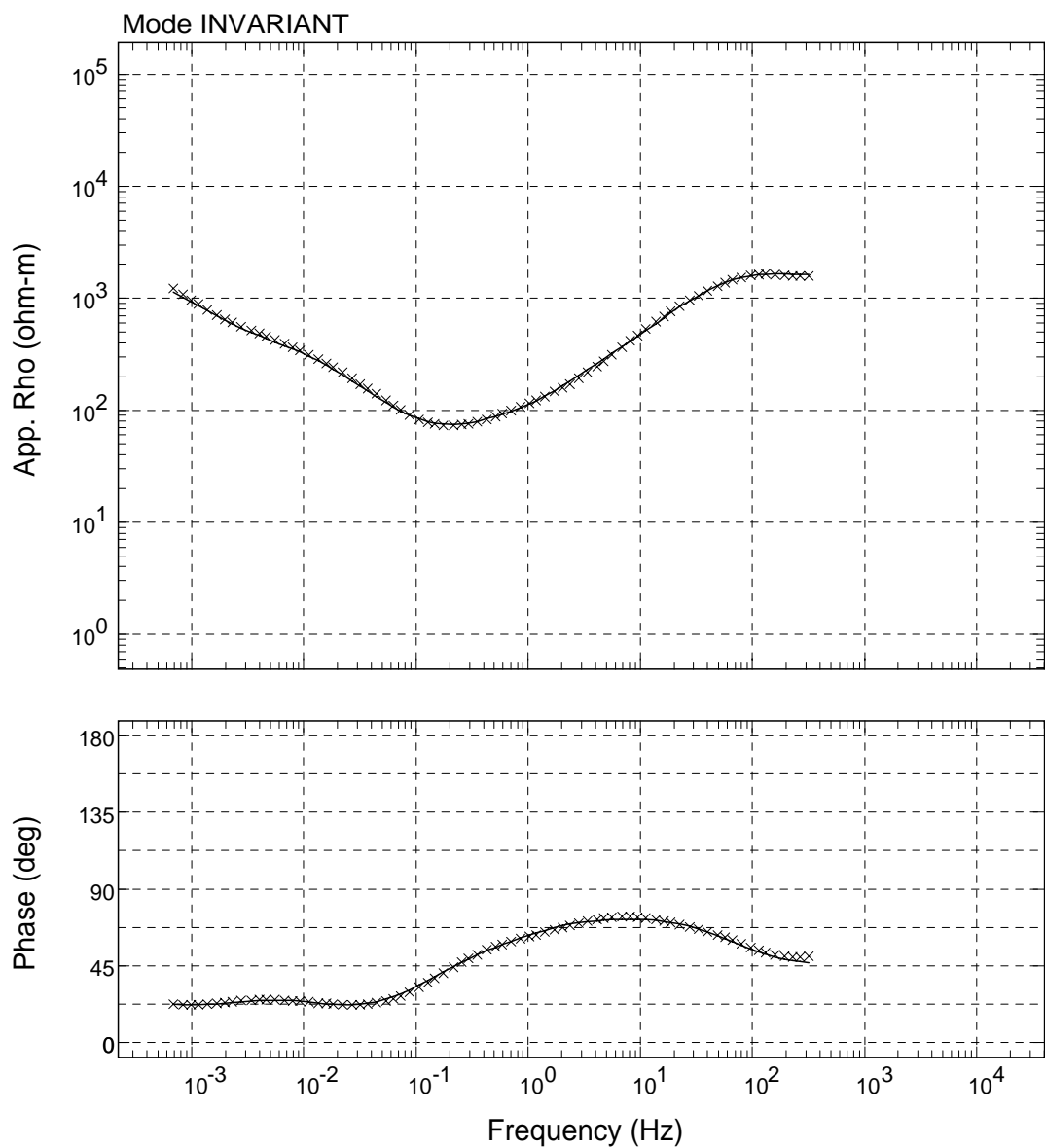
USGS - 01/Jun/2009



Sounding: MKR1

Area: Hawaii

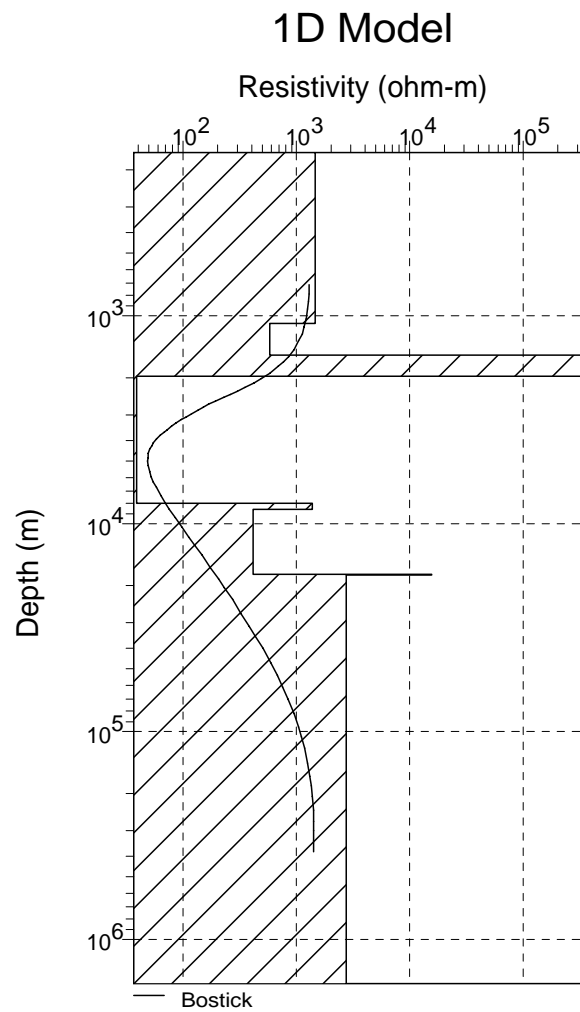
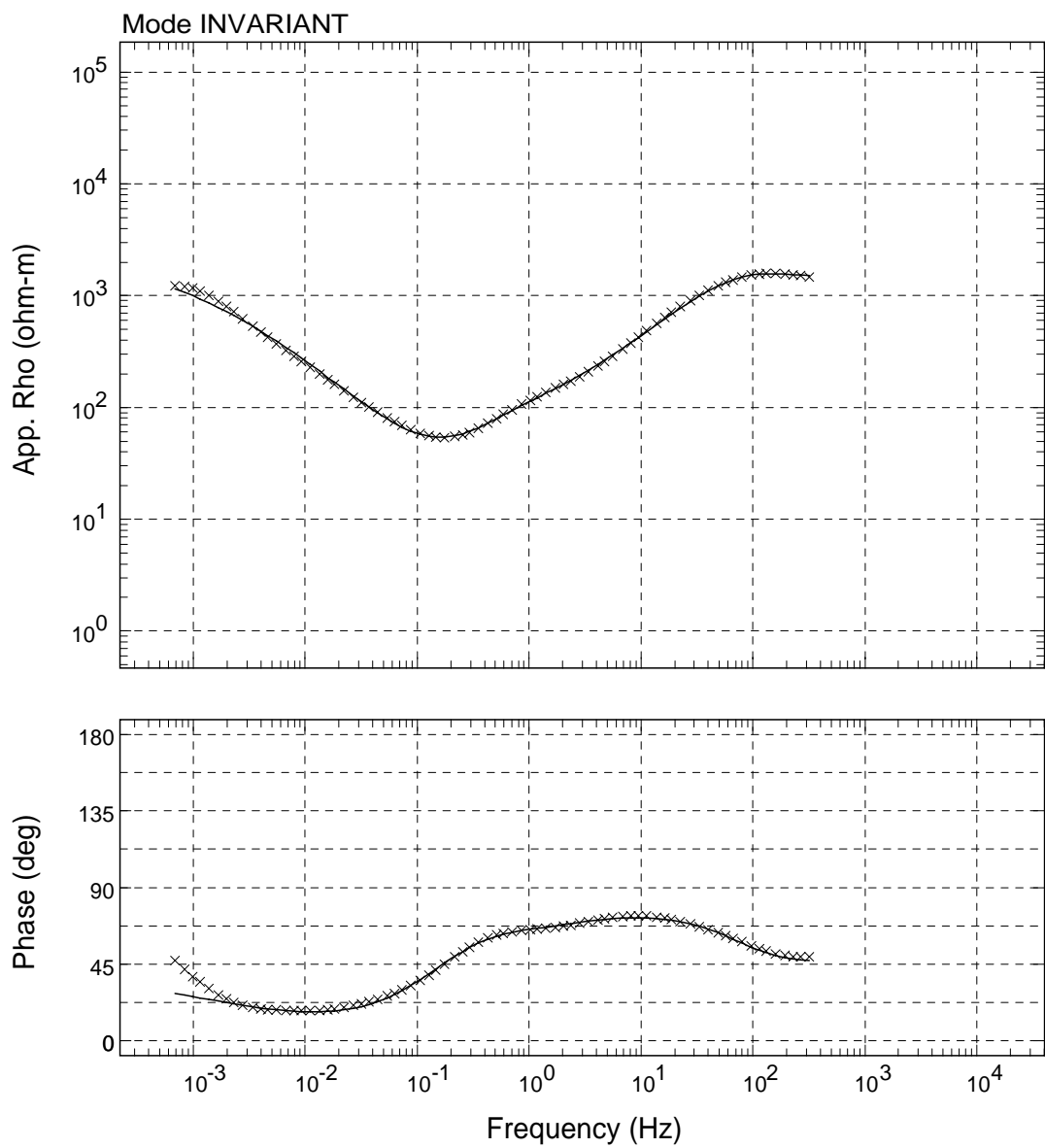
USGS - 01/Jun/2009



Sounding: ML01

Area: Hawaii

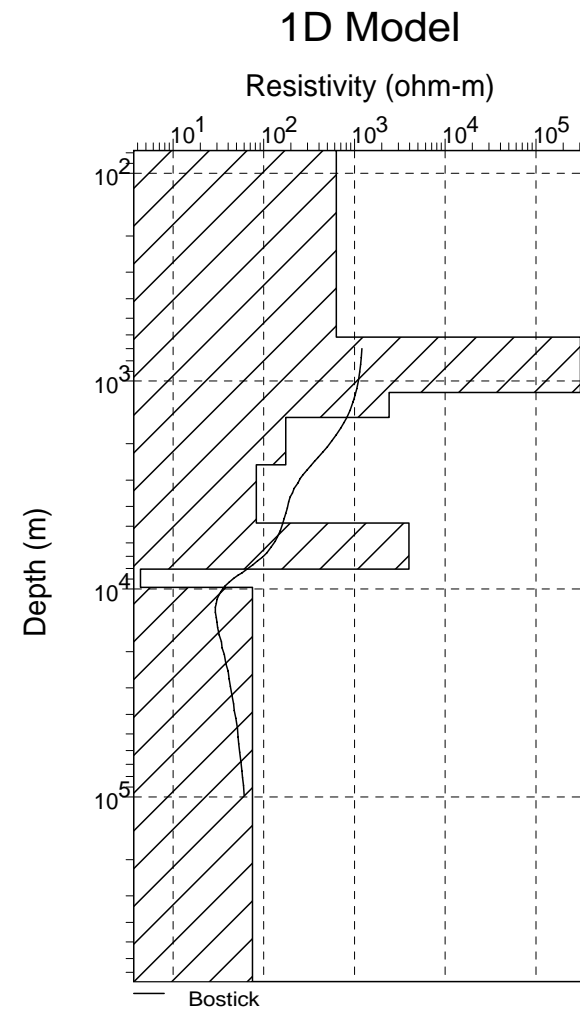
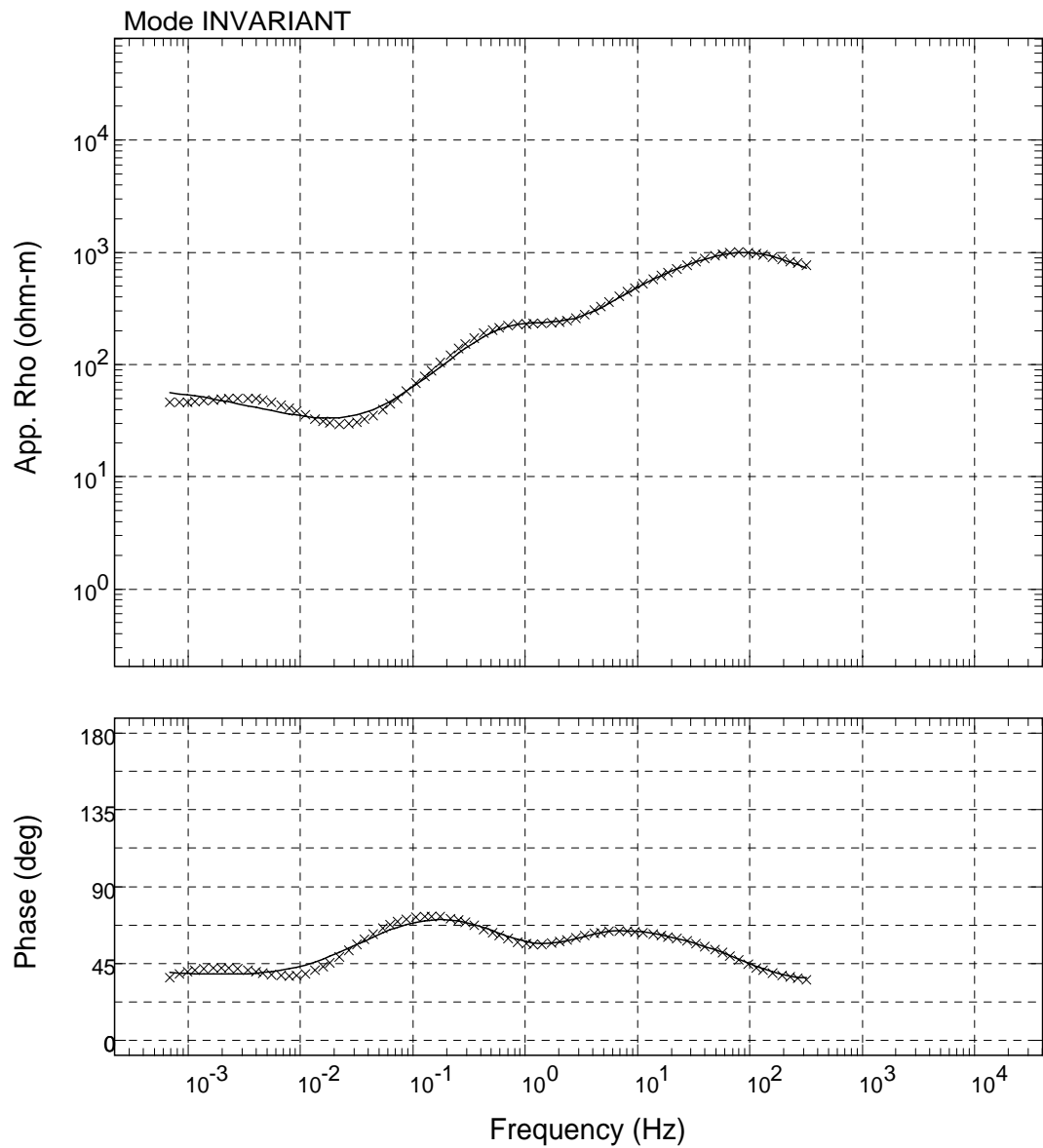
USGS - 01/Jun/2009



Sounding: ML02

Area: Hawaii

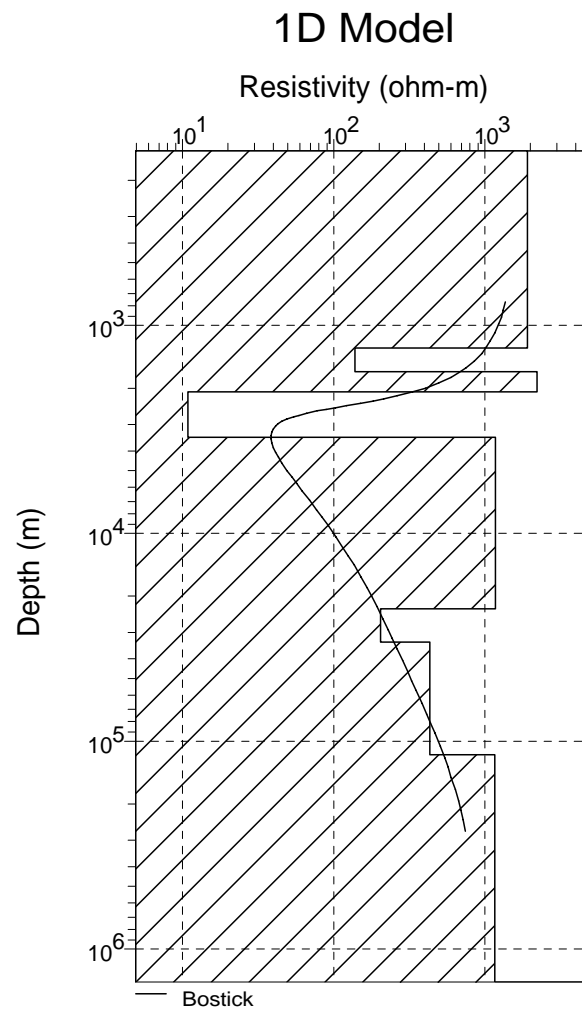
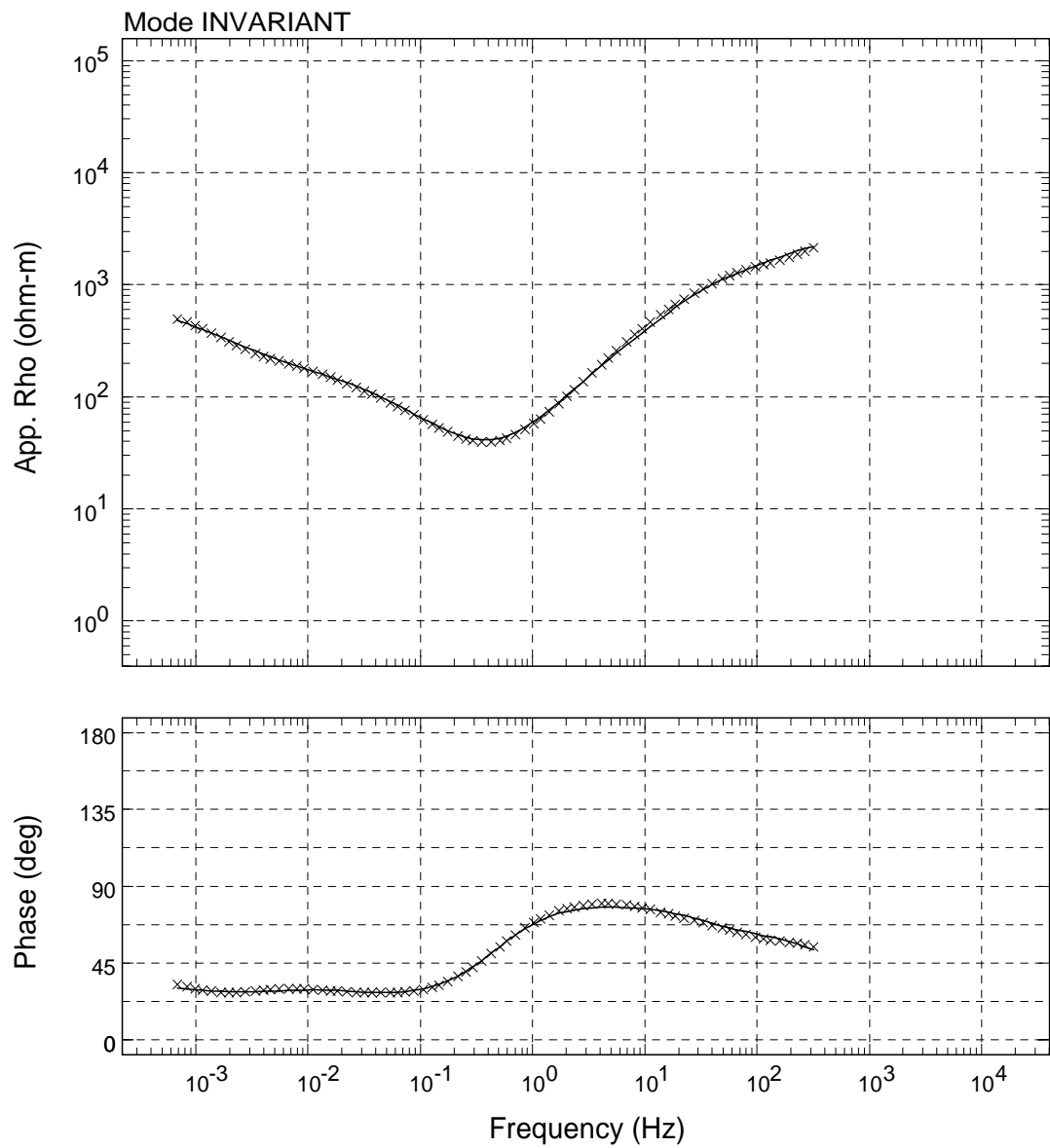
USGS - 01/Jun/2009



Sounding: MM13

Area: Hawaii

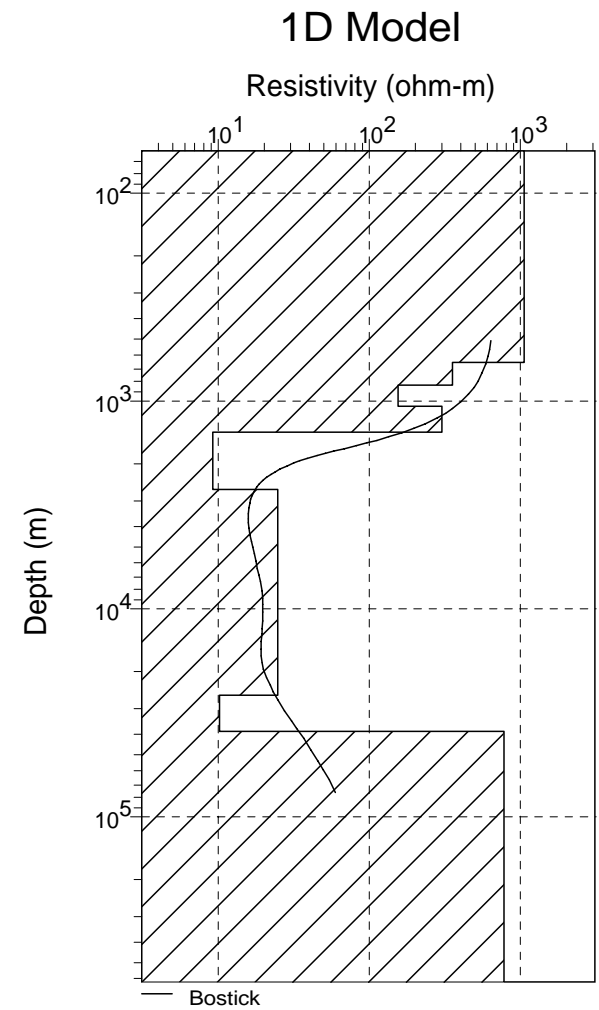
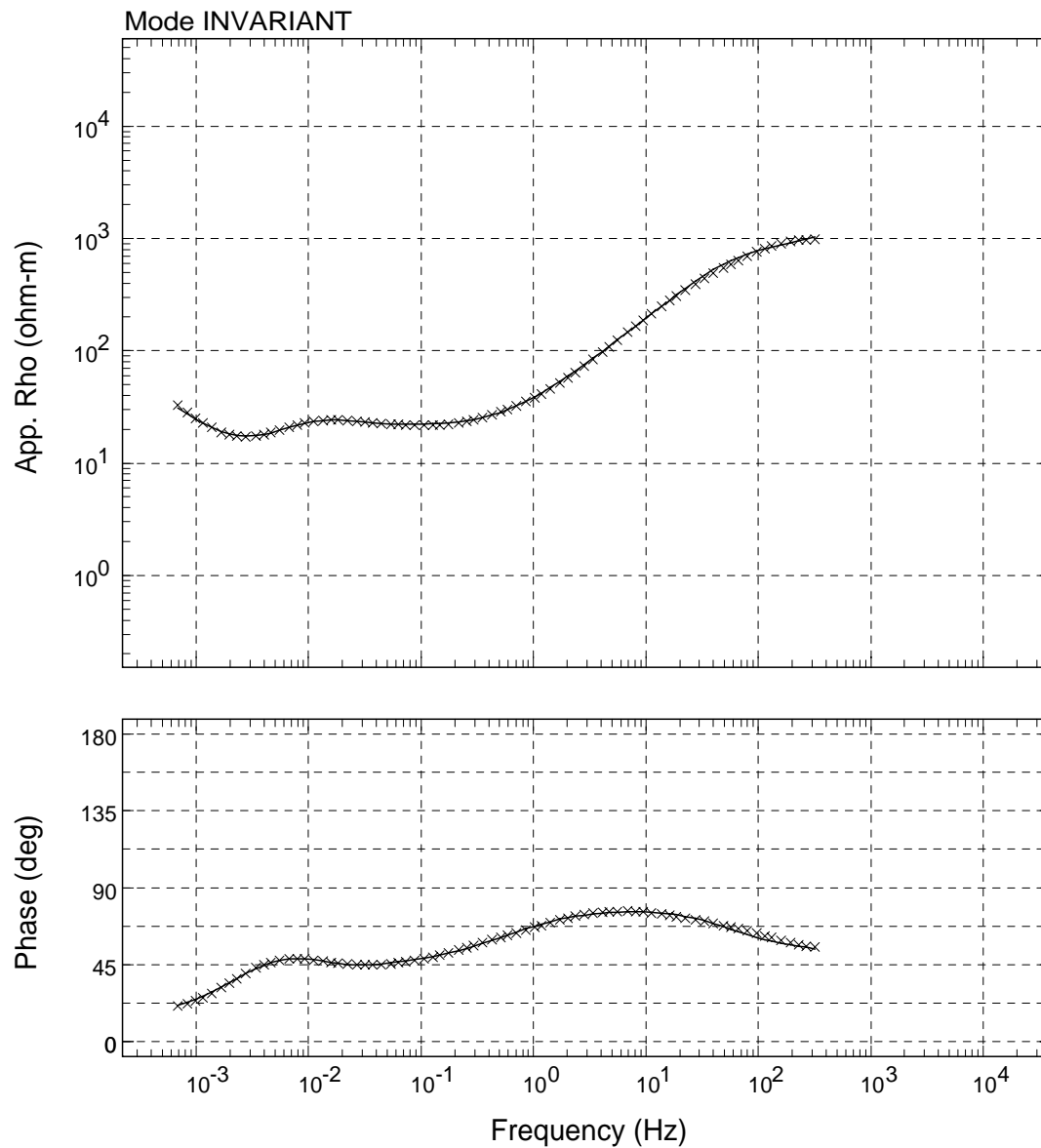
USGS - 01/Jun/2009



Sounding: OR01

Area: Hawaii

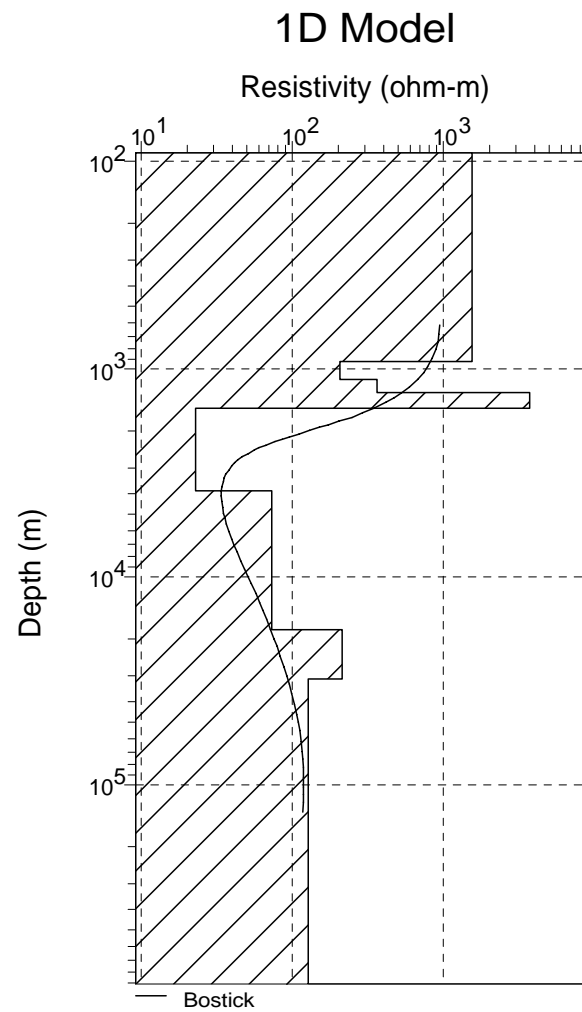
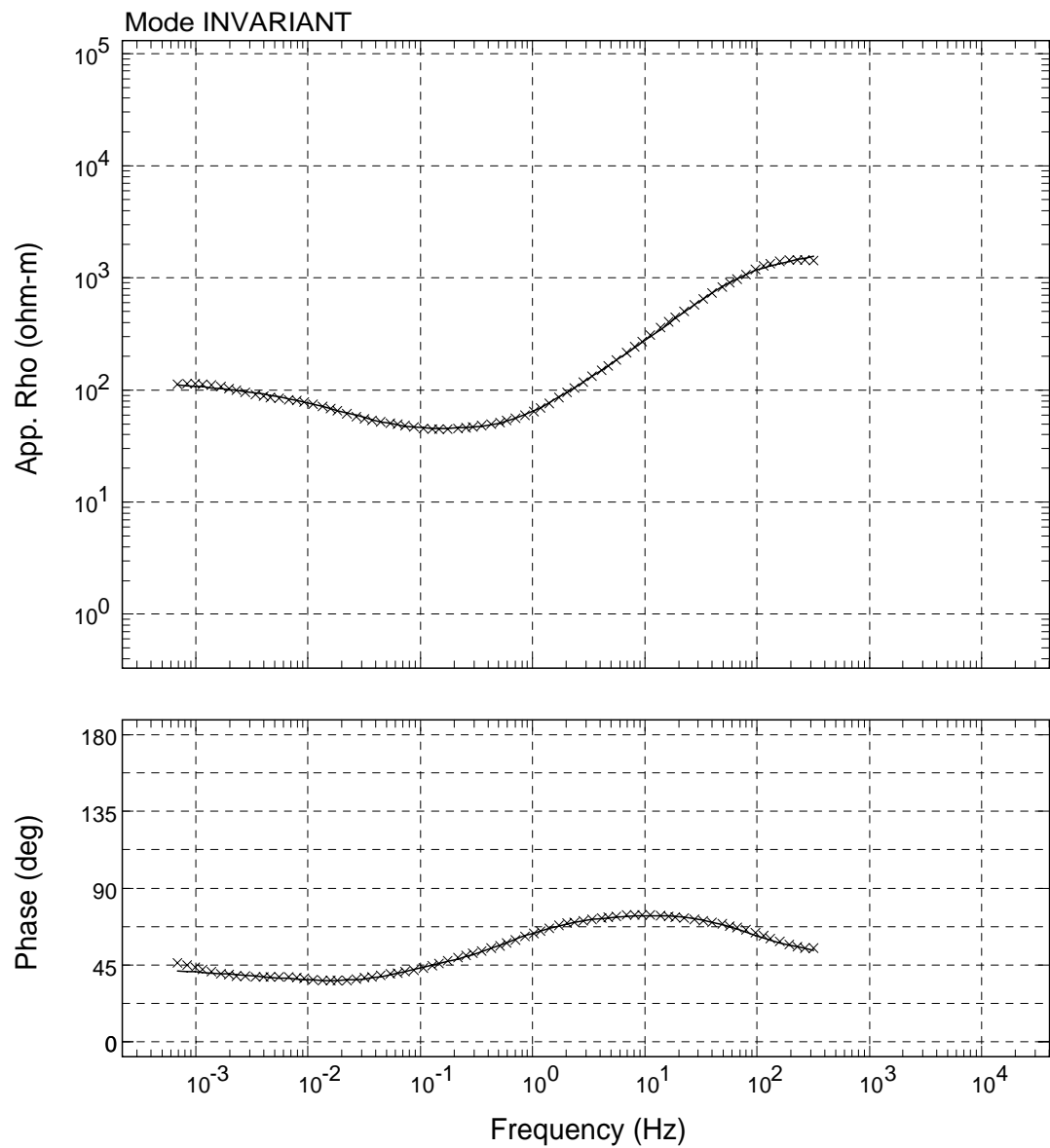
USGS - 01/Jun/2009



Sounding: PK01

Area: Hawaii

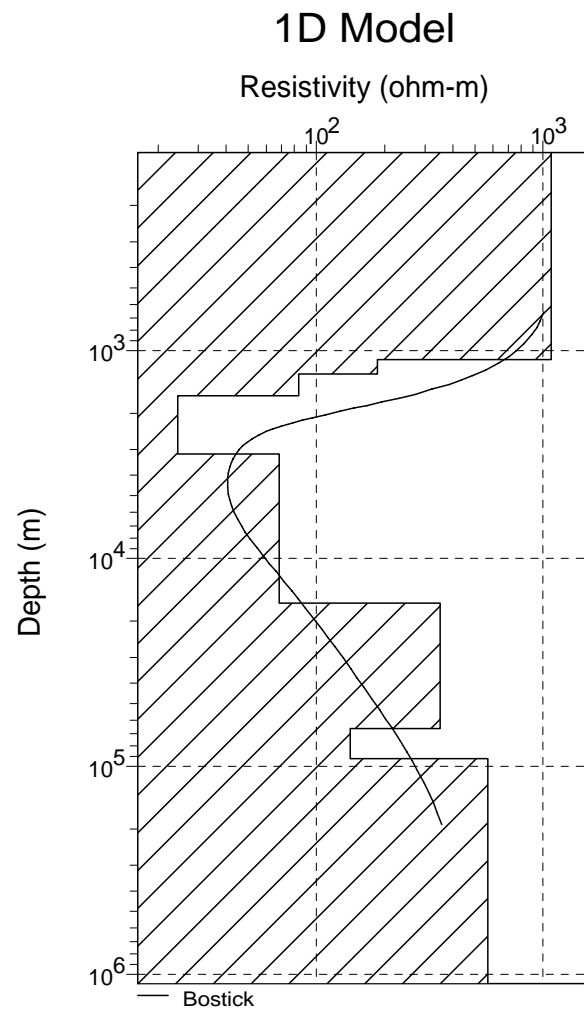
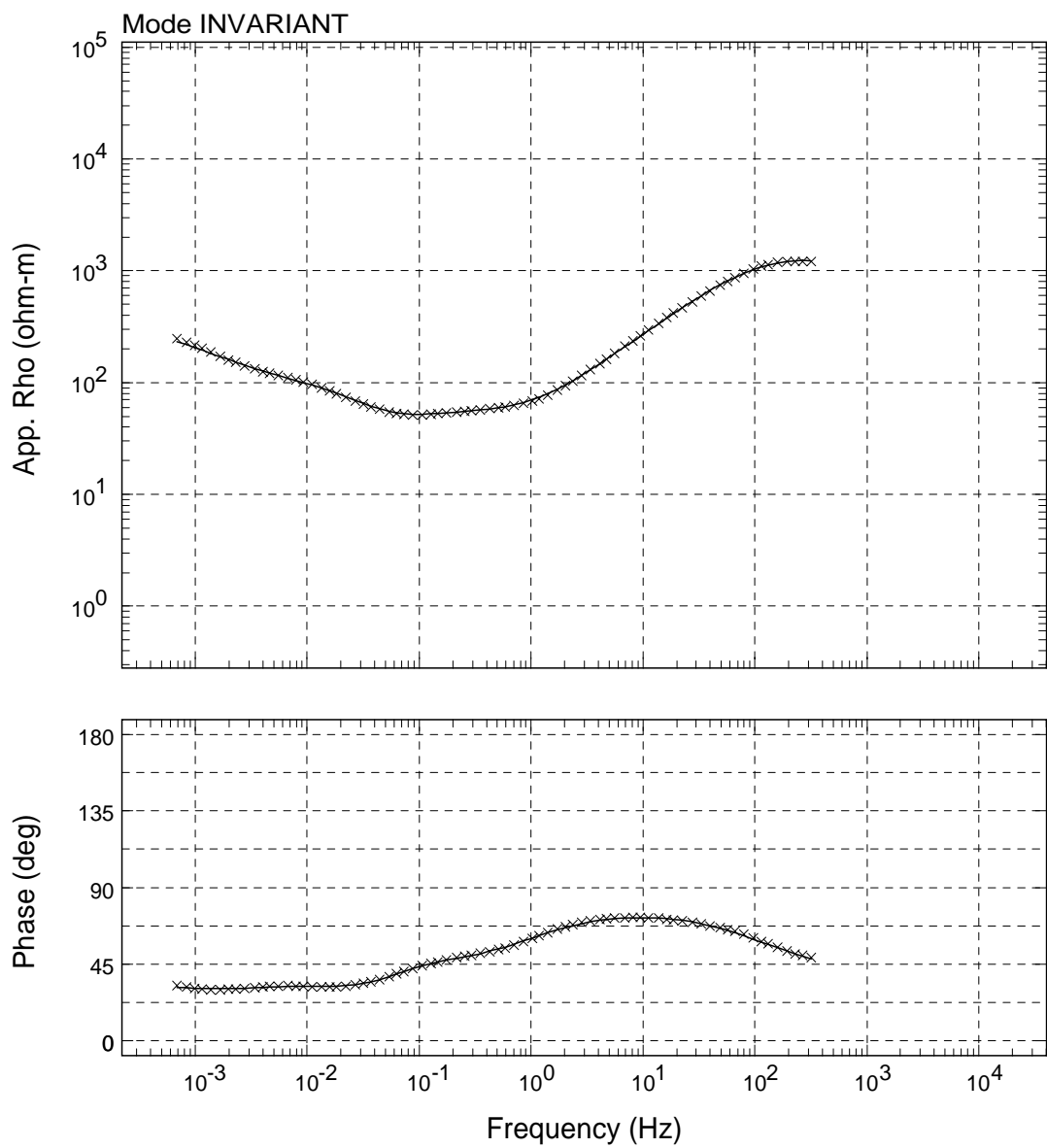
USGS - 01/Jun/2009



Sounding: PK02

Area: Hawaii

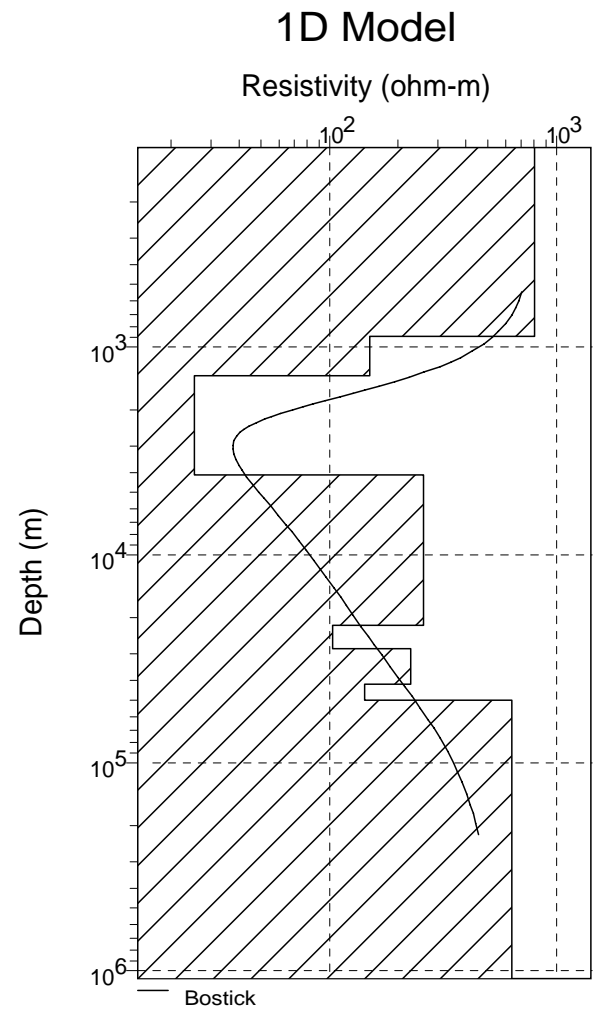
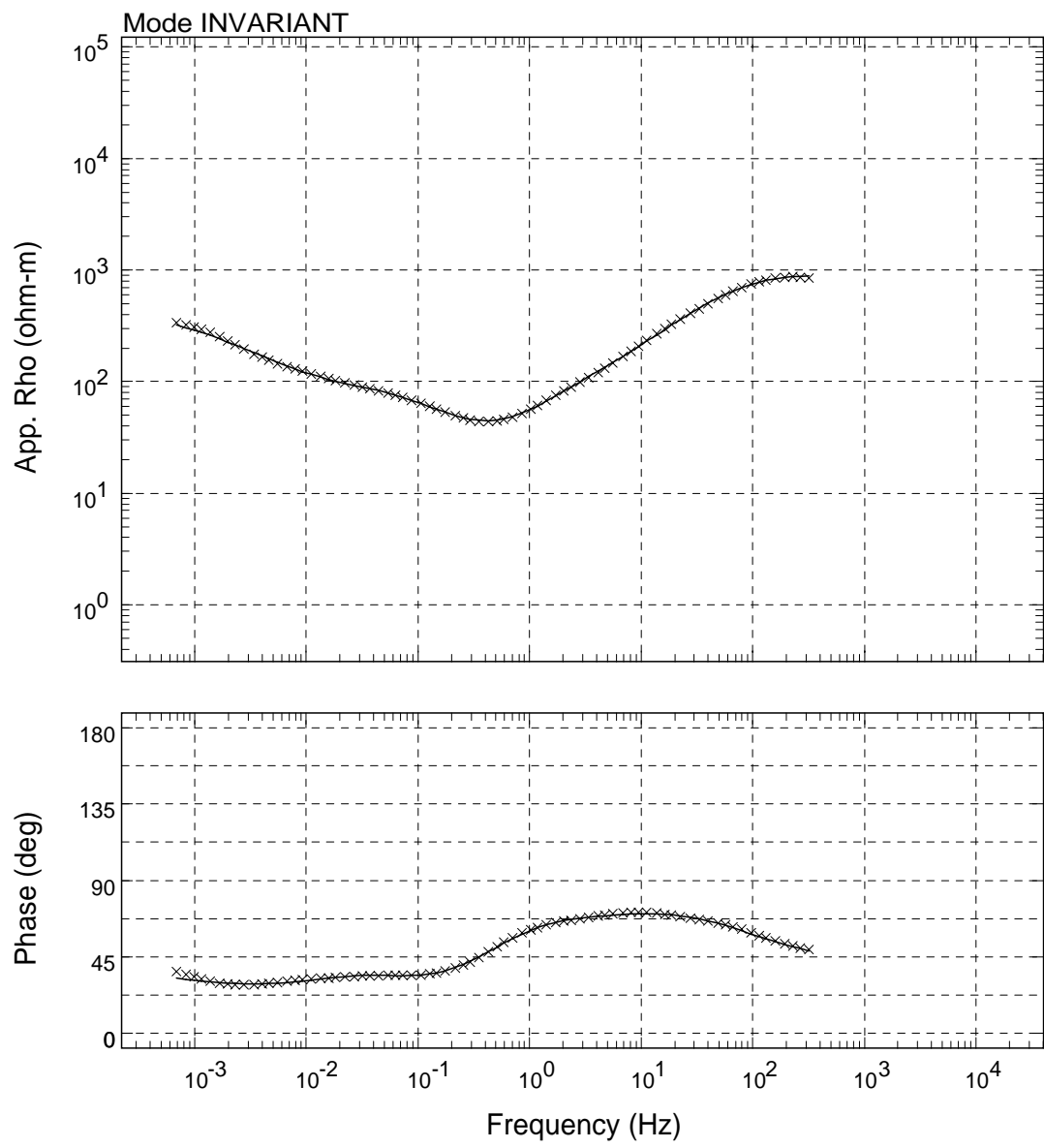
USGS - 01/Jun/2009



Sounding: PK03

Area: Hawaii

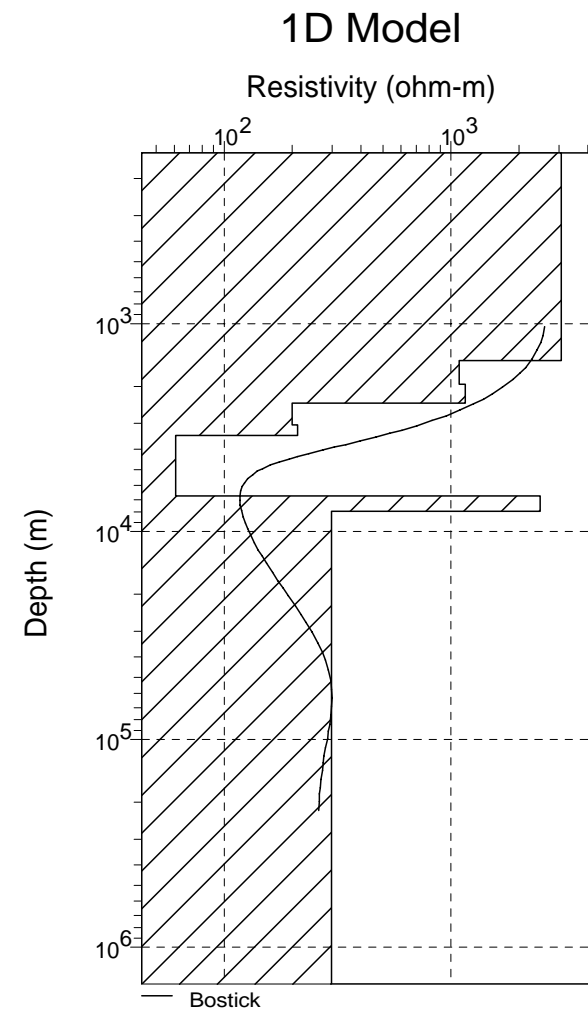
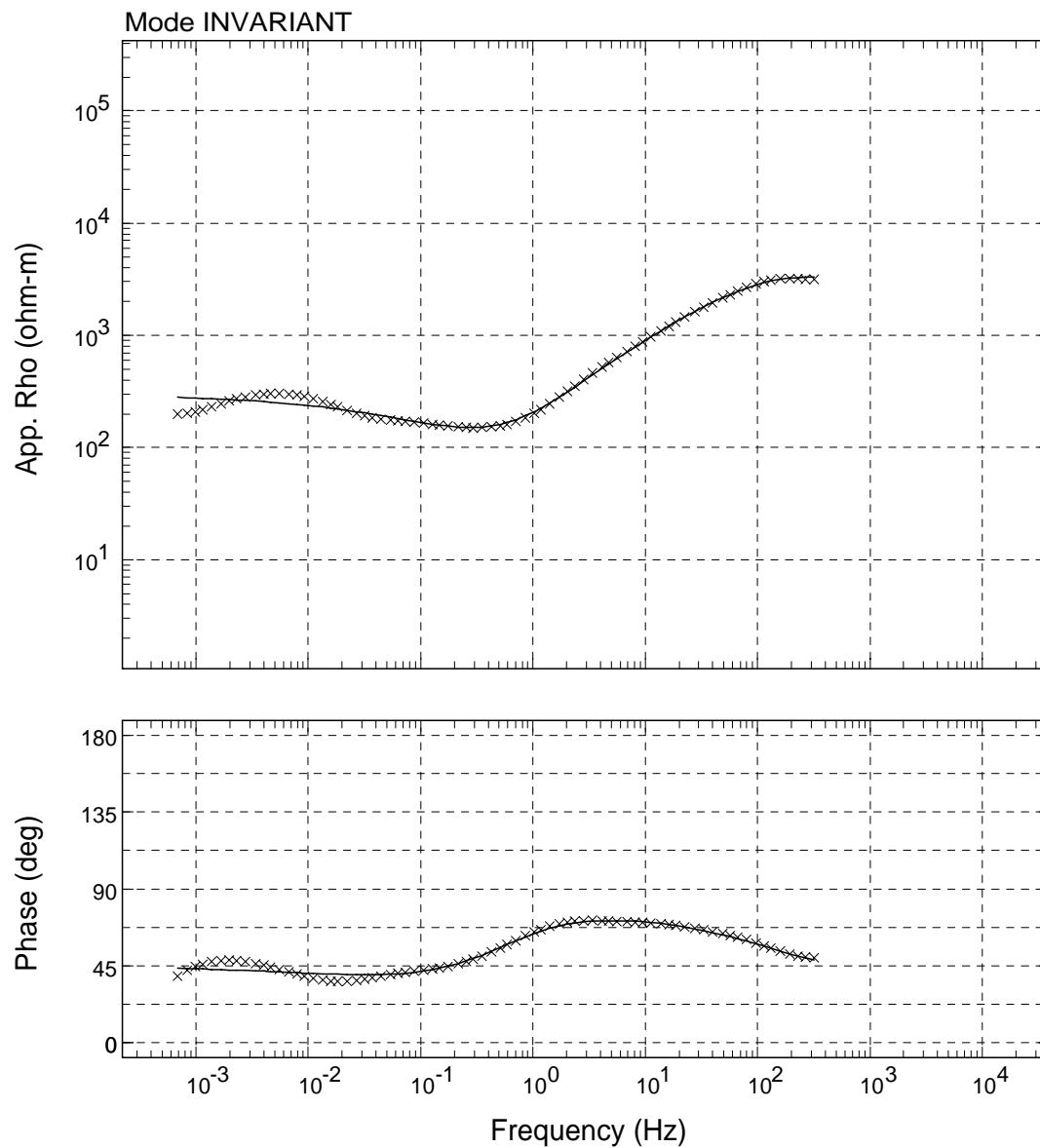
USGS - 01/Jun/2009



Sounding: PK04

Area: Hawaii

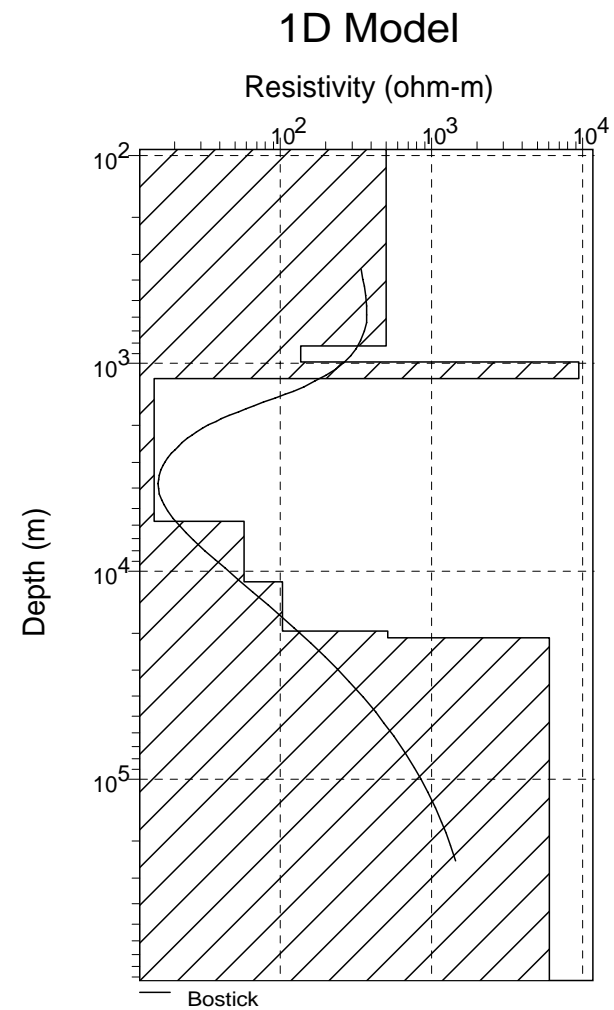
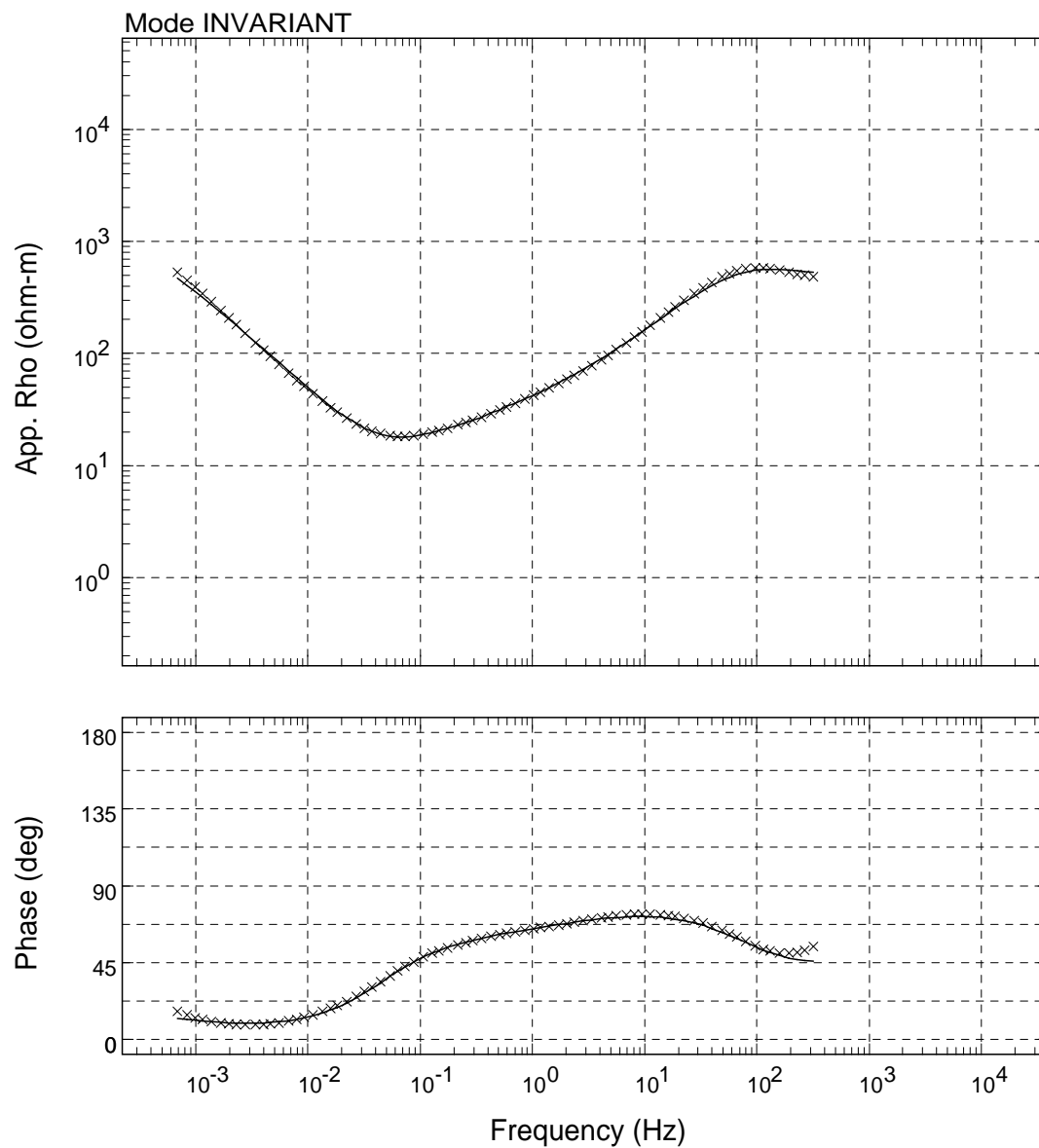
USGS - 01/Jun/2009



Sounding: PK05

Area: Hawaii

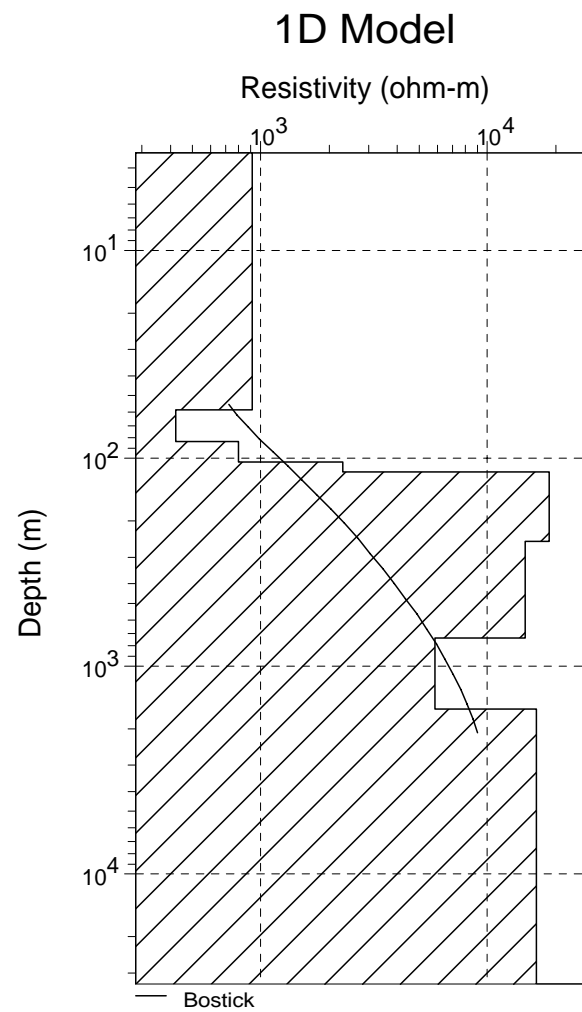
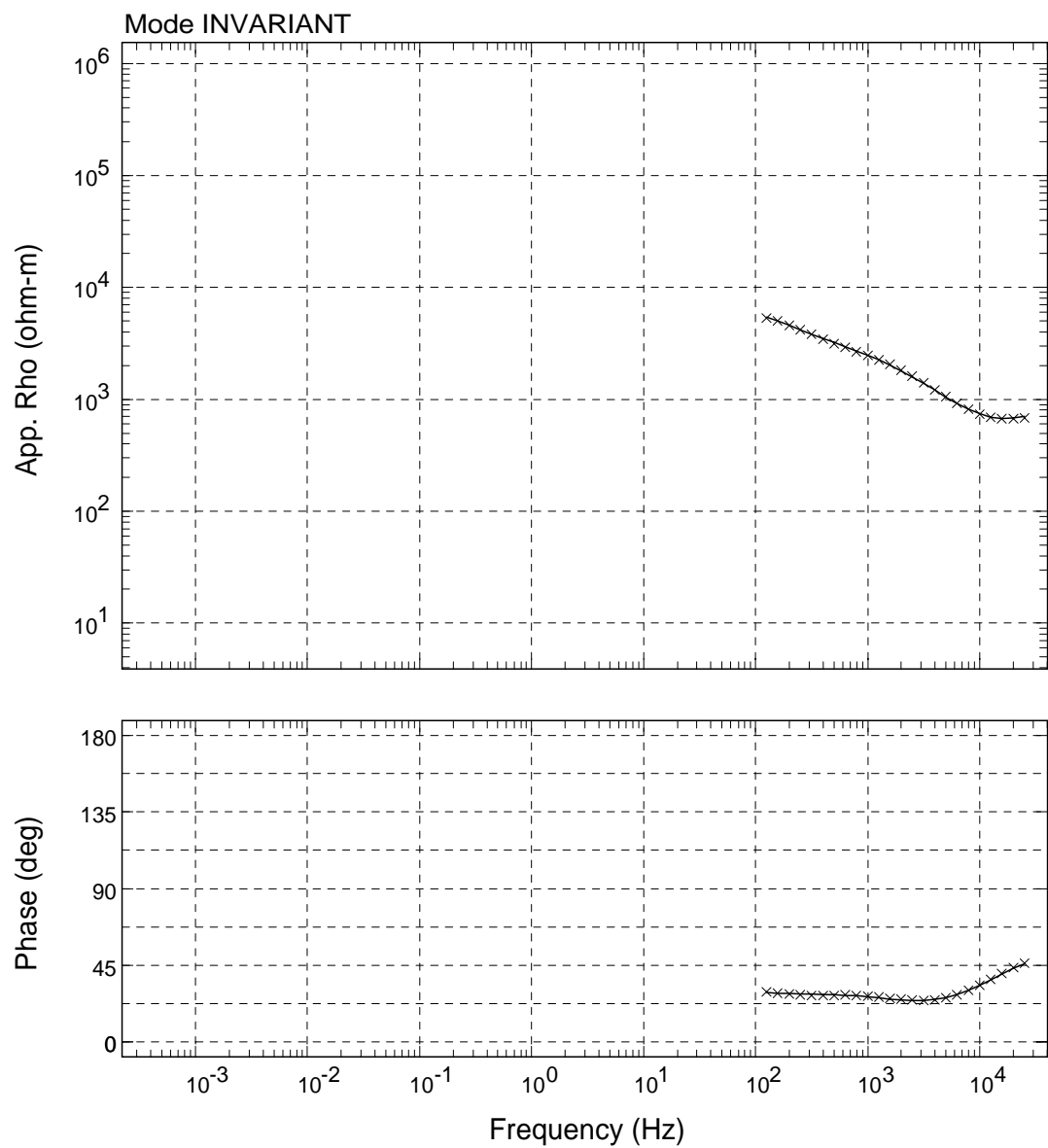
USGS - 01/Jun/2009



Sounding: REF1

Area: Hawaii

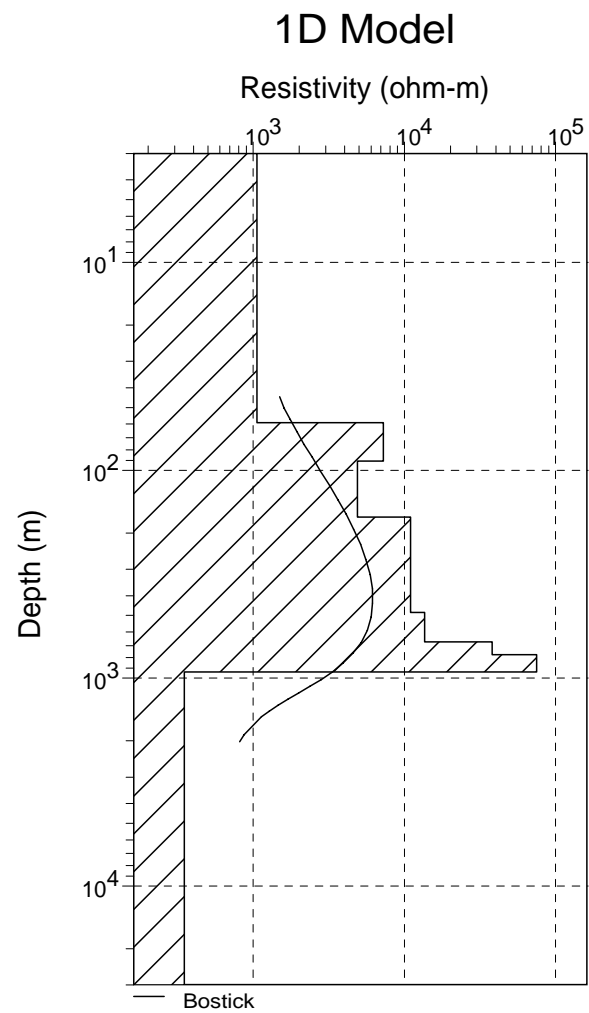
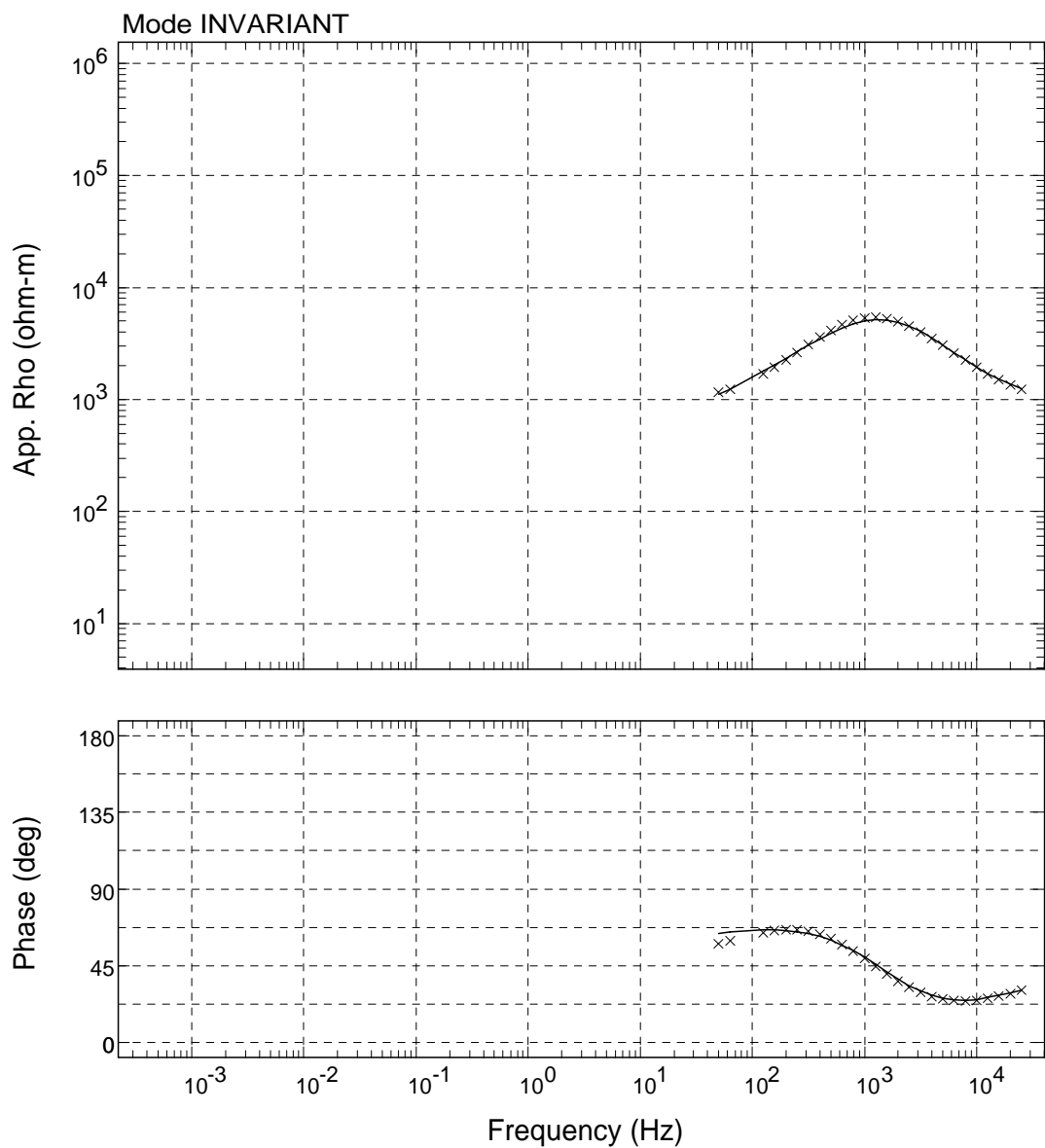
USGS - 01/Jun/2009



Sounding: SR005

Area: Hawaii

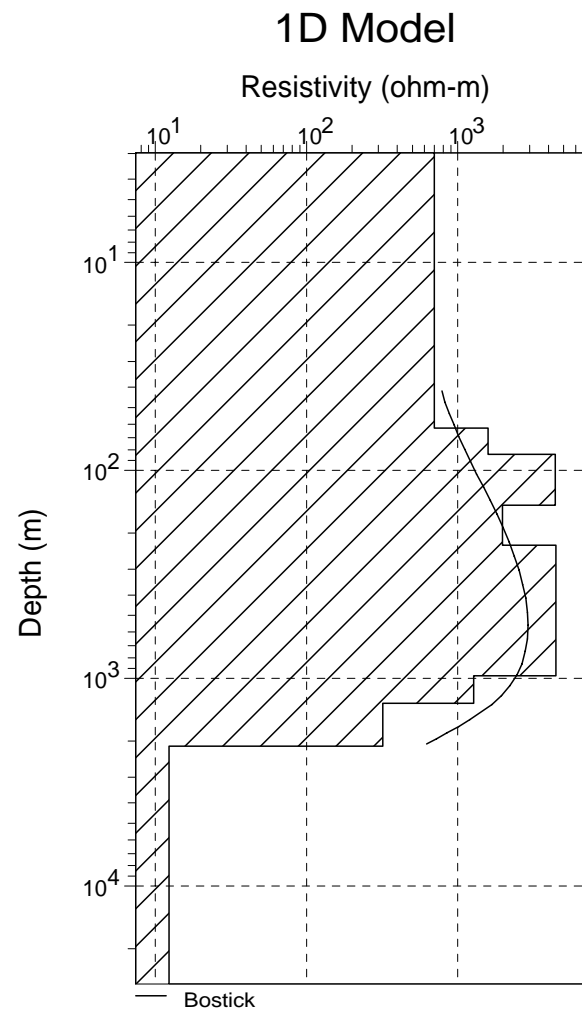
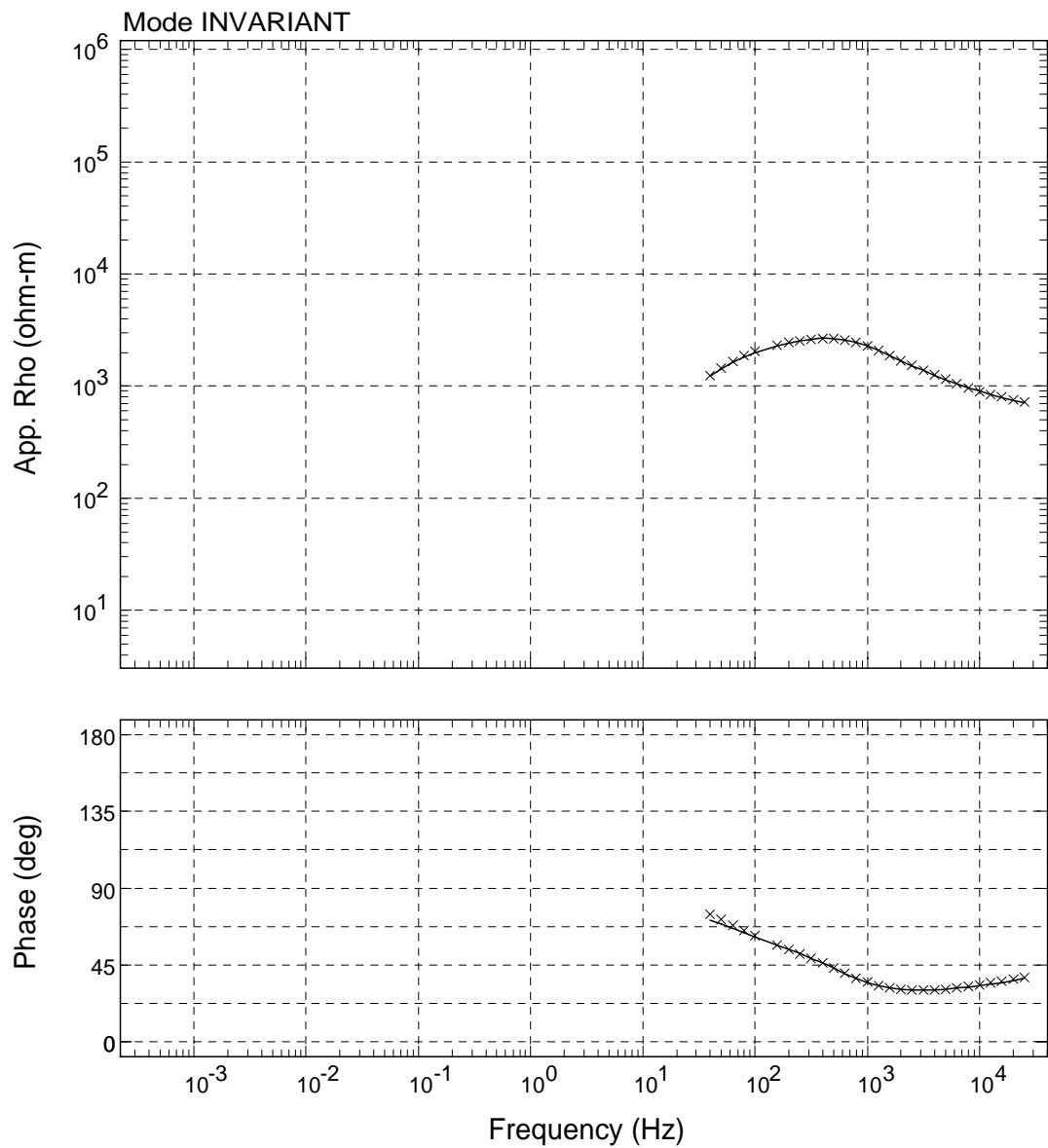
USGS - 01/Jun/2009



Sounding: SR006

Area: Hawaii

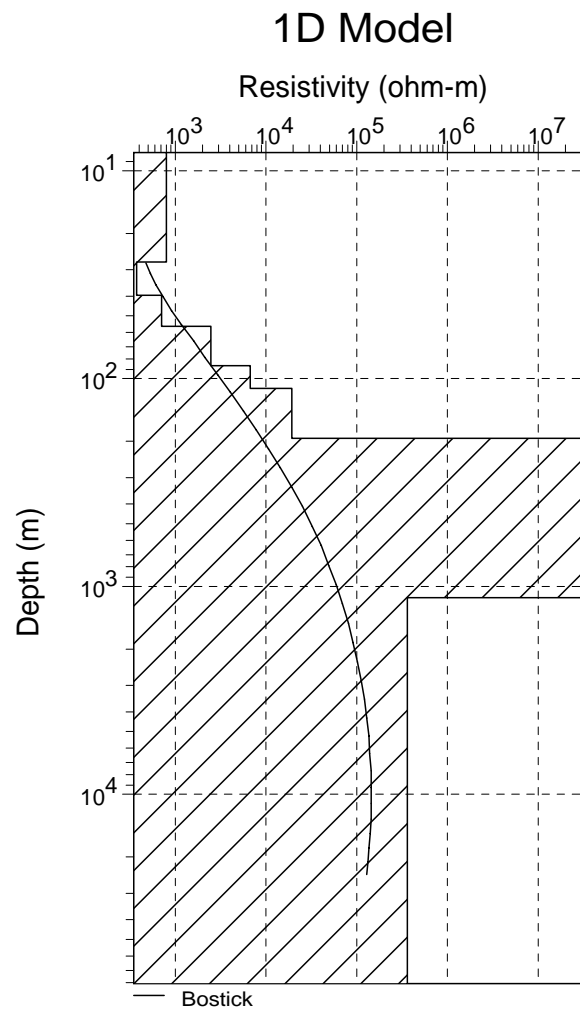
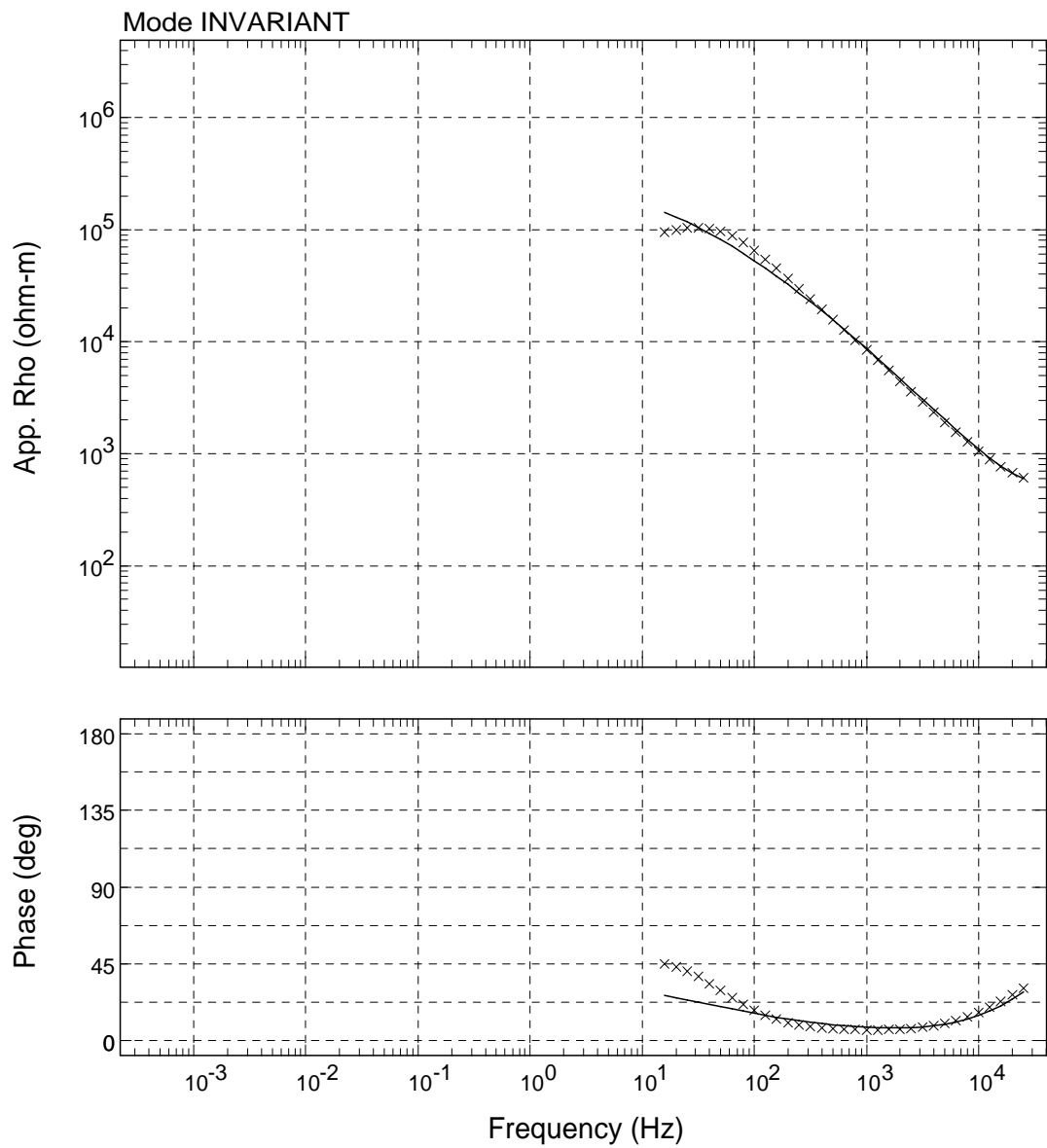
USGS - 01/Jun/2009



Sounding: SR007

Area: Hawaii

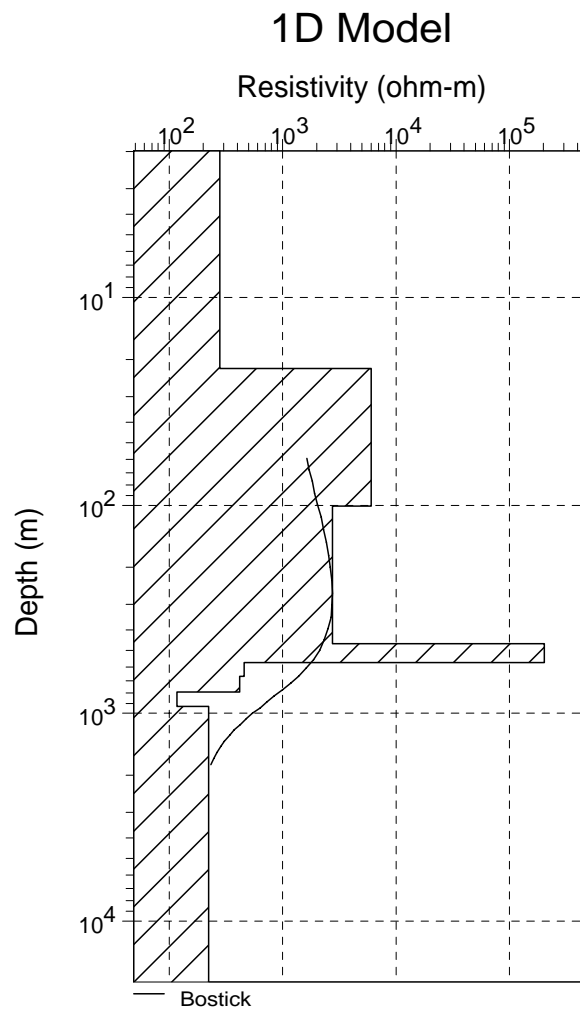
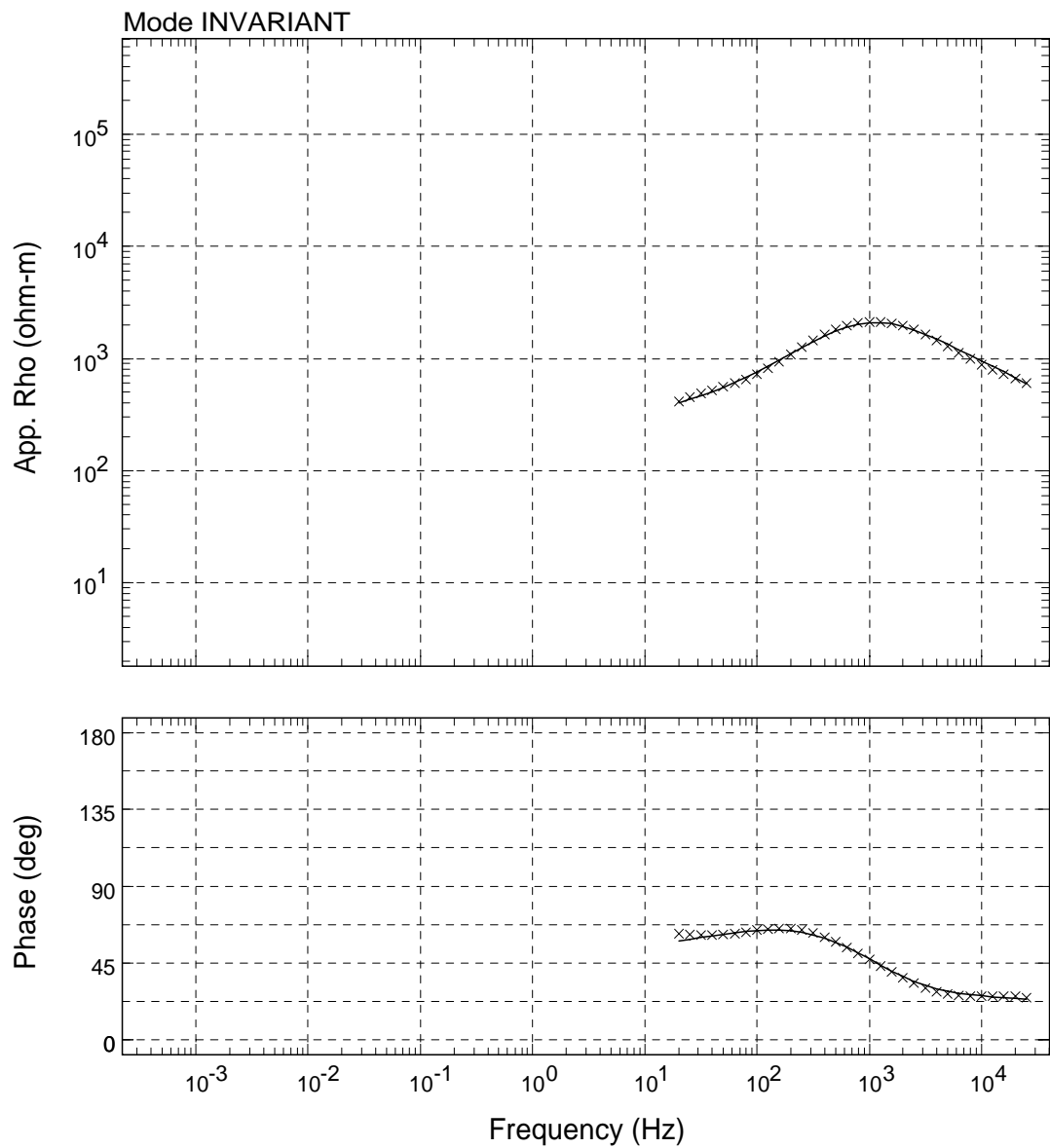
USGS - 01/Jun/2009



Sounding: SR008

Area: Hawaii

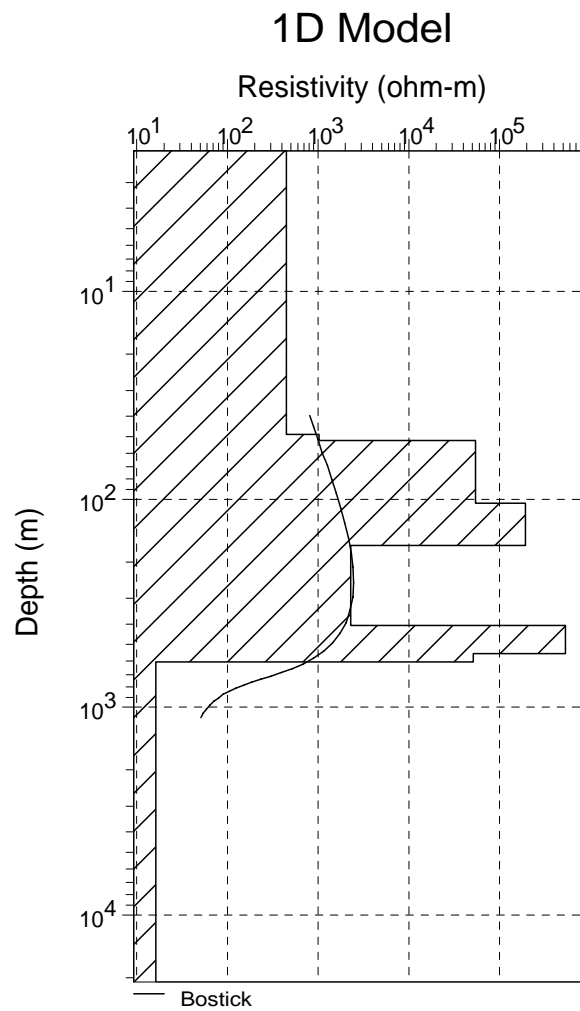
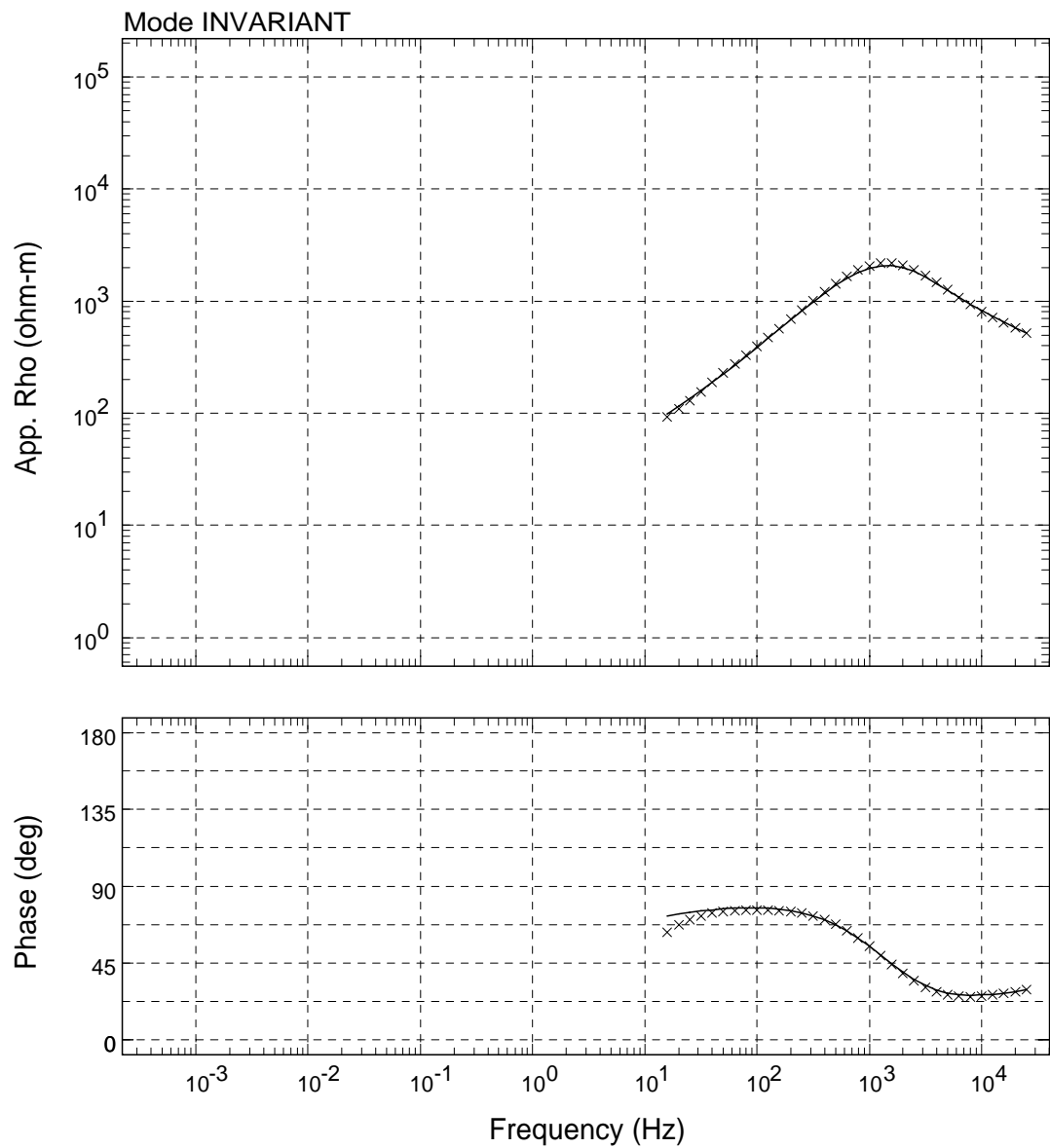
USGS - 01/Jun/2009



Sounding: SR009

Area: Hawaii

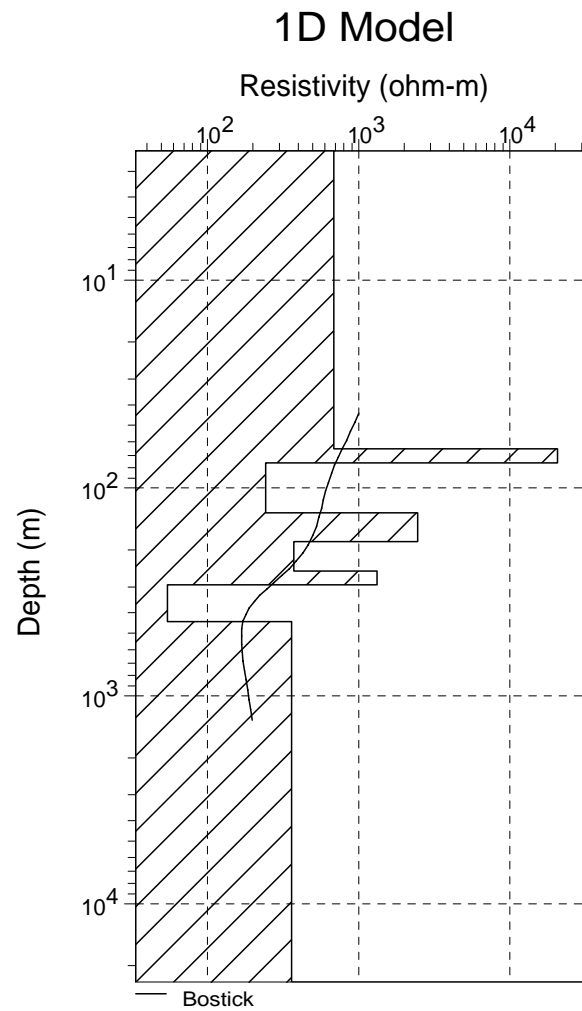
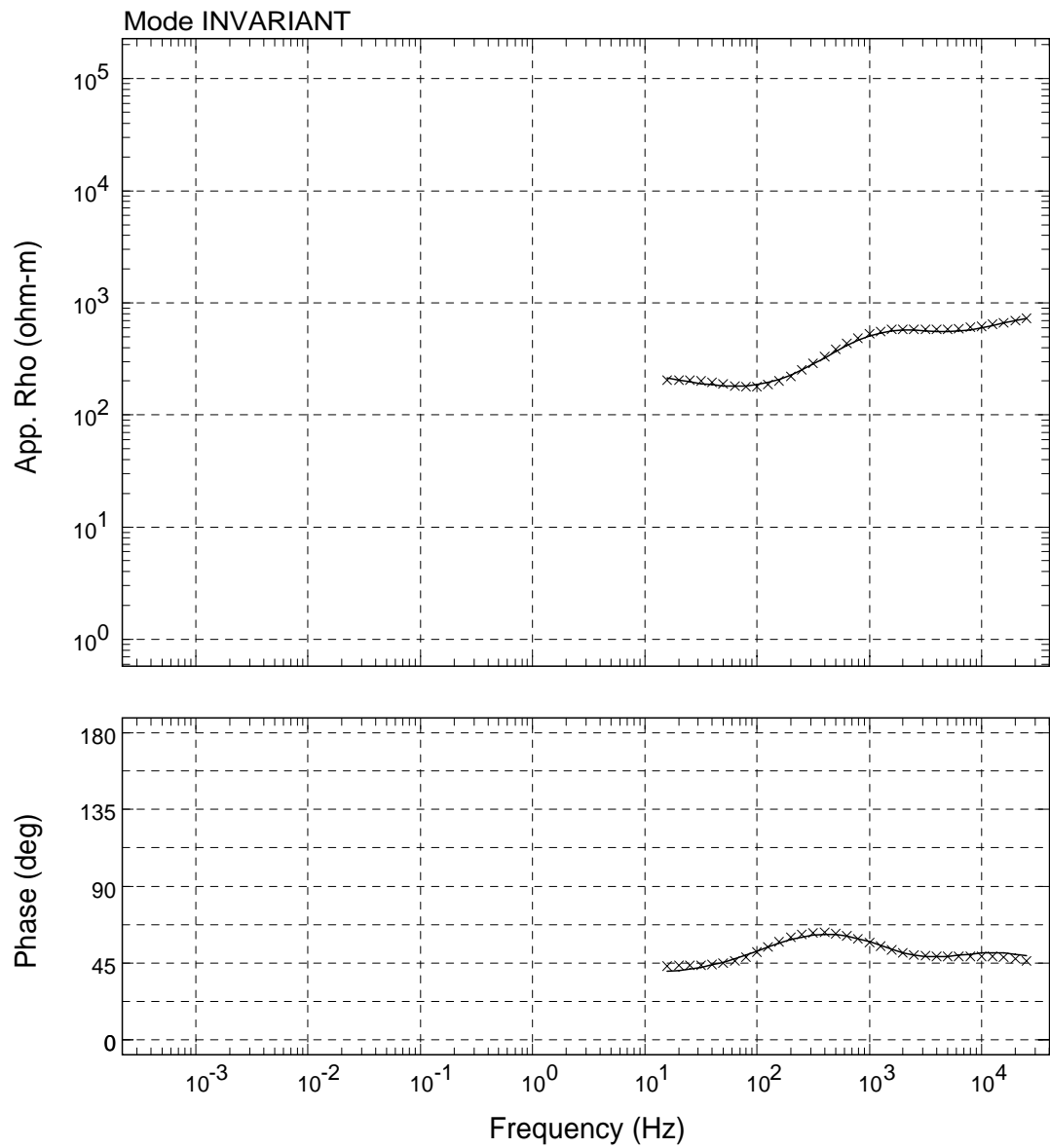
USGS - 01/Jun/2009



Sounding: SR010

Area: Hawaii

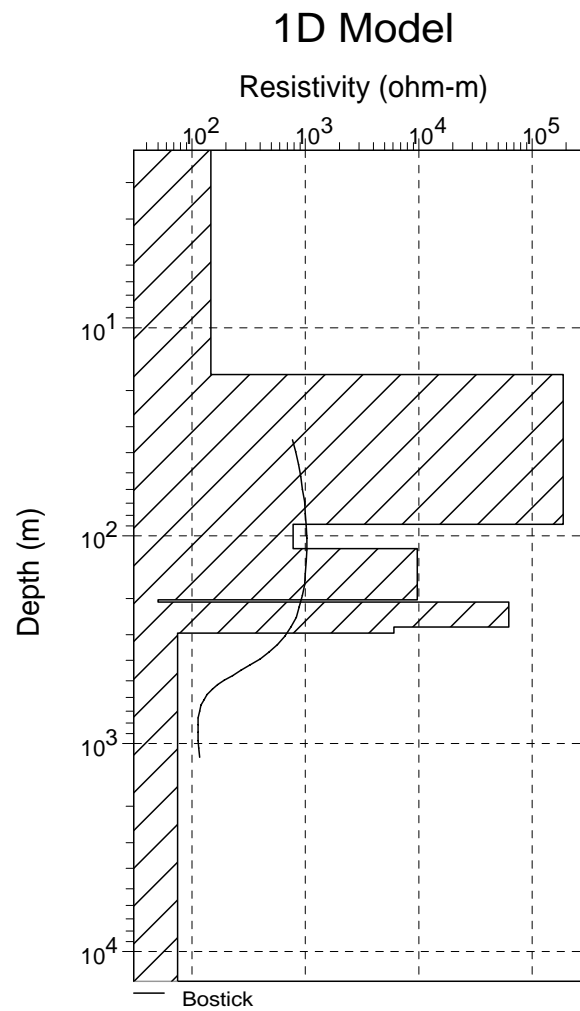
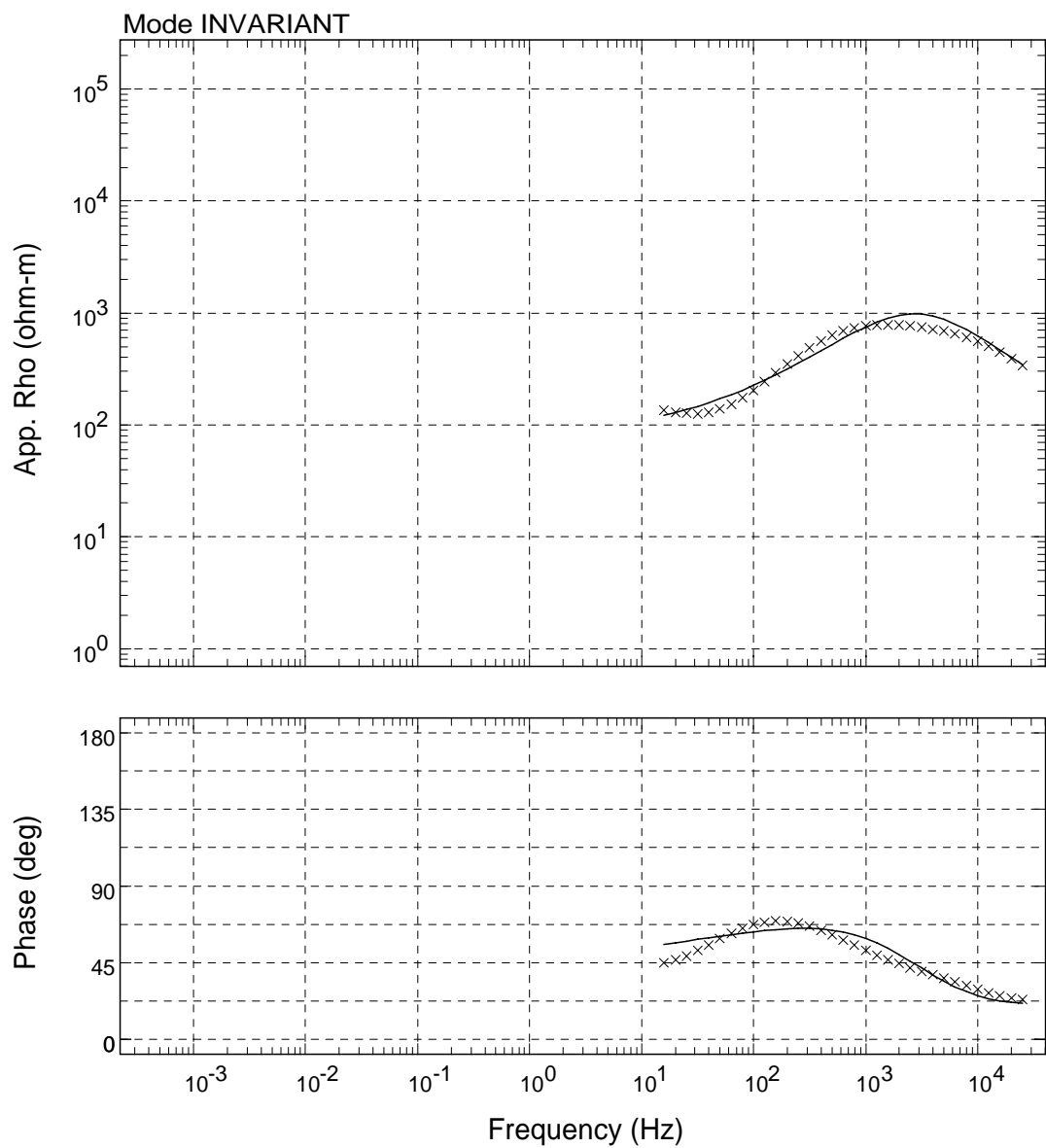
USGS - 01/Jun/2009



Sounding: SR011

Area: Hawaii

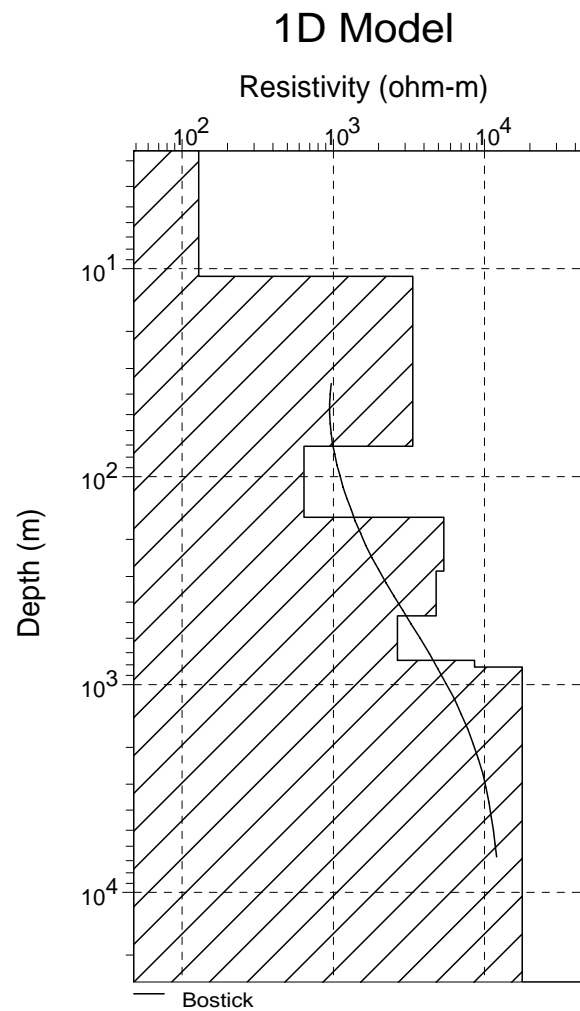
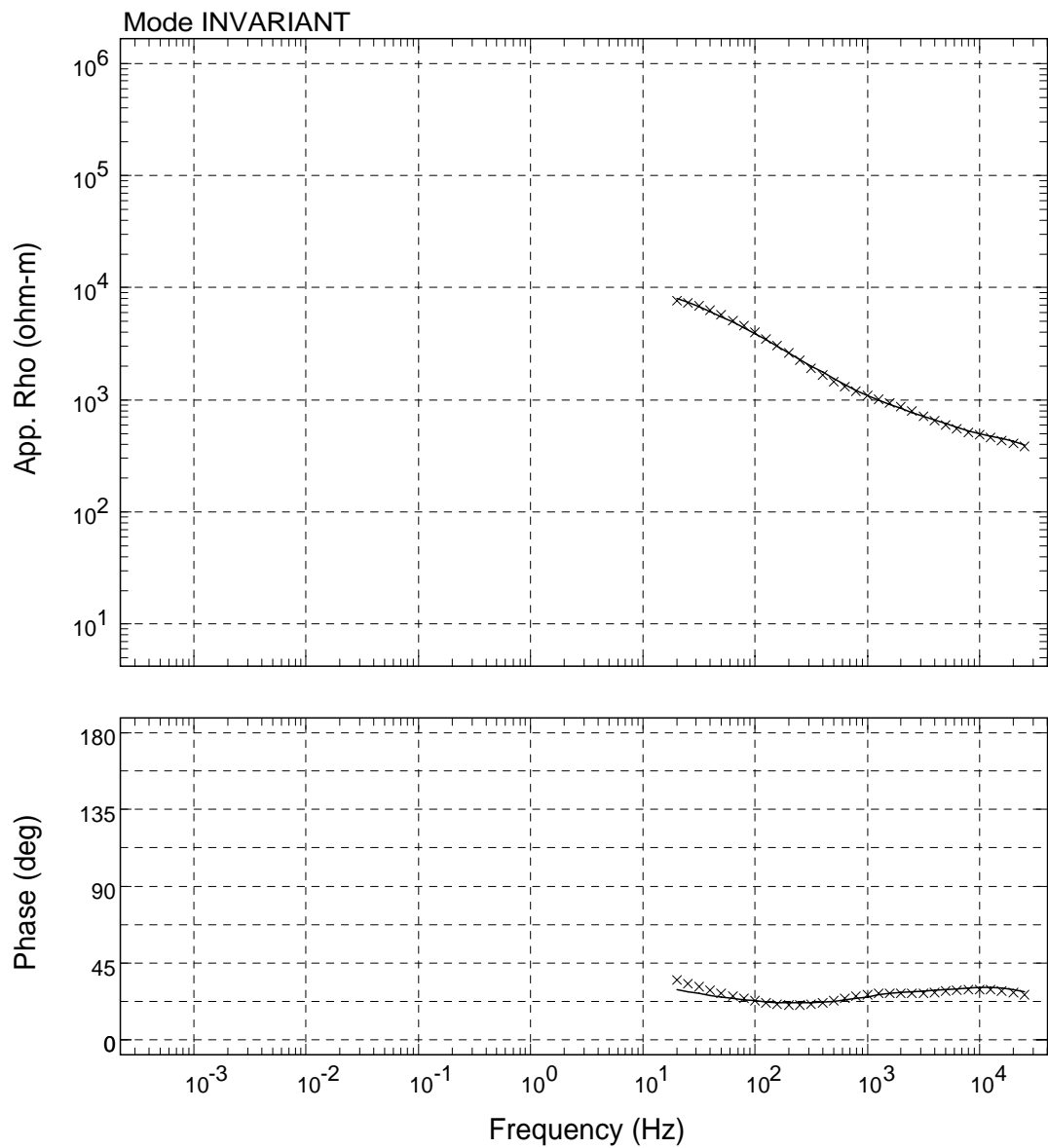
USGS - 01/Jun/2009



Sounding: SR012

Area: Hawaii

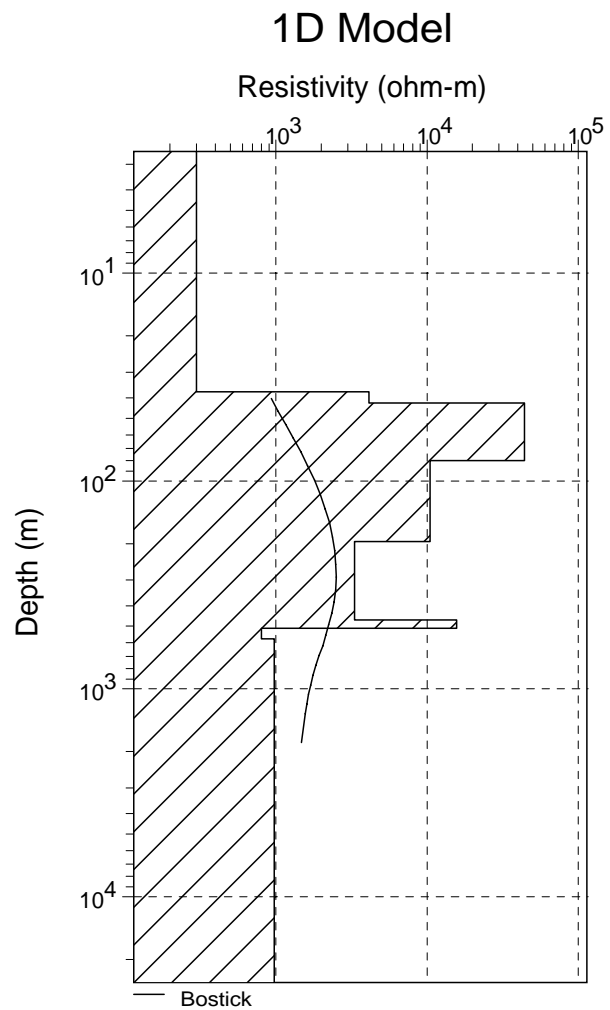
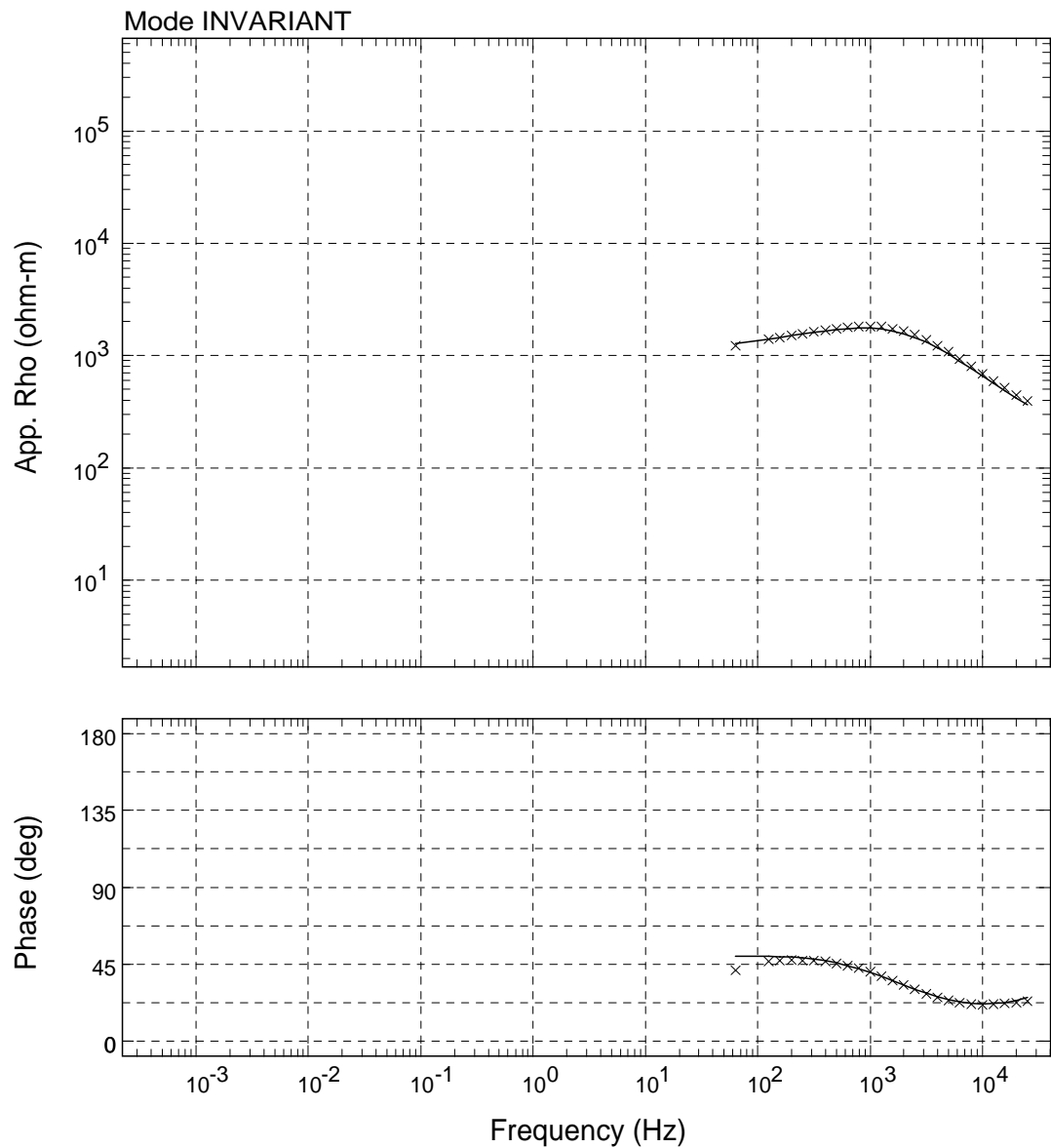
USGS - 01/Jun/2009



Sounding: SR013

Area: Hawaii

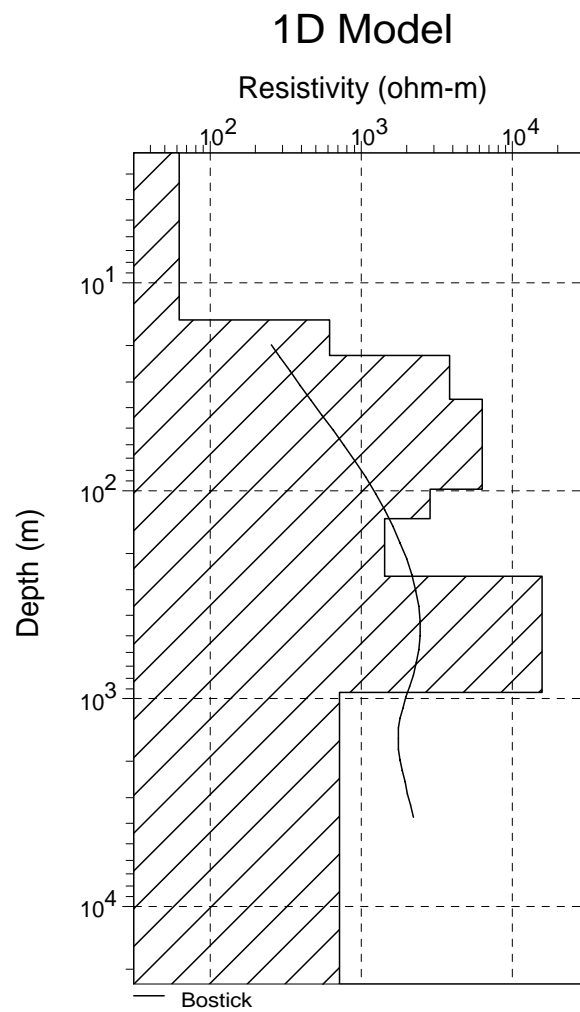
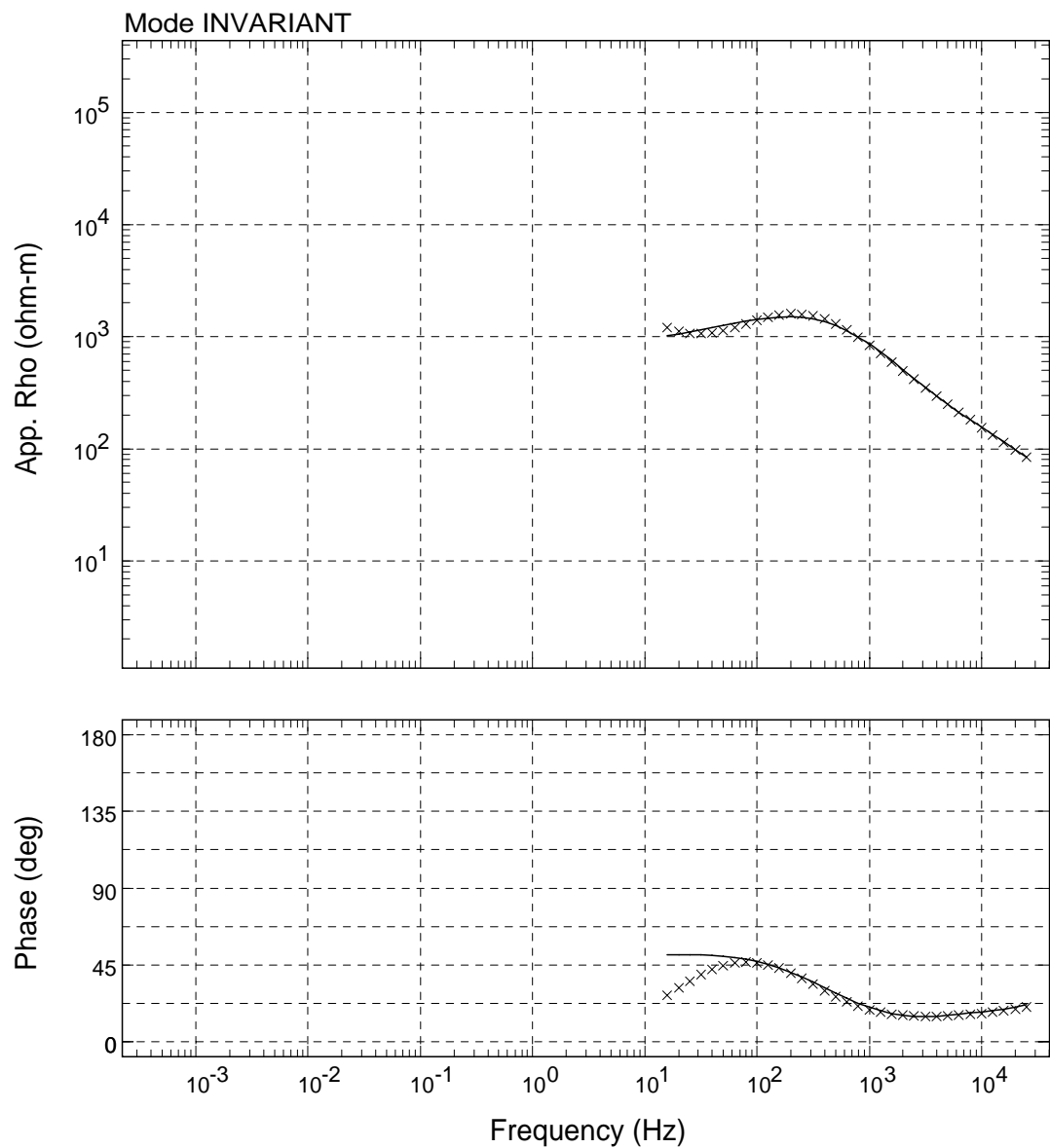
USGS - 01/Jun/2009



Sounding: SR014

Area: Hawaii

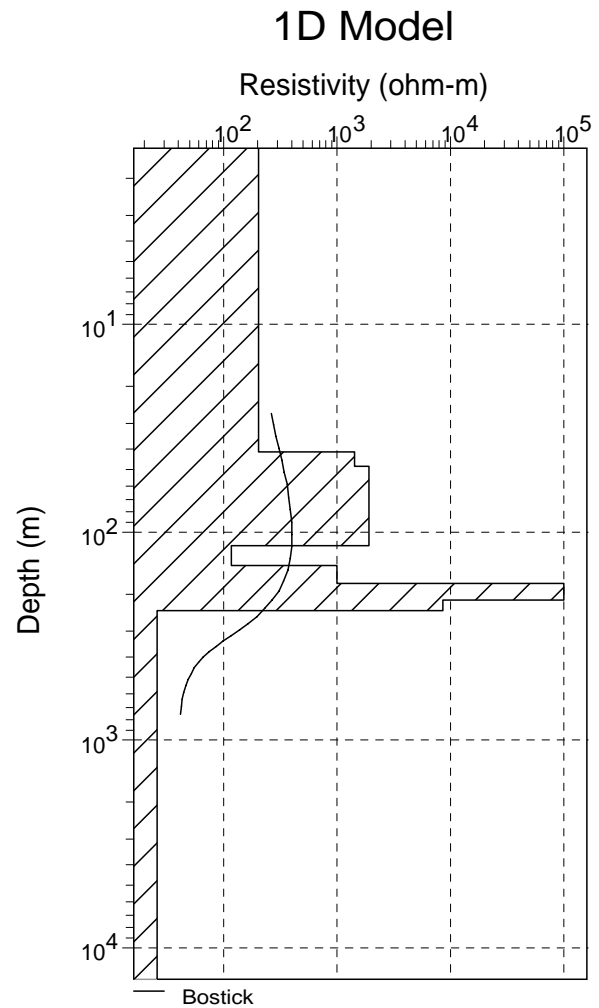
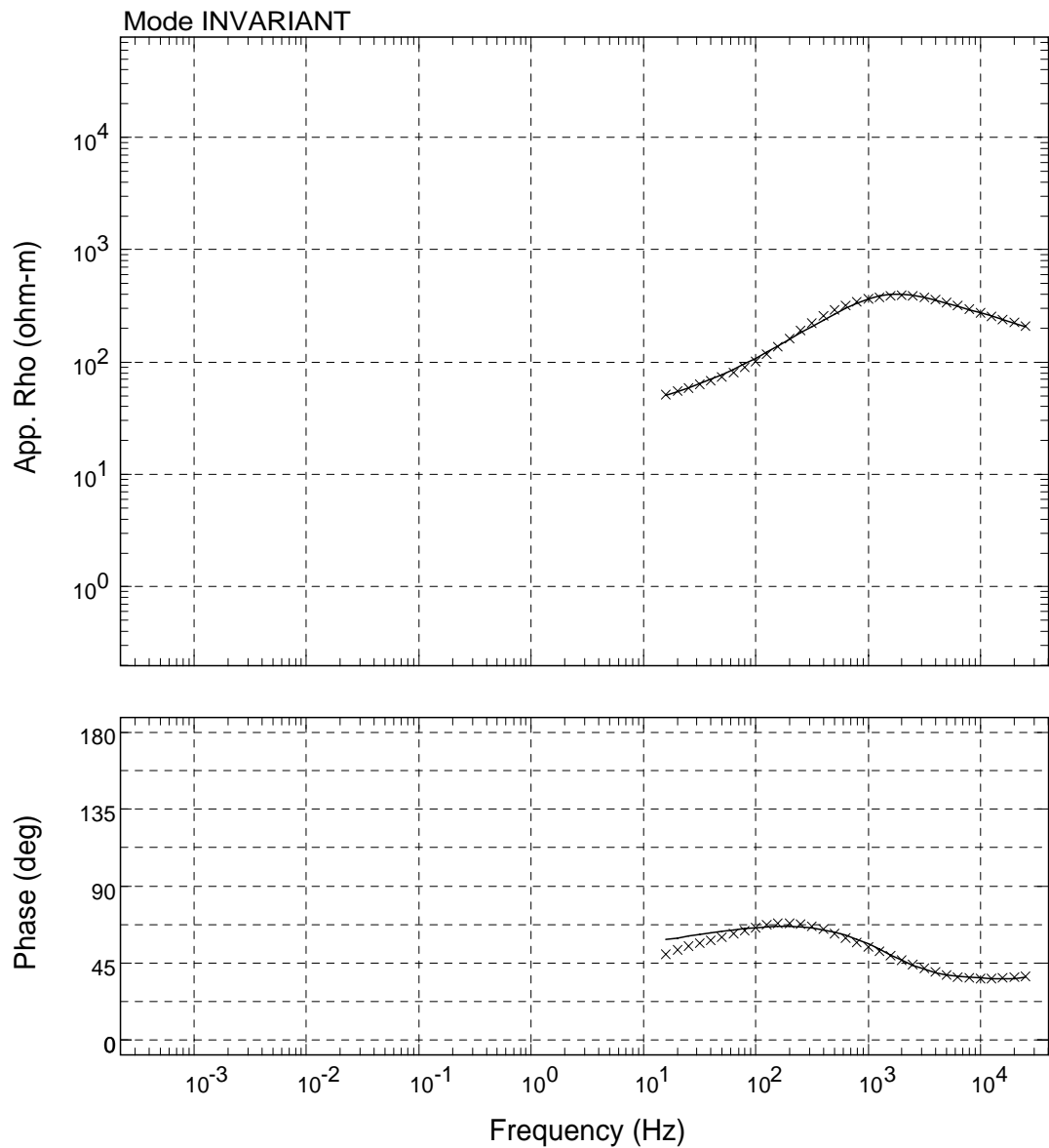
USGS - 01/Jun/2009



Sounding: SR015

Area: Hawaii

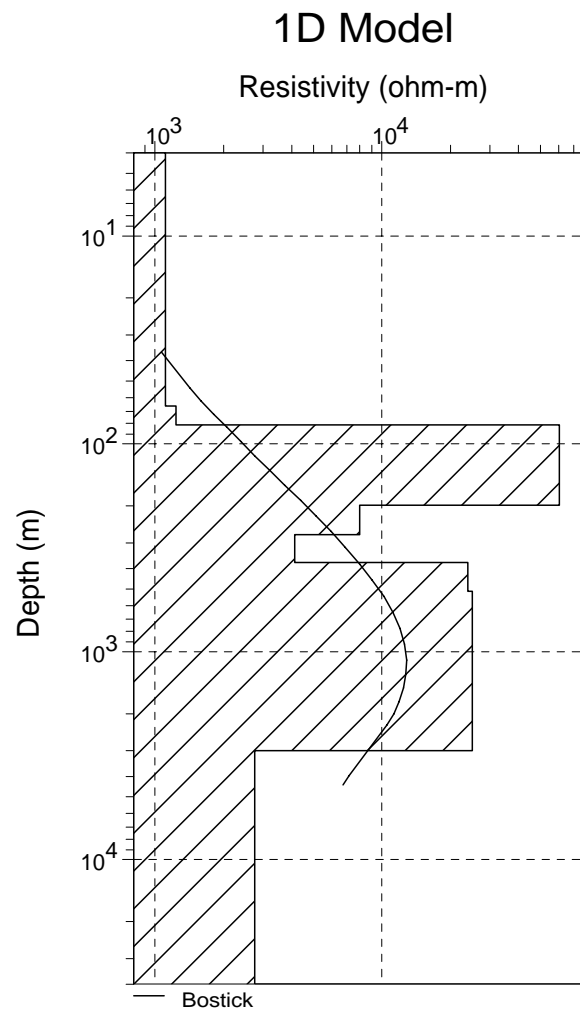
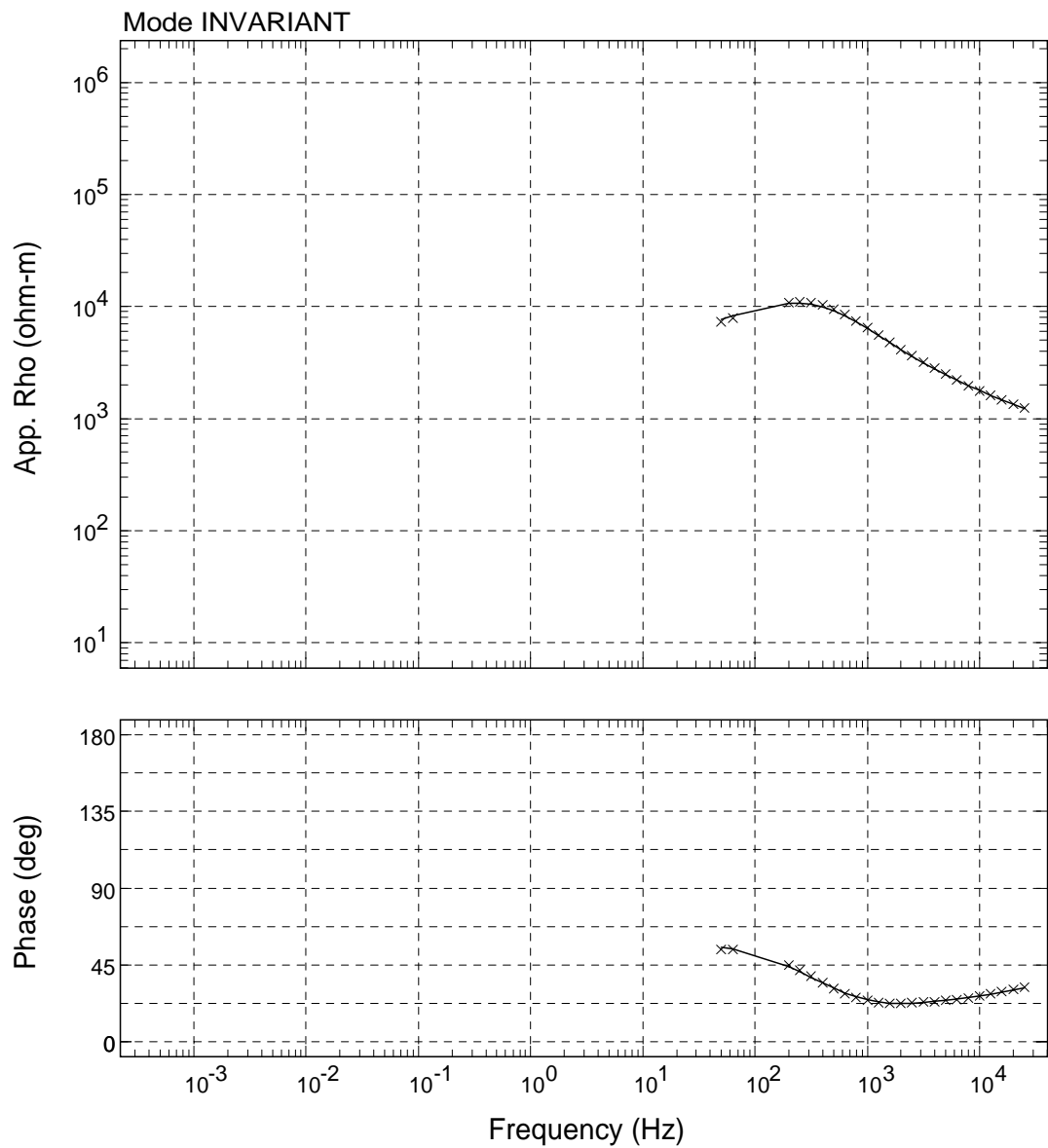
USGS - 01/Jun/2009



Sounding: SR016

Area: Hawaii

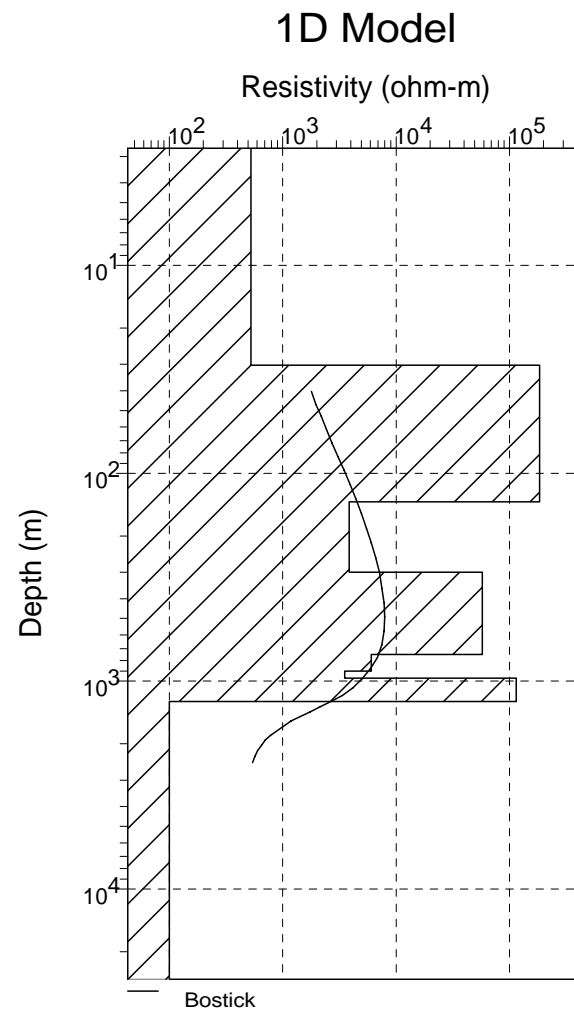
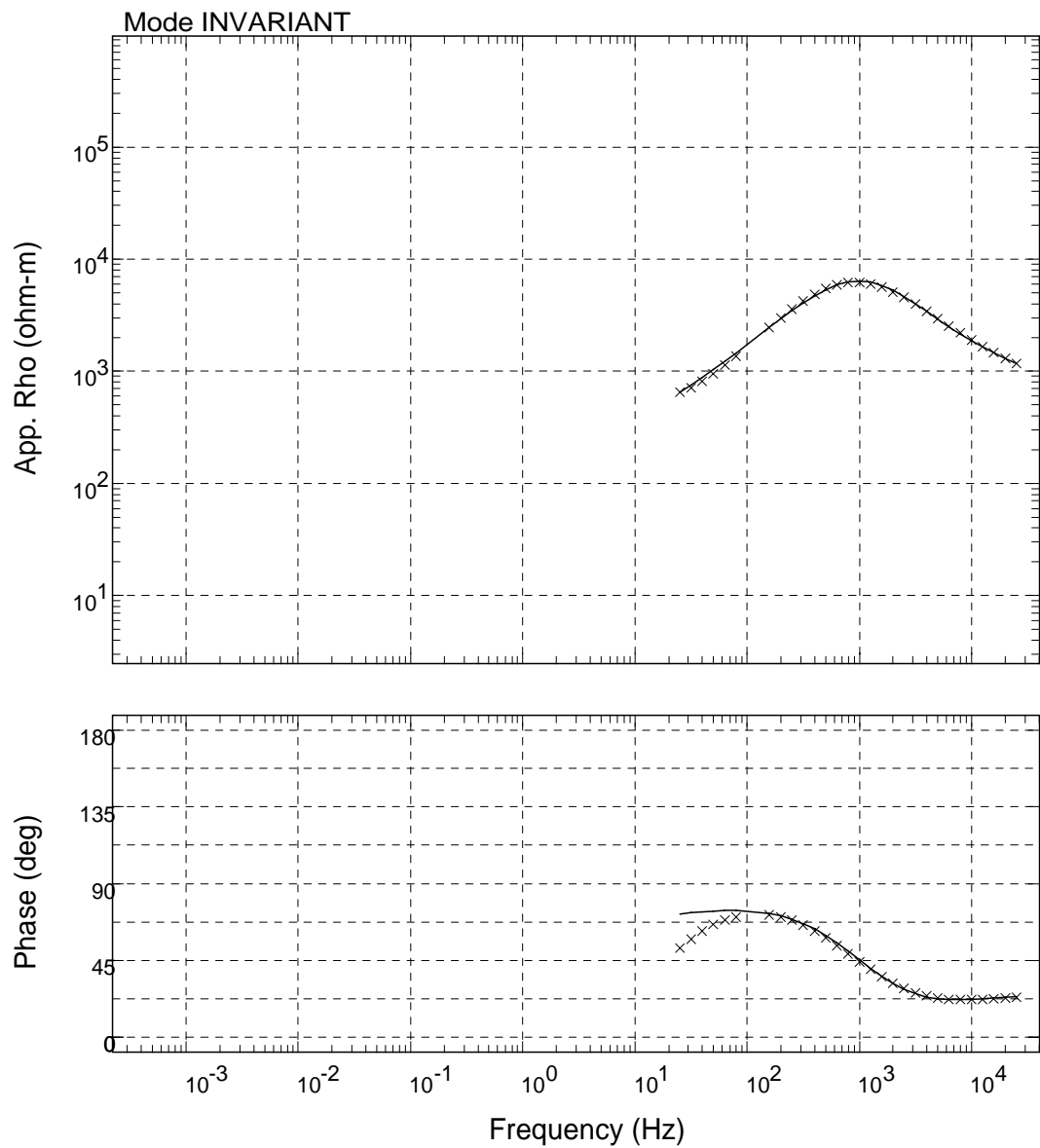
USGS - 01/Jun/2009



Sounding: SR017

Area: Hawaii

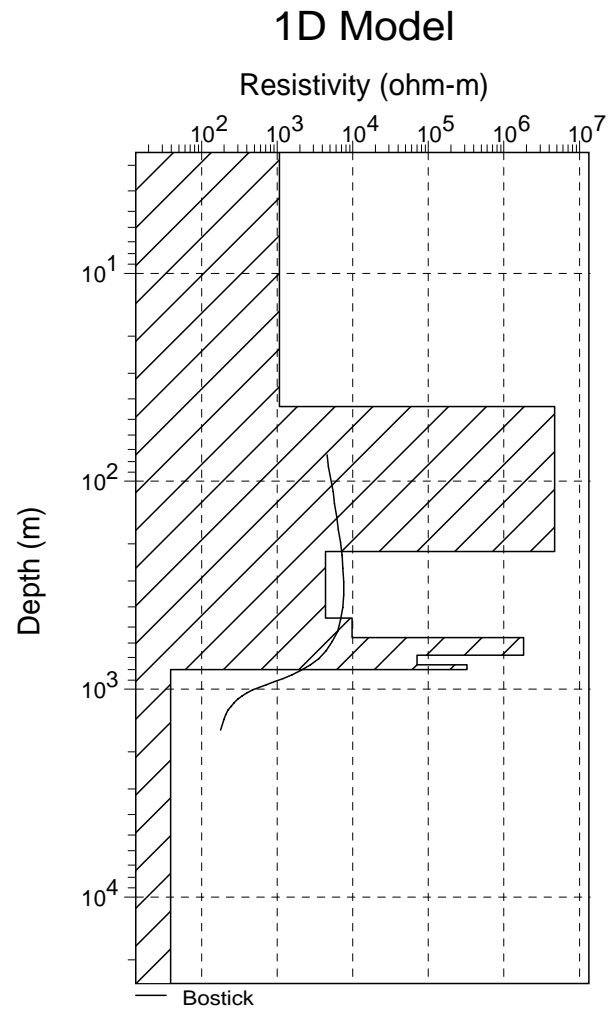
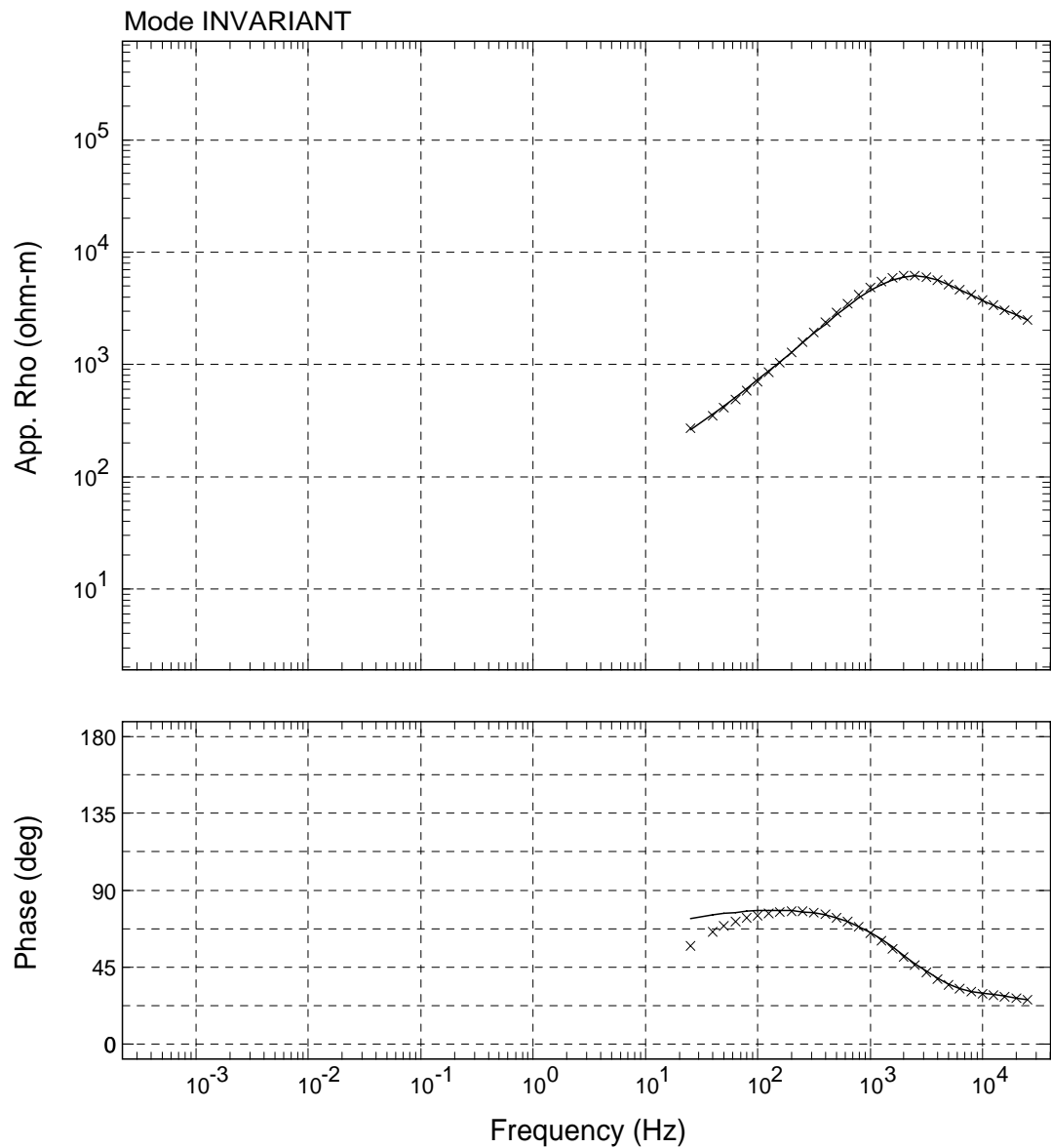
USGS - 01/Jun/2009



Sounding: SR018

Area: Hawaii

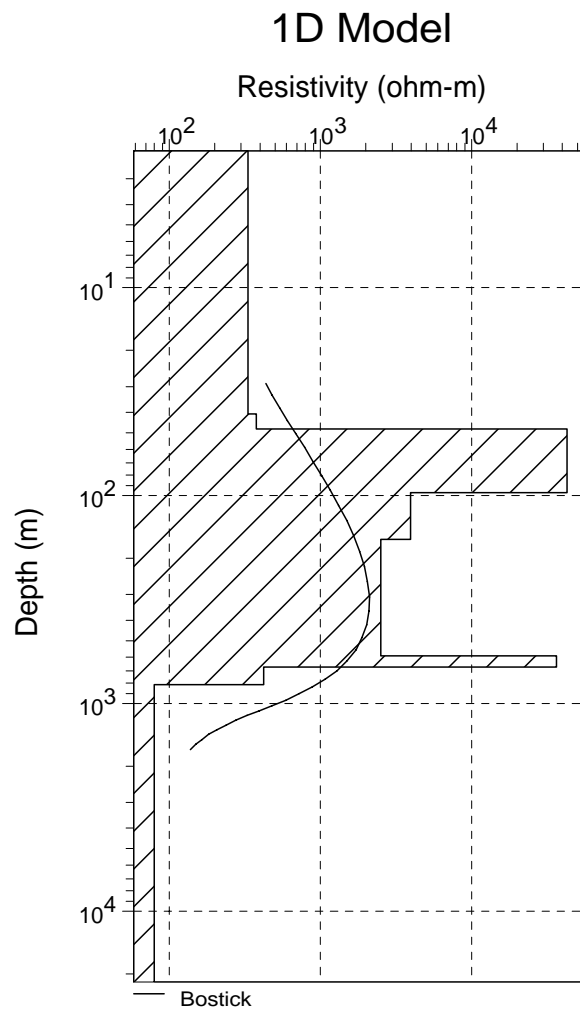
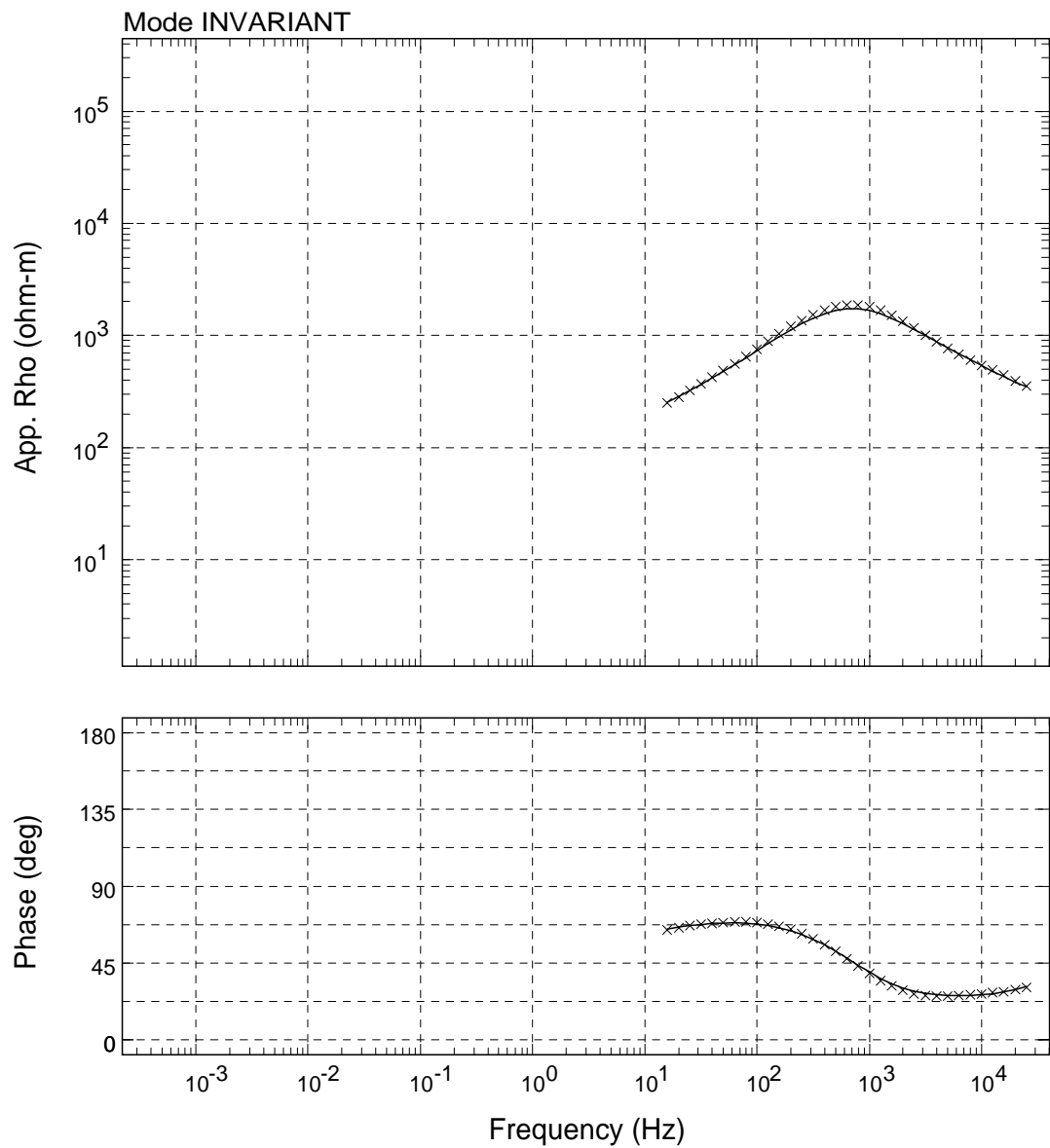
USGS - 01/Jun/2009



Sounding: SR019

Area: Hawaii

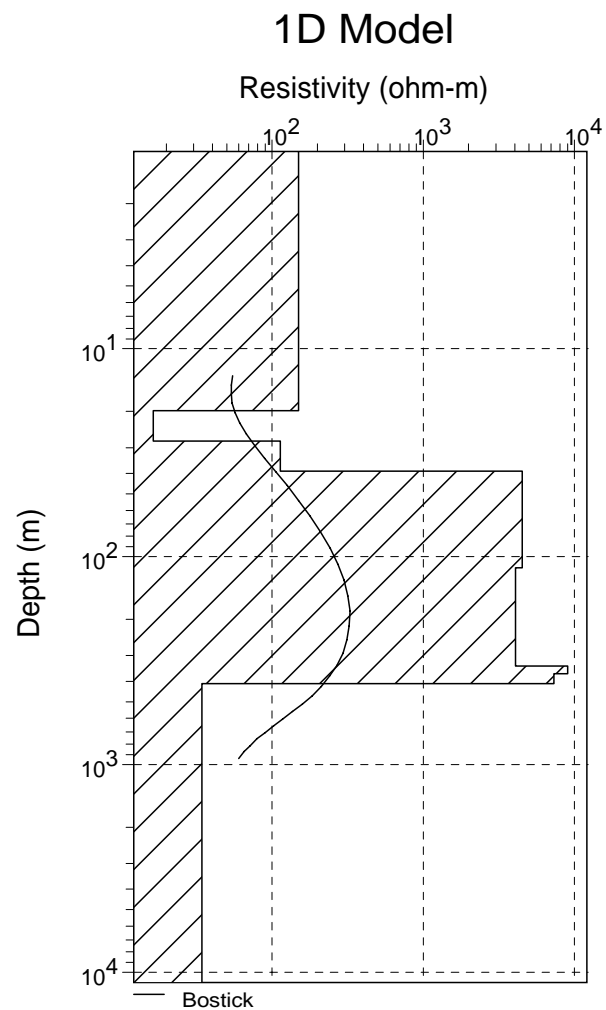
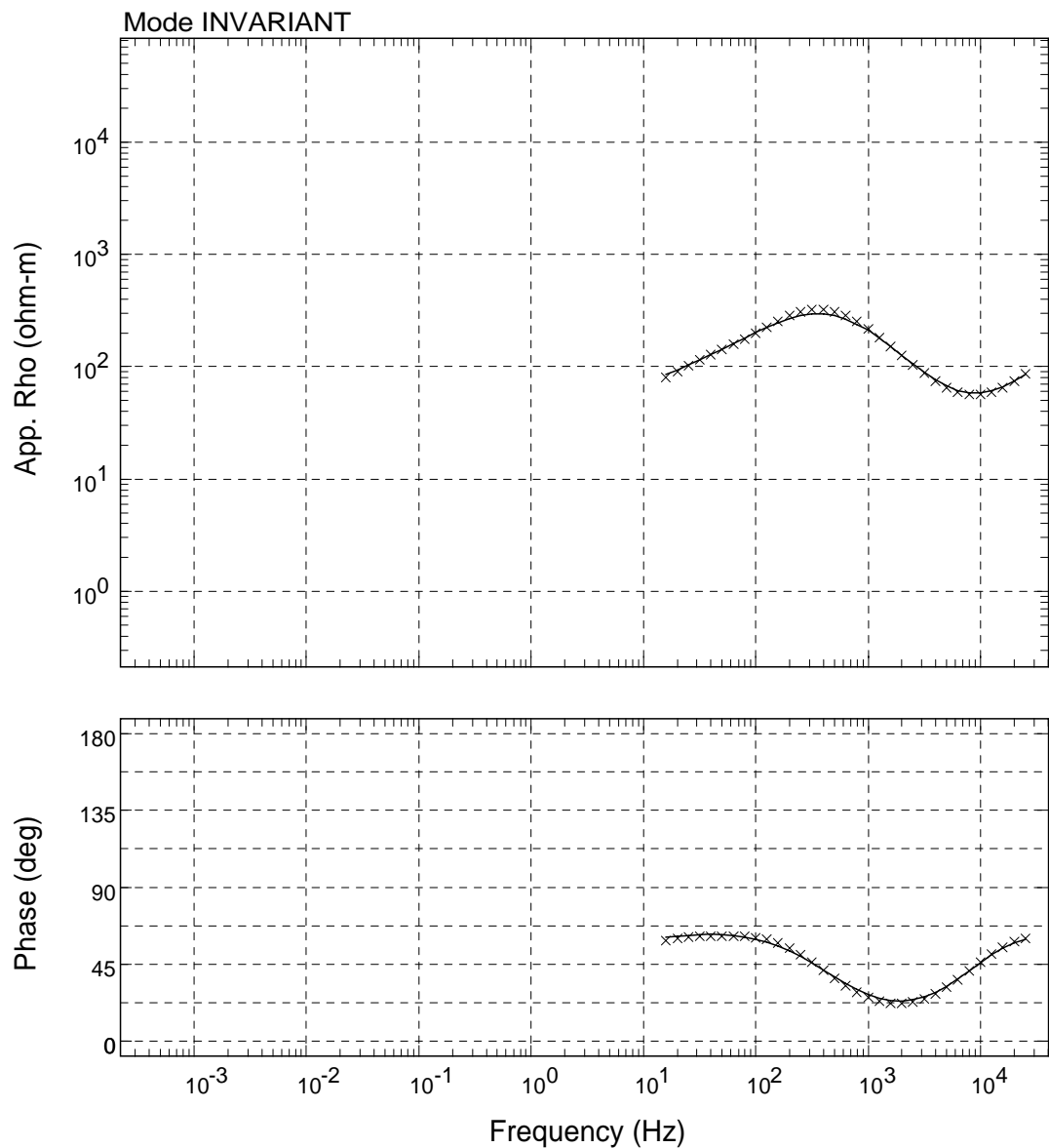
USGS - 01/Jun/2009



Sounding: SR020

Area: Hawaii

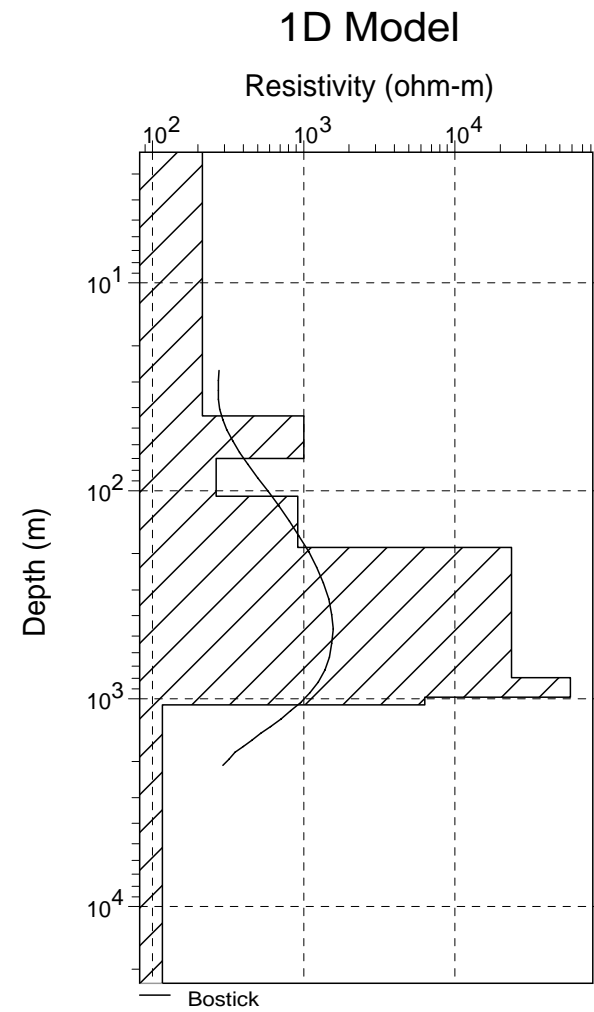
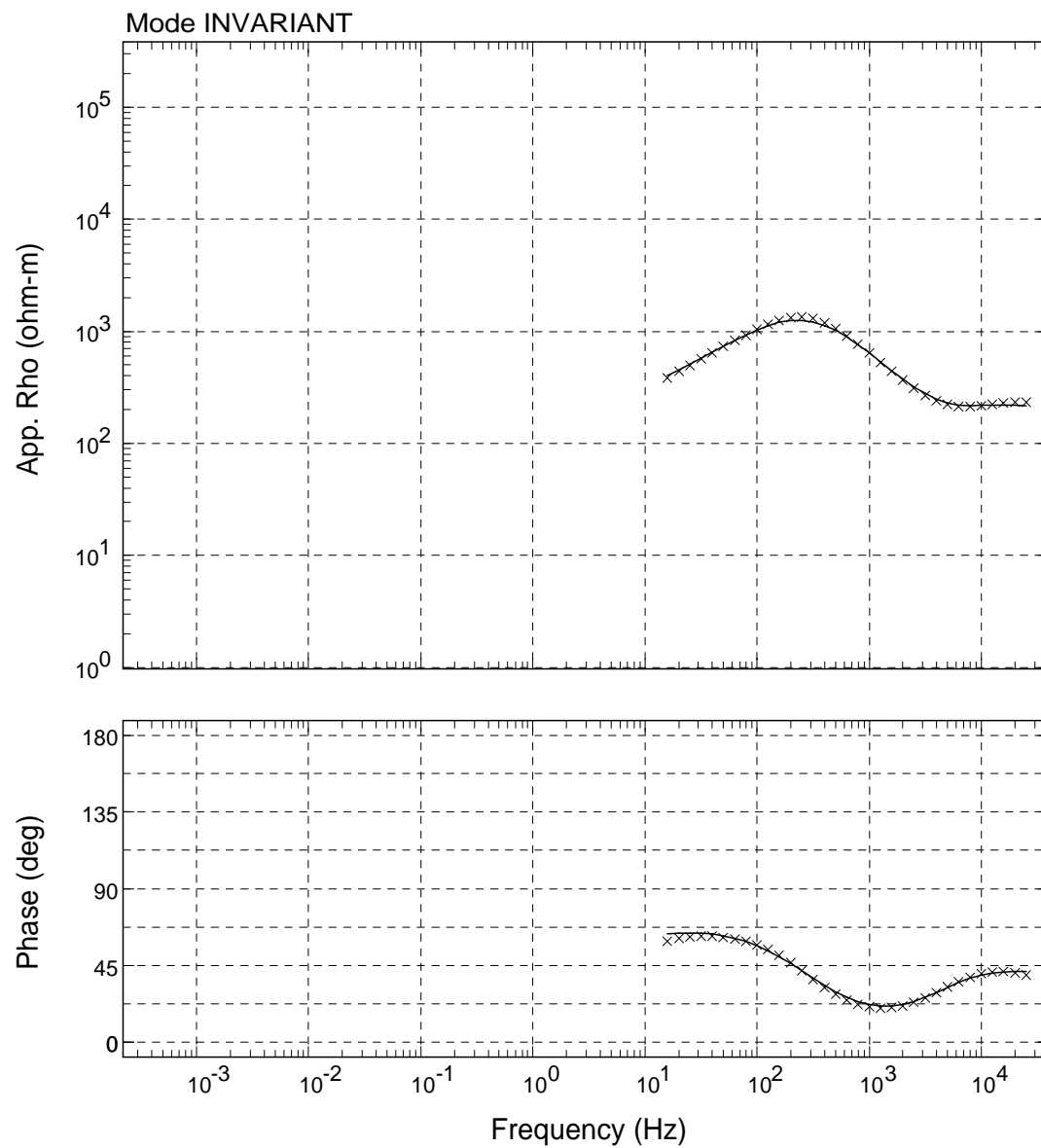
USGS - 01/Jun/2009



Sounding: SR021

Area: Hawaii

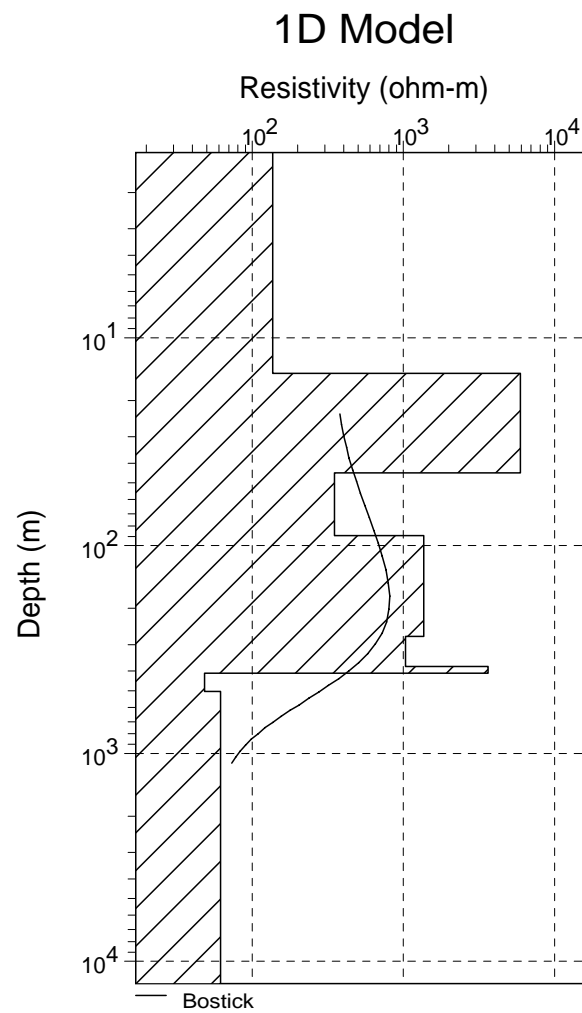
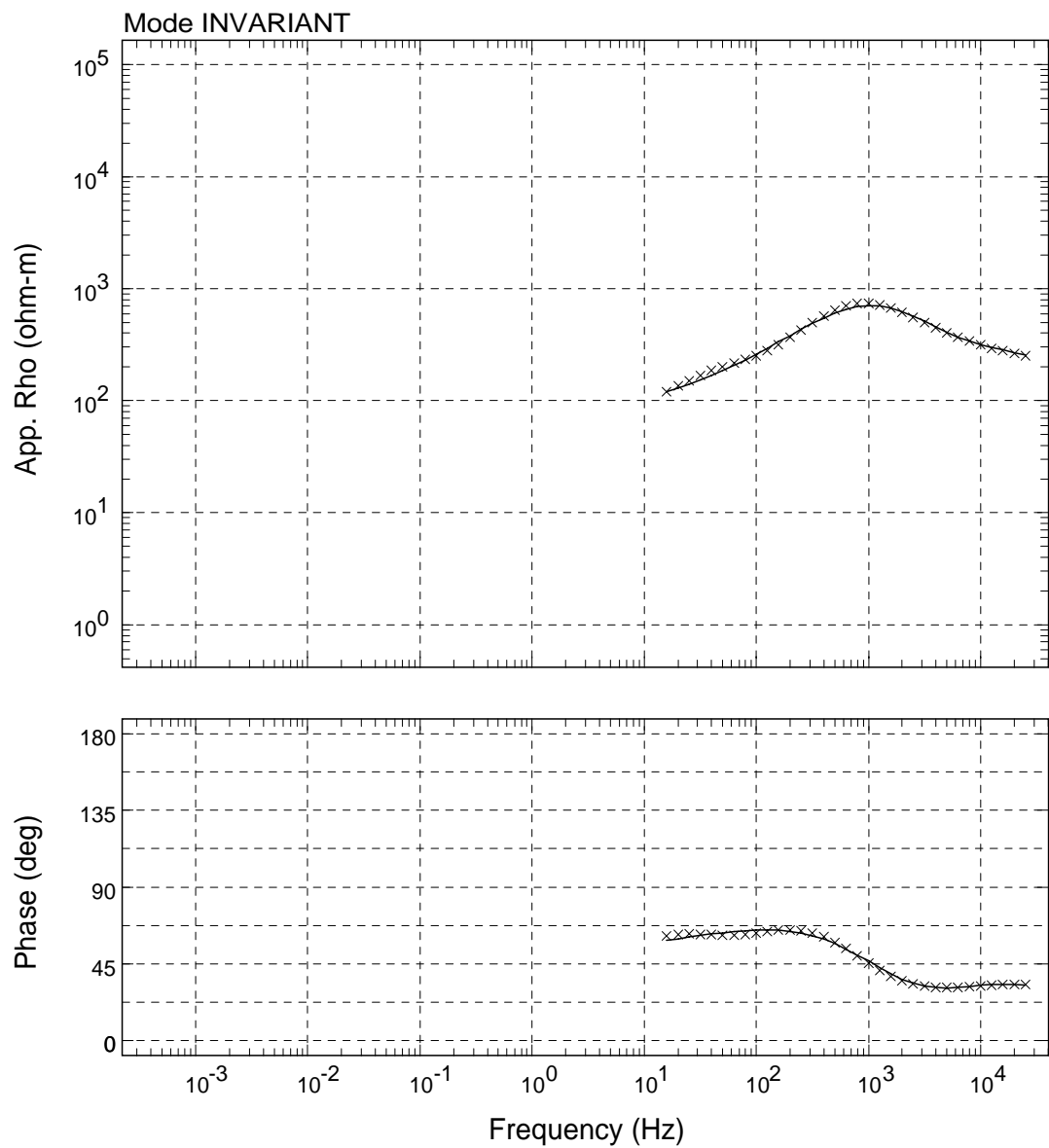
USGS - 01/Jun/2009



Sounding: SR022

Area: Hawaii

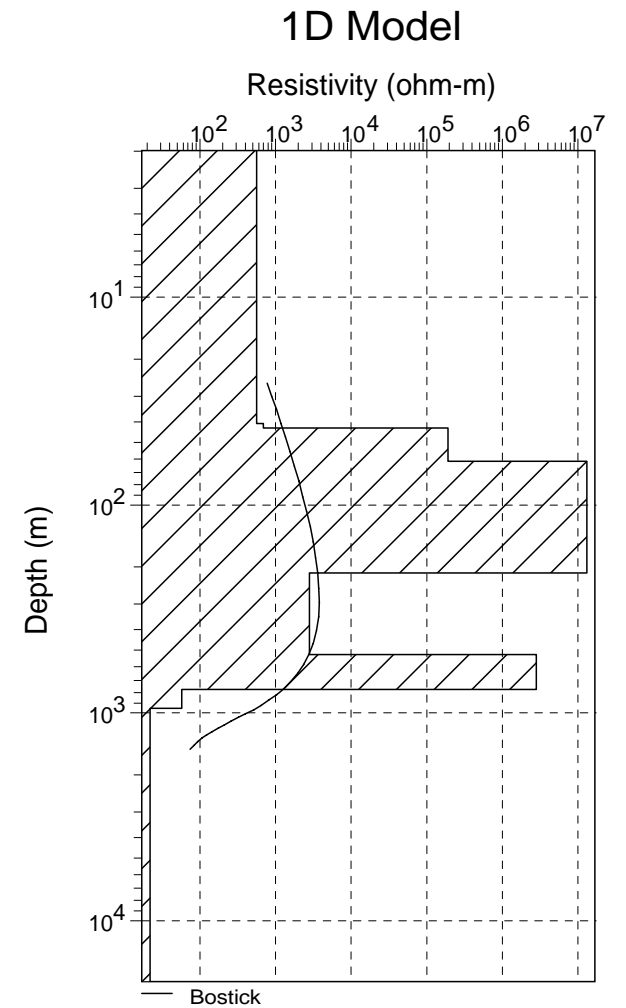
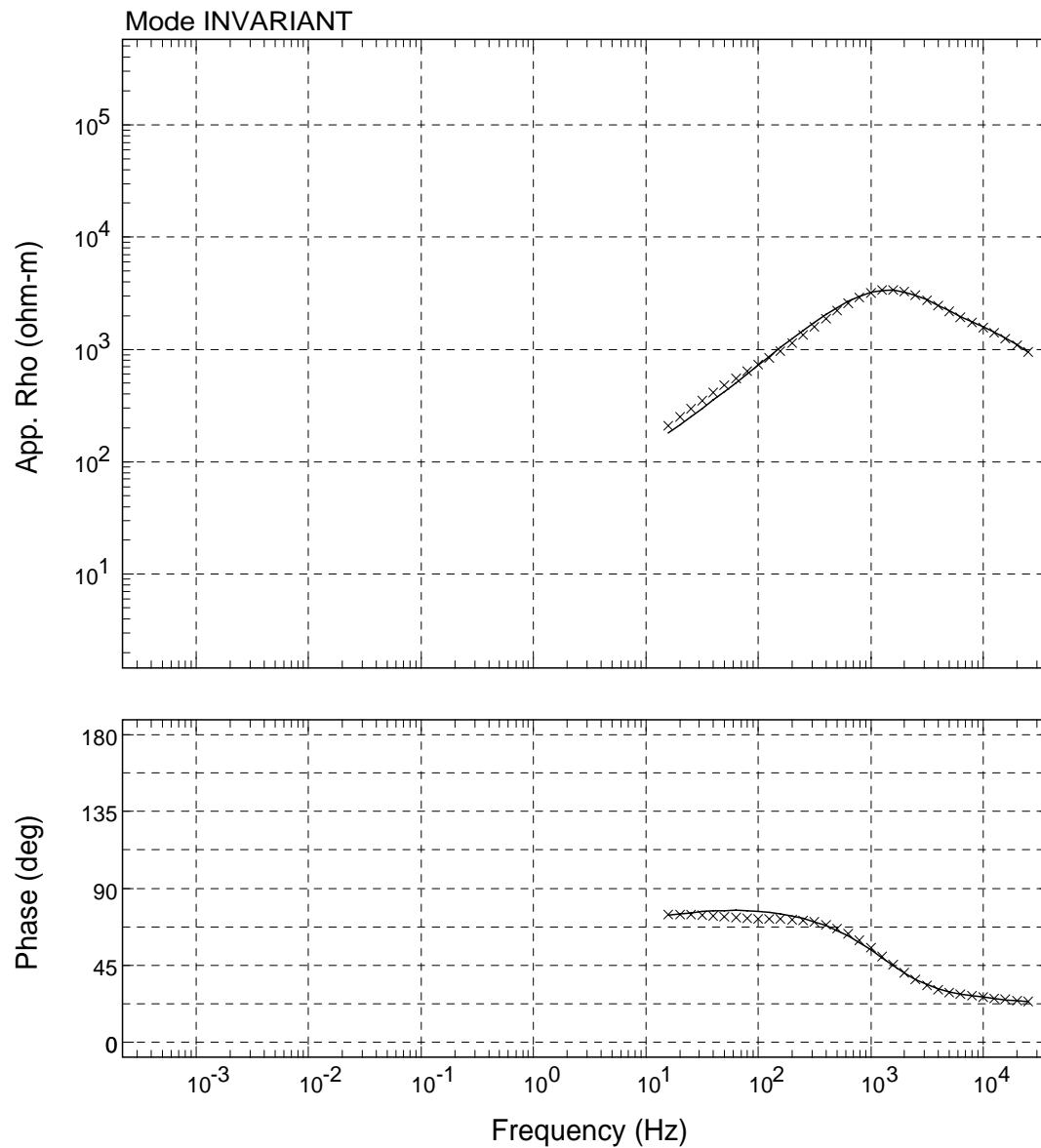
USGS - 01/Jun/2009



Sounding: SR023

Area: Hawaii

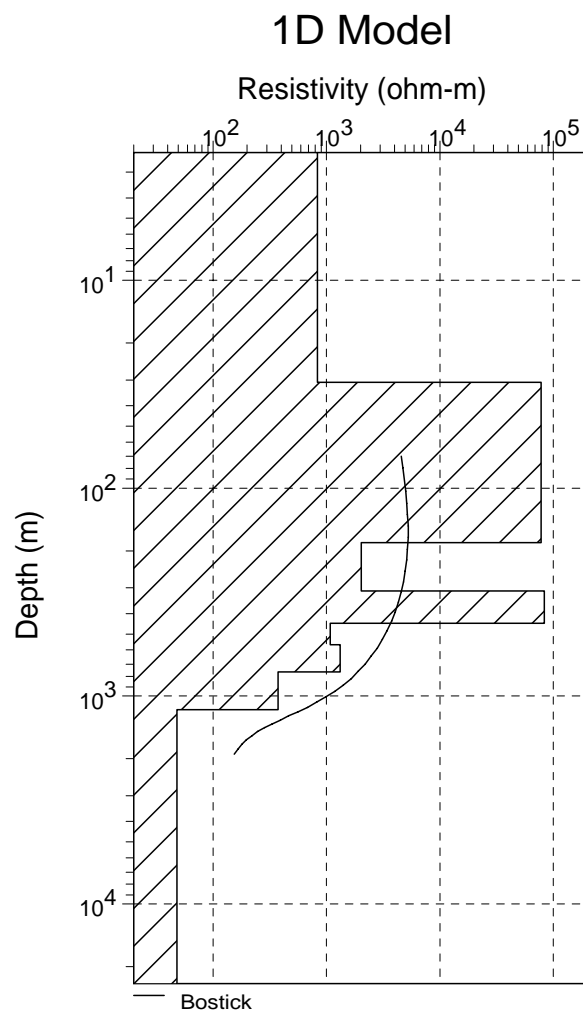
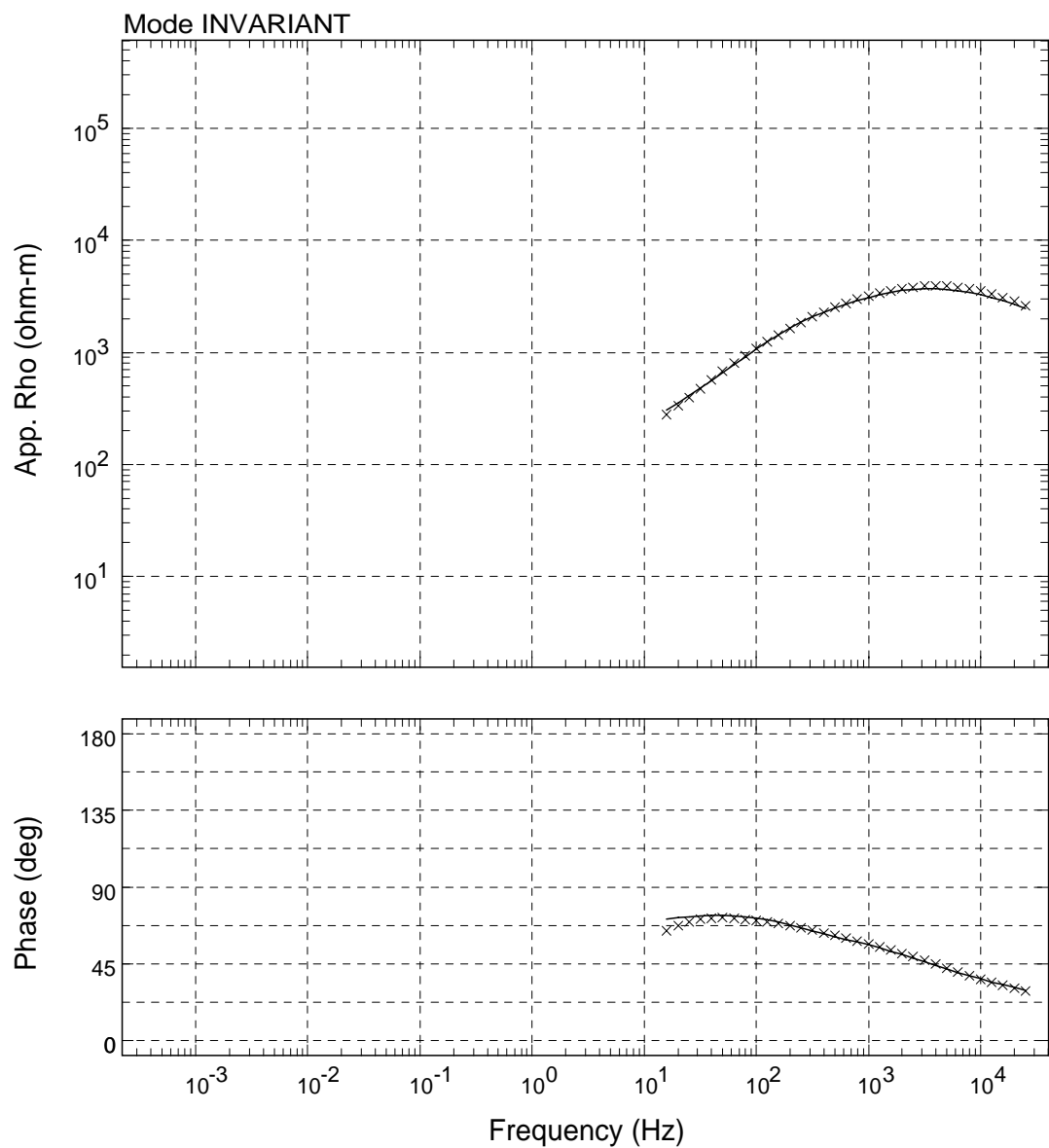
USGS - 01/Jun/2009



Sounding: SR025

Area: Hawaii

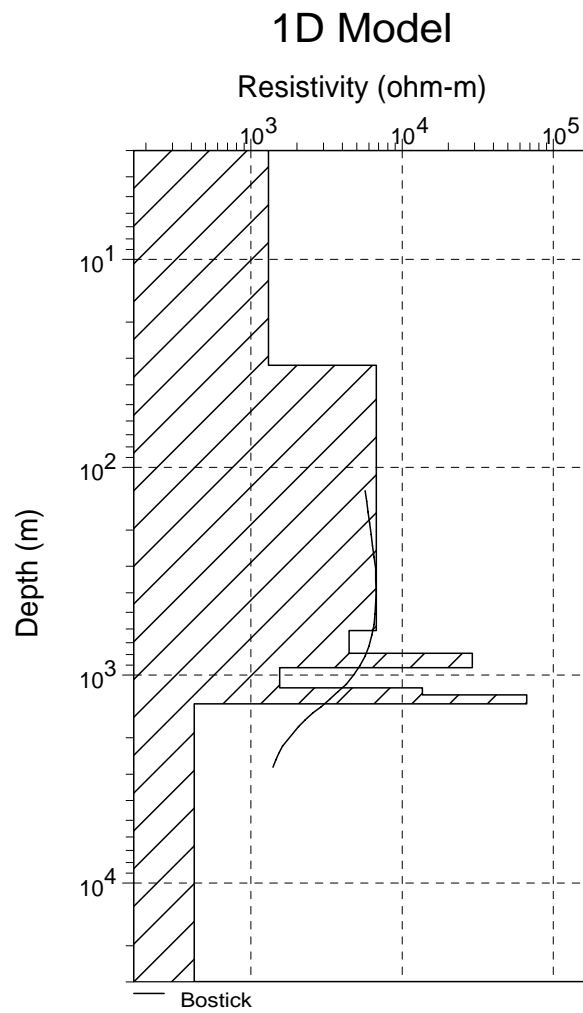
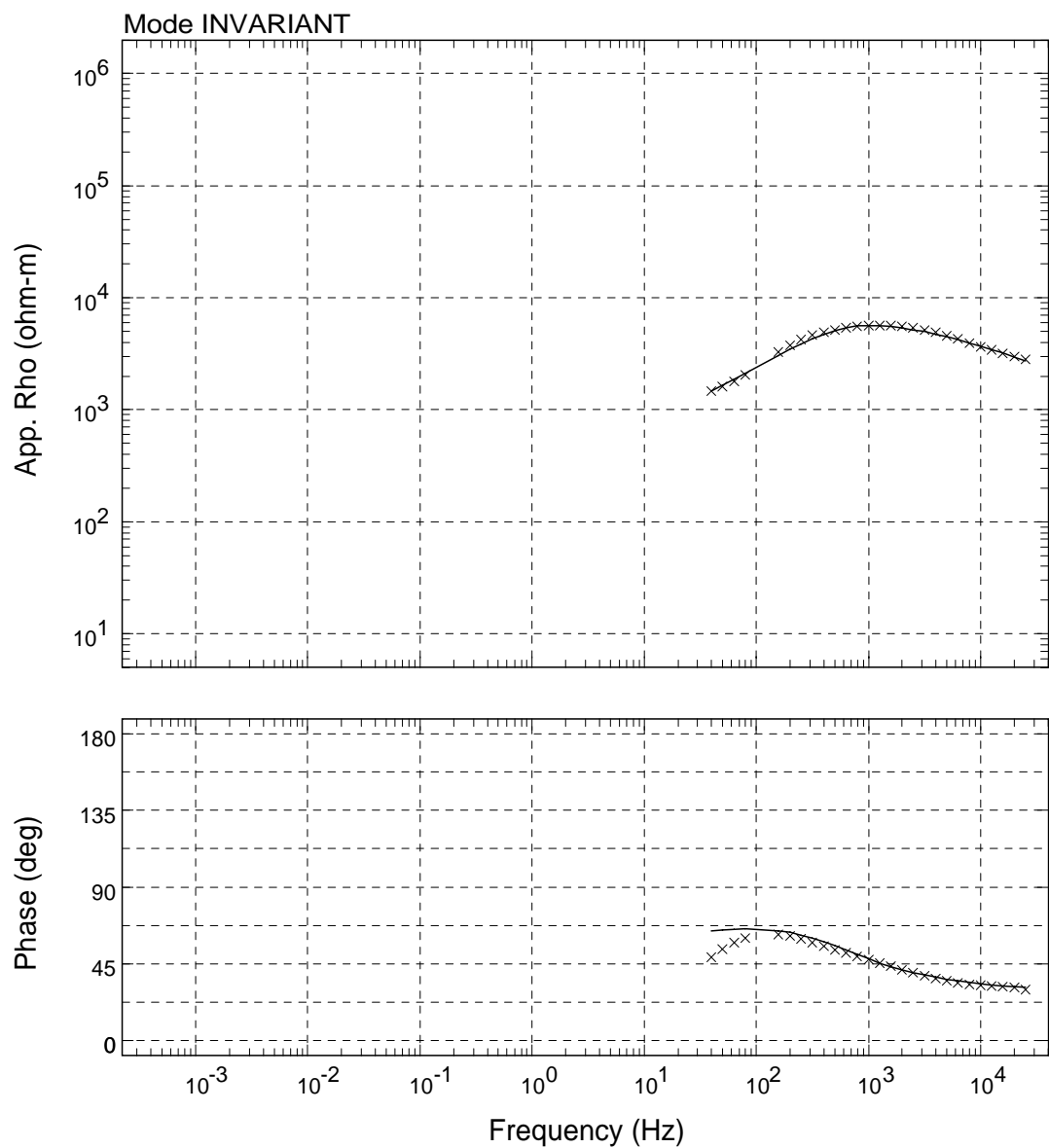
USGS - 01/Jun/2009



Sounding: SR026

Area: Hawaii

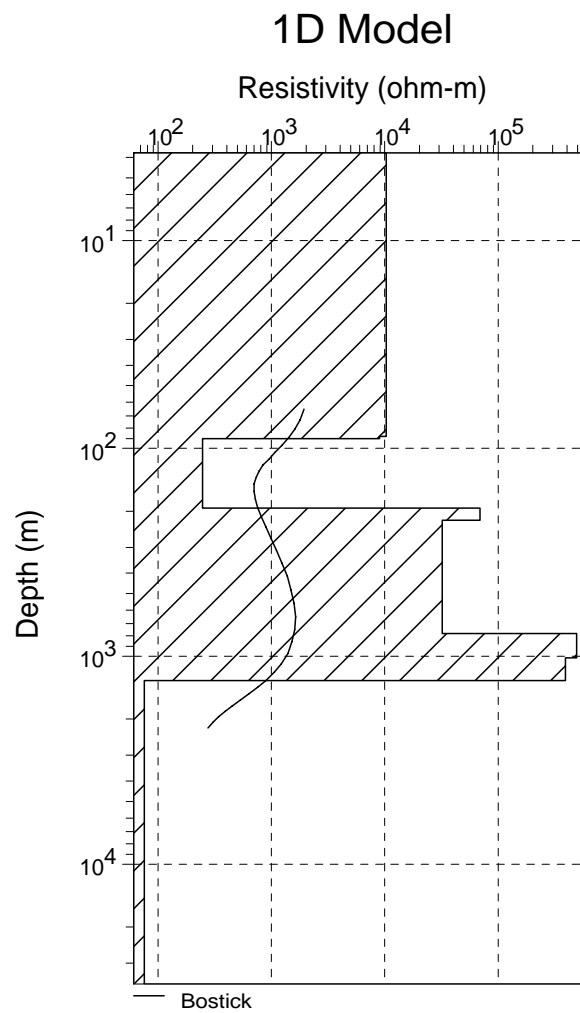
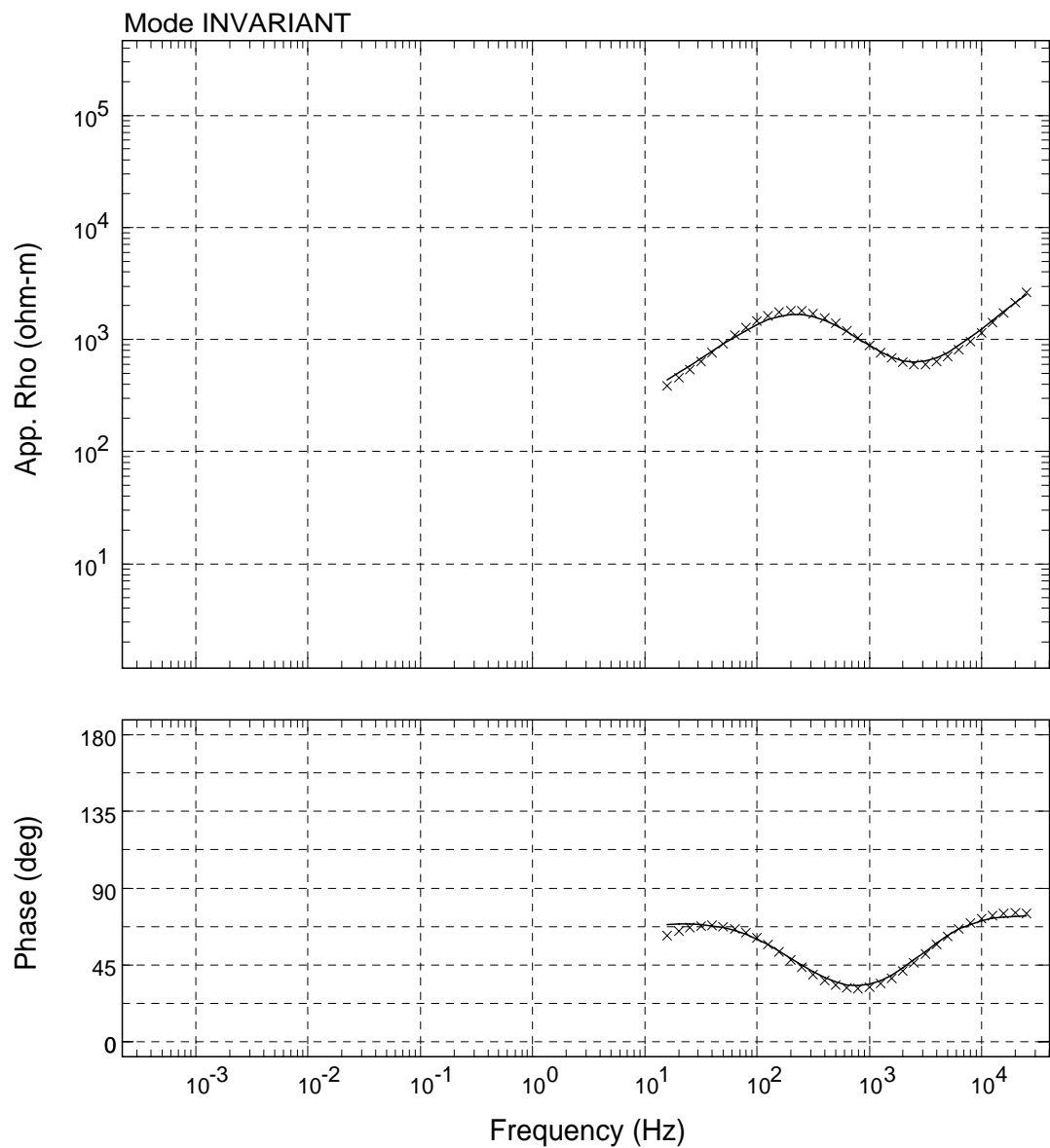
USGS - 01/Jun/2009



Sounding: SR028

Area: Hawaii

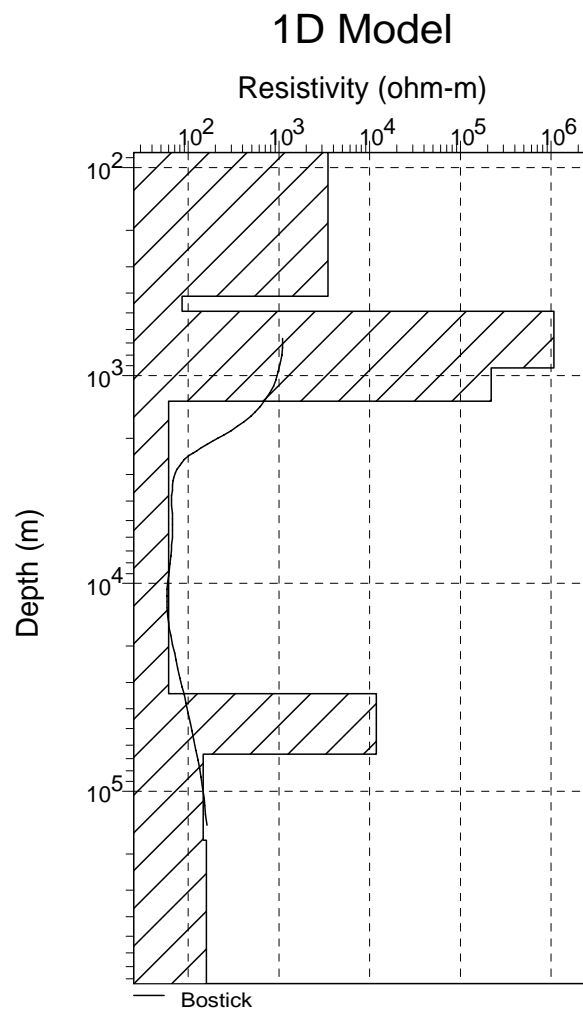
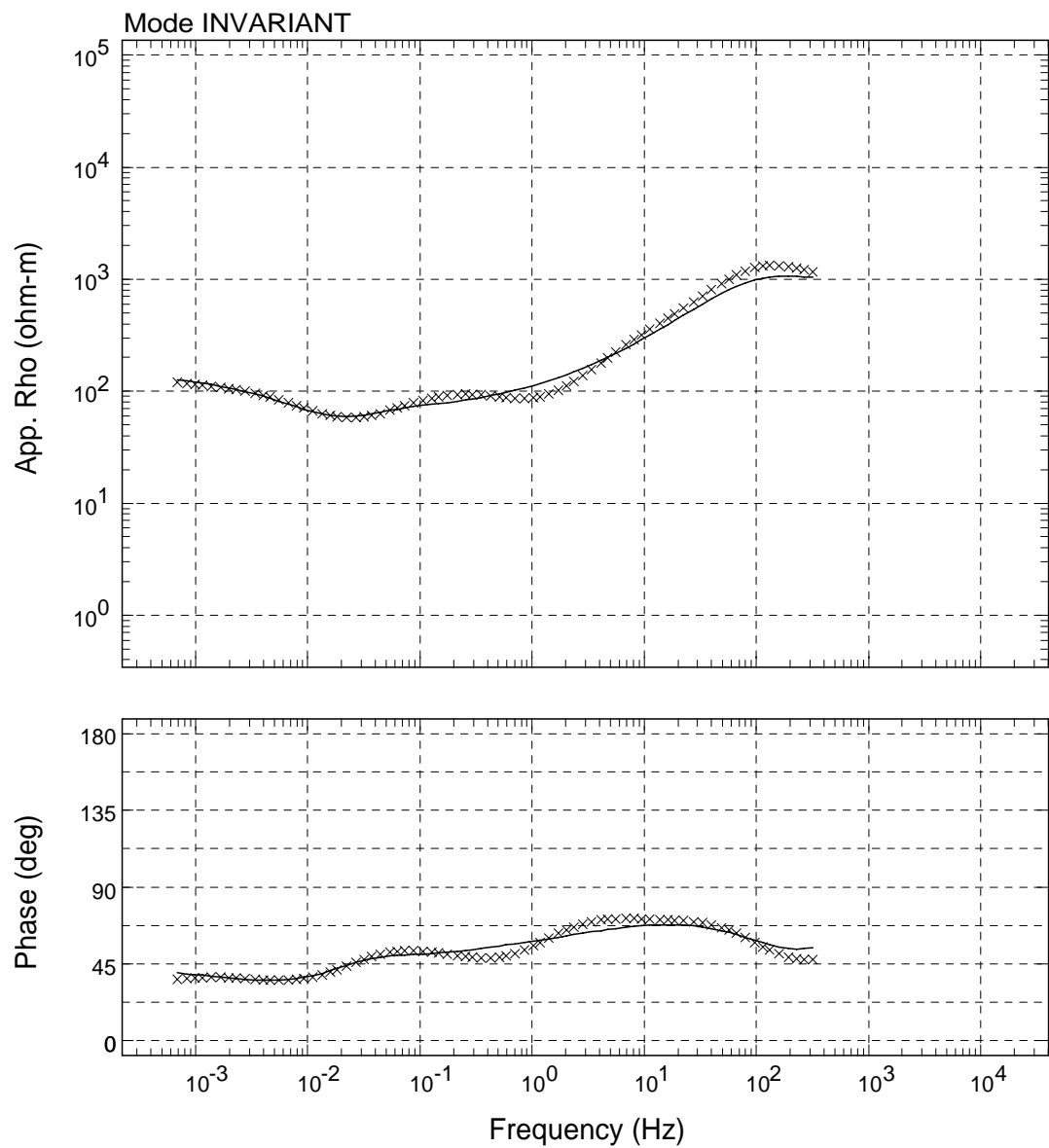
USGS - 01/Jun/2009



Sounding: SR029

Area: Hawaii

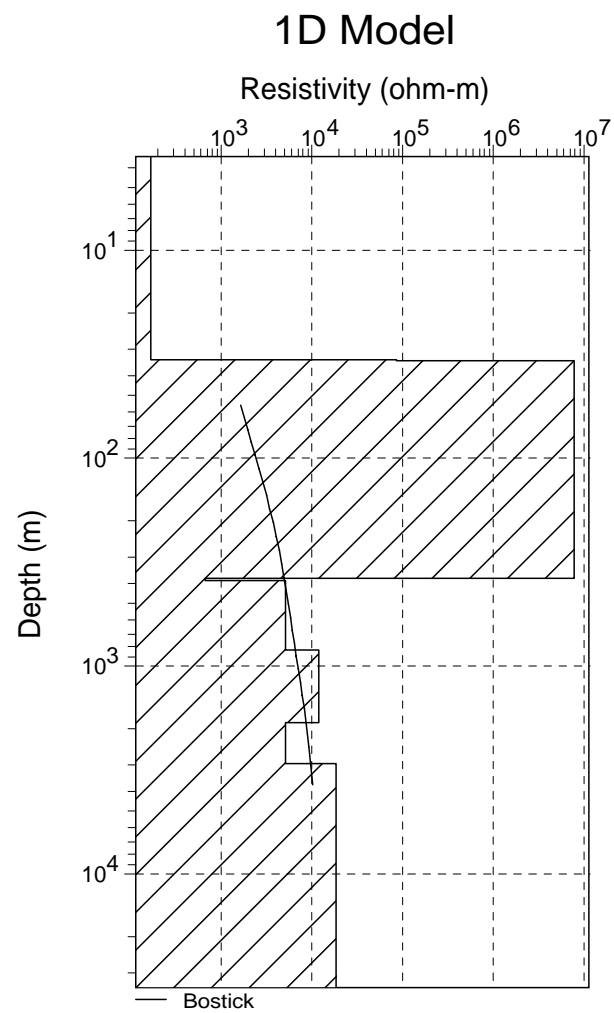
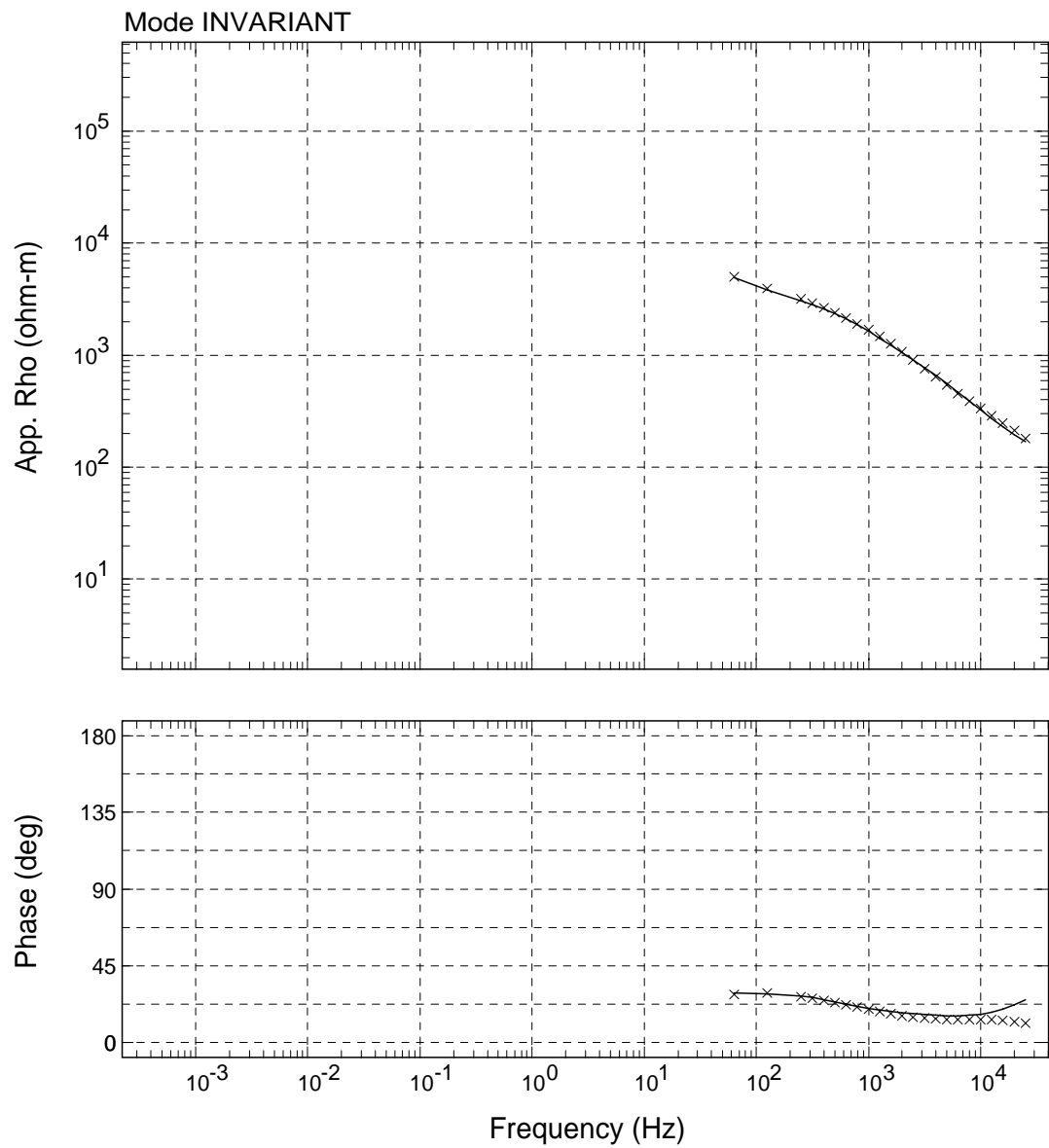
USGS - 01/Jun/2009



Sounding: WF01

Area: Hawaii

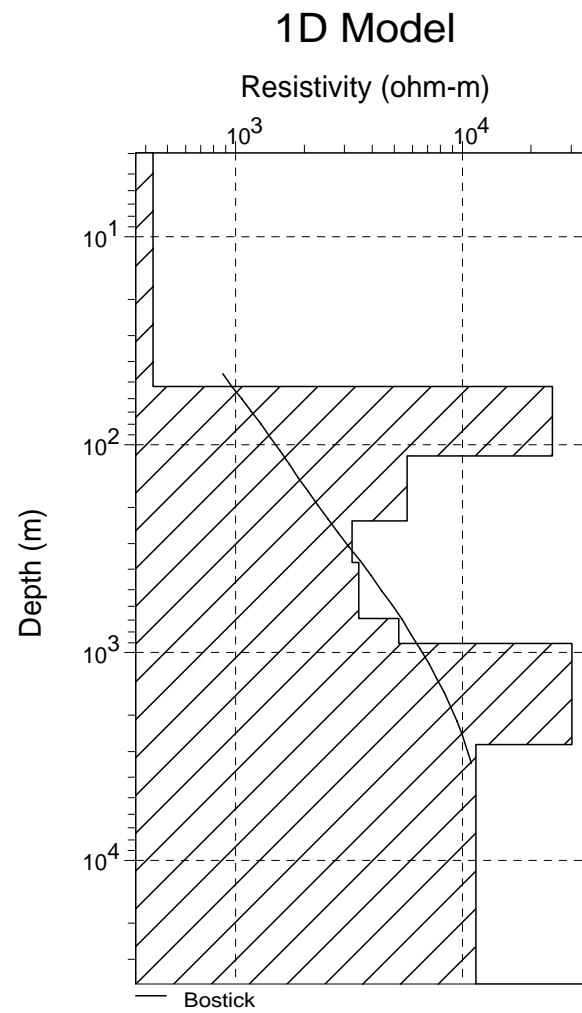
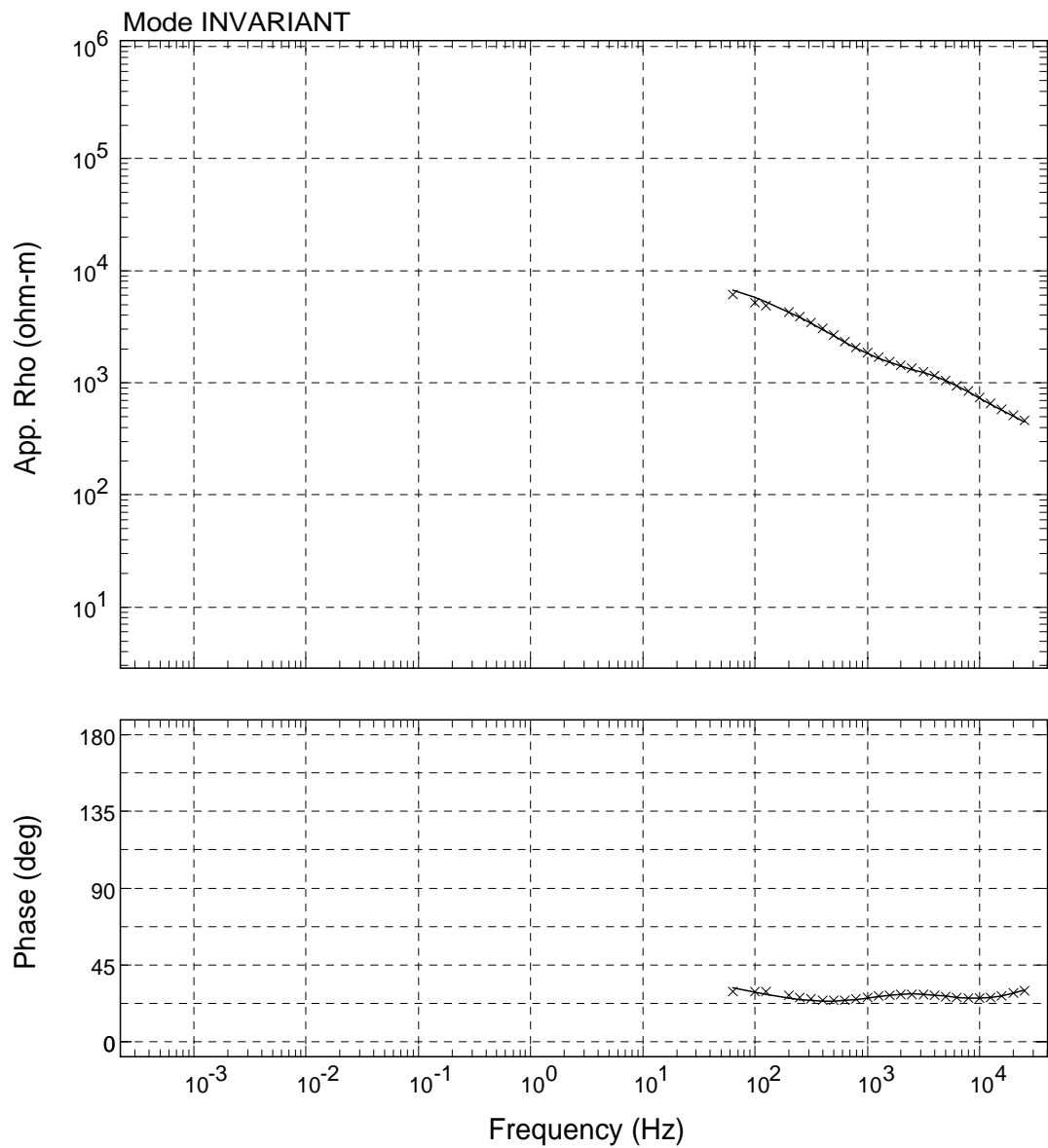
USGS - 01/Jun/2009



Sounding: WR002

Area: Hawaii

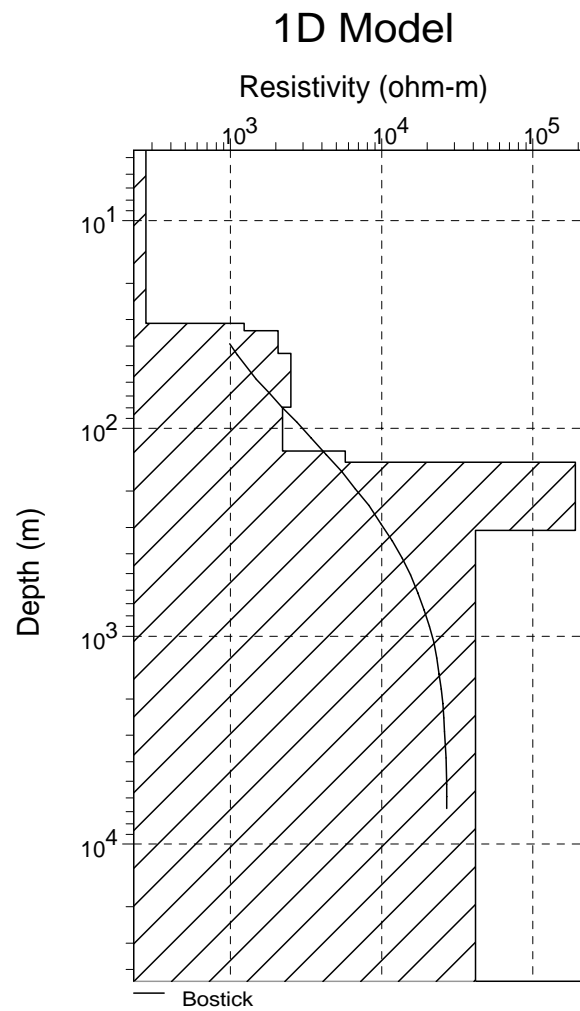
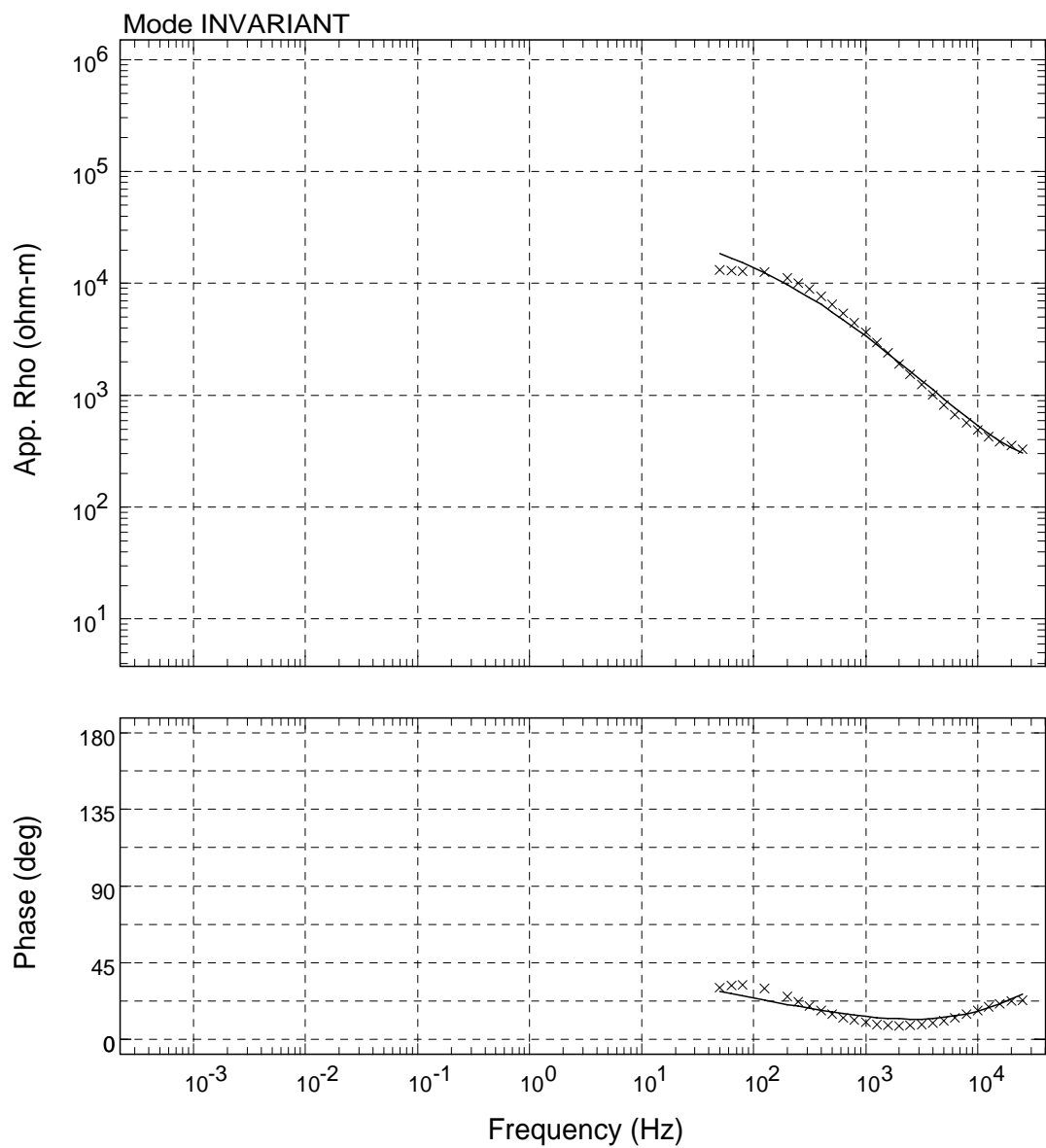
USGS - 01/Jun/2009



Sounding: WR003

Area: Hawaii

USGS - 01/Jun/2009



Sounding: WR004

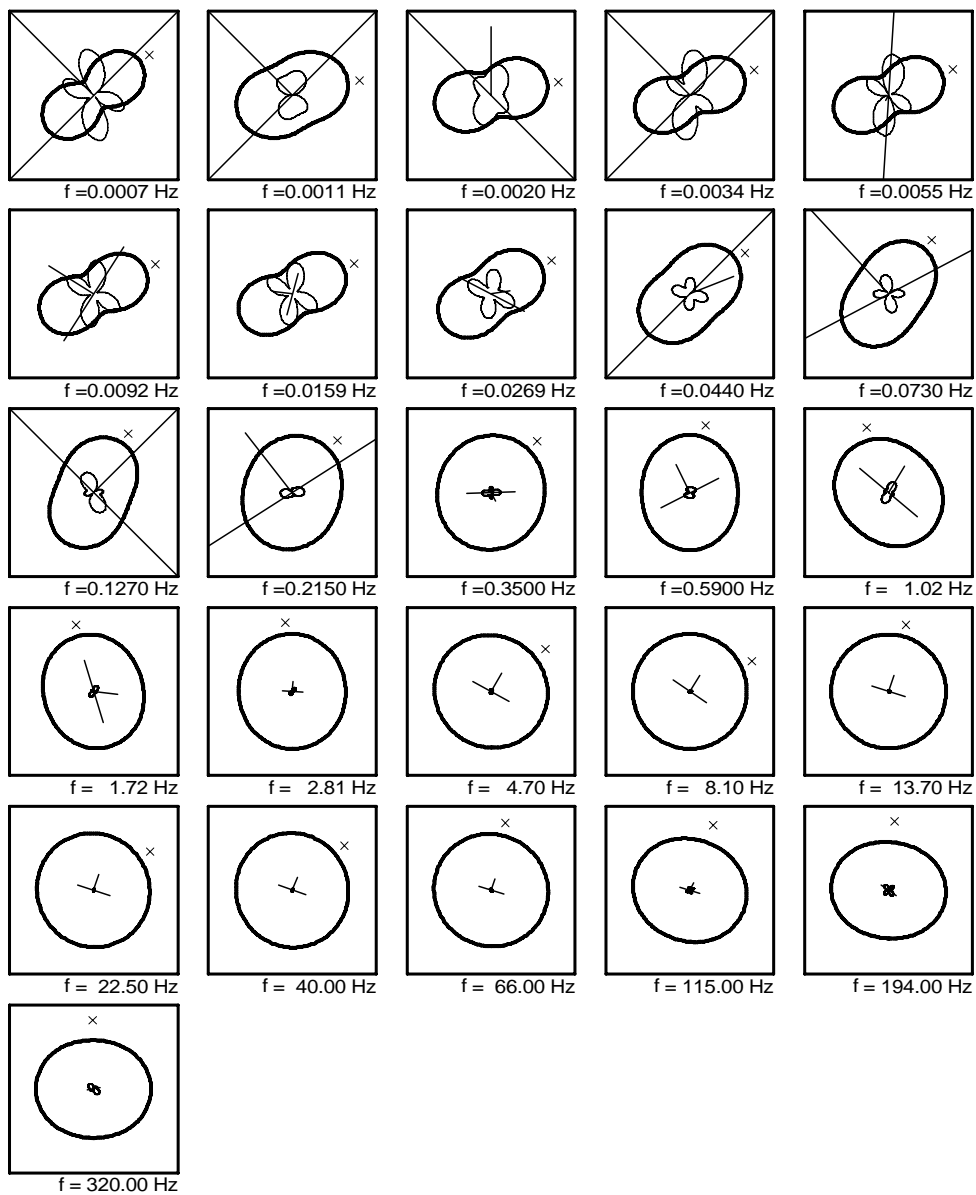
Area: Hawaii

USGS - 01/Jun/2009

Appendix D—Polar Diagrams of Selected Frequencies

USGS

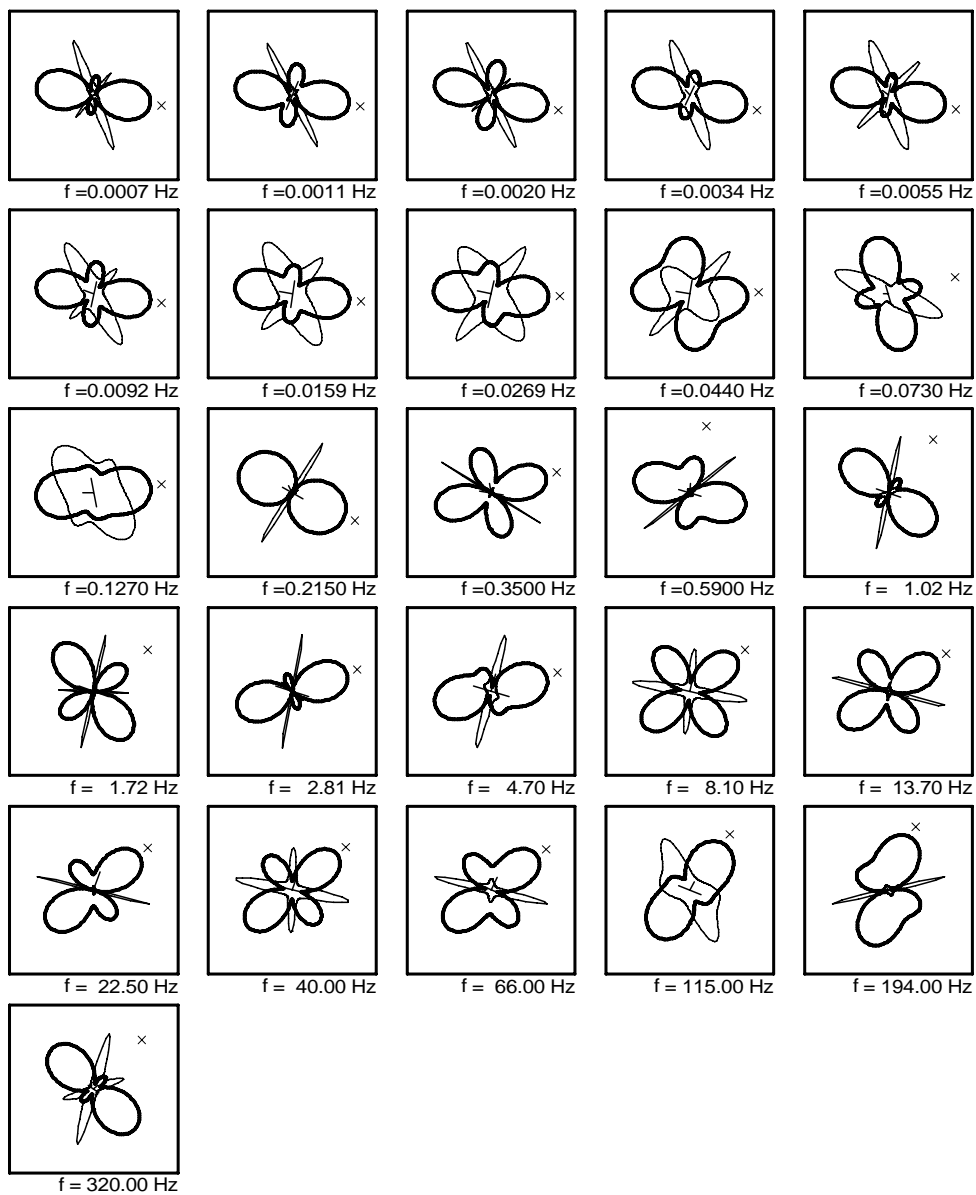
Sounding 1PT1



————— = Zxy Impedance
 ————— = Zxx Impedance
 × = Impedance Strike
 ————— = Tipper Magnitude / Strike
 0 1
 ————— = Induction Arrow (to conductor)
 0 1

USGS

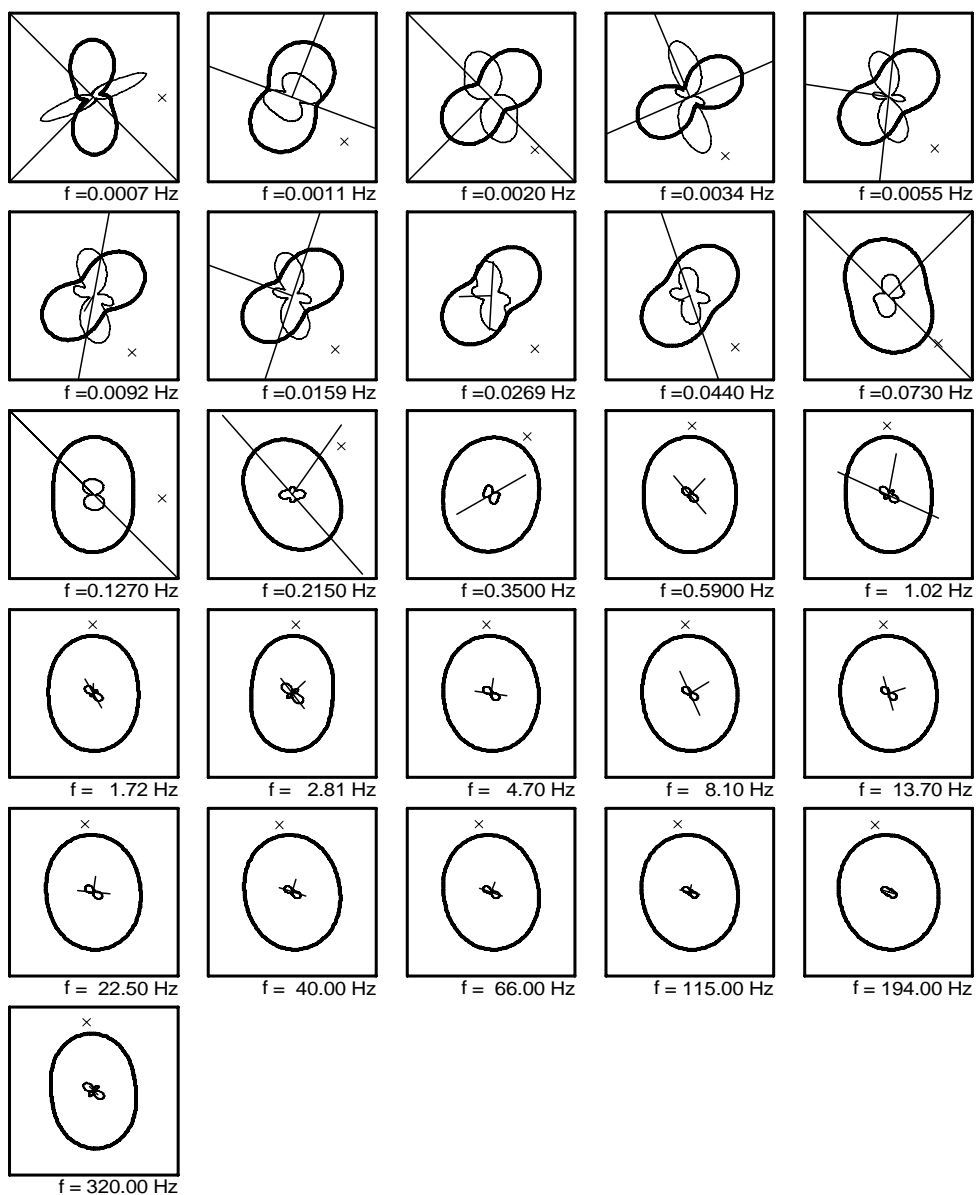
Sounding 2PT1

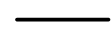
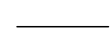


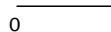


— = Zxy Impedance
 — = Zxx Impedance
 × = Impedance Strike
 — = Tipper Magnitude / Strike
 0 1
 — = Induction Arrow (to conductor)
 0 1

USGS

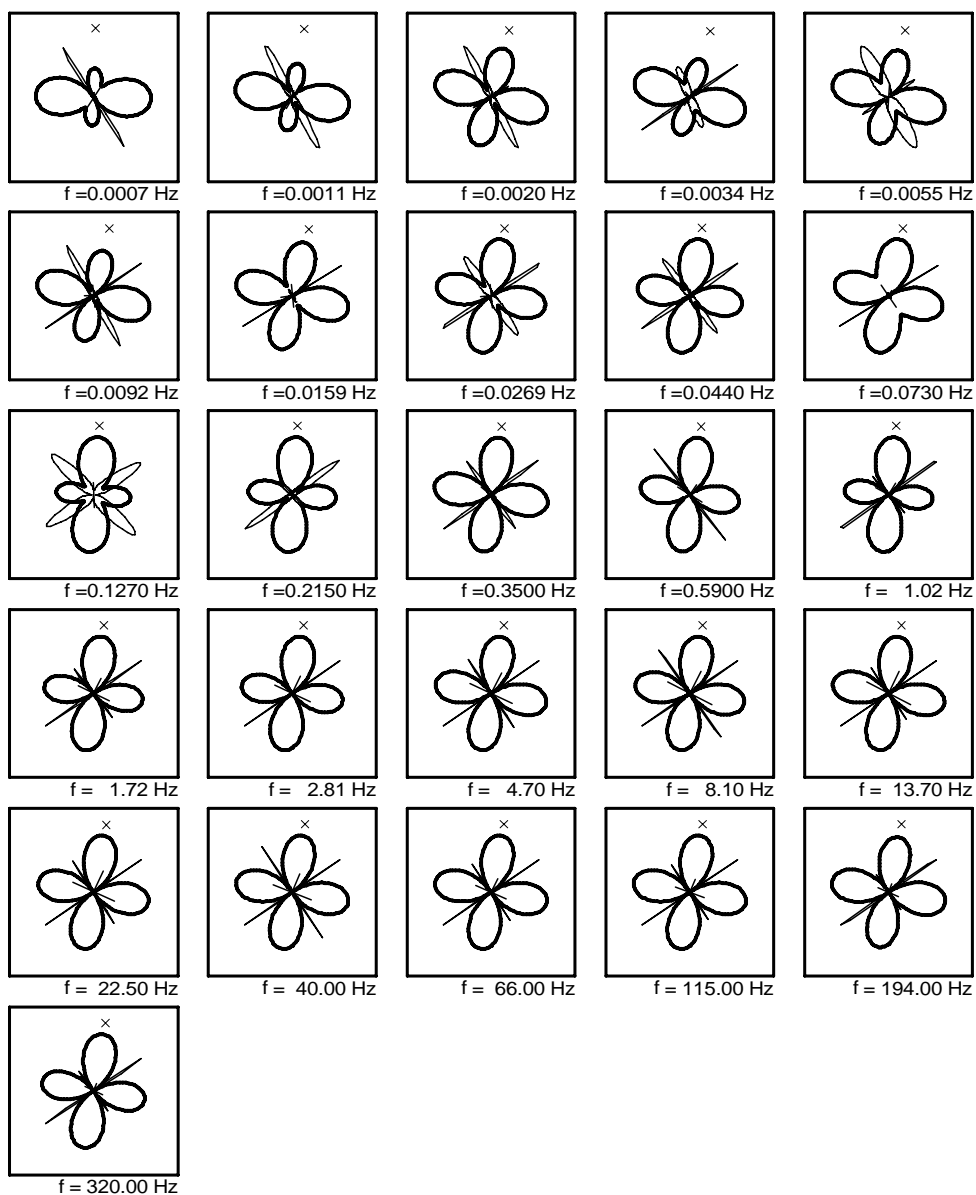
Sounding 3PT1



 = Zxy Impedance
 = Zxx Impedance
 = Impedance Strike
 = Tipper Magnitude / Strike
 = Induction Arrow (to conductor)

USGS

Sounding 4PT1



= Zxy Impedance

 = Zxx Impedance

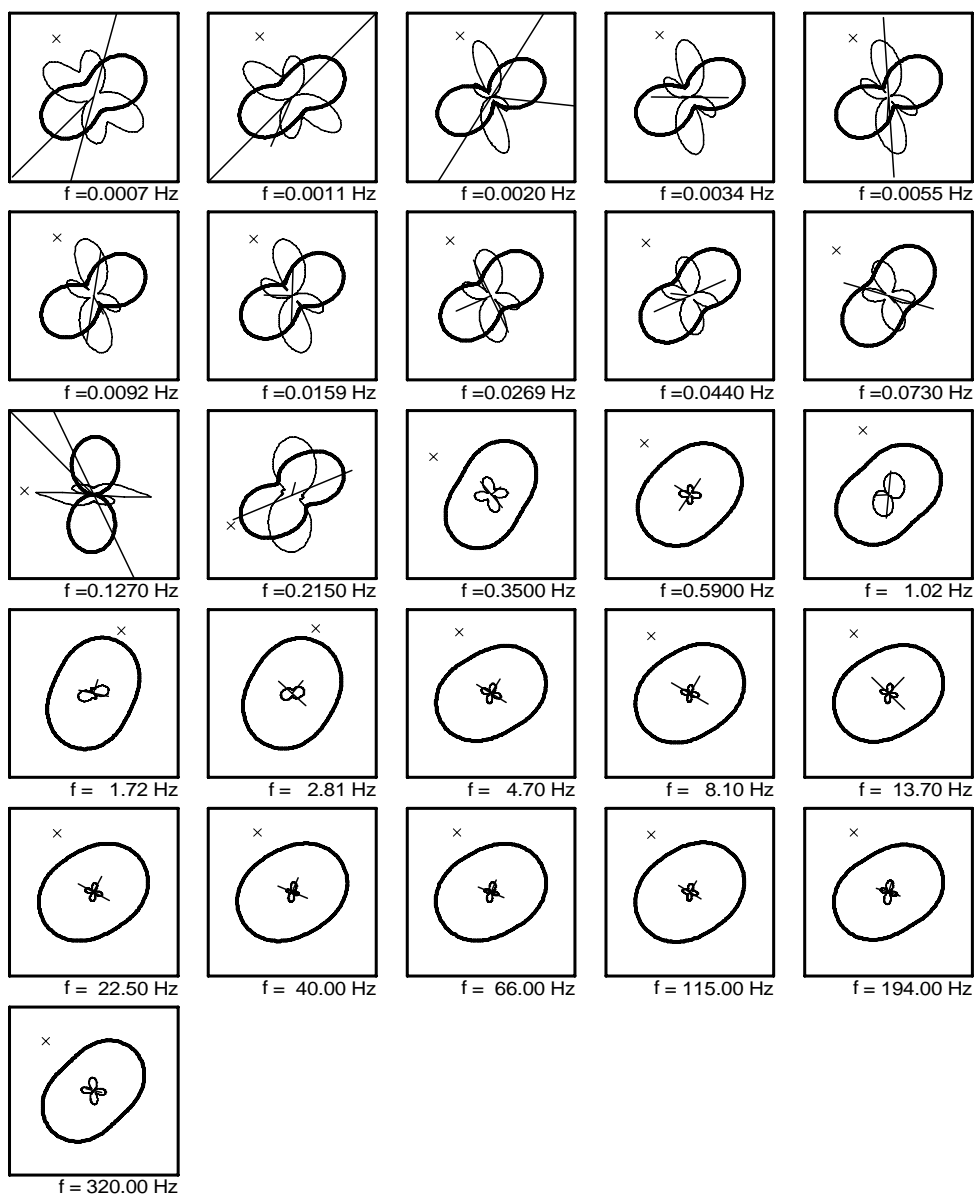
 x = Impedance Strike

 = Tipper Magnitude / Strike

 = Induction Arrow (to conductor)

USGS

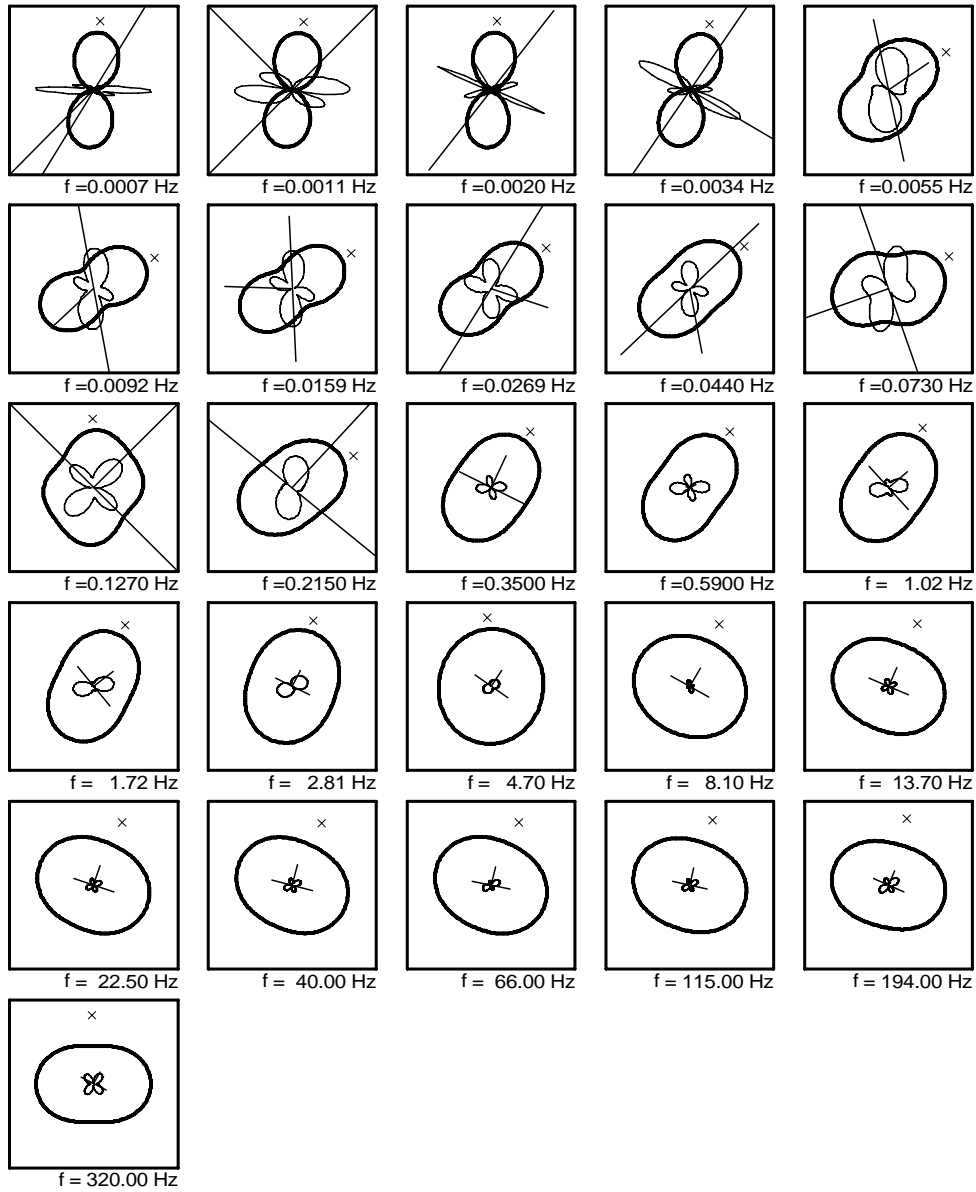
Sounding 6PT1



— = Zxy Impedance
 — = Zxx Impedance
 × = Impedance Strike
 — = Tipper Magnitude / Strike
 0 — 1
 — = Induction Arrow (to conductor)
 0 — 1

USGS

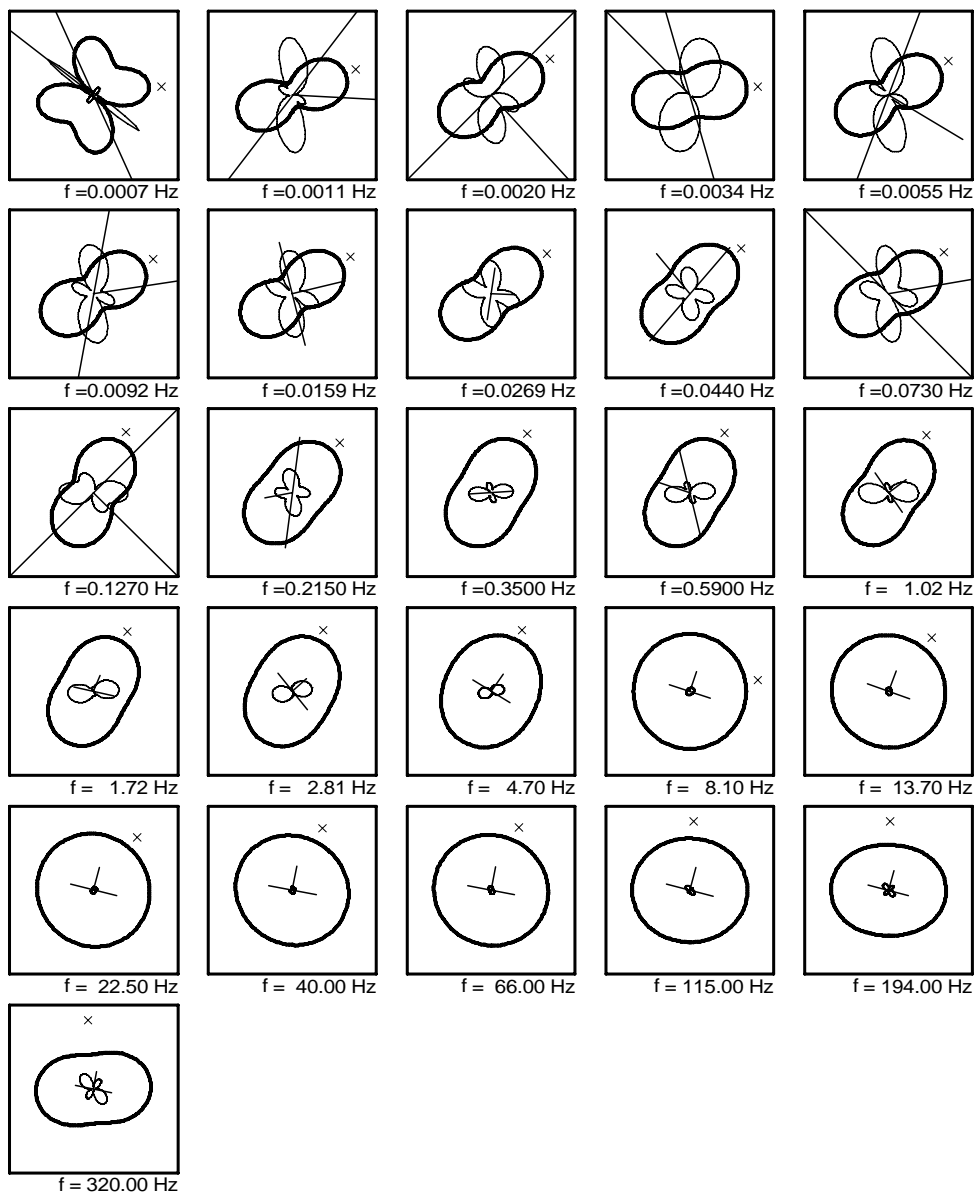
Sounding 7PT1



— = Zxy Impedance
 — = Zxx Impedance
 x = Impedance Strike
 — = Tipper Magnitude / Strike
 — = Induction Arrow (to conductor)

USGS

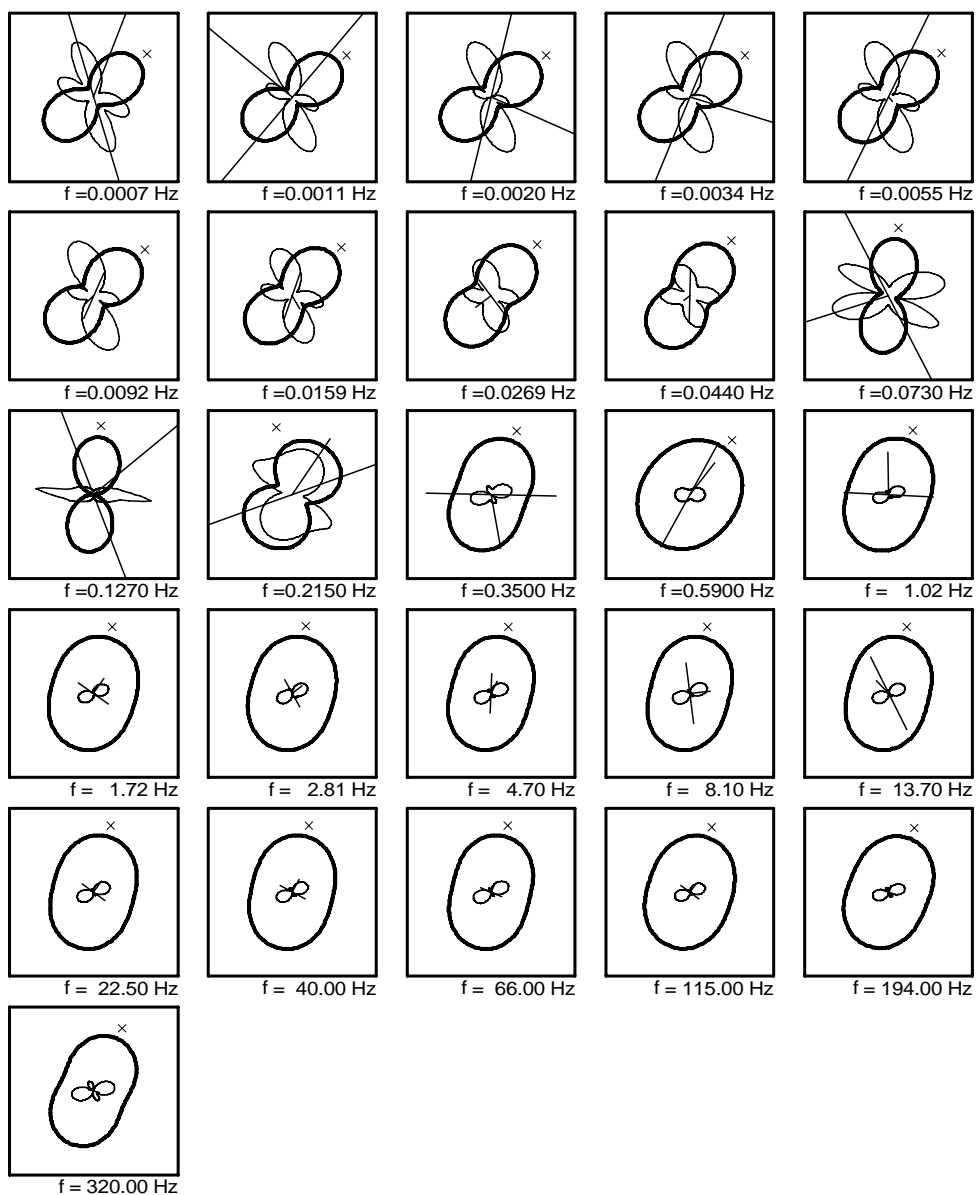
Sounding 8PT1

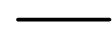
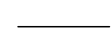
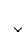

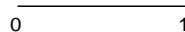


— = Zxy Impedance
 — = Zxx Impedance
 × = Impedance Strike
 — = Tipper Magnitude / Strike
 0 — 1
 — = Induction Arrow (to conductor)
 0 — 1

USGS

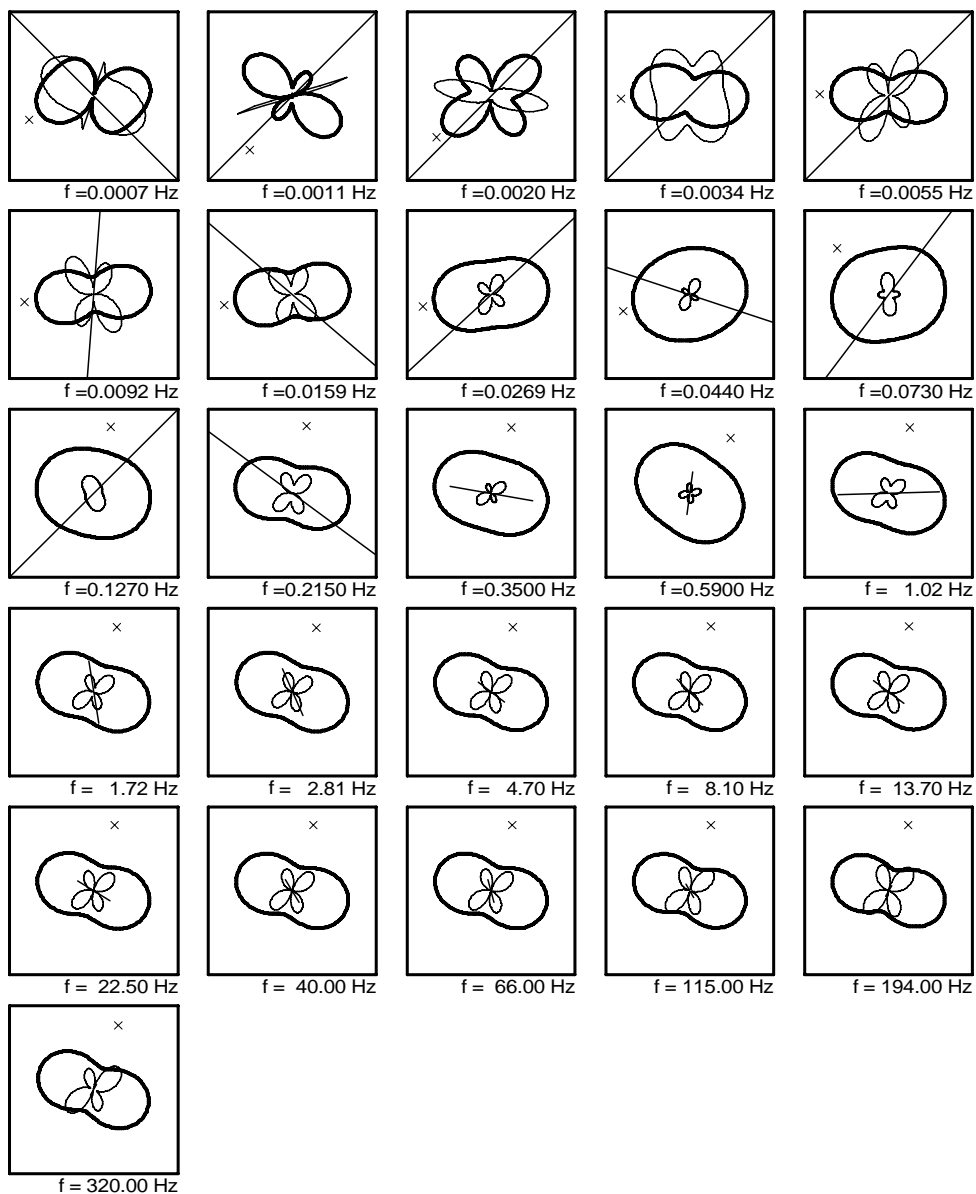
Sounding 9PT1



 = Zxy Impedance
 = Zxx Impedance
 = Impedance Strike
 = Tipper Magnitude / Strike
 = Induction Arrow (to conductor)

USGS

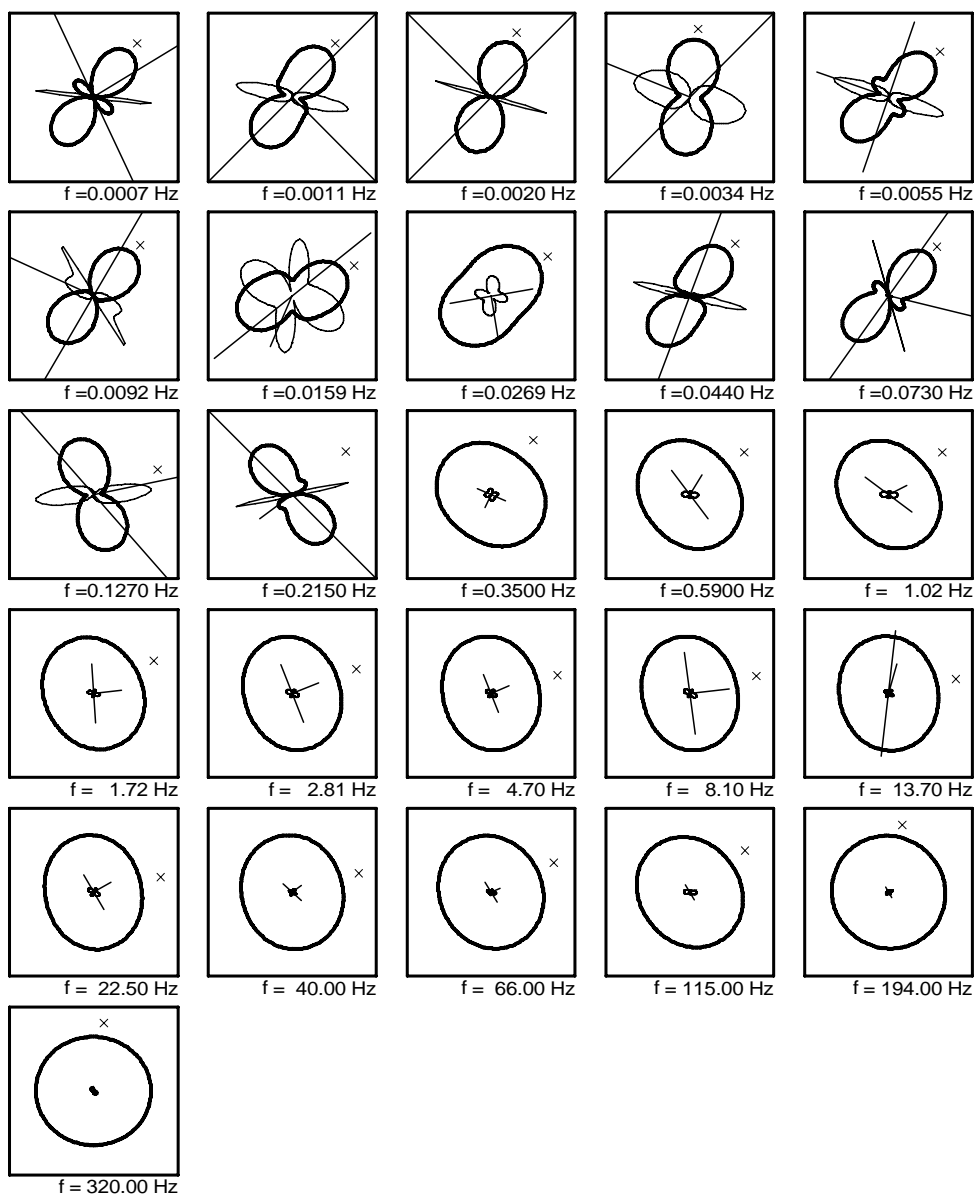
Sounding 12PT



— = Zxy Impedance
 — = Zxx Impedance
 x = Impedance Strike
 — = Tipper Magnitude / Strike
 0 1

USGS

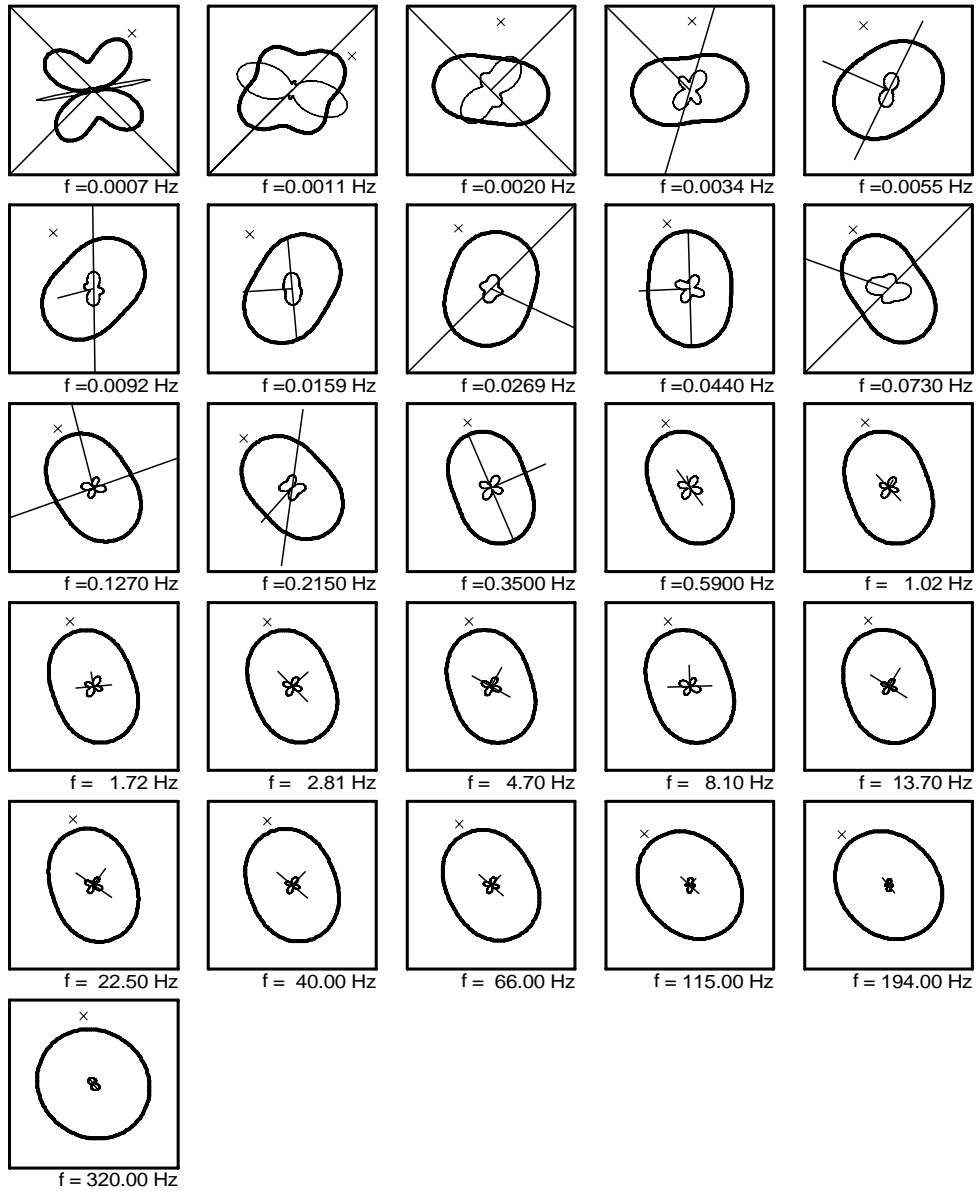
Sounding 13PT

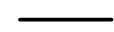
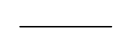

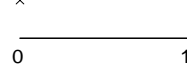



— = Zxy Impedance
 — = Zxx Impedance
 x = Impedance Strike
 — = Tipper Magnitude / Strike
 0 — 1
 — = Induction Arrow (to conductor)
 0 — 1

USGS

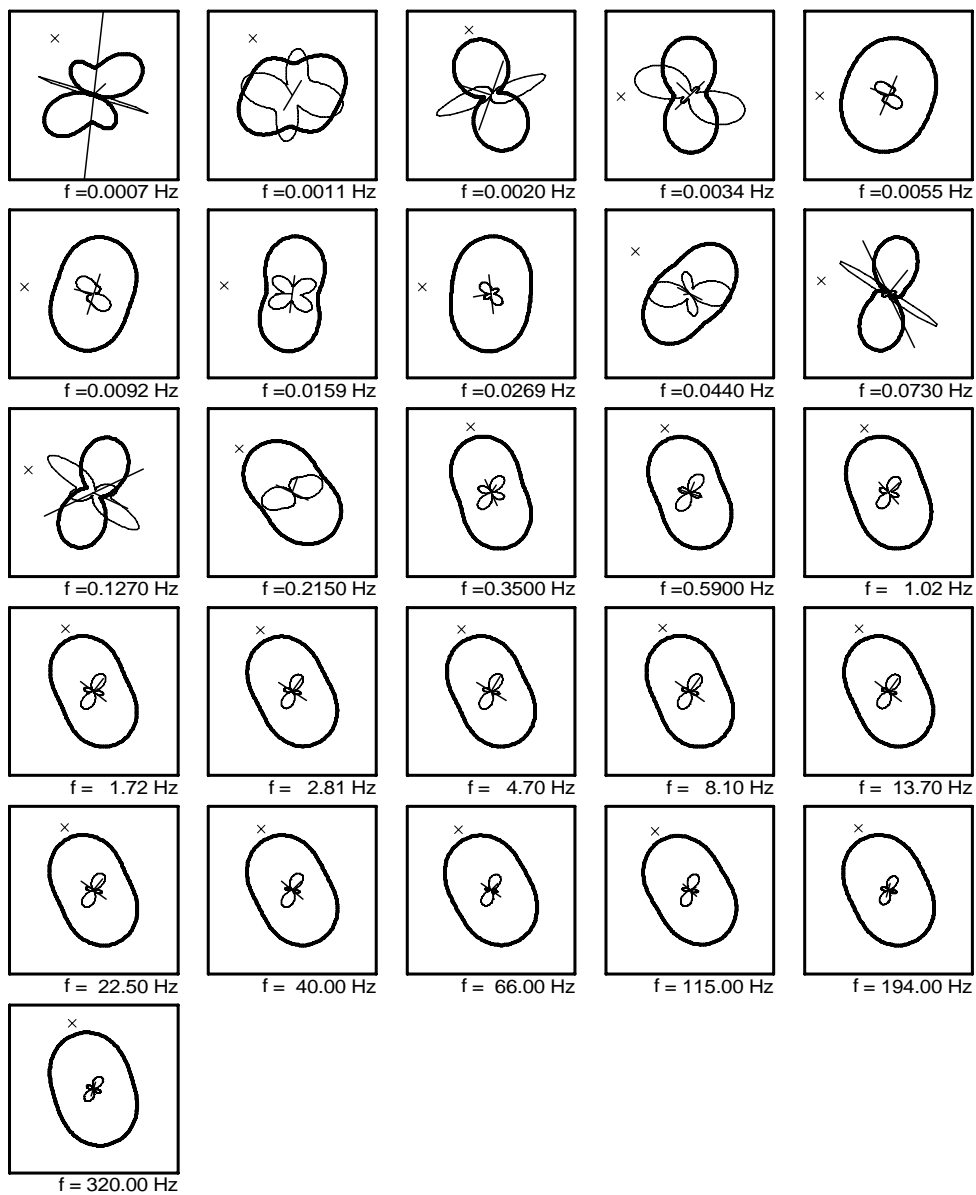
Sounding 15PT



 = Zxy Impedance
 = Zxx Impedance
 = Impedance Strike
 = Tipper Magnitude /Strike
 = Induction Arrow (to conductor)

USGS

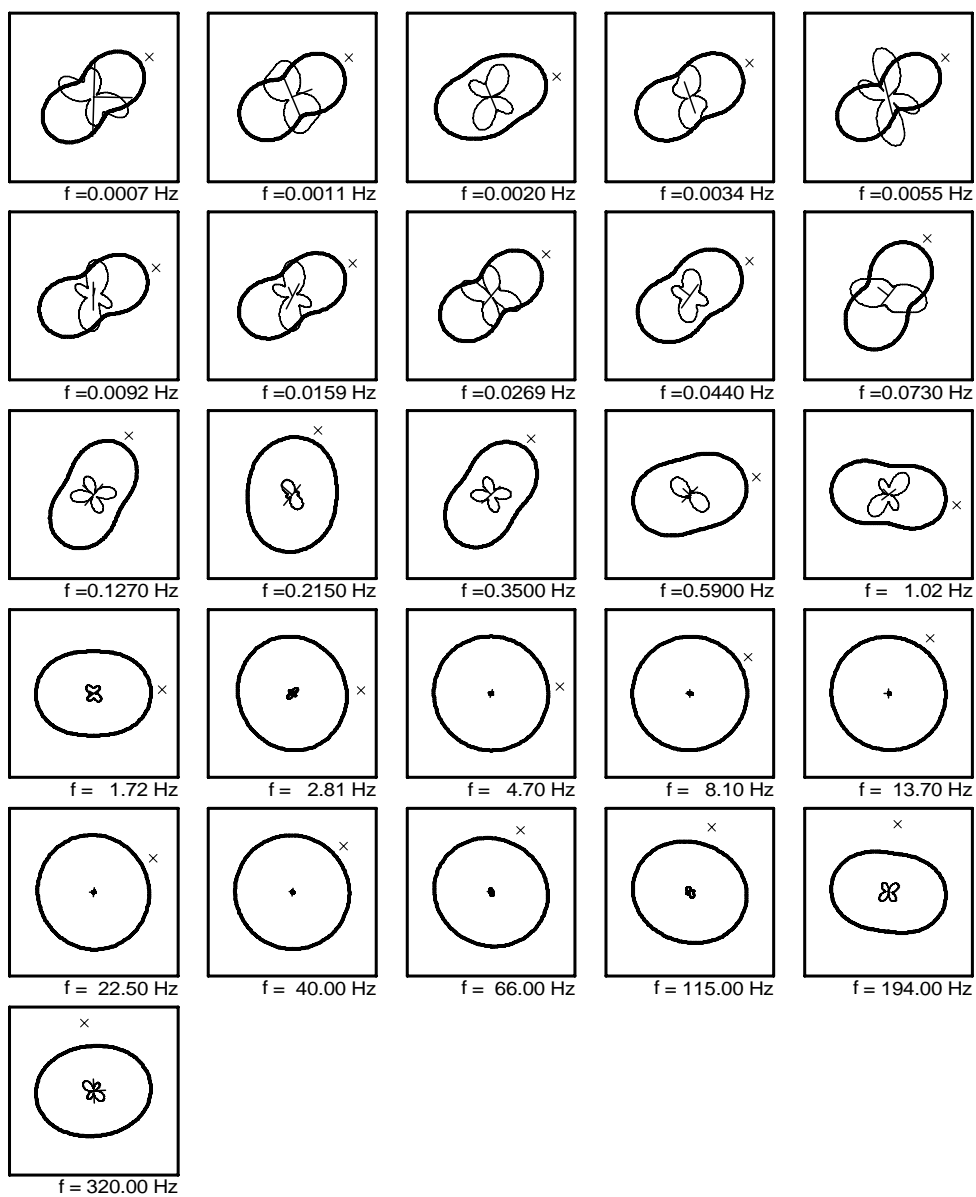
Sounding 16PT



————— = Zxy Impedance
 ————— = Zxx Impedance
 × = Impedance Strike
 0 ————— 1 = Tipper Magnitude /Strike
 0 ————— 1 = Induction Arrow (to conductor)

USGS

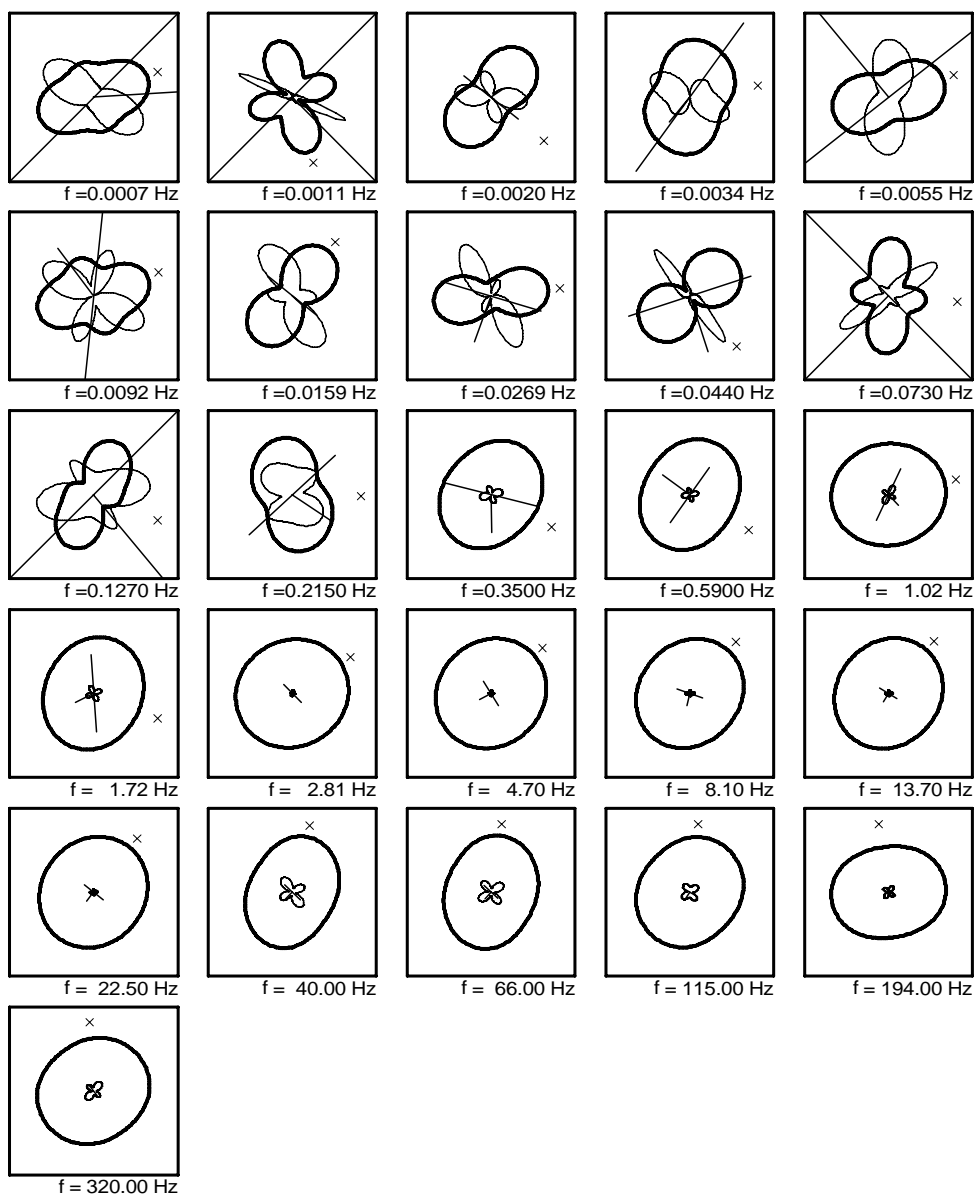
Sounding HH01



— = Zxy Impedance
 — = Zxx Impedance
 x = Impedance Strike
 — = Tipper Magnitude / Strike
 0 — 1
 — = Induction Arrow (to conductor)
 0 — 1

USGS

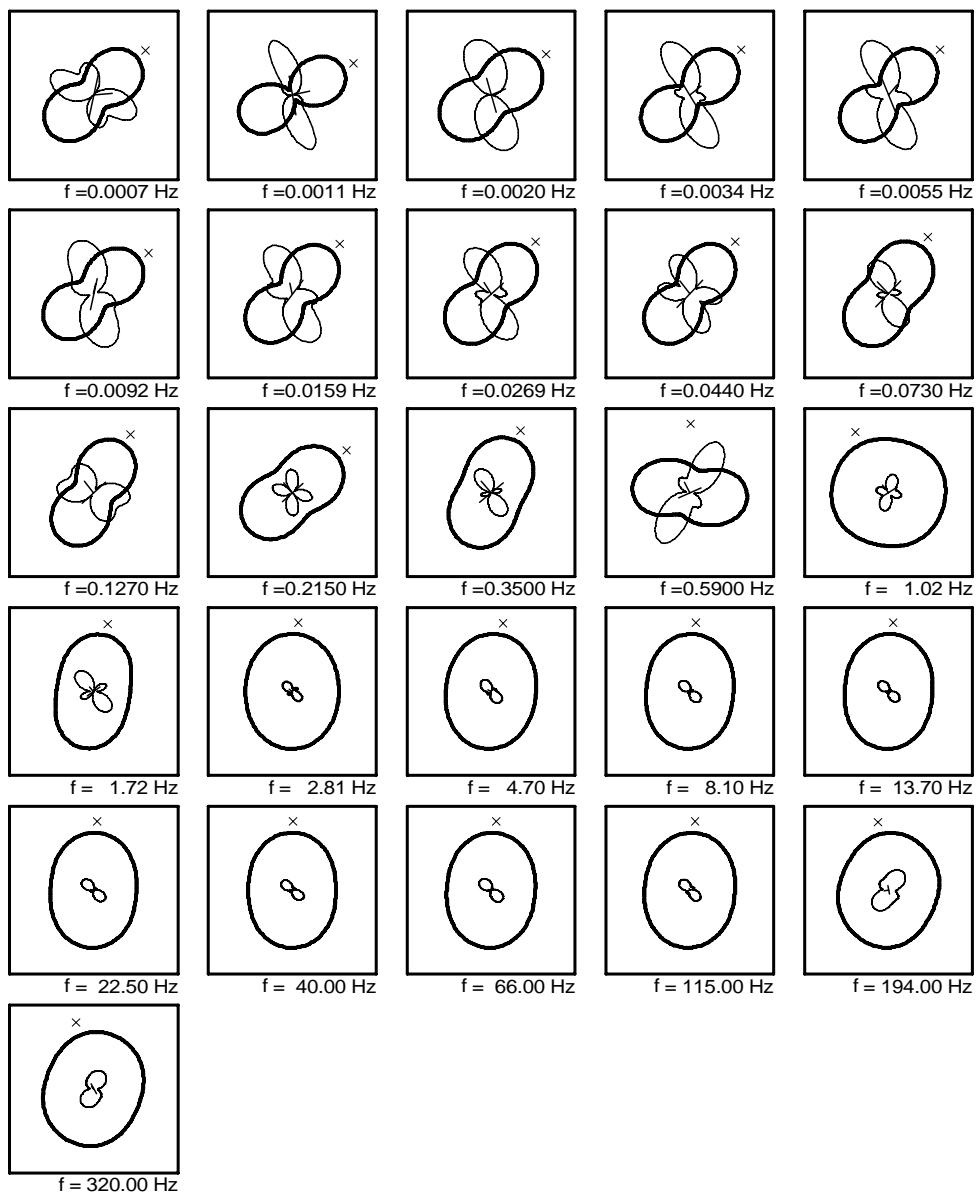
Sounding HH02

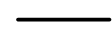
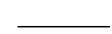
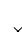

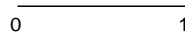


— = Zxy Impedance
 — = Zxx Impedance
 x = Impedance Strike
 — = Tipper Magnitude / Strike
 — = Induction Arrow (to conductor)

USGS

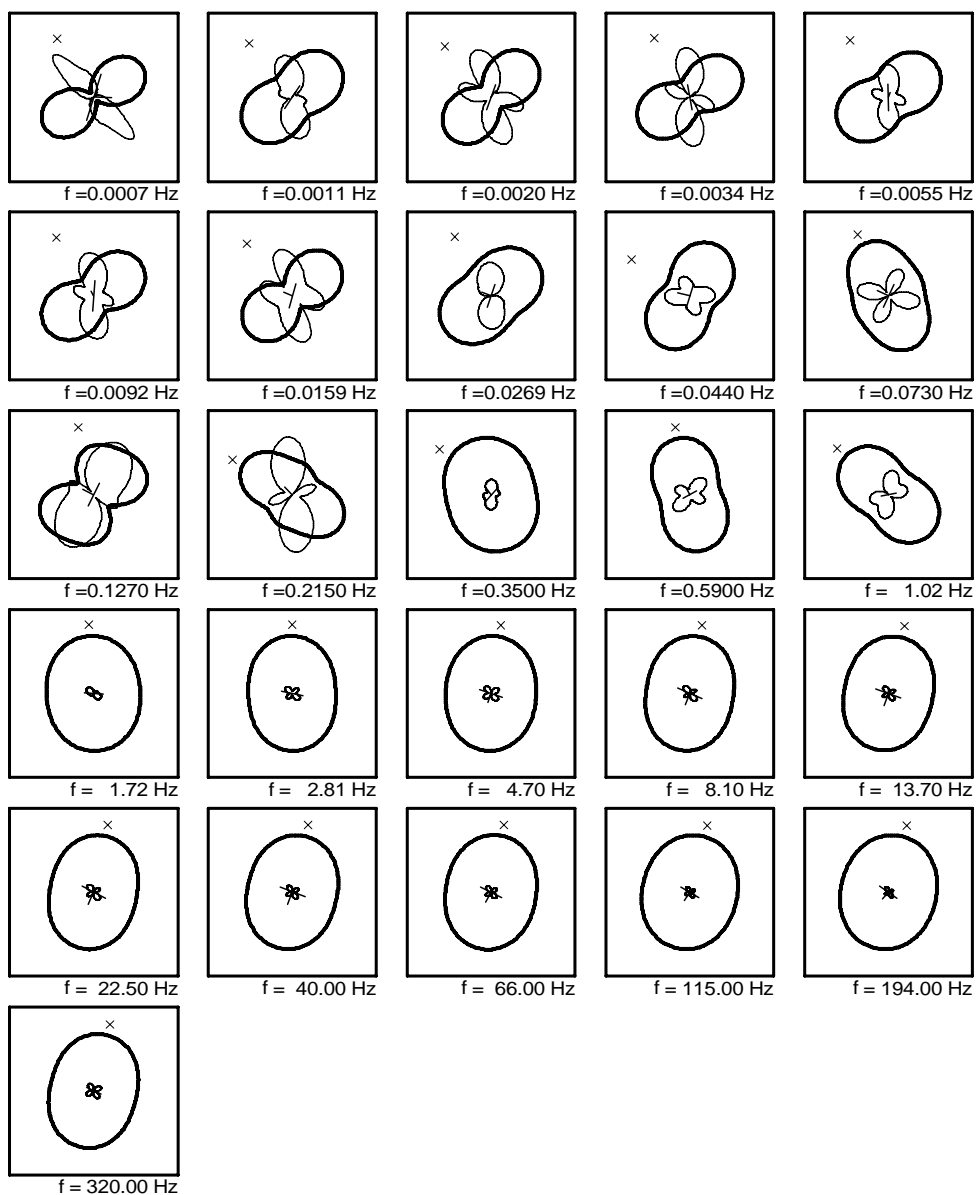
Sounding HH03



 = Zxy Impedance
 = Zxx Impedance
 = Impedance Strike
 = Tipper Magnitude / Strike
 = Induction Arrow (to conductor)

USGS

Sounding KK01



= Zxy Impedance

 = Zxx Impedance

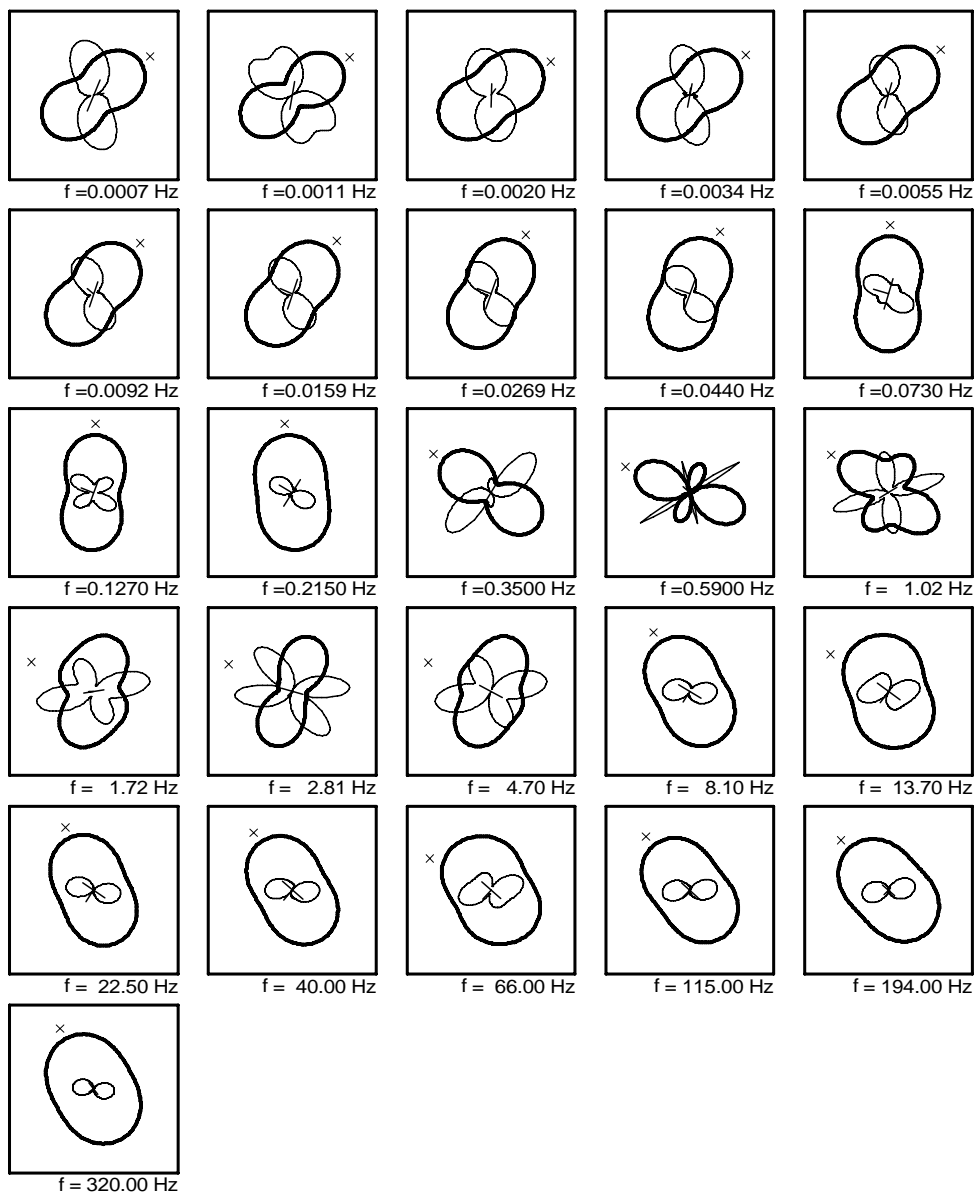
 x = Impedance Strike

 = Tipper Magnitude / Strike

 = Induction Arrow (to conductor)

USGS

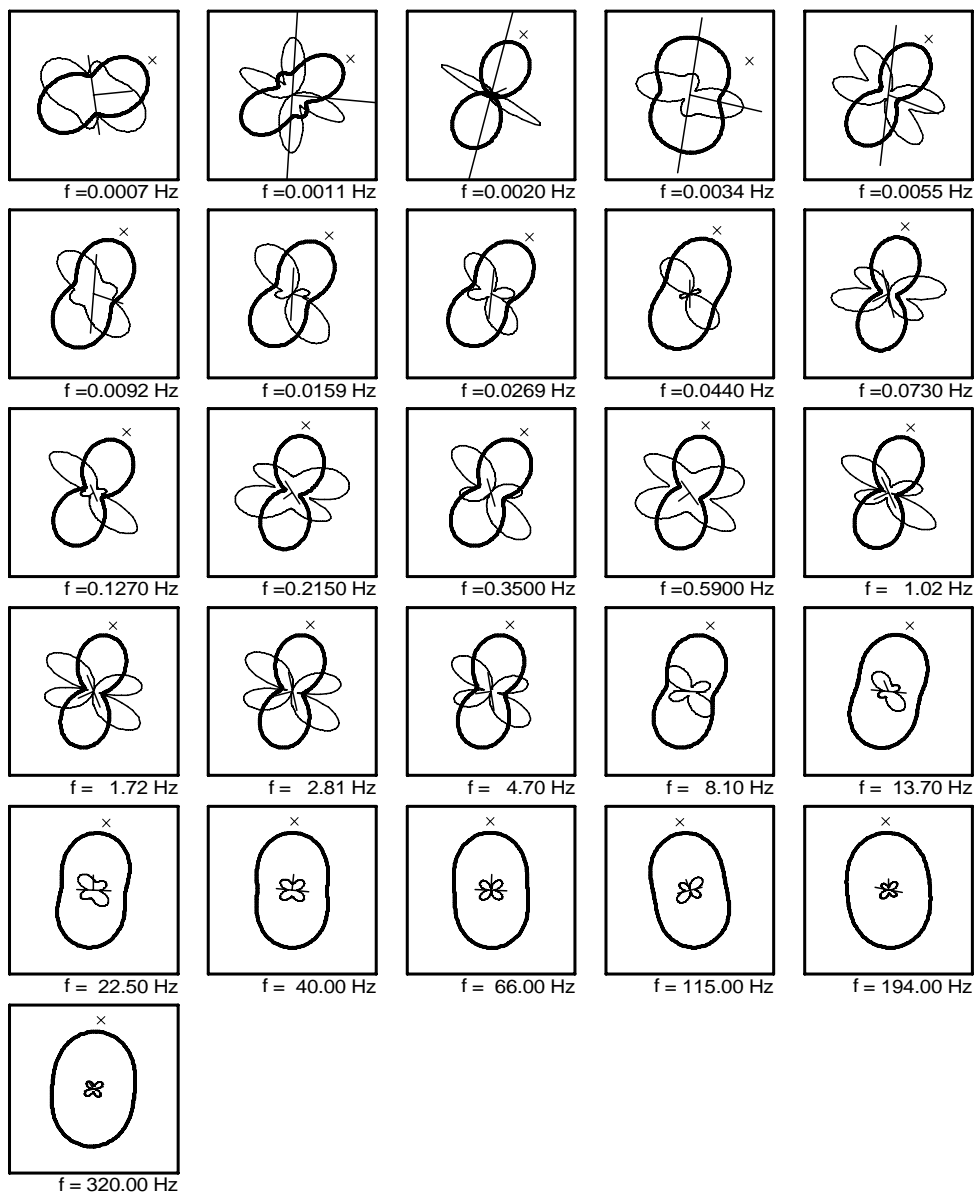
Sounding KK02



— = Zxy Impedance
 — = Zxx Impedance
 × = Impedance Strike
 — = Tipper Magnitude / Strike
 0 — 1
 — = Induction Arrow (to conductor)
 0 — 1

USGS

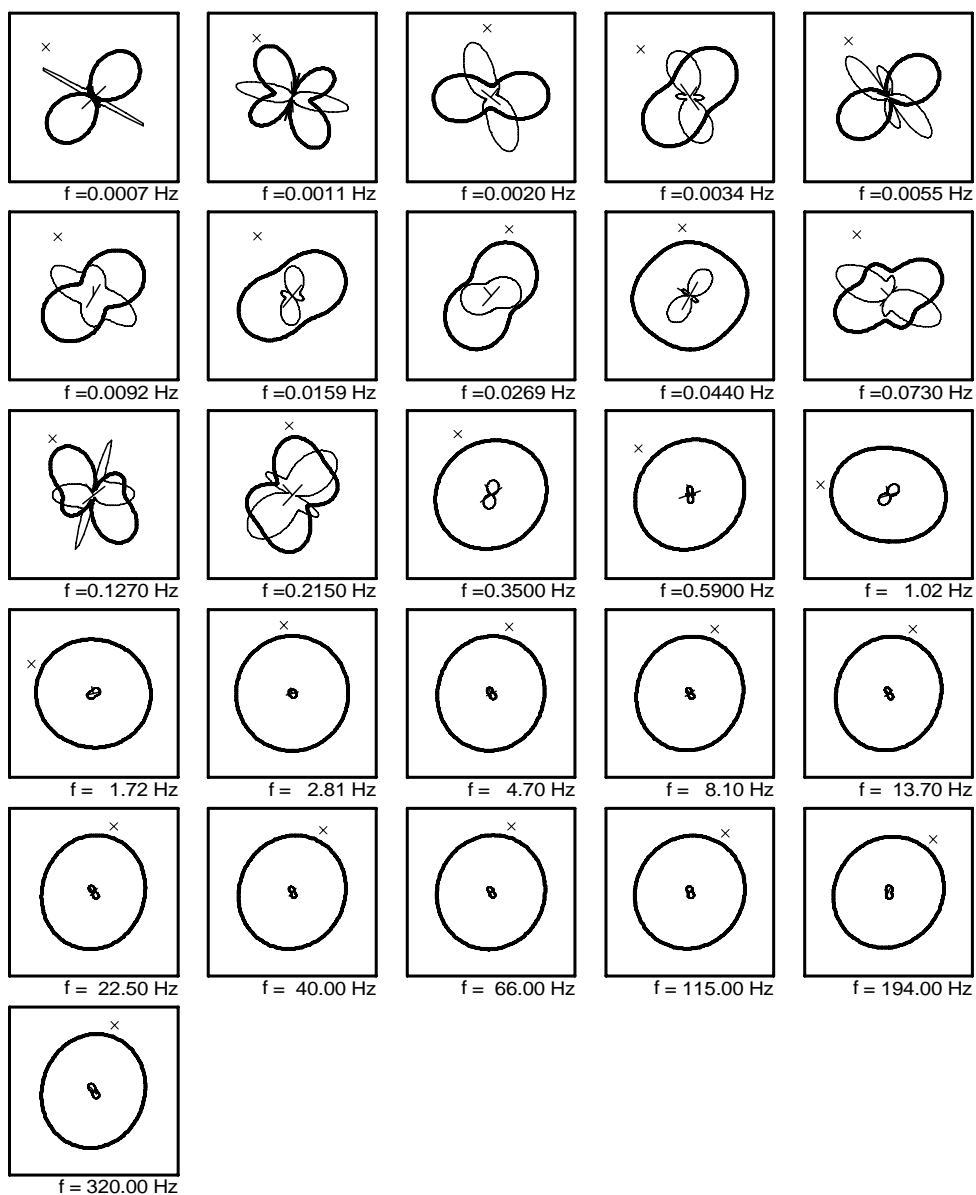
Sounding KM01



= Zxy Impedance
 = Zxx Impedance
 = Impedance Strike
 = Tipper Magnitude / Strike
 = Induction Arrow (to conductor)

USGS

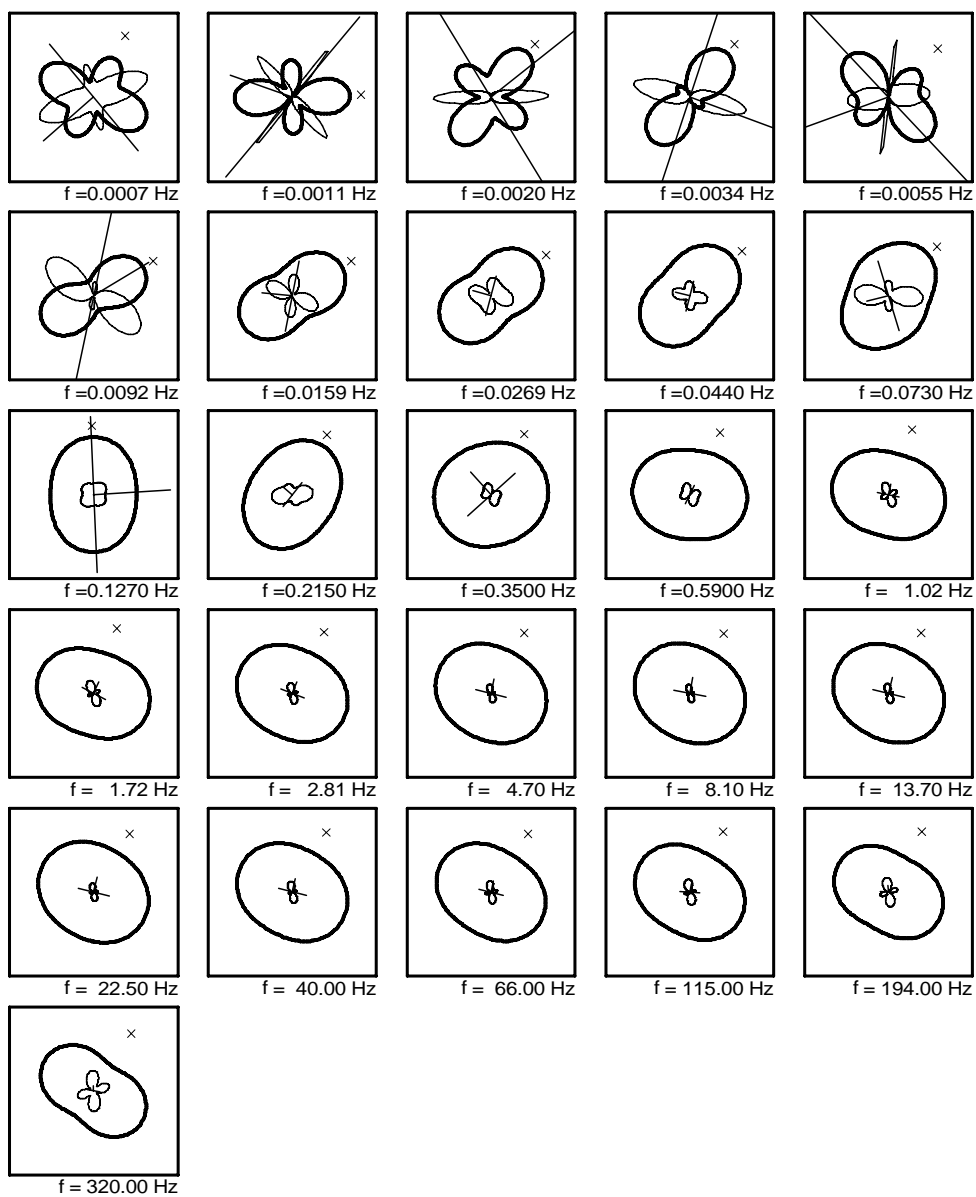
Sounding MKR1



— = Zxy Impedance
 — = Zxx Impedance
 x = Impedance Strike
 — = Tipper Magnitude / Strike
 0 1
 — = Induction Arrow (to conductor)
 0 1

USGS

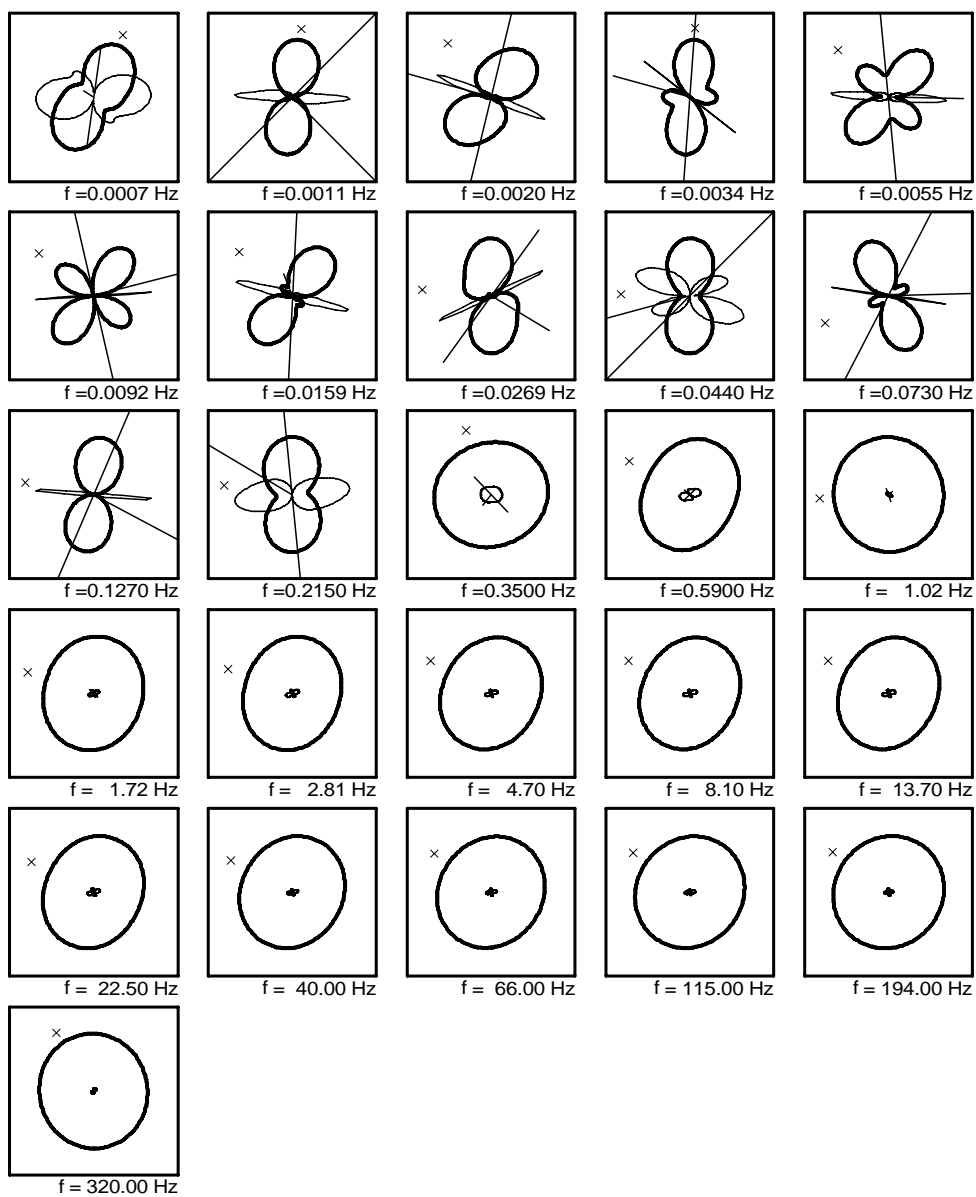
Sounding ML01



— = Zxy Impedance
 — = Zxx Impedance
 x = Impedance Strike
 — = Tipper Magnitude / Strike
 0 1
 — = Induction Arrow (to conductor)
 0 1

USGS

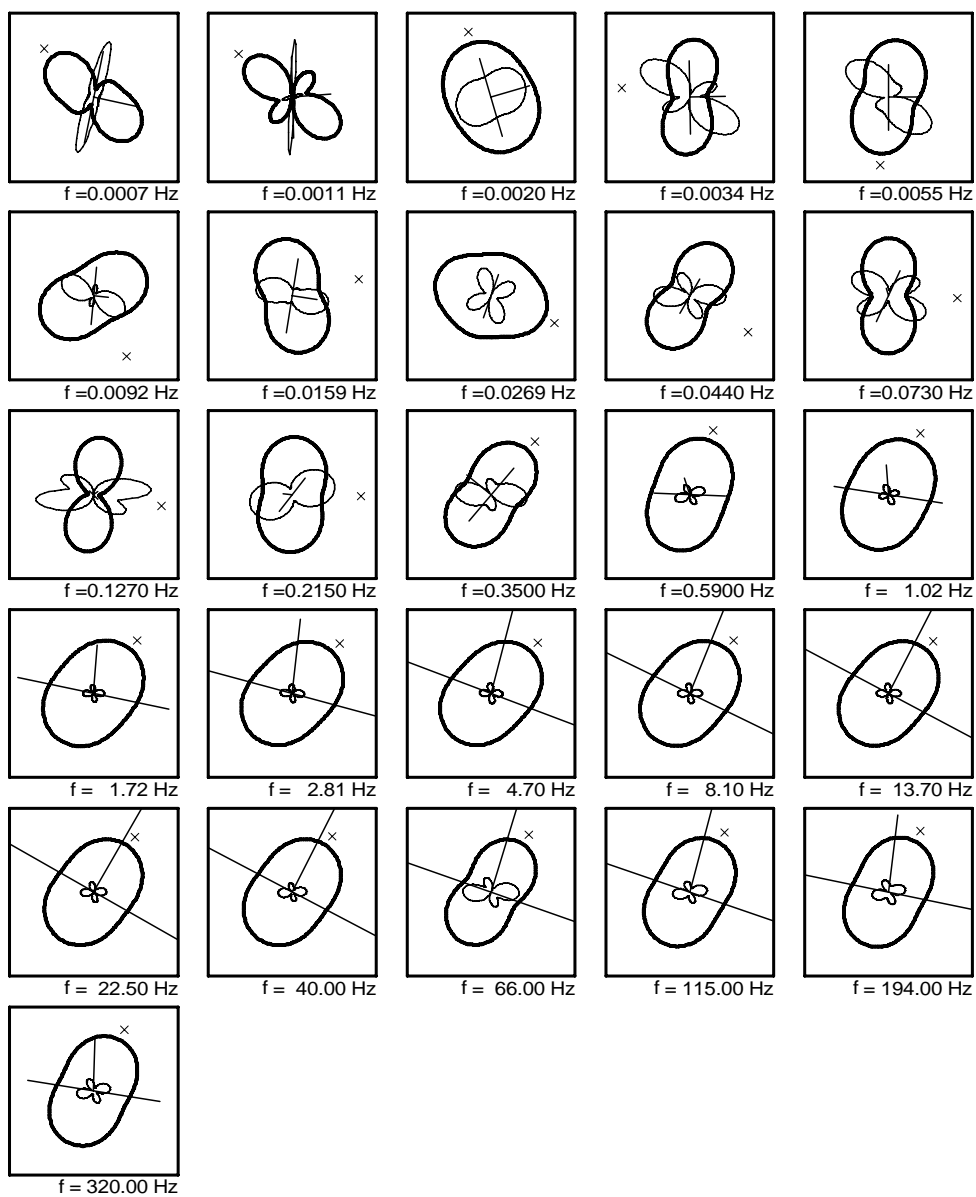
Sounding ML02



= Zxy Impedance
 = Zxx Impedance
 = Impedance Strike
 = Tipper Magnitude / Strike
 = Induction Arrow (to conductor)

USGS

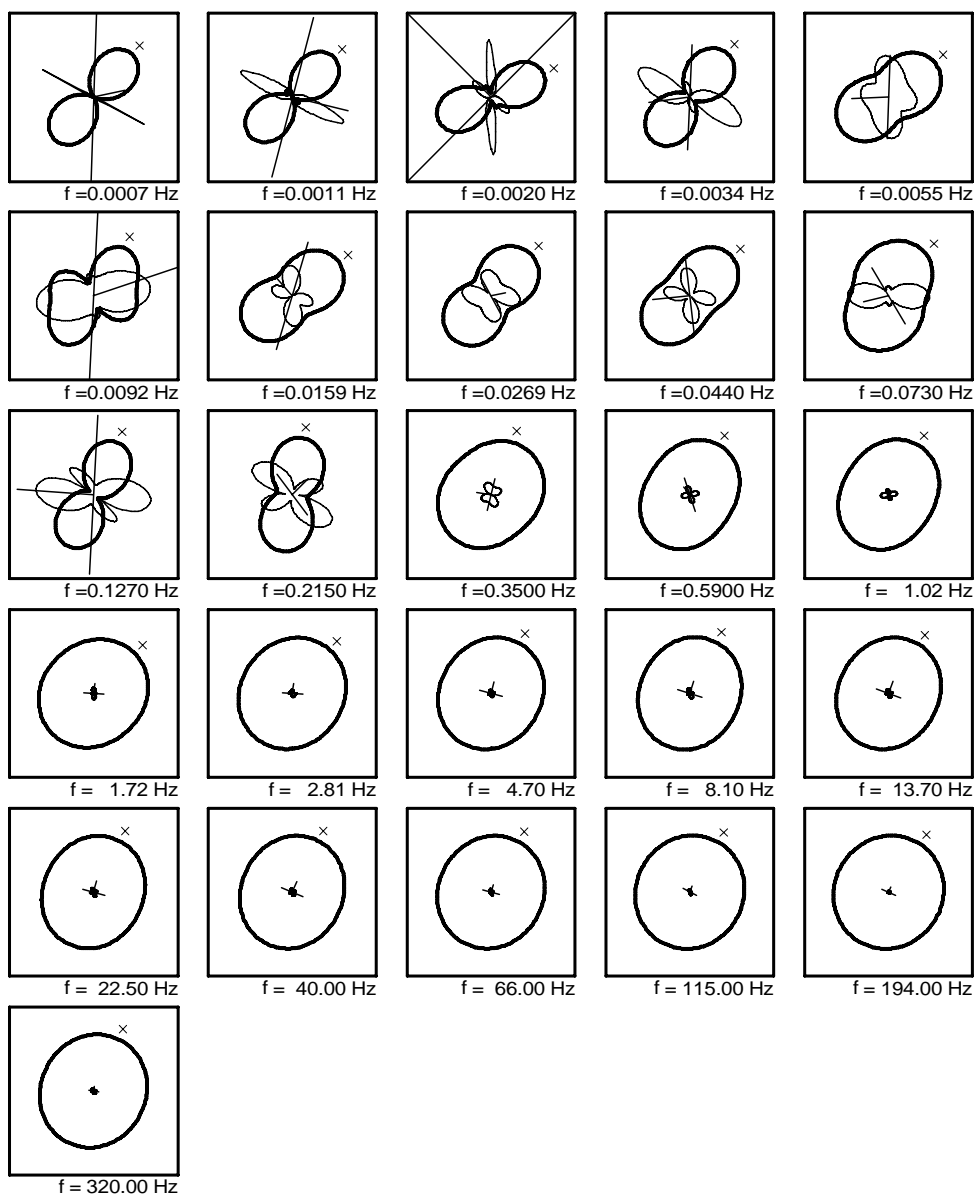
Sounding MM13


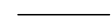





— = Zxy Impedance
 - - - = Zxx Impedance
 x = Impedance Strike
 — = Tipper Magnitude / Strike
 0 1
 — = Induction Arrow (to conductor)
 0 1

USGS

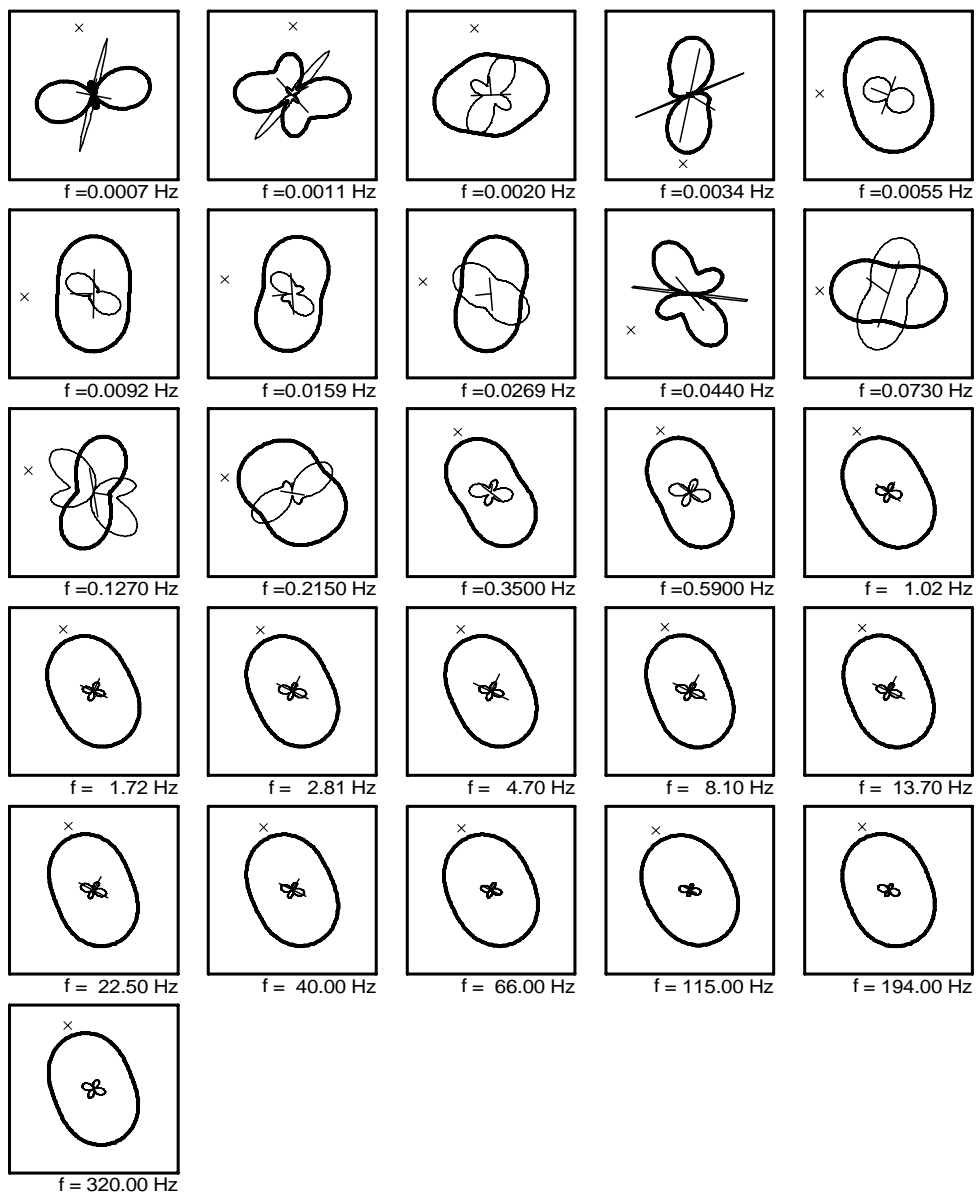
Sounding OR01



 = Z_{xy} Impedance
 = Z_{xx} Impedance
 = Impedance Strike
 = Tipper Magnitude / Strike
 = Induction Arrow (to conductor)

USGS

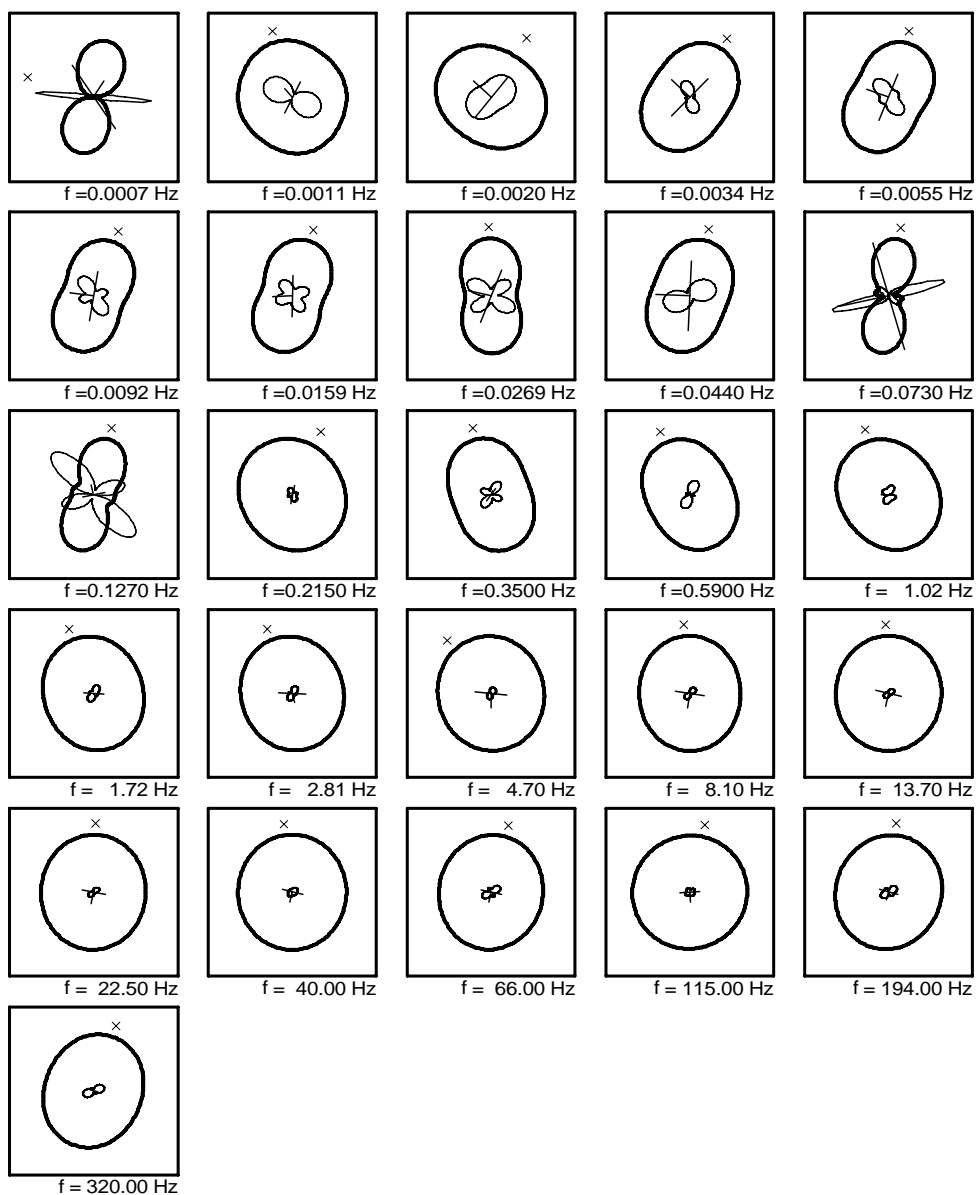
Sounding PK01



— = Zxy Impedance
 — = Zxx Impedance
 x = Impedance Strike
 — = Tipper Magnitude / Strike
 0 — 1
 — = Induction Arrow (to conductor)
 0 — 1

USGS

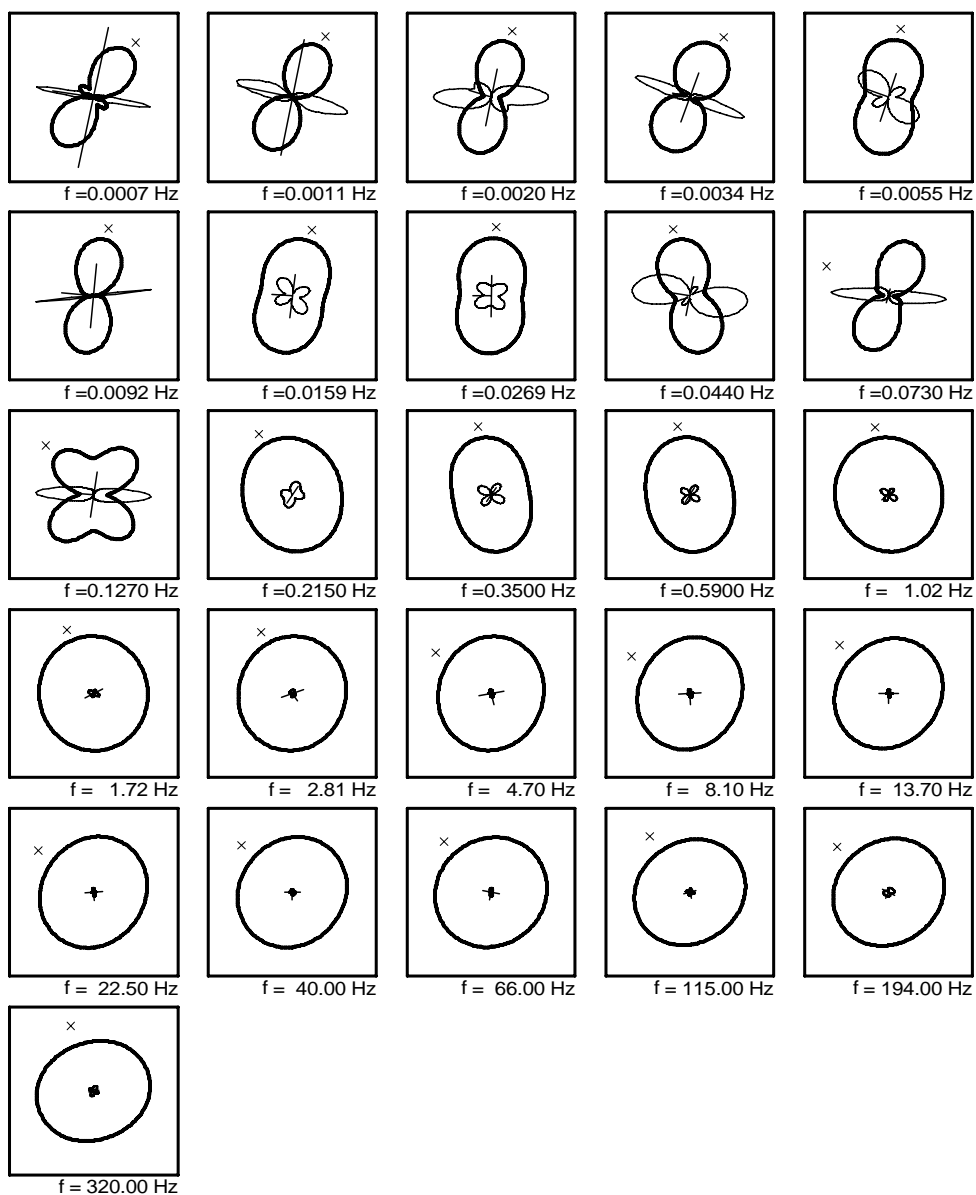
Sounding PK02



————— = Zxy Impedance
 ————— = Zxx Impedance
 × = Impedance Strike
 0 ————— 1 = Tipper Magnitude /Strike
 0 ————— 1 = Induction Arrow (to conductor)

USGS

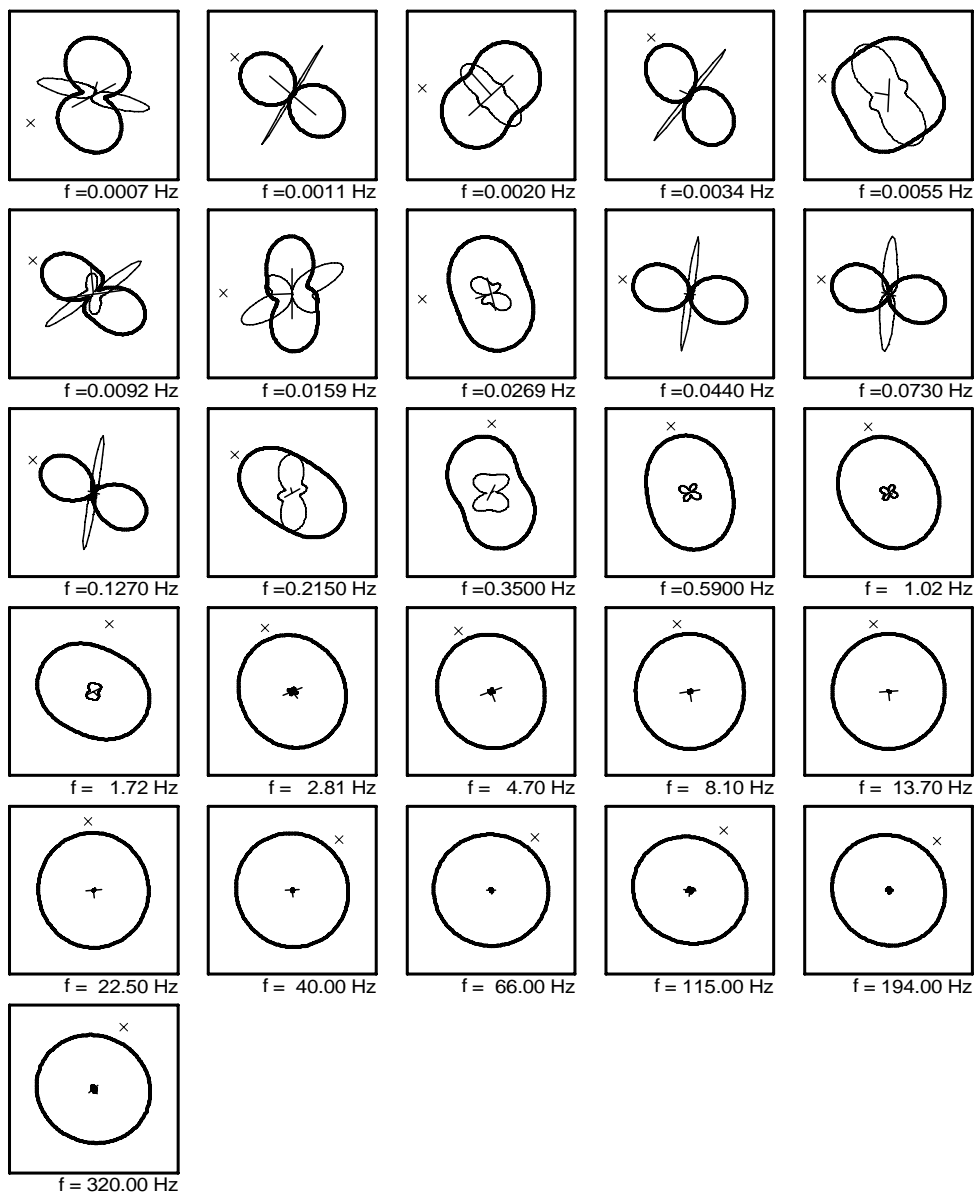
Sounding PK03



————— = Zxy Impedance
 ————— = Zxx Impedance
 × = Impedance Strike
 ————— = Tipper Magnitude / Strike
 0 1
 ————— = Induction Arrow (to conductor)
 0 1

USGS

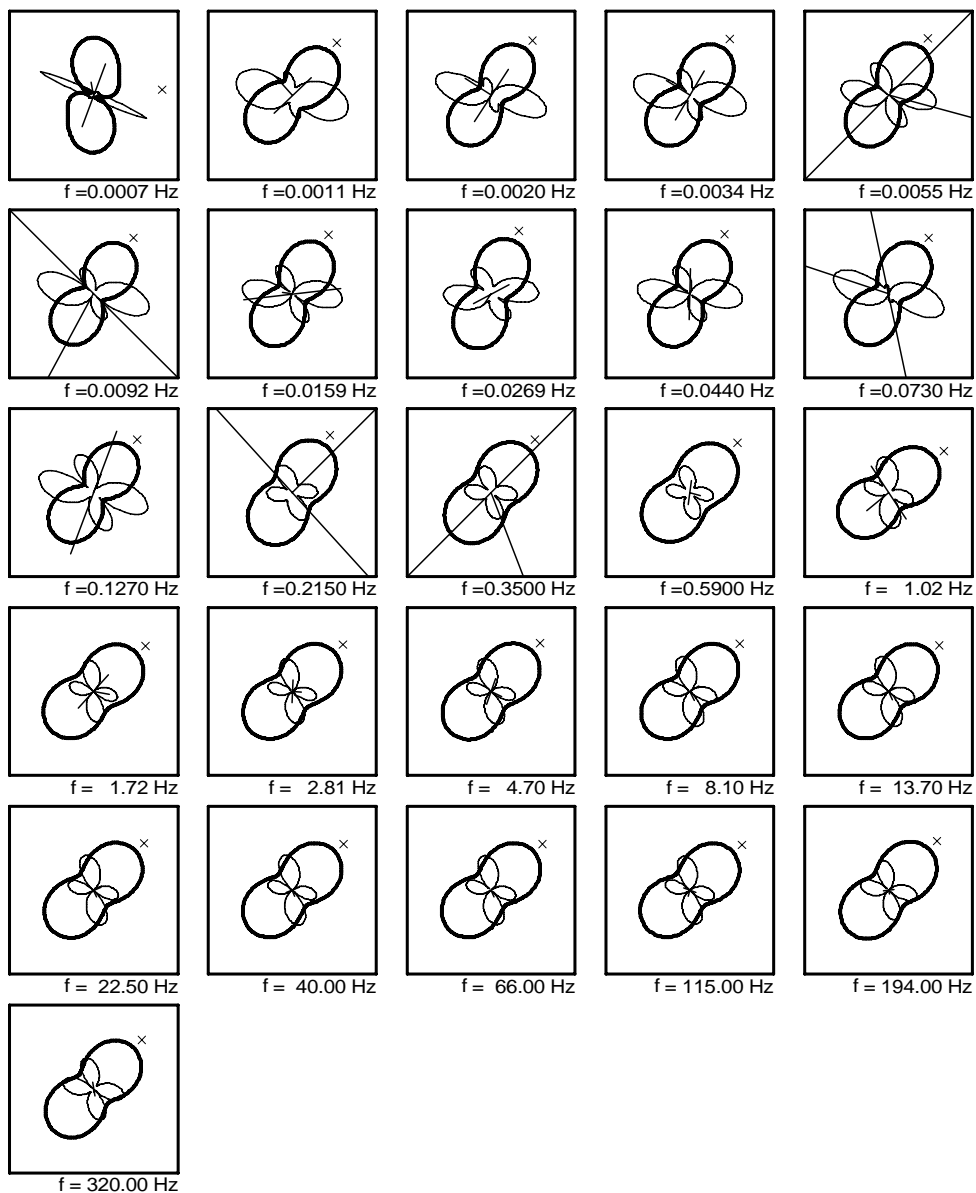
Sounding PK04

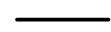
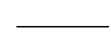


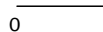


= Zxy Impedance
 = Zxx Impedance
 = Impedance Strike
 = Tipper Magnitude / Strike
 = Induction Arrow (to conductor)

USGS

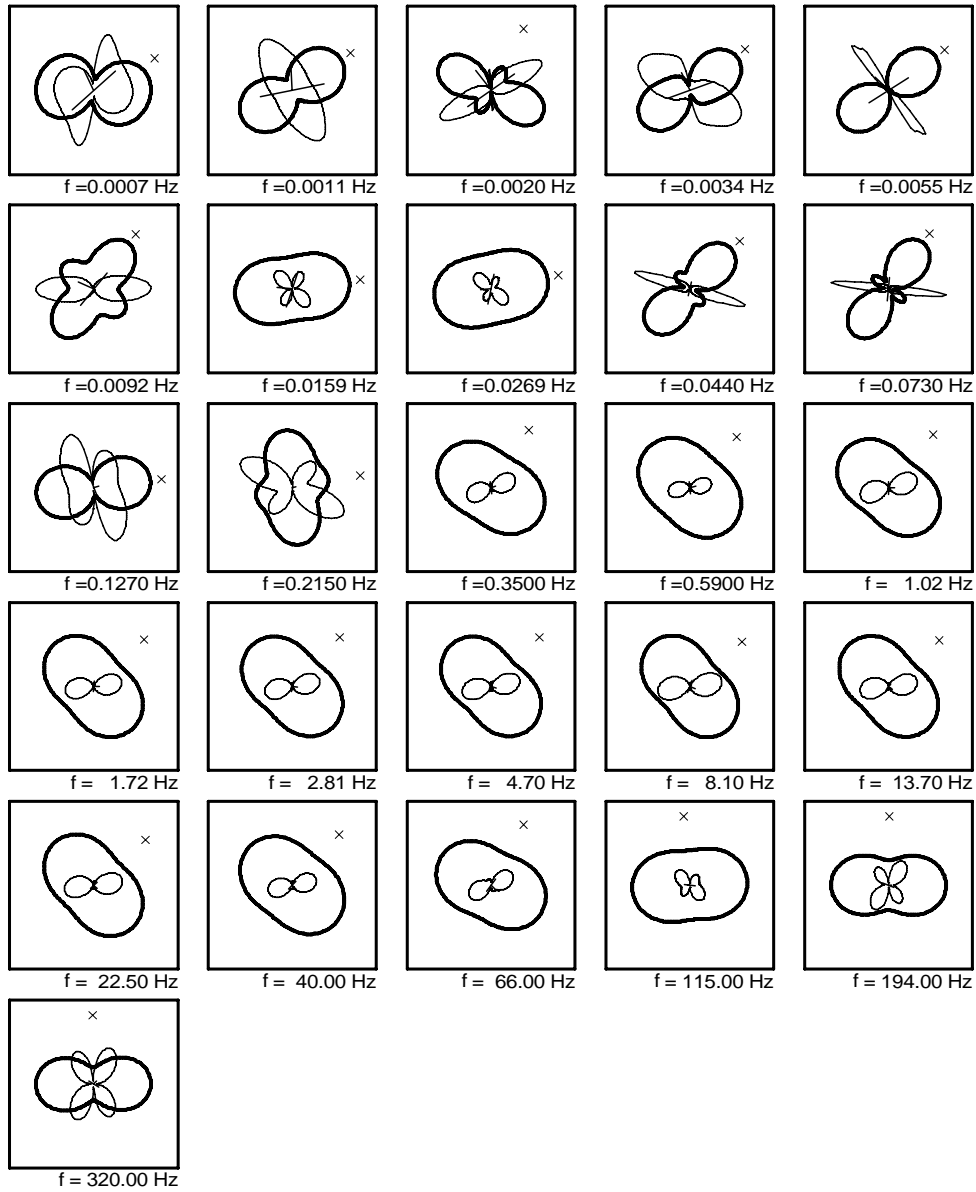
Sounding PK05



 = Zxy Impedance
 = Zxx Impedance
 = Impedance Strike
 = Tipper Magnitude / Strike
 = Induction Arrow (to conductor)

USGS

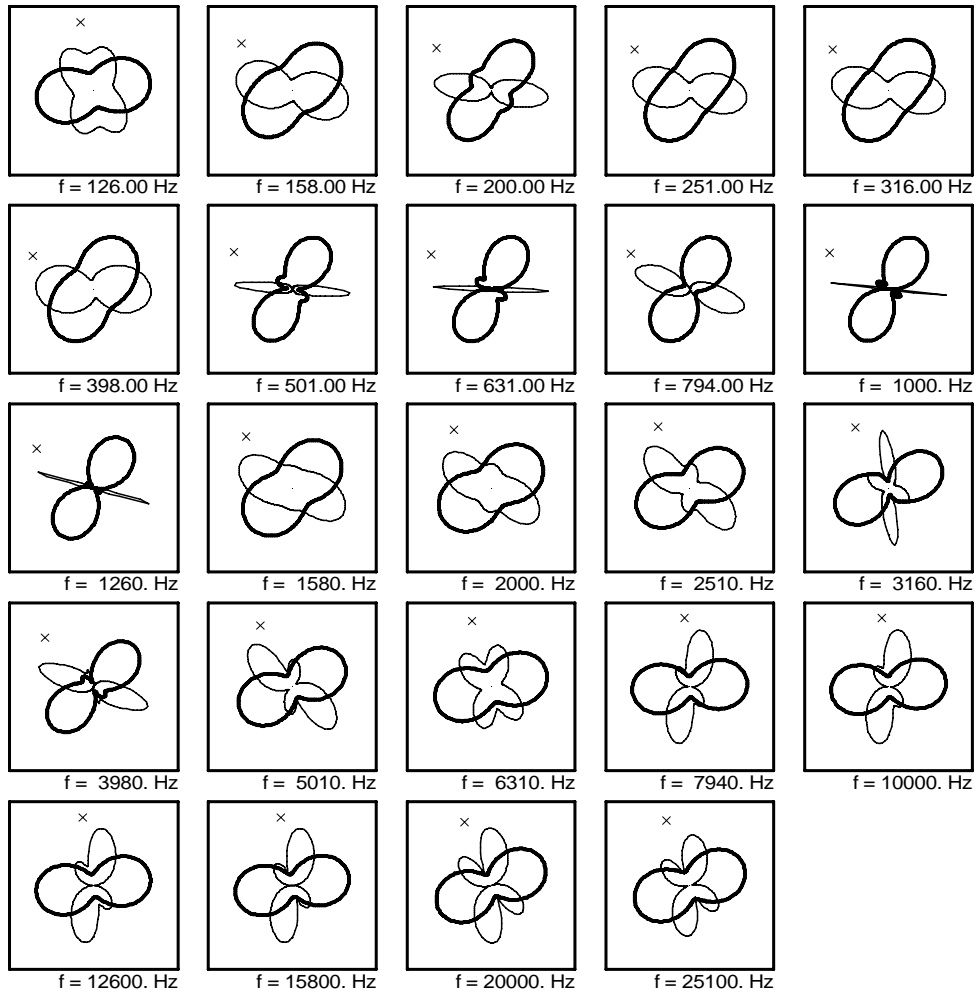
Sounding REF1



— = Zxy Impedance
 — = Zxx Impedance
 x = Impedance Strike
 — = Tipper Magnitude / Strike
 0 — 1
 — = Induction Arrow (to conductor)
 0 — 1

USGS

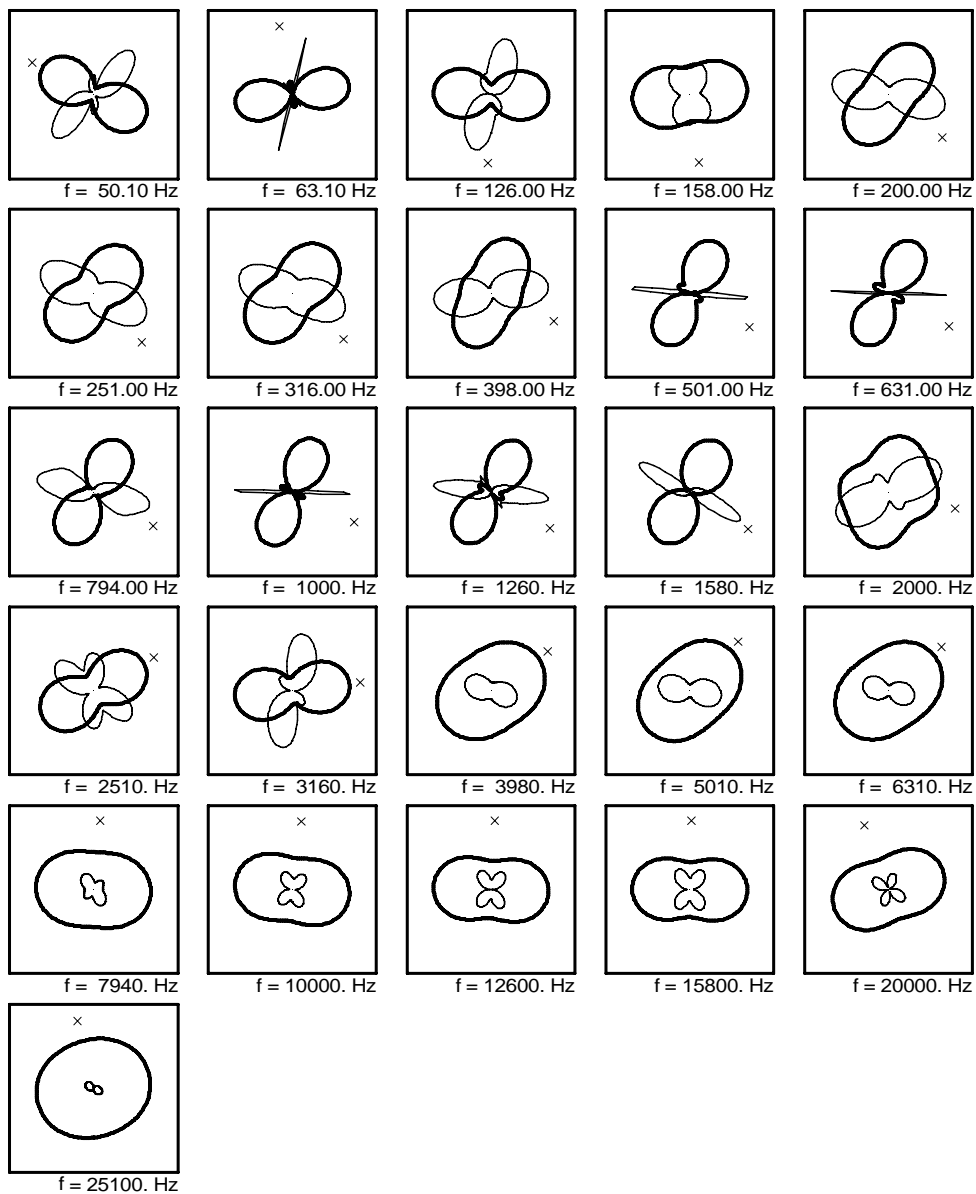
Sounding SR005



— = Zxy Impedance
 — = Zxx Impedance
 x = Impedance Strike

USGS

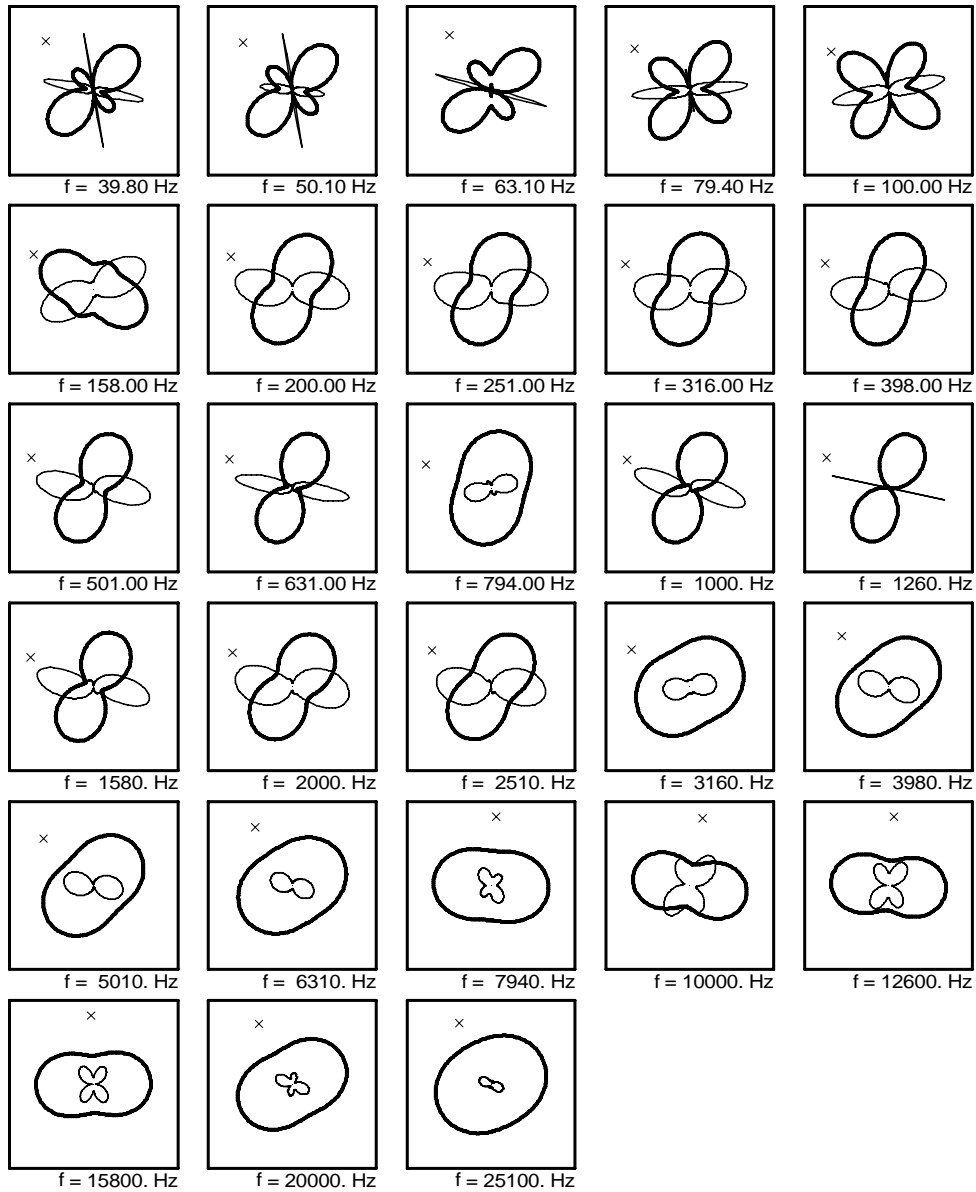
Sounding SR006



— = Zxy Impedance
 - - - = Zxx Impedance
 x = Impedance Strike

USGS

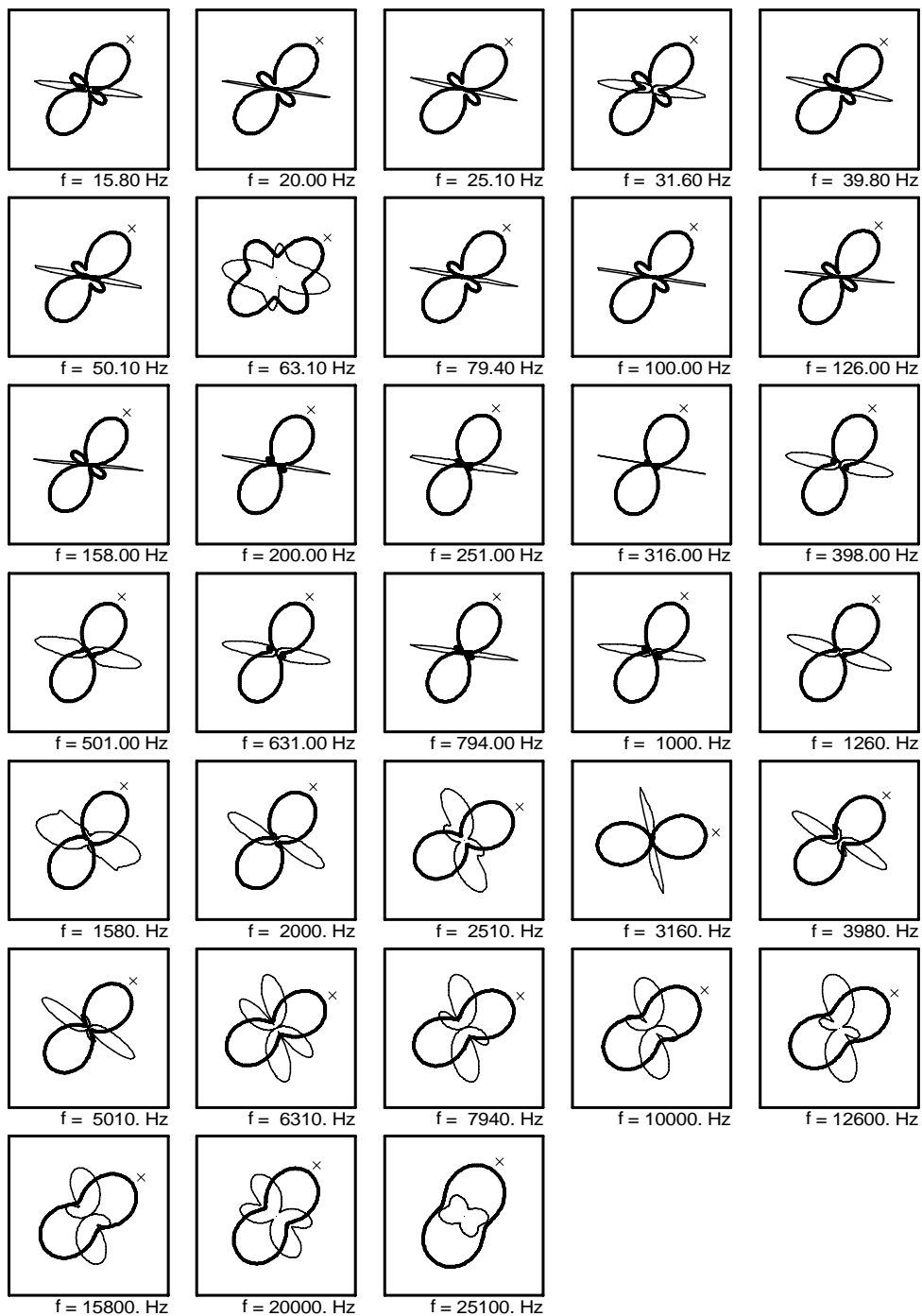
Sounding SR007



— = Zxy Impedance
 — = Zxx Impedance
 x = Impedance Strike

USGS

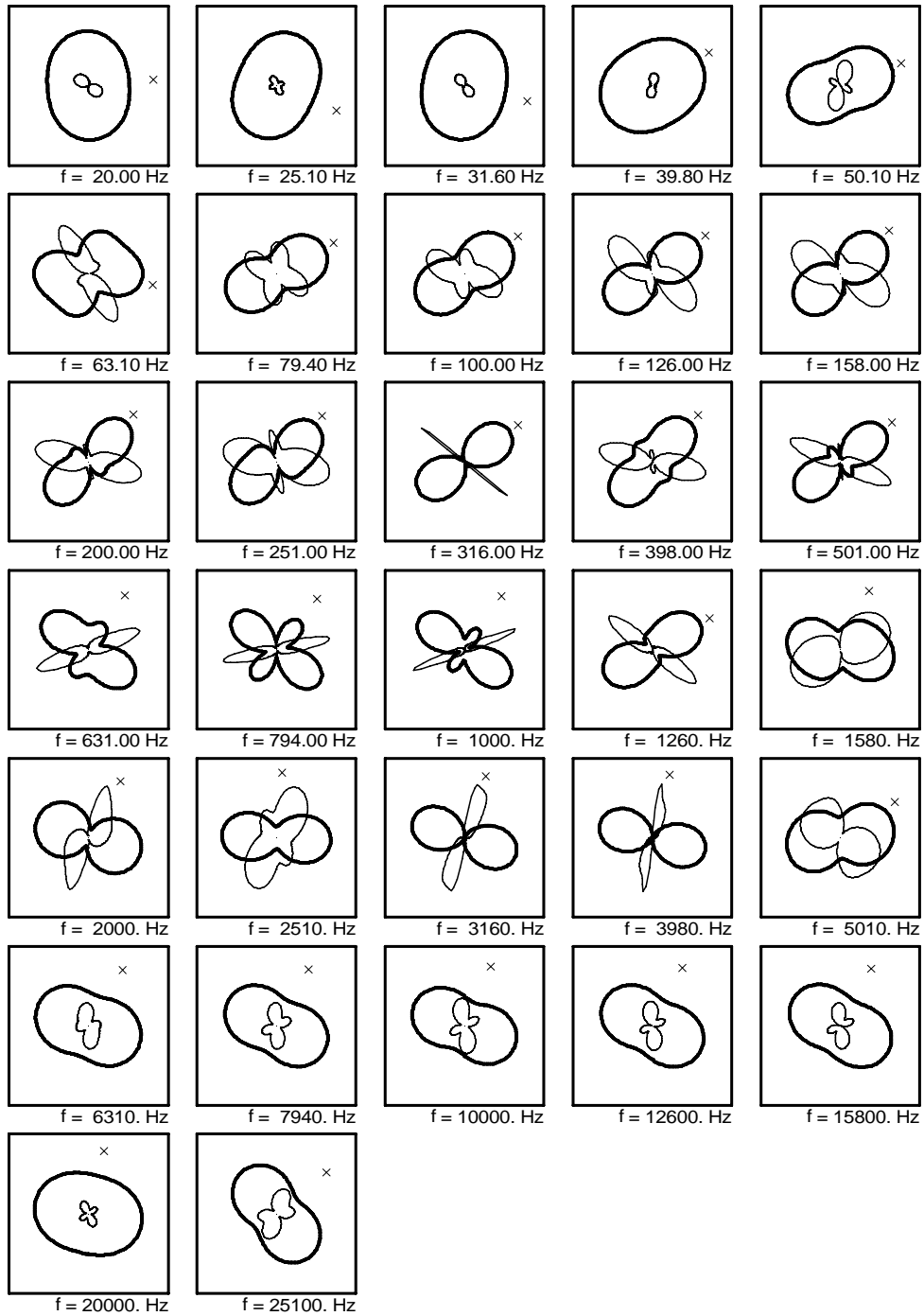
Sounding SR008



— = Zxy Impedance
 - - = Zxx Impedance
 x = Impedance Strike

USGS

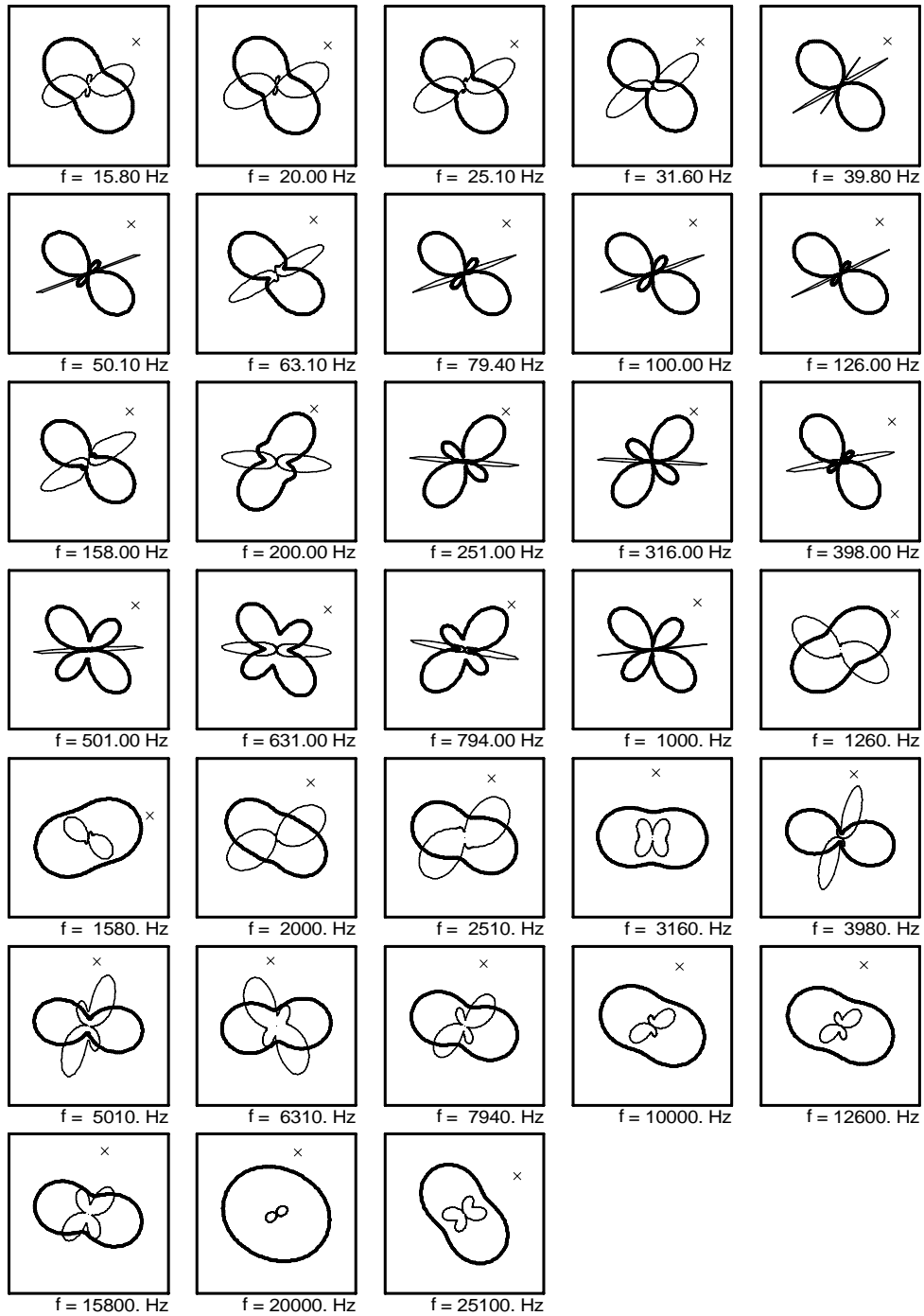
Sounding SR009



— = Zxy Impedance
 — = Zxx Impedance
 x = Impedance Strike

USGS

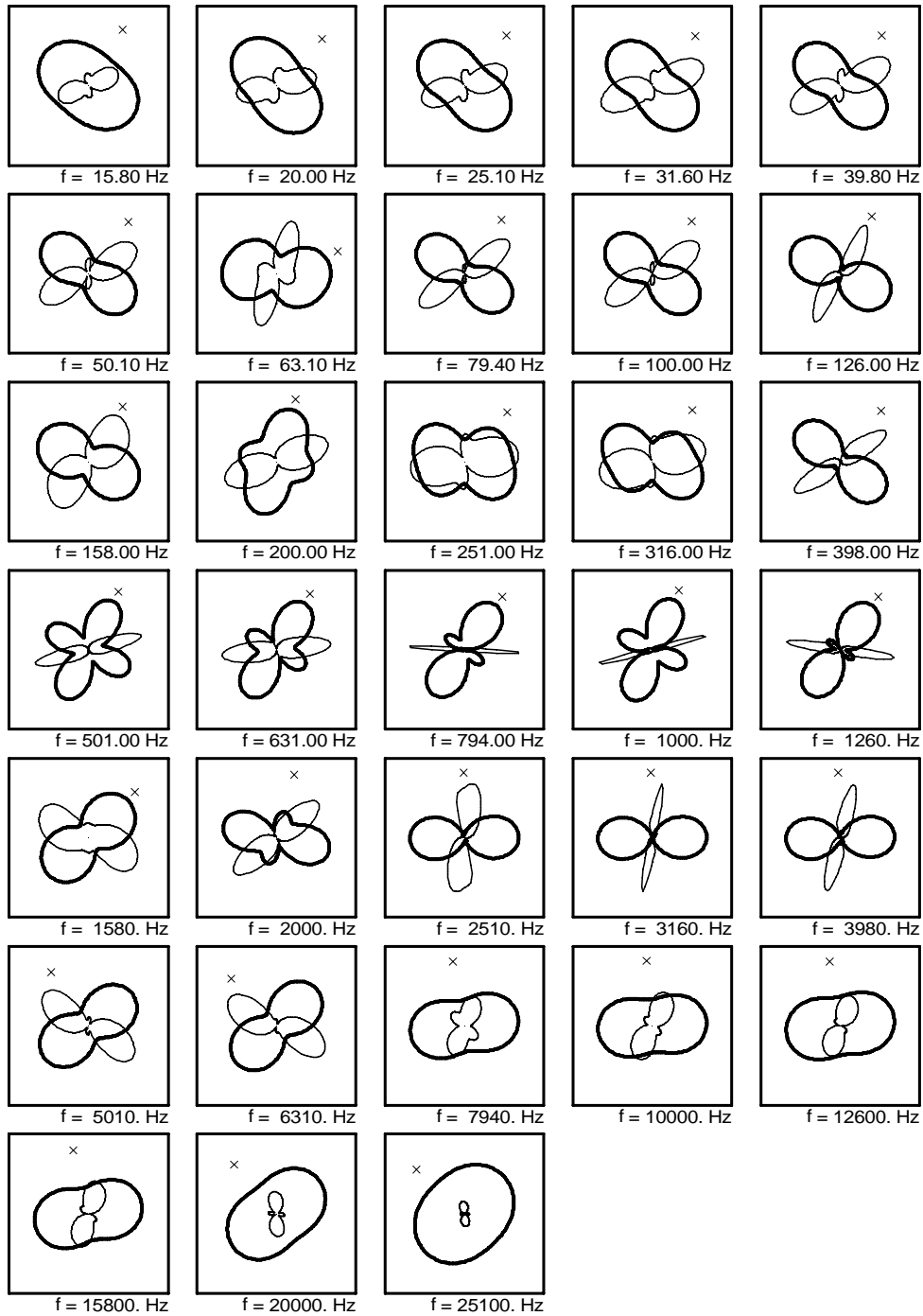
Sounding SR010



— = Zxy Impedance
 — = Zxx Impedance
 x = Impedance Strike

USGS

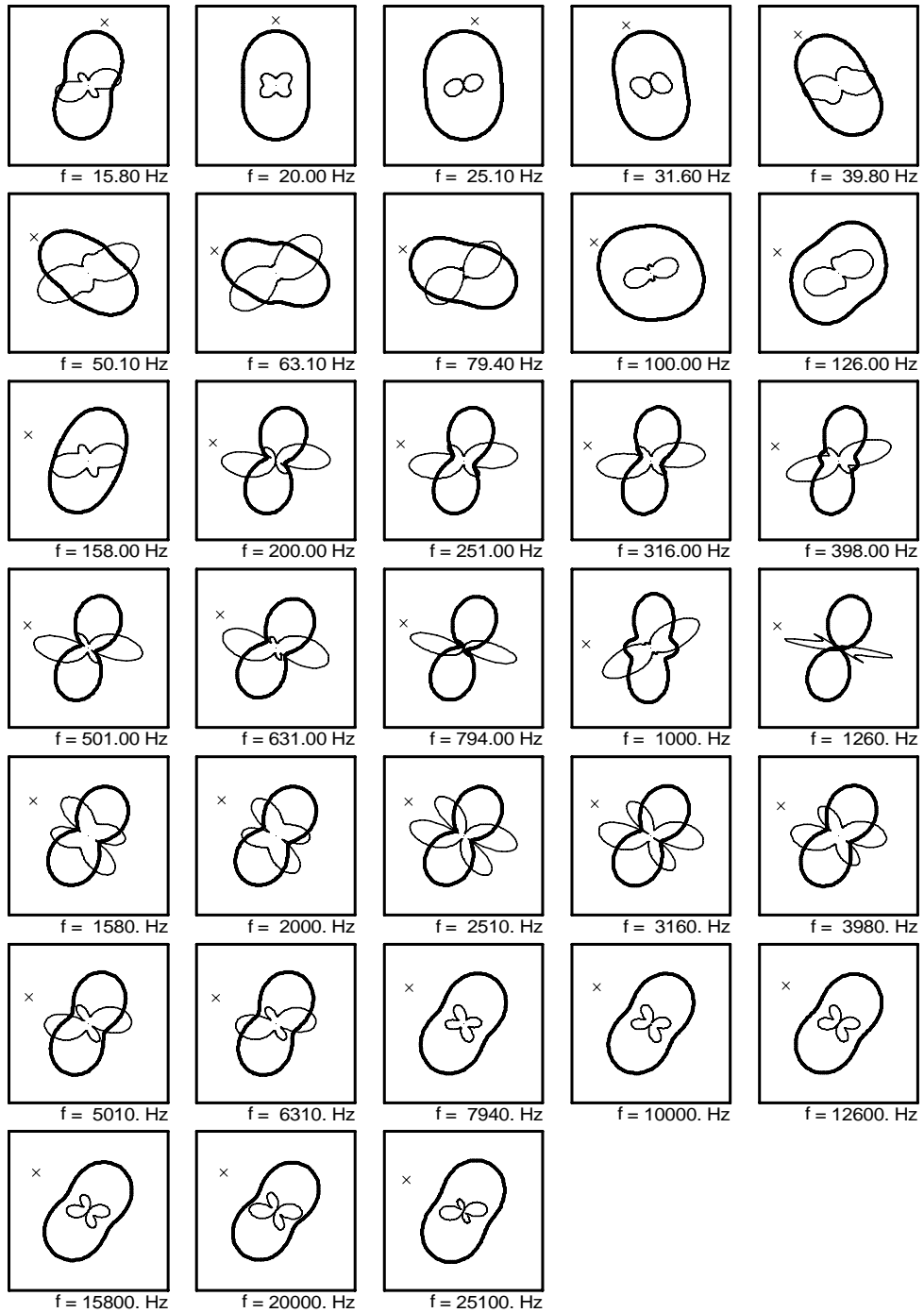
Sounding SR011



— = Zxy Impedance
 — = Zxx Impedance
 x = Impedance Strike

USGS

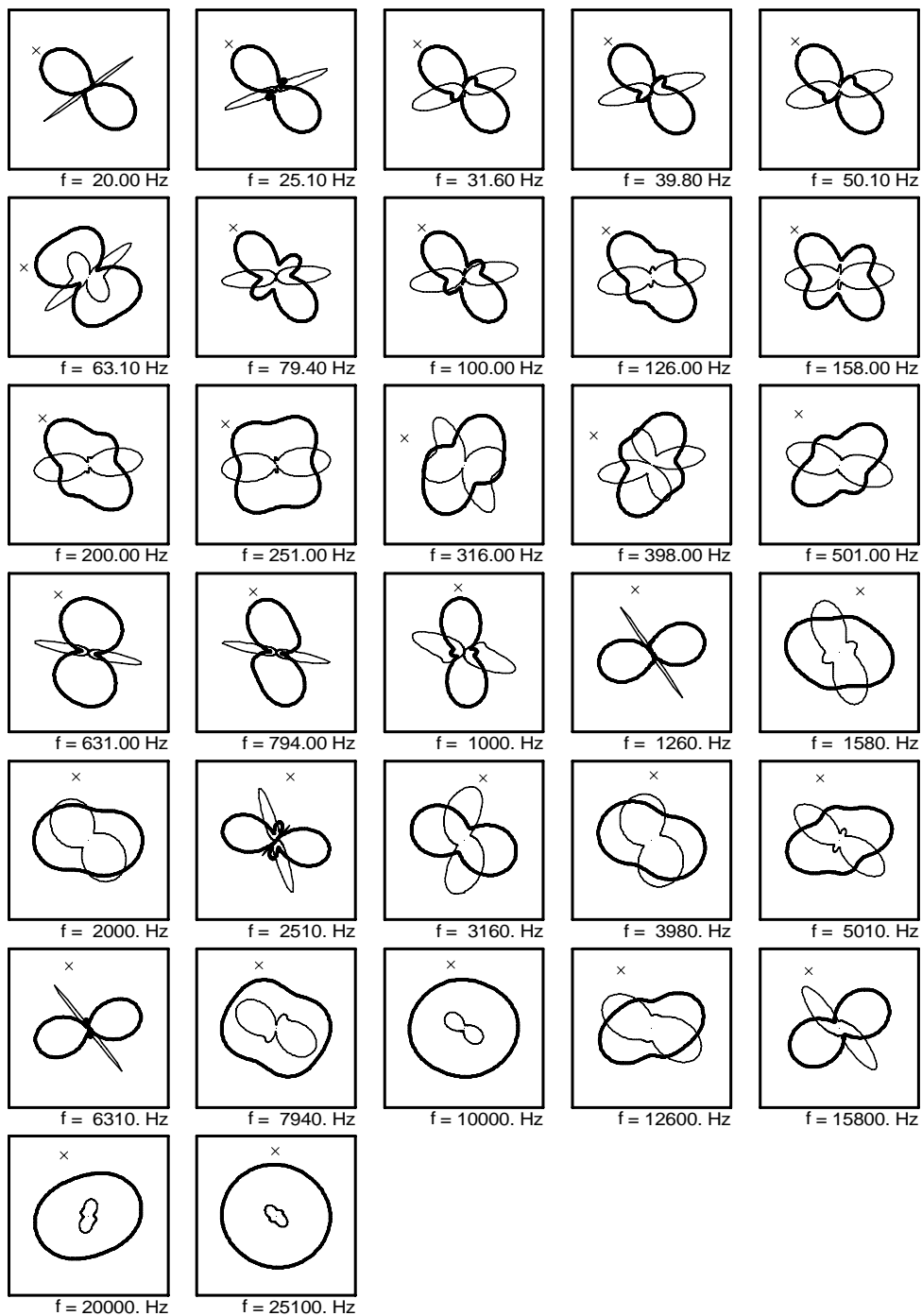
Sounding SR012



— = Zxy Impedance
 — = Zxx Impedance
 x = Impedance Strike

USGS

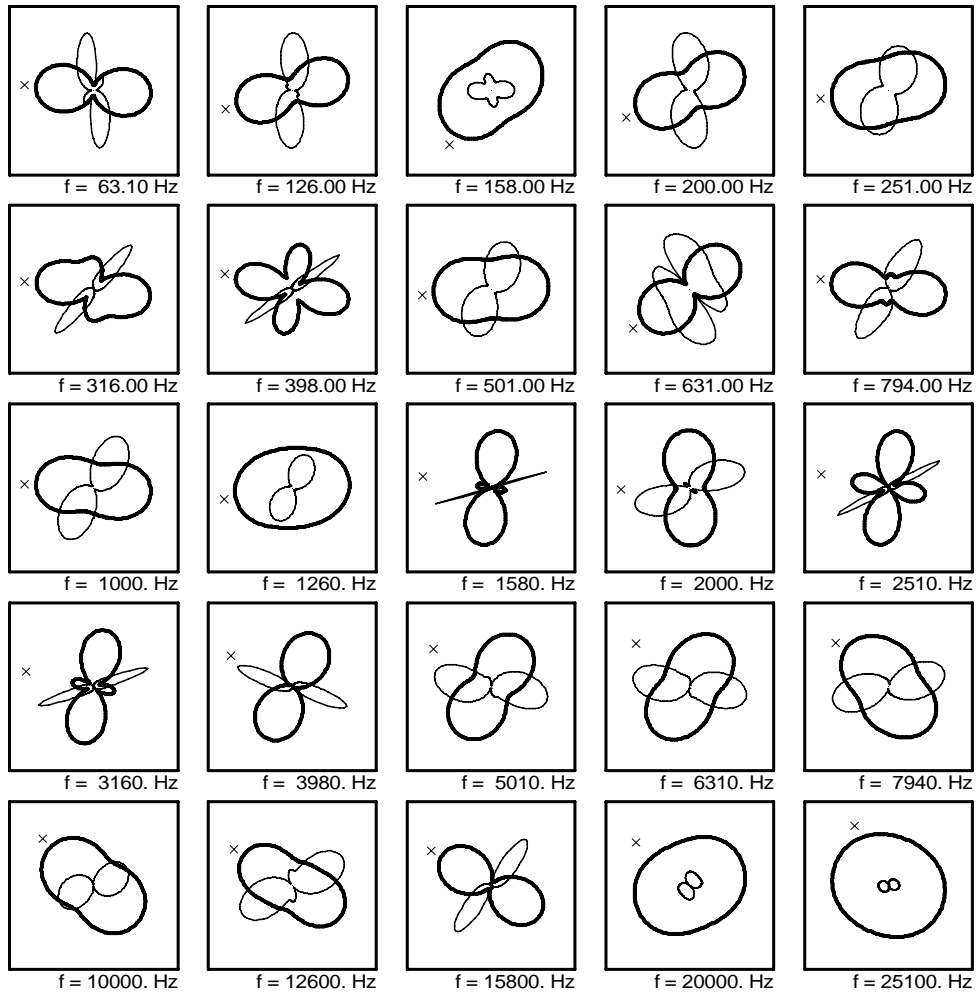
Sounding SR013



— = Zxy Impedance
 - - - = Zxx Impedance
 x = Impedance Strike

USGS

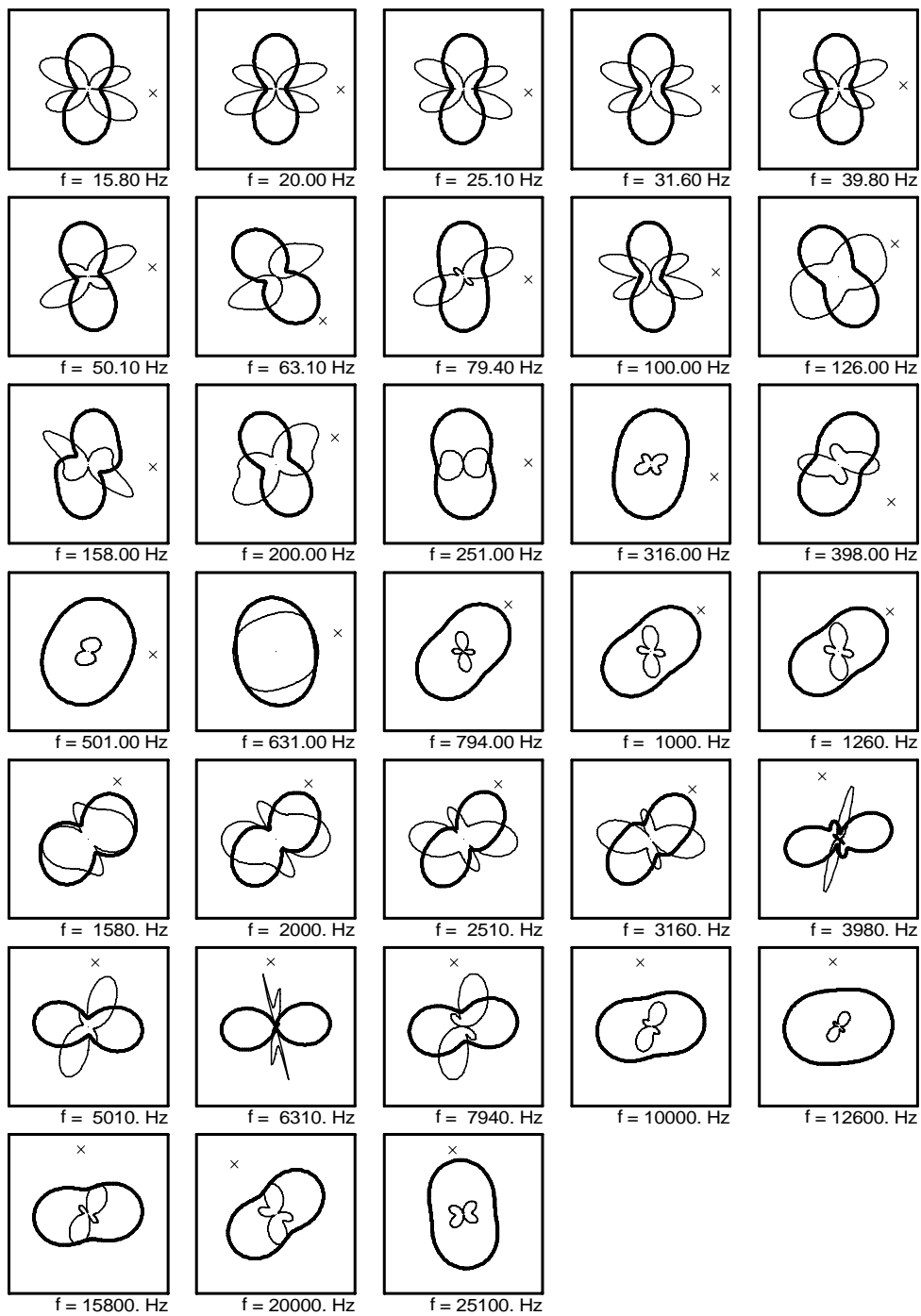
Sounding SR014



— = Zxy Impedance
 — = Zxx Impedance
 x = Impedance Strike

USGS

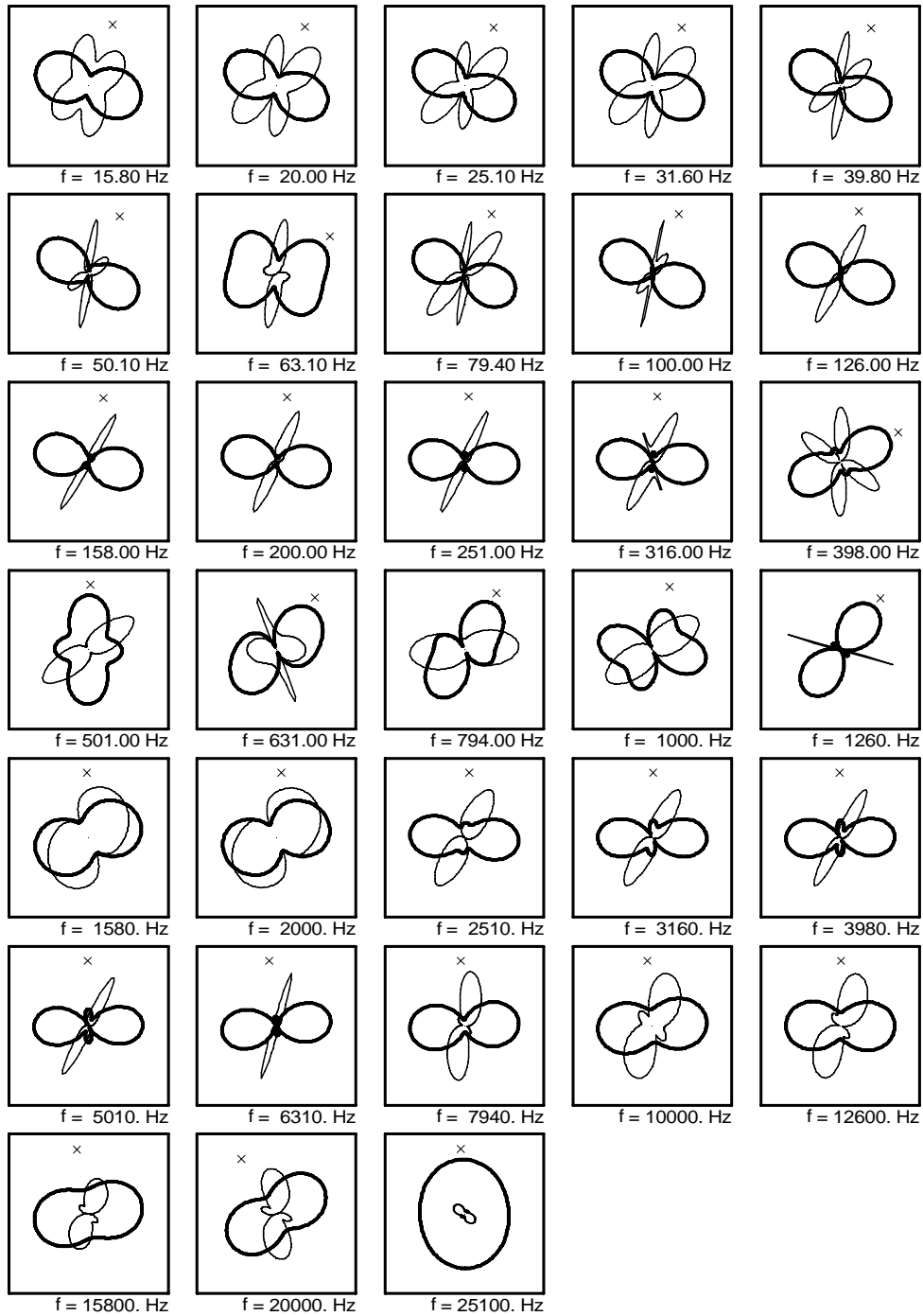
Sounding SR015



— = Zxy Impedance
 - - - = Zxx Impedance
 x = Impedance Strike

USGS

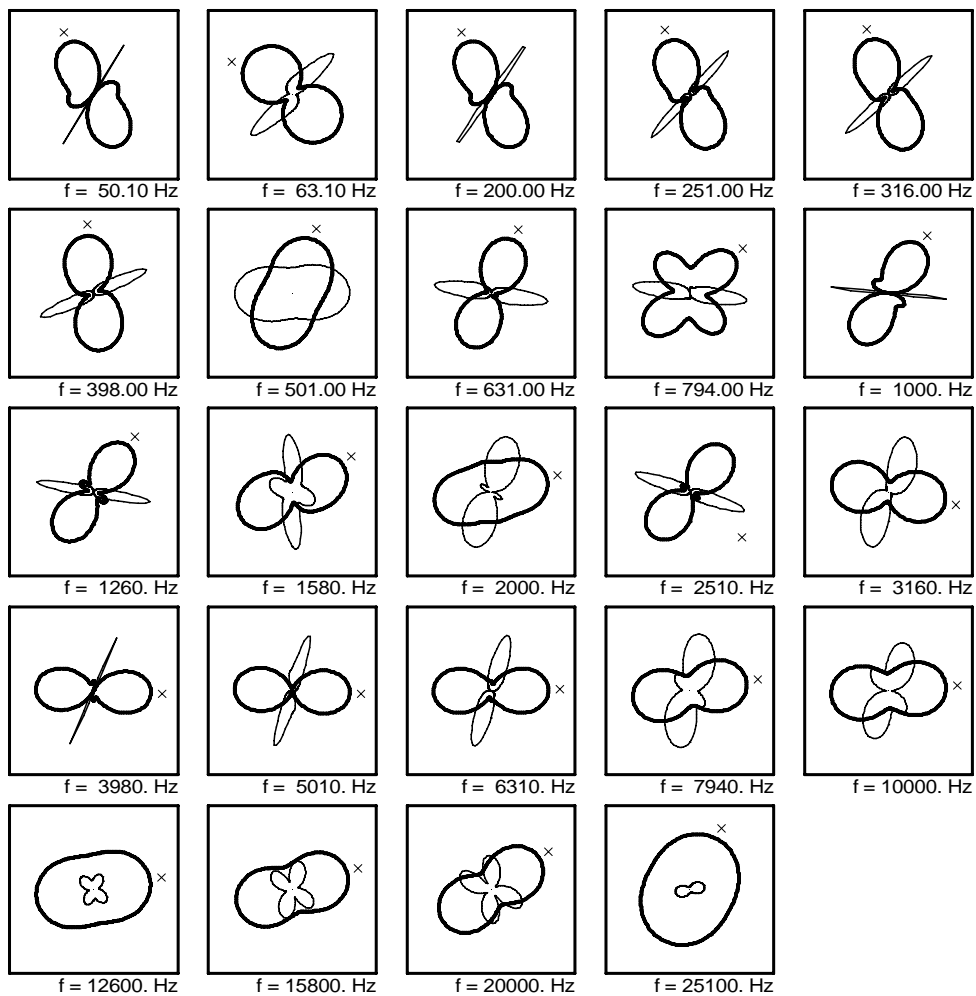
Sounding SR016



— = Zxy Impedance
 — = Zxx Impedance
 x = Impedance Strike

USGS

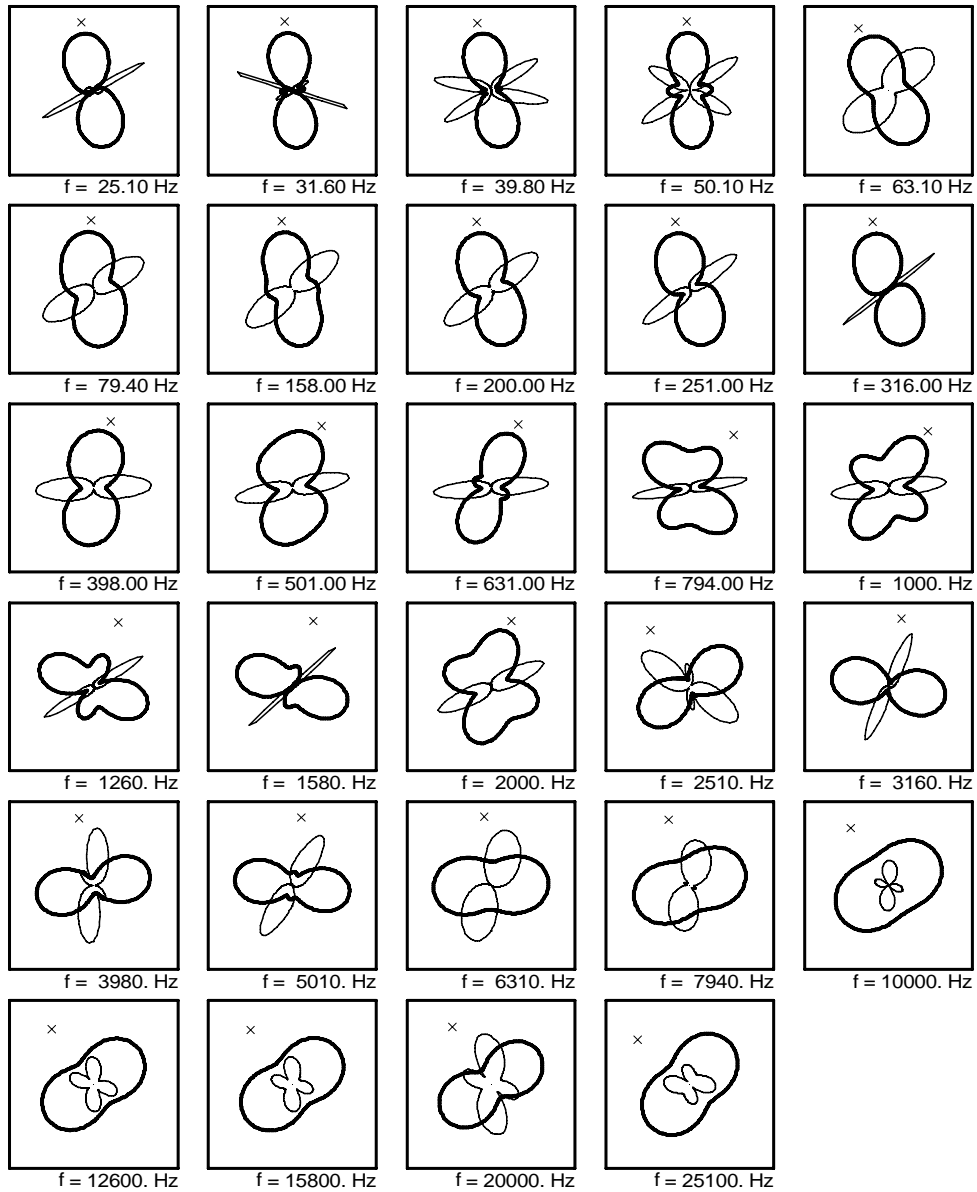
Sounding SR017



= Zxy Impedance
 = Zxx Impedance
 = Impedance Strike

USGS

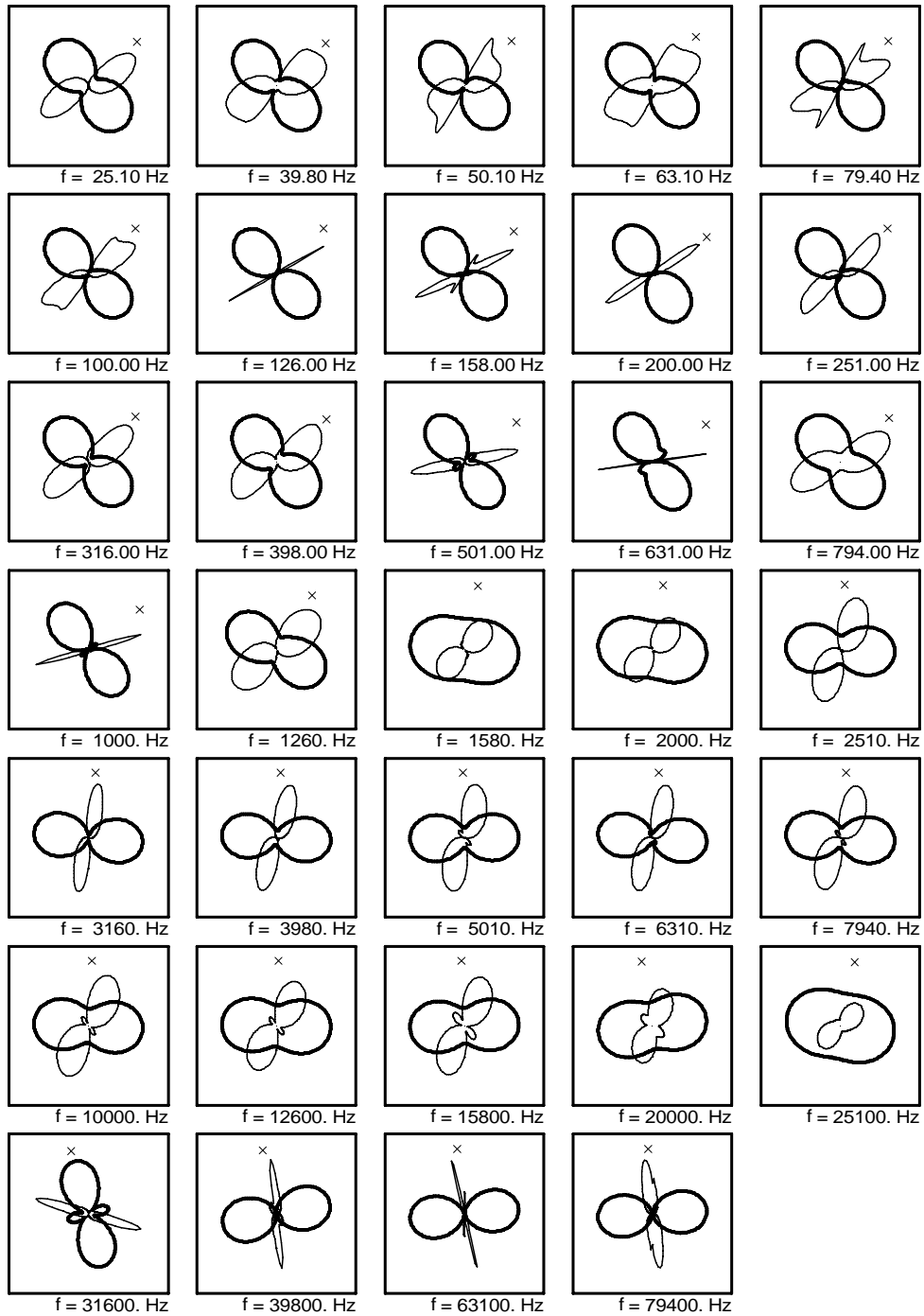
Sounding SR018



— = Zxy Impedance
 — = Zxx Impedance
 x = Impedance Strike

USGS

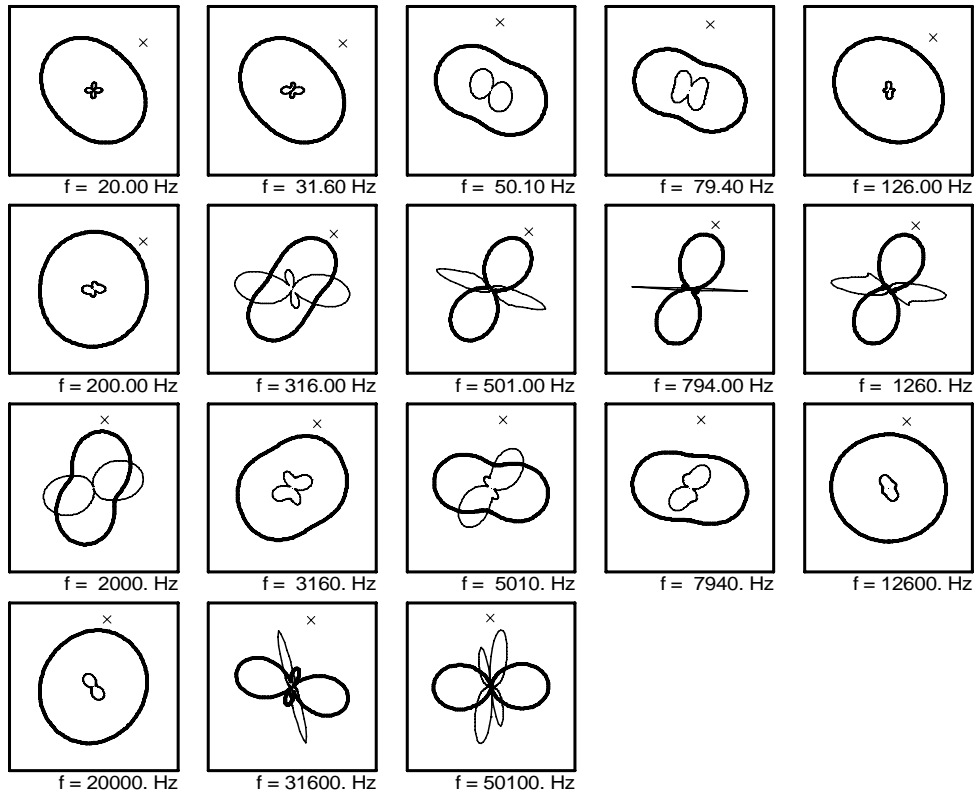
Sounding SR019



= Zxy Impedance
 = Zxx Impedance
 = Impedance Strike

USGS

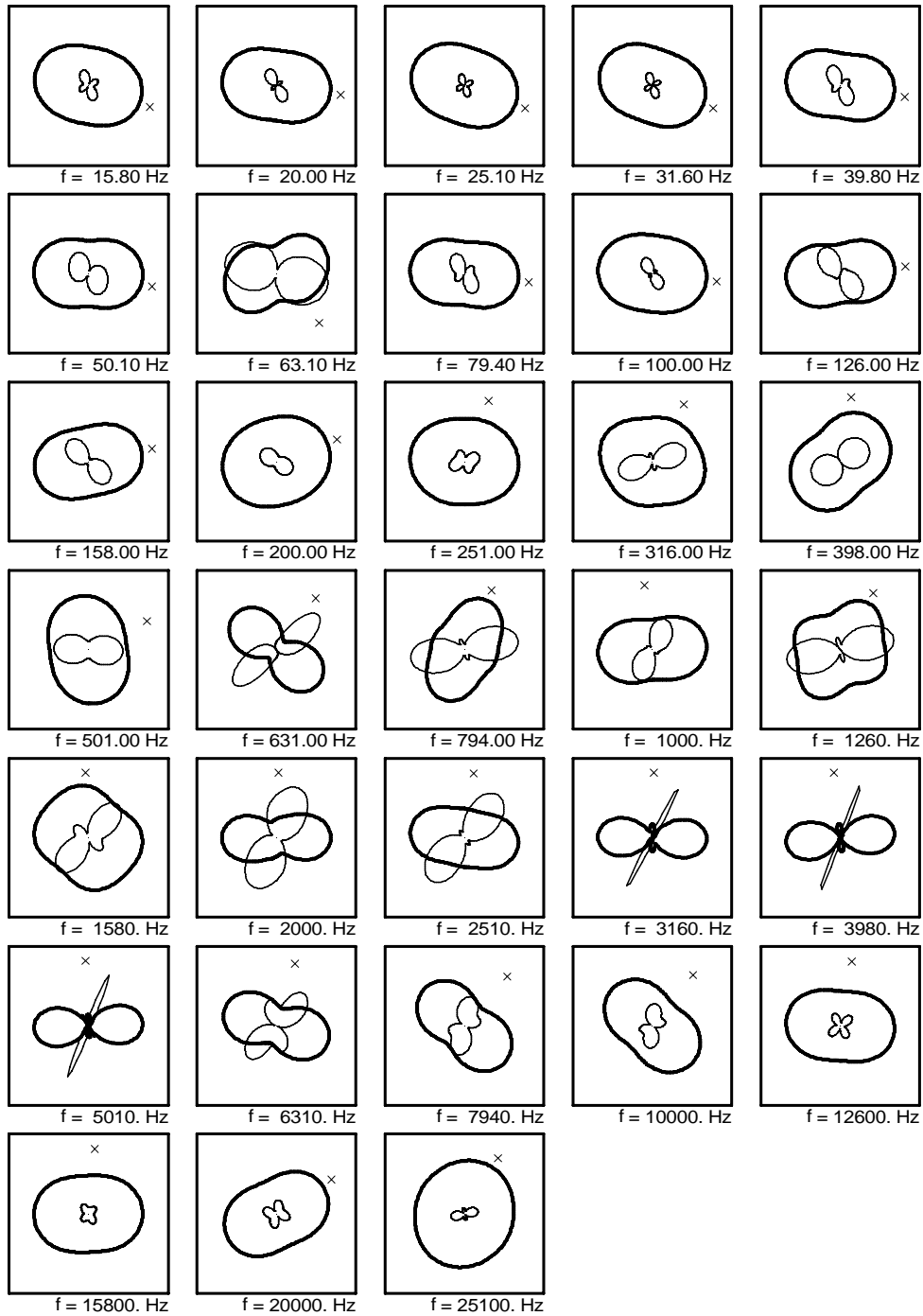
Sounding SR020



= Zxy Impedance
 = Zxx Impedance
 = Impedance Strike

USGS

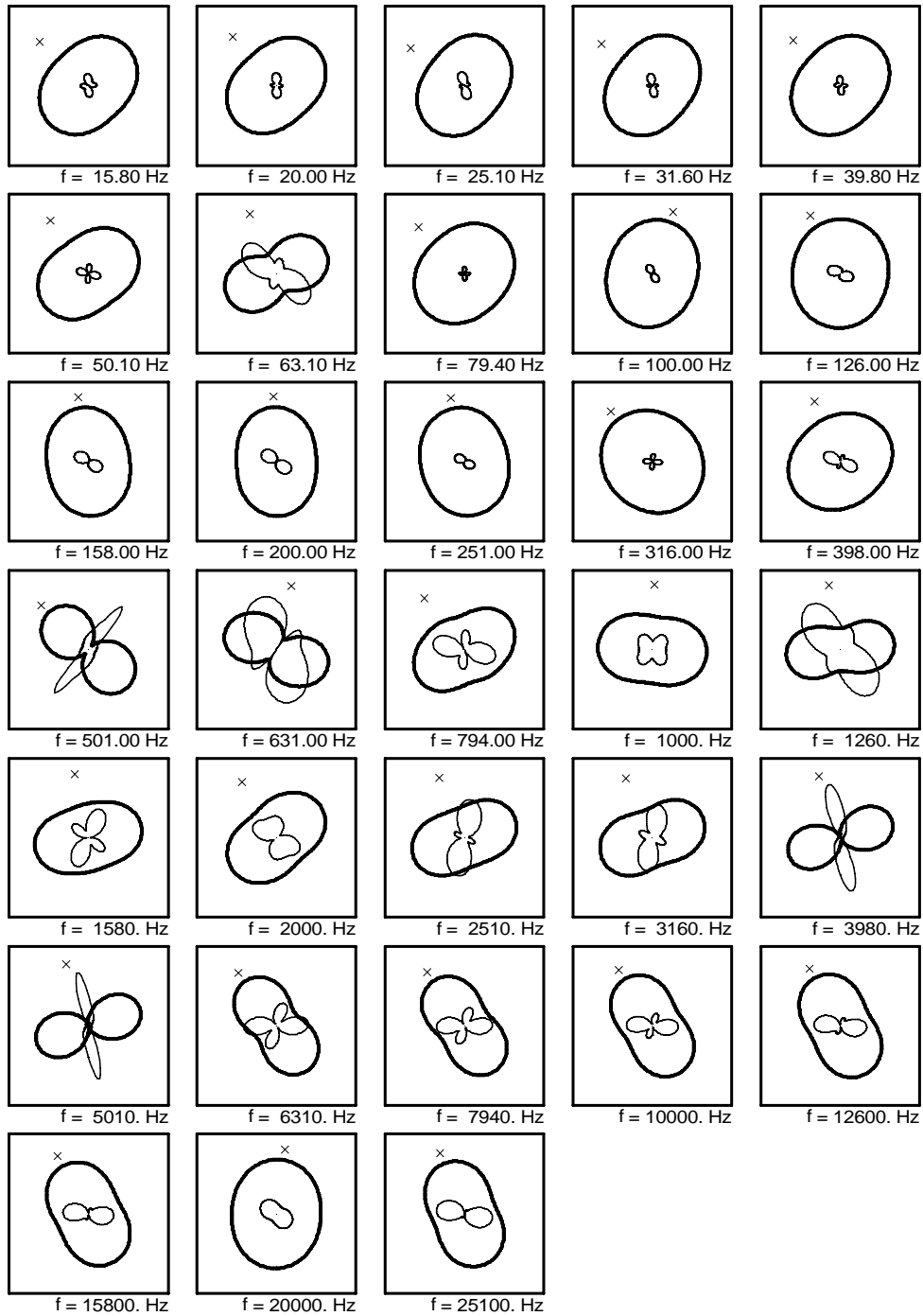
Sounding SR021



— = Zxy Impedance
 - - - = Zxx Impedance
 x = Impedance Strike

USGS

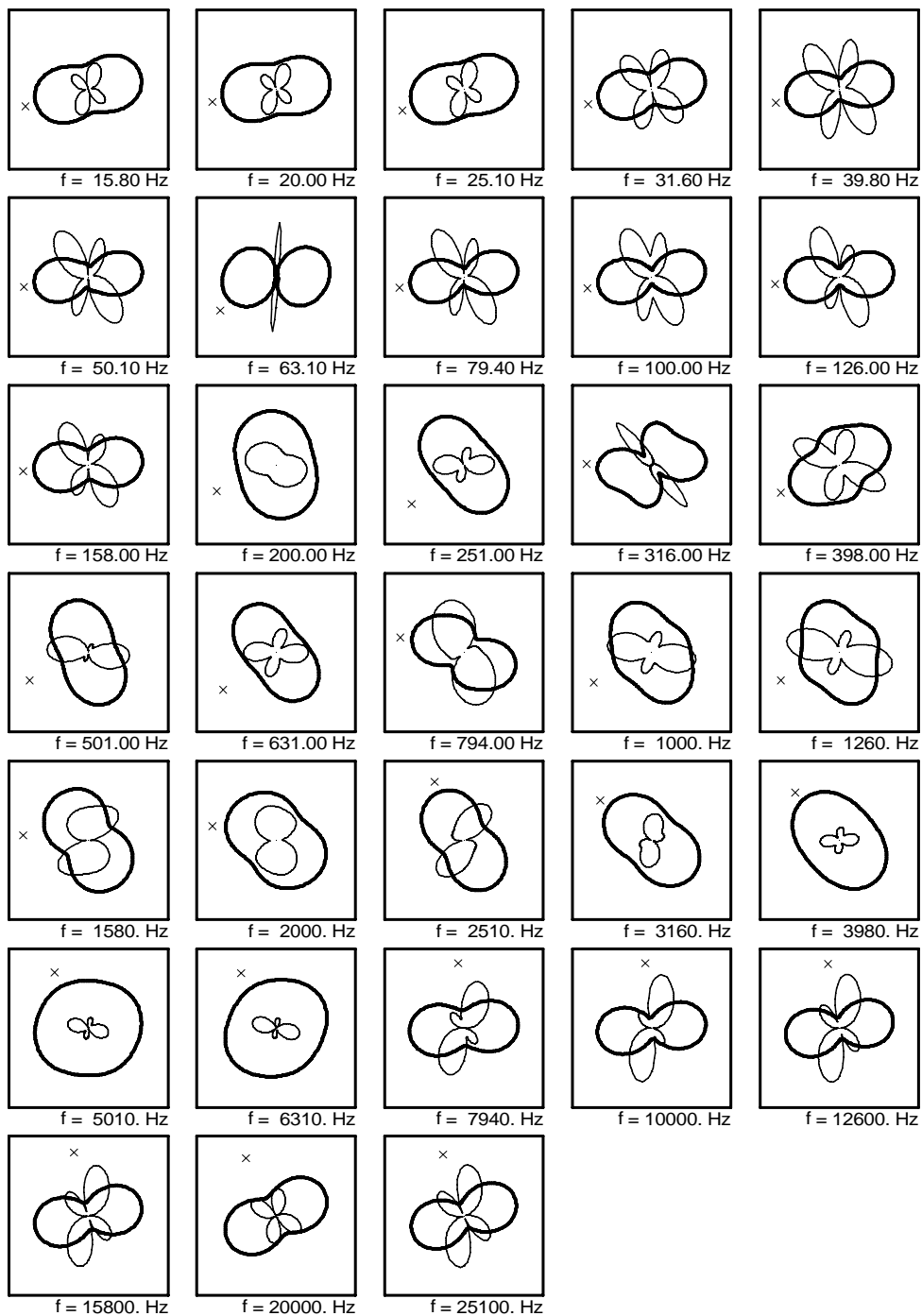
Sounding SR022



— = Z_{xy} Impedance
 - - - = Z_{xx} Impedance
 x = Impedance Strike

USGS

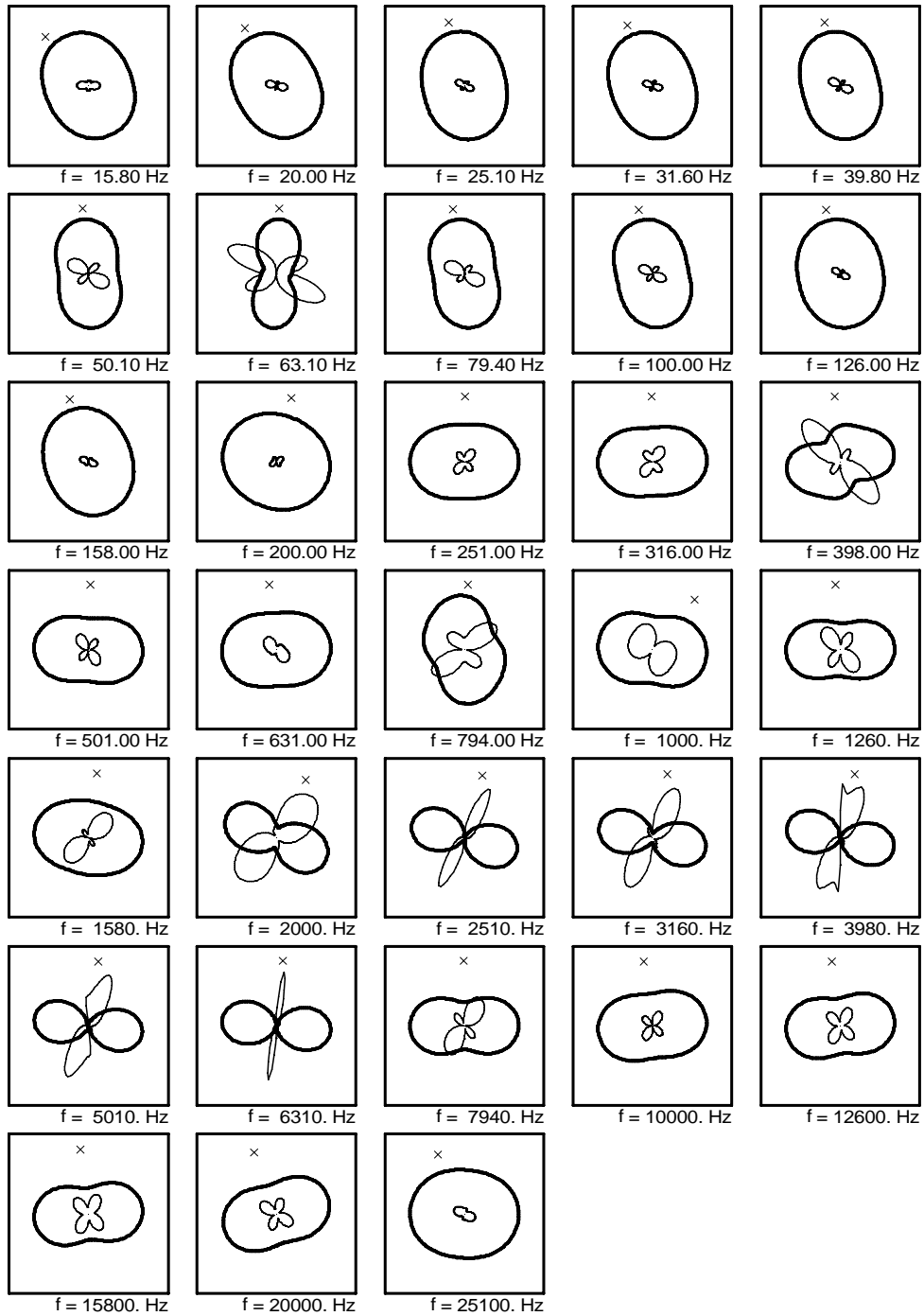
Sounding SR023



— = Zxy Impedance
 - - - = Zxx Impedance
 x = Impedance Strike

USGS

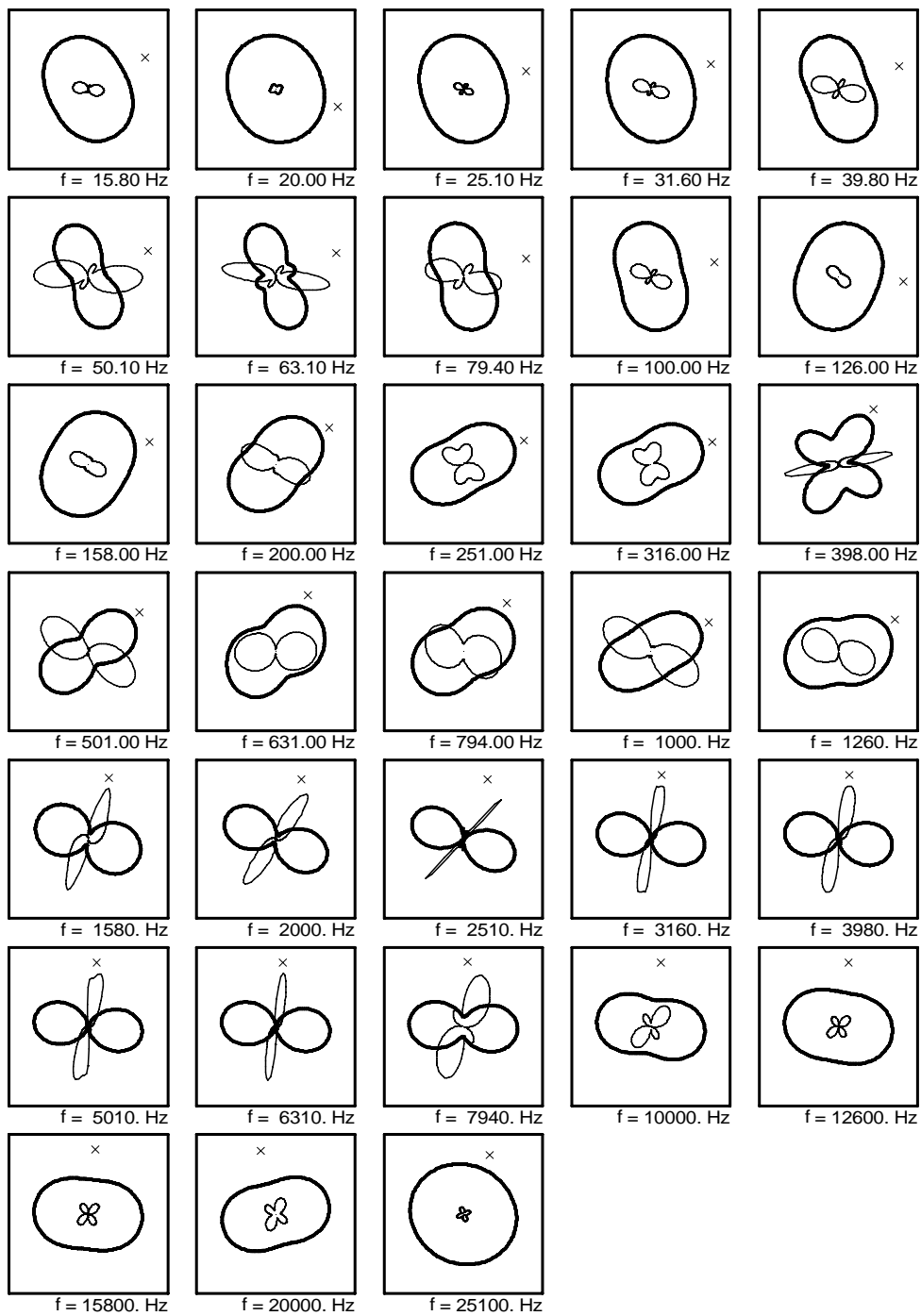
Sounding SR025



— = Zxy Impedance
 - - - = Zxx Impedance
 x = Impedance Strike

USGS

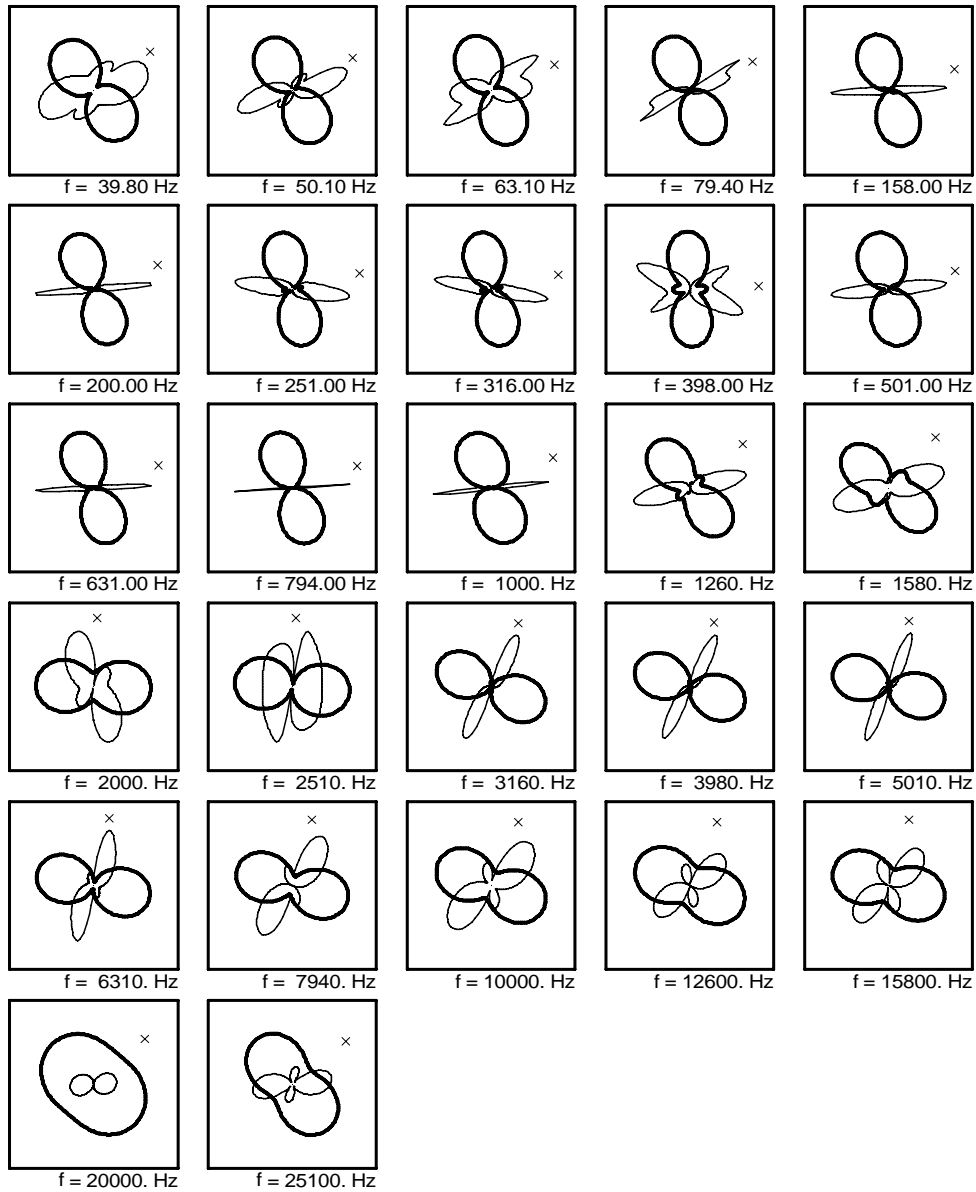
Sounding SR026



— = Zxy Impedance
 — = Zxx Impedance
 x = Impedance Strike

USGS

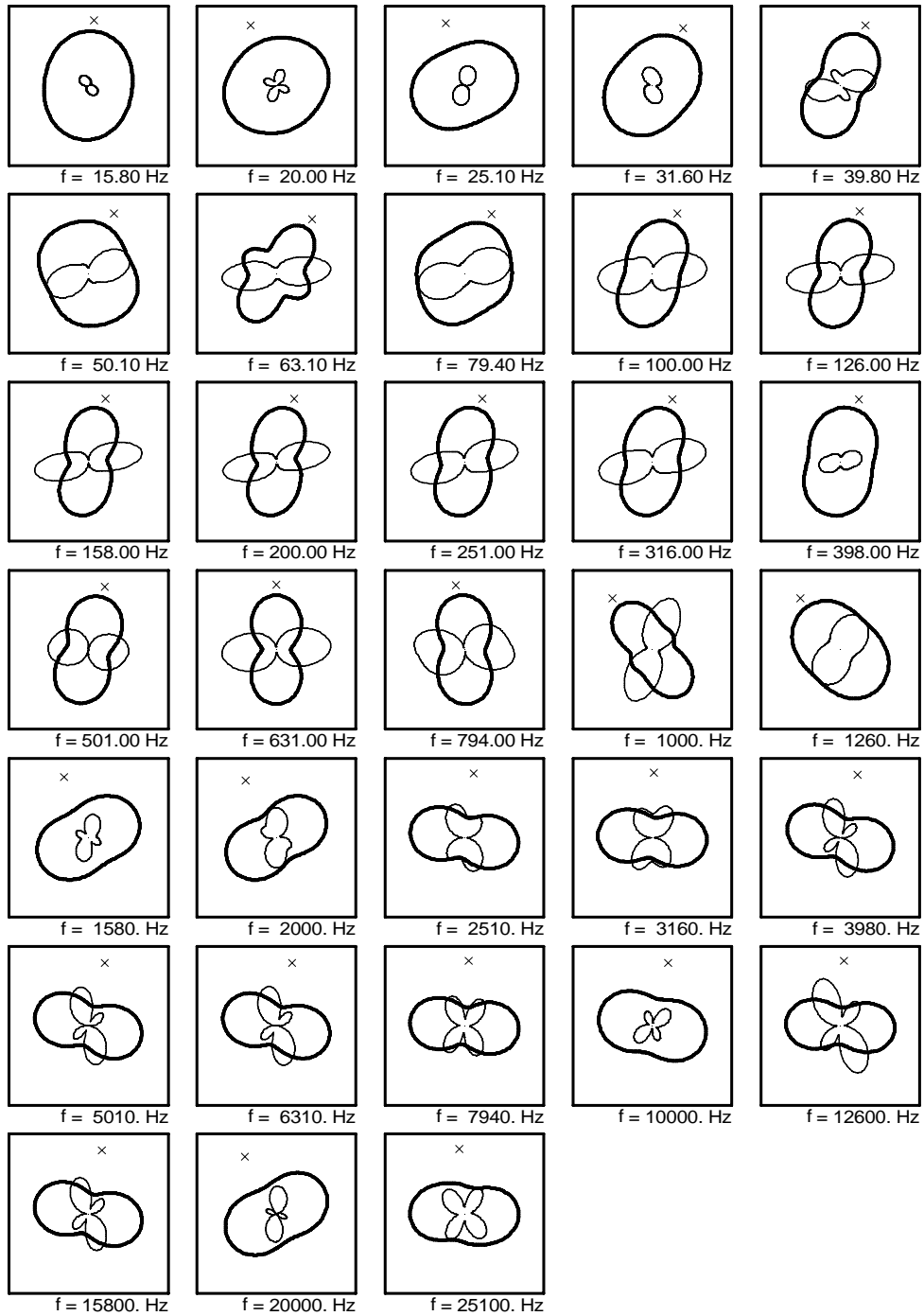
Sounding SR028



— = Zxy Impedance
 - - - = Zxx Impedance
 x = Impedance Strike

USGS

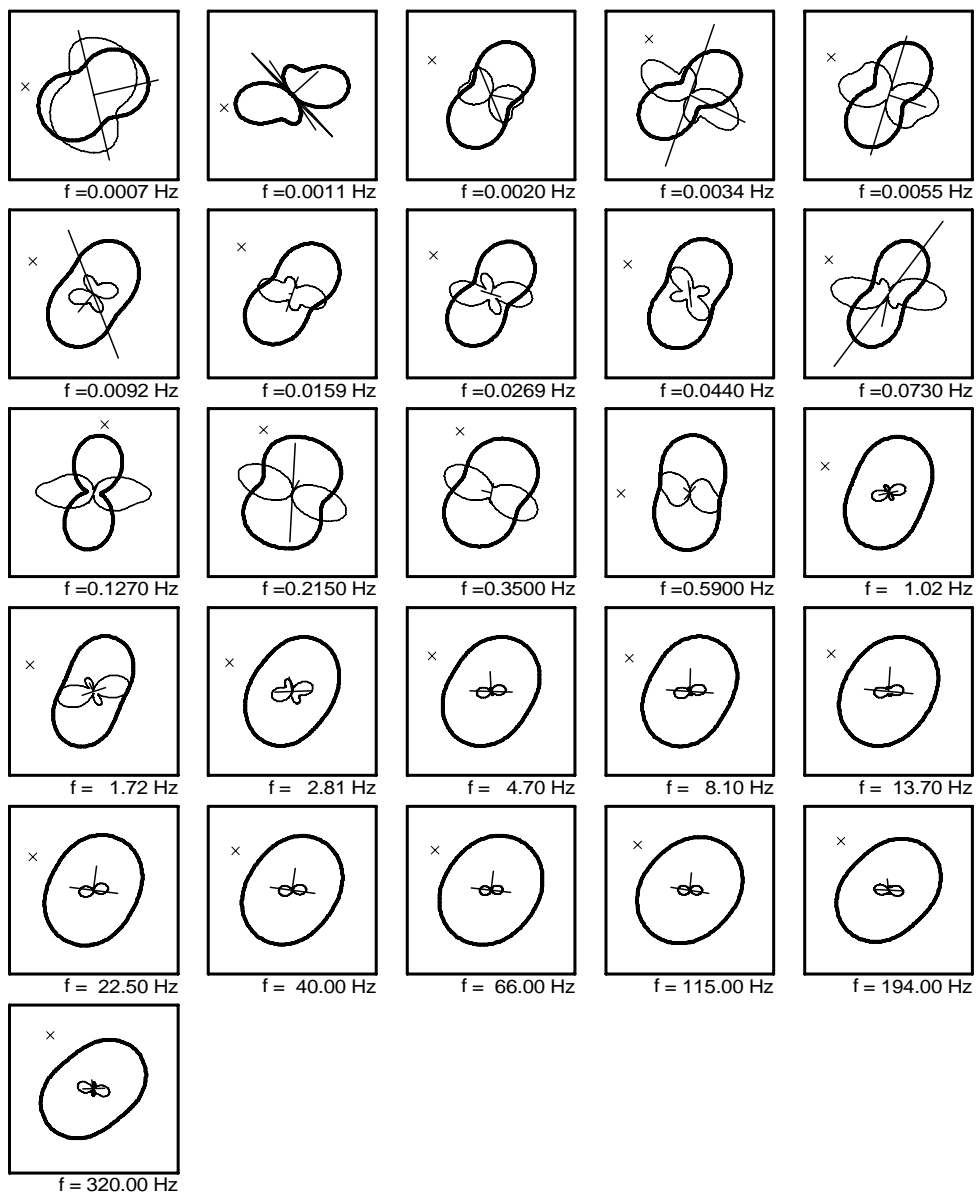
Sounding SR029



— = Z_{xy} Impedance
 — = Z_{xx} Impedance
 x = Impedance Strike

USGS

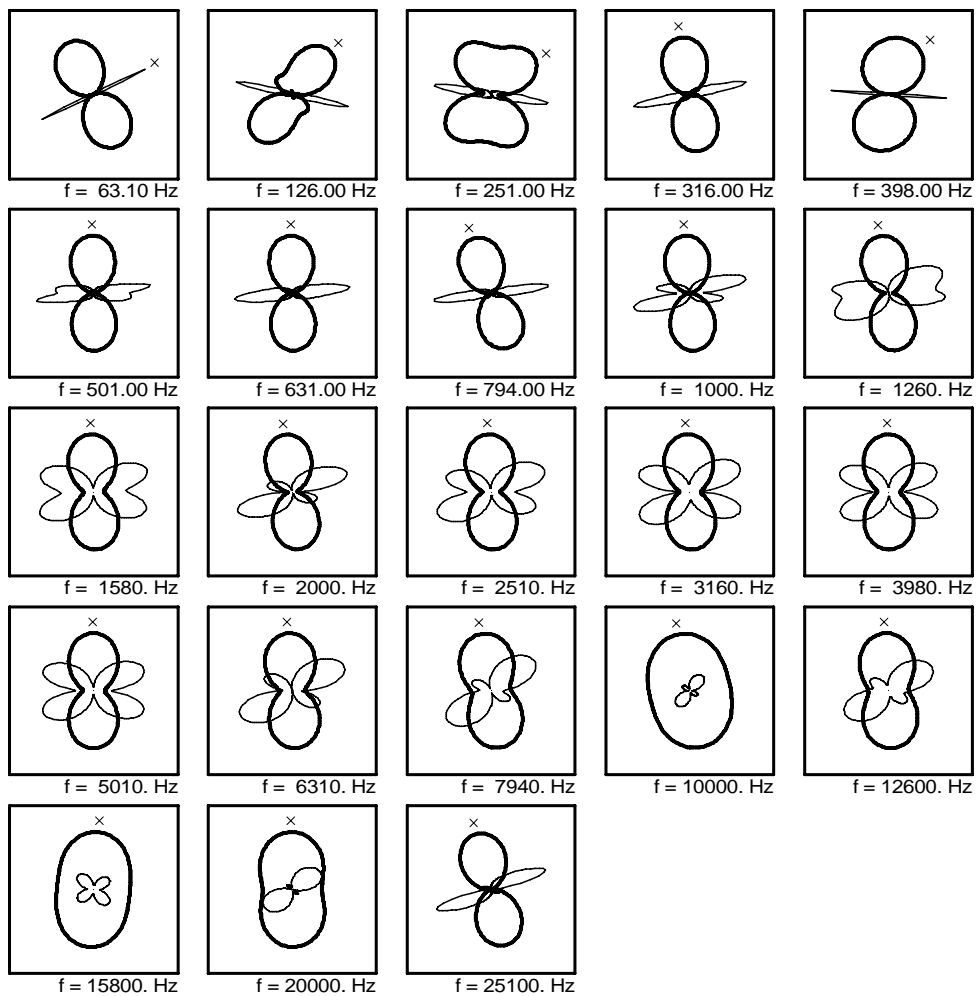
Sounding WF01



————— = Zxy Impedance
 ————— = Zxx Impedance
 × = Impedance Strike
 ————— = Tipper Magnitude / Strike
 0 1
 ————— = Induction Arrow (to conductor)
 0 1

USGS

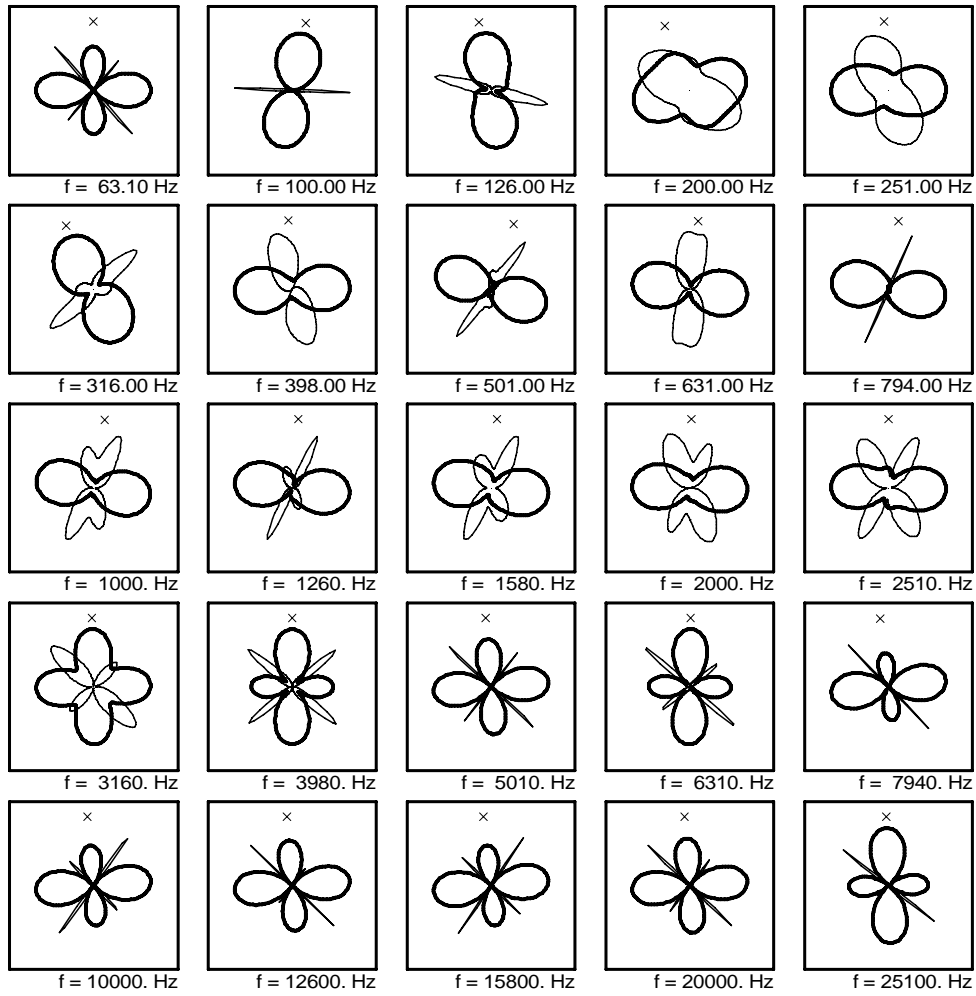
Sounding WR002



— = Zxy Impedance
 — = Zxx Impedance
 x = Impedance Strike

USGS

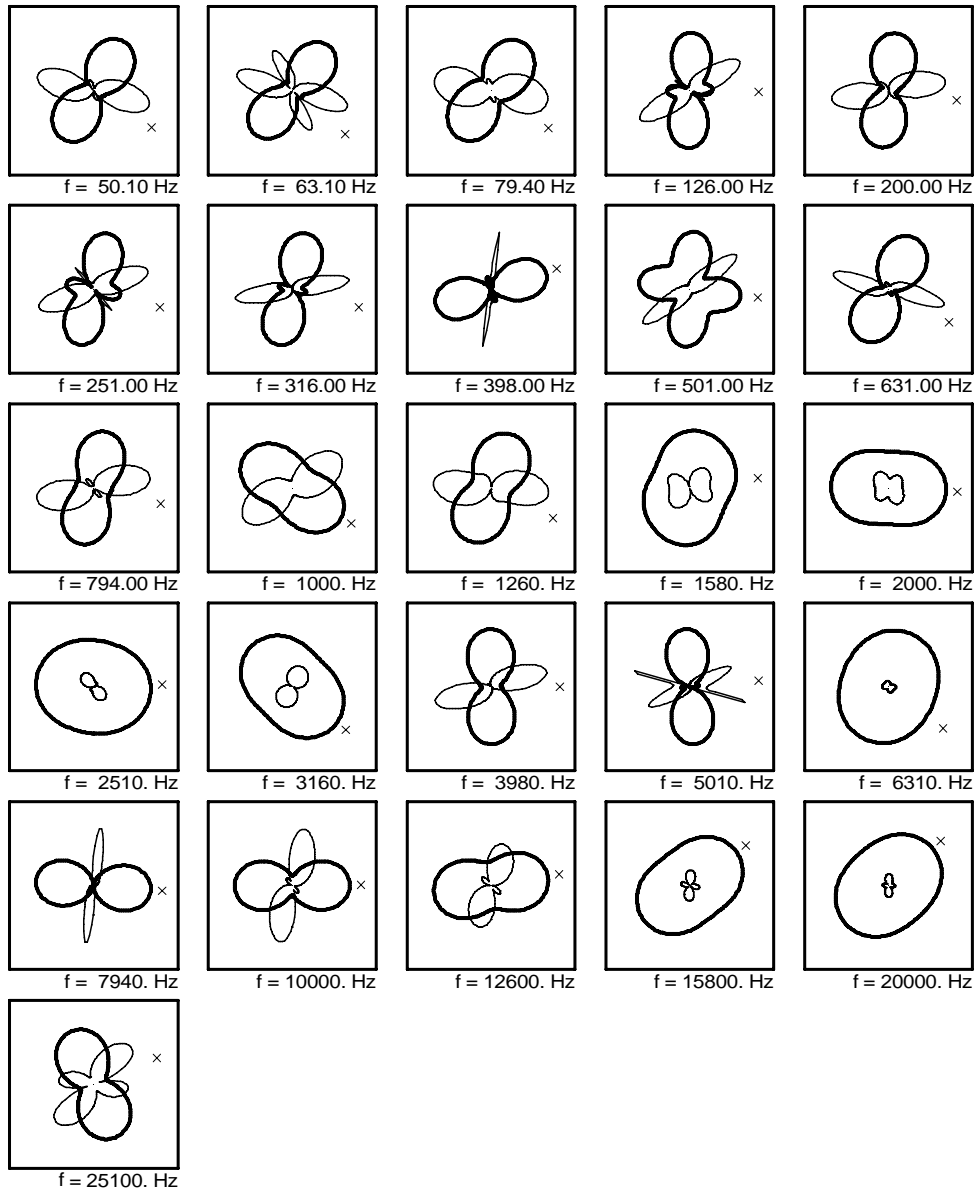
Sounding WR003



= Zxy Impedance
 = Zxx Impedance
 = Impedance Strike

USGS

Sounding WR004



— = Zxy Impedance
 — = Zxx Impedance
 x = Impedance Strike